DOCTOR OF PHILOSOPHY

Synthesis and bioactivation of redox-activated quinone prodrugs of guanidine

Martin, Claire Marie

Award date:
2012

Awarding institution:
Bangor University

Synthesis and Bioactivation of Redox-Activated Quinone Prodrugs of Guanidine

---

A thesis presented for the

Degree of

Philosophy Doctor

In the

School of Chemistry

By

Claire Marie Martin

Prifysgol Bangor • Bangor University

September 2012

Acknowledgements

Firstly I would like to dedicate my thesis to the memory of one very special lady, my incredible nana Mary Martin. I will never forget her support and encouragement throughout my time in Bangor. Every day she is a constant reminder to why cancer research is so important. She is my inspiration.

To my supervisor Dr. Paddy Murphy for giving me the opportunity to stay another three years and for all his help and guidance. Also to all of the PhD, Masters, third year undergraduates and exchange students that have worked alongside me on the sixth floor. In particular I would like to thank my wonderful boyfriend Deiniol, lab associates Iestyn, Elliot, Zainab, Hisham, Dan and Manji, my fume cupboard partner and friend for life.

To Morvus Technology Ltd, my sponsor, for allowing me the opportunity to work in an area of Chemistry I am passionate about and for their generous financial support. In particular I would like to thank my company supervisors Prof. Terry Jenkins and Dr. Mohammed Jaffar for their time in assisting me these past years. To the EPSRC; without their financial support this PhD would not have been possible.

To all of the technical staff Louise (NMR), Gwynfor, Glynne, Nick, Denis and Sam for all of their help and patience.

To my amazing family my Mum, Dad, Rebecca, James, Kate, Dan and grandparents who have supported me throughout every single exam and thesis write-up.

Lastly but by no means least to my close friends from home Vicky and Gary for always being there and to Helen and Susan for making my time in Bangor the very best!

Abbreviations

ADEPT	Antibody-directed enzyme prodrug therapy
aq.	Aqueous
br.	Broad
CI	Chemical ionisation
conc.	Concentrated
DCC	Dicyclohexylcarbodiimide
DEPT	Distortionless enhancement by polarisation transfer
DIAD	Diisopropyl azodicarboxylate
DMA	Dimethylaniline
DMF	*N*,*N*-Dimethylformamide
DMSO	Dimethyl sulfoxide
DNA	Deoxyribonucleic acid
EDCI	1-Ethyl-3-(3-dimethylaminopropyl)carbodiimide
EI	Electron impact
EO9	*E*-3-(5-(Aziridin-1-yl)-4,7-dioxo-3-hydroxymethyl-1-methylindol-2-yl)prop-2-en-1-ol
Equiv.	Equivalent (s)
ESI	Electrospray ionisation
FAD/ $FADH_2$	Flavin adenine dinucleotide (oxidised/reduced form)
FTIR	Fourier transform infrared
GDEPT	Gene-directed enzyme prodrug therapy
h	Hour (s)
hNQO1	Human quinone-oxidoreductase 1
HOBT	4-Hydroxybenzotriazole
HPLC	High performance liquid chromatography
HRMS	High resolution mass spectrometry
Lit.	Literature
LRMS	Low resolution mass spectrometry
min	Minute (s)
m.p.	Melting point

NADH	Nicotinamide adenine dinucleotide
NADPH	Nicotinamide adenine dinucleotide phosphate
NBS	*N*-Bromosuccinimide
NHS	*N*-Hydroxysuccinimide
NMR	Nuclear magnetic resonance
QR1	Quinone reductase 1
RMSD	Root mean square deviation
r.t	Room temperature
TAP	Tumour activated prodrug
THF	Tetrahydrofuran
TLC	Thin layer chromatography
TOF	Time of flight
UV	Ultraviolet

Abstract

This thesis describes the preparation of several novel guanidine derivatives (where X= tetramethyl, dipiperidine and dimorpholine); three containing a previously described trimethyl-substituted quinone **I** and three analogous guanidines containing the novel phenyl-substituted quinone **II**. These conformationally locked derivatives were tested as substrates in a benzoquinone-based drug delivery system which is activated by the enzyme human quinone-oxidoreductase 1 (hNQO1). Molecular modelling studies were initially performed and demonstrated that all six derivatives were viable substrates of the enzyme hNQO1, as determined by the drug/hNQO1 interactions. Following their successful preparation, these derivatives were subsequently analysed by high performance liquid chromatography (HPLC). Preliminary findings confirmed their ability to act as substrates for the enzyme hNQO1 and showed they followed the intended mechanistic pathway for this drug delivery system. These results also indicated that the rate of reaction with hNQO1 was faster for quinone **I** versus **II** and the reaction of **II** did not proceed to completion.

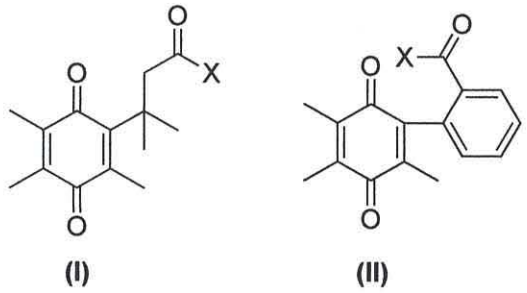

X =

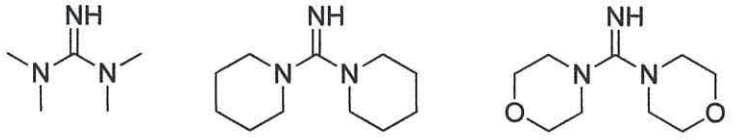

Contents

Introduction

1.0 Cancer chemotherapy

In recent years, many different strategies have been exploited concerning the development of new chemotherapeutic drugs. The problem is lack of tumour specificity,[1] resulting in systemic toxicity and a low therapeutic index.[2] These drugs can interfere with cells by attacking some aspects of their deoxyribonucleic acid (DNA) synthesis, replication or processing.[3] Since they preferentially kill rapidly dividing cells, some normal cells are also exposed to toxic levels, resulting in severe undesirable side effects such as damage to hair follicles, the kidney, liver, bone marrow[4] and gut epithelia.[3] However, chemotherapy still remains the primary systemic treatment of cancer. Consequently there is a need to develop new and improved drugs which are more selective in their function but still maintain their cytotoxic activity.

2.0 Prodrugs

2.1 Introduction

One approach first introduced by Albert[5] and Harper[6] in the late 1950s is the design of relatively non-toxic prodrugs. These can be converted either through metabolism by endogenous enzymes or spontaneously into the pharmacologically active species and activated within the tumour mass.[7] They have essentially been employed to improve the efficacy of anti-cancer agents by the modification of their physicochemical[8] and/or pharmacokinetic[9] properties. More specifically this includes their (i) solubility and lipophilicity (ii) bioavailability[8] (iii) stability[10] (iv) toxicity (v) transport properties[9] (vi) site and duration of action[10, 11] and (vii) first-pass metabolic effects.[12]

2.2 Classes of prodrug

There are many different types of prodrug which exploit various aspects of the tumour physiology, such as selective enzyme expression, hypoxia and low extracellular pH. Others relate to tumour-specific delivery techniques such as antibody- and gene-directed enzyme prodrug therapy (ADEPT and GDEPT).

2.3 Hypoxia-activated prodrugs

Our interest lies with hypoxia-selective tumour-activated prodrugs (known as hypoxia-TAP). Hypoxia is a deficiency of oxygen[13] that can be classified into two broad types, the first (i) chronic or diffusion hypoxia keeps cells that are ample distance (approx 150 μm) away from the nearest functional blood capillary hypoxic in the long term. The second (ii) transient or perfusion hypoxia is due to a temporary shutdown of blood vessels keeping sections of tissue hypoxic in the short term.[7, 14] Hypoxia has been shown to exist in a number of different diseases including some cancers i.e. brain, head and neck, breast and cervix,[15] rheumatoid arthritis and diabetes.[16] It is often characterised by low oxygen tension, nutrient levels[17, 18] and pH.[17-19] Hypoxic cells are commonly found in most solid tumours as the result of a poor blood supply,[14] high interstitial pressures,[14, 20] enhanced metabolic rate[4] and an inefficient vasculature system.[14] They have been found to be resistant to both radiotherapy and chemotherapy.[21] Since severe hypoxia only exists in tumours, an opportunity arose to exploit this phenomenon for its potential therapeutic advantage[22] and to develop non-toxic hypoxia-activated prodrugs. By concentrating the cytotoxic anti-cancer agents inside the tumour mass could dramatically minimise the risk of destroying normal cells.

2.4 Classes of hypoxia-activated prodrugs

The major classes of hypoxia-TAP include nitroaromatic heterocyclics, quinones, aromatic and aliphatic *N*-oxides and transition metal complexes. Each class can be activated under hypoxic conditions and in the presence of reductive enzymes (Figure 1).

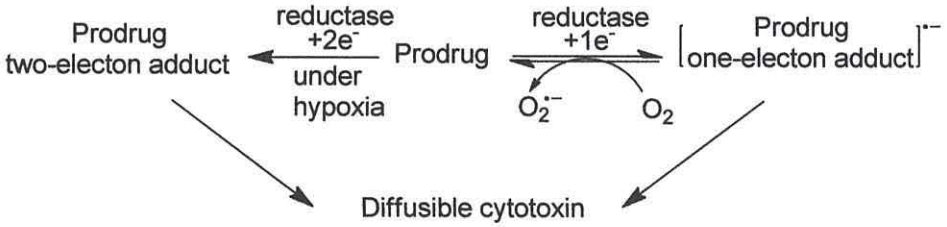

Figure 1. General mechanism of prodrug activation under hypoxia (adapted from[3, 7])

2.4.1 Nitroaromatic heterocyclics

Nitro compounds can undergo a series of up to six one-electron reductions starting with the nitro group **1** to give the nitro anion radical **2** (Scheme 1). This intermediate can be back-oxidised by molecular oxygen present in normoxic tissues to regenerate the parent compound **1**. Further reduction produces the nitroso **3**, radical **4**, hydroxylamine **5** and

amine **6** as the subsequent products. Only in hypoxic tissue will the reduction proceed to these highly cytotoxic species.[9]

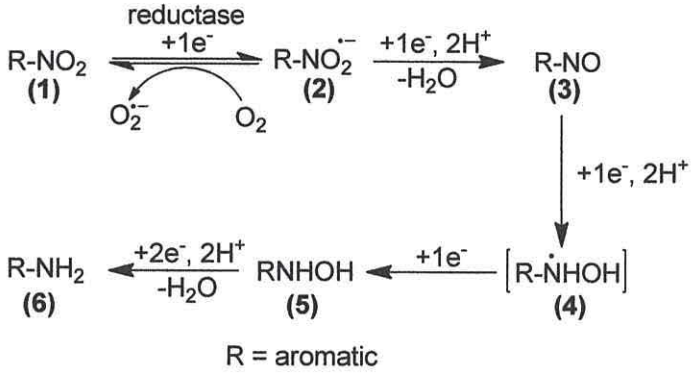

Scheme 1. Pathway of reductive activation for a nitroaromatic drug

Among the nitroaromatics, the most extensively studied compounds are the 2-nitroimidazoles such as misonidazole **7**[23] and etanidazole **8**[7] (Figure 2).

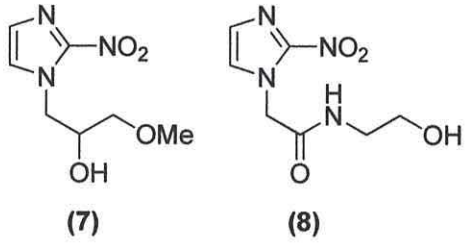

Figure 2. Structure of misonidazole and etanidazole

These were originally developed as oxygen-mimetic radiosensitisers[24-26] but are also metabolised selectively under hypoxia to give an ill-defined electrophilic species. However, they are only weakly cytotoxic and have moderate selective toxicity for hypoxic cells over oxygenated cells in tissue culture.[7] Another hypoxia-activated nitroaromatic prodrug is dinitrobenzamide 5-(1-aziridinyl)-2,4-dinitrobenzamide **9**[23, 27] (CB-1954) (Figure 3), although this has been more widely used for GDEPT.[28]

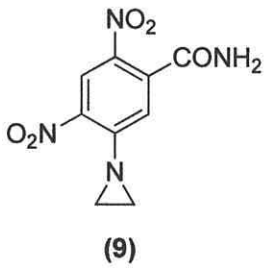

Figure 3. Structure of 5-(1-aziridinyl)-2,4-dinitrobenzamide

2.4.2 *N*-oxides

N-oxides are an important class of hypoxia-selective anti-tumour agents, such as the 1,2,4-benzotriazine 1,4-dioxides, represented by their leading compound the bioreductive prodrug tirapazamine **10** (3-amino-1,2,4-benzotriazine 1,4-dioxide) (Figure 4).[29]

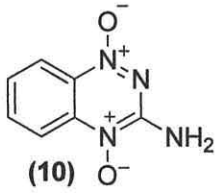

(10)

Figure 4. Structure of tirapazamine

Tirapazamine **10** can be synthesised using 3-aminobenzo-1,2,4-triazine 1-*N*-oxide **15**. There are two different synthetic routes to prepare this compound (Scheme 2). The first, known as the Arndt[30] reaction involves the addition of cyanamide to the nitroaniline **11** which is then melted and treated with concentrated (conc.) hydrochloric acid. The resulting intermediate[31] **12** is then made alkaline by the addition of sodium hydroxide and cooled to precipitate out the benzotriazine **15** in 80% yield.[32] The second method involves boiling 3-hydroxybenzo-1,2,4-triazine 1-*N*-oxide **13** under reflux with dimethylaniline (DMA) and phosphorus oxychloride ($POCl_3$) followed by cooling to crystallise out 3-chlorobenzo-1,2,4-triazine 1-*N*-oxide **14** in 64% yield. In the final step, this is boiled in ethanol under reflux whilst anhydrous ammonia is passed through the solution to afford the desired benzotriazine **15** this time in 54% yield.[33, 34]

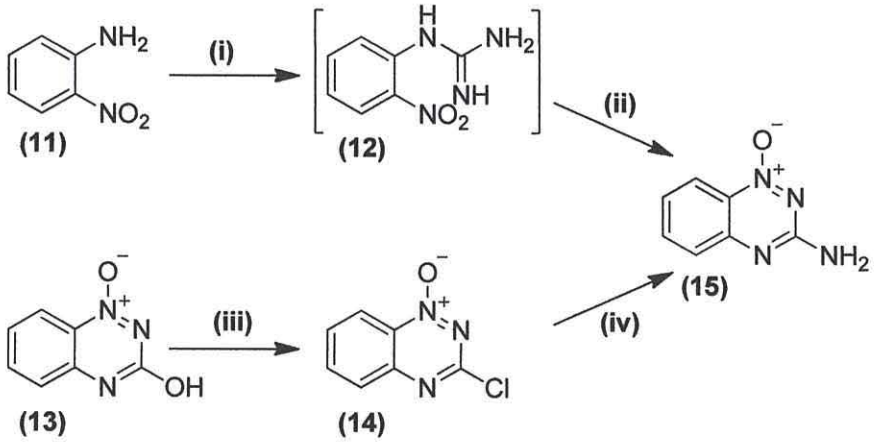

Scheme 2. (i) 0.5 equiv. cyanamide, 100 °C then r.t, HCl then 100 °C (ii) NaOH, r.t then 100 °C, 30 min (iii) DMA, $POCl_3$, Δ, 45 min (iv) NH_3, EtOH, Δ, 7 h

In the final step, a suspension of the benzotriazine **15** in acetic acid is stirred and heated at 45 – 50 °C with 30% aqueous (aq.) hydrogen peroxide for 20-60 hours (h). The mixture is then treated with sodium hydrogen carbonate and recrystallised from acetic acid and water to give tirapazamine **10** in 89% yield (Scheme 3).[32]

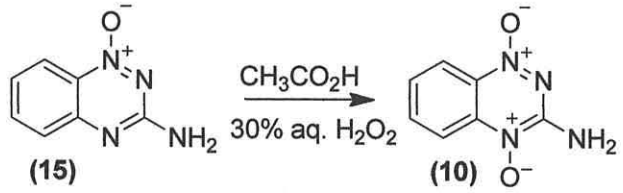

Scheme 3. Final step in the synthesis of tirapazamine

The mechanism by which a benzotriazine 1,4-dioxide produces oxidising radicals has been investigated using tirapazamine **10**[35] (Scheme 4).

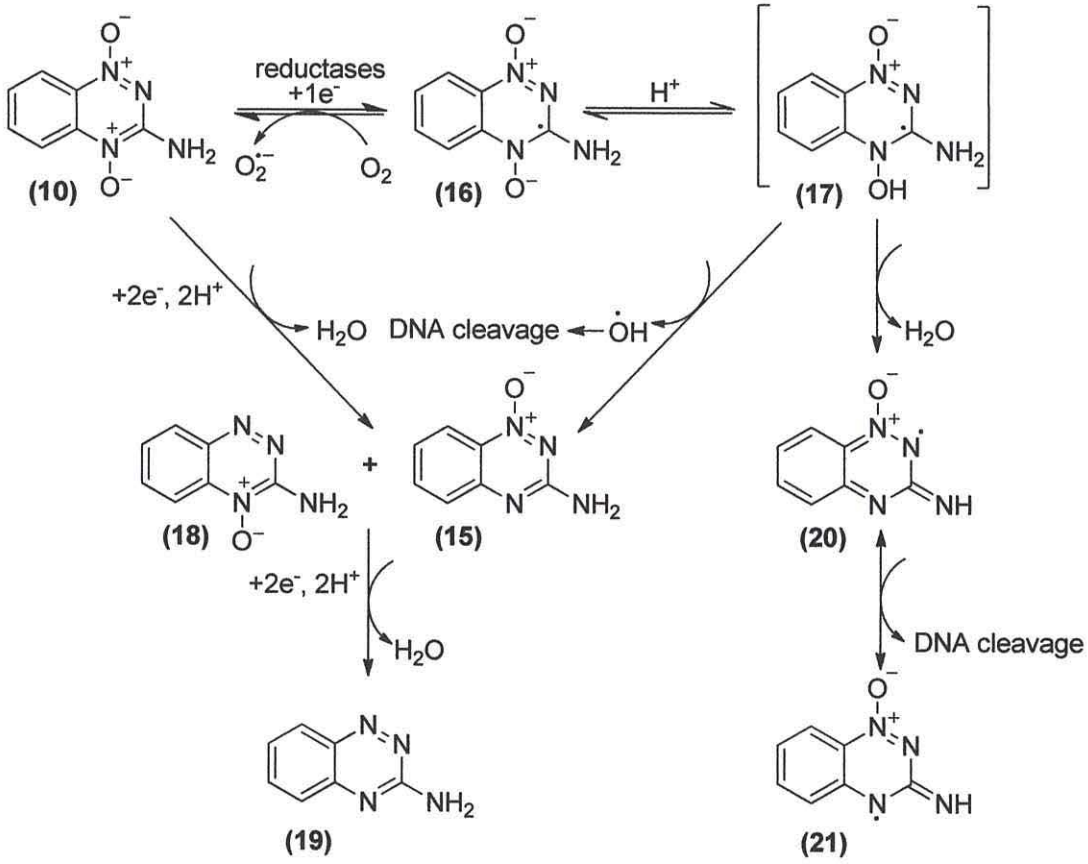

Scheme 4. Pathway of tirapazamine reductive activation (adapted from[29, 36-39])

Tirapazamine **10** can undergo one-electron reduction by the enzymes xanthine/xanthine oxidase and nicotinamide adenine dinucleotide phosphate (NADPH):cytochrome P450 oxidoreductase[29] to form the free radical anion nitroxide **16**[40] and in the presence of acid the protonated radical **17**. However, in normal aerobic cells, these radicals are destroyed

by oxidation by molecular oxygen to regenerate the parent compound **10** with release of a superoxide radical as a by-product.[36] Normally this redox cycling can be cytotoxic but, in the context of tirapazamine **10**, it is the reactions of the protonated radical **17** in the absence of molecular oxygen that are more lethal.[41] Tirapazamine **10** is relatively non-toxic to oxygenated cells.[29] However, under hypoxic conditions, its activated form, the protonated radical **17**, can fragment to release the hydroxyl radical, a known DNA-damaging cytotoxin,[29, 41] and the metabolite **15**, which is not highly cytotoxic.[36] This intermediate **15** can then undergo two-electron reduction to give the reduced species **19** which is non-toxic.[35] In 2001 Fuchs *et al.*[29] reported the formation of a second metabolite **18** which undergoes the same reduction. It has also been reported that the protonated radical **17** can also undergo a dehydration reaction to form the highly reactive benzotriazinyl radicals **20** and **21**,[37-39, 42] capable of causing oxidative damage to DNA.[39] Therefore it is the products of the one-electron reduction species that are believed to be the key radical intermediates in the cytotoxic action of tirapazamine **10**. The propensity for this increases at lower pHs since more of the protonated radical **17** is present.[35]

Tirapazamine **10** is selectively toxic towards hypoxic cells found in solid tumours. Over the past 25 years it has been in phase I,[43] II[44] and III[45] clinical trials for the treatment of certain cancers. However, tirapazamine **10** has a number of limitations; one of which is it's lower hypoxic selectivity *in vivo* compared to *in vitro*. This is thought to be due to the rapid rate of metabolism in hypoxic tissue resulting in limited penetration of the drug. Tirapazamine **10** also has moderate solubility. Therefore it would be an advantage to design analogues which improve on some or all of these limitations.[46, 47]

Other examples of aromatic *N*-oxides are the quinoxaline 1,4-di-*N*-oxides, represented by 3-amino-2-quinoxalinecarbonitrile-1,4-di-*N*-oxide **22** (Figure 5).[48]

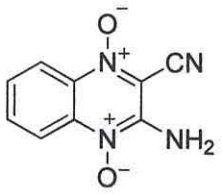

(22)

Figure 5. Structure of 3-amino-2-quinoxalinecarbonitrile-1,4-di-*N*-oxide

These compounds show interesting medicinal properties (anti-bacterial, anti-viral and anti-cancer)[49] and have been found to exhibit hypoxia-selective toxicity in preclinical tests.[41] More recently they have been studied for their potential for treating tuberculosis.[49]

2.4.3 Quinones

Quinones were among the first compounds to be explored for their role as hypoxia-TAP. Even the simplest 1,4-benzoquinone **23** (Figure 6), isolated by oxidation of quinic acid obtained from cinchona bark is bioactive being used as a defence agent in beetles to warn off attackers.[50]

(23)

Figure 6. Structure of 1,4-benzoquinone

Quinones are known to undergo both one-electron reduction to afford a semiquinone species **25** (by cytochrome P450 reductase) or a two-electron reduction to afford a hydroquinone species **24** (by hNQO1)[51] (Scheme 5).[3, 9] Both can potentially fragment and lead to the release of a therapeutic drug. However, the semiquinone **25** can be back-oxidised to the original quinone **23** by molecular oxygen present in normal cells. Since this is an oxygen-sensitive intermediate, this protects normal tissues, since it ensures that further reduction is confined only to hypoxic cells. In contrast, two-electron reduction using hNQO1 is oxygen independent and therefore is capable of reducing and activating quinones in non-hypoxic cells.[21] The result would be the destruction of normal cells by the intended therapeutic drug giving rise to unwanted side effects. This limiting factor has meant that, despite a large number of quinones being studied, very few have been shown to possess hypoxia selectivity.[9]

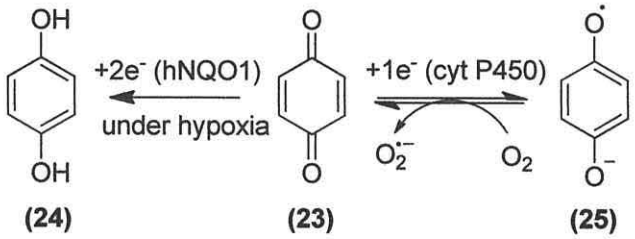

(24) **(23)** **(25)**

Scheme 5. Mechanistic pathway of reductive activation for a quinone drug

Several quinones have been studied for their potential application as hypoxia-TAP. In 1956 Hata *et al.*[52, 53] discovered two new antibiotics mitomycin A **26** and B **27** from the *Streptomyces caespitosus* bacteria (Figure 7).

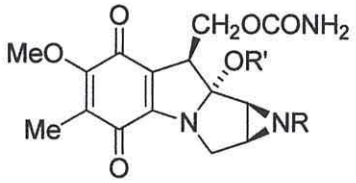

(26) R = H R' = Me
(27) R = Me R' = H

Figure 7. Structure of mitomycin A and B

Two years later mitomycin C **28** was isolated from the same strain by Wakaki *et al.*[54, 55] and found to be a potent anti-tumour agent for cancer chemotherapy.[56] In 1962 Webb *et al.*[57] reported the structural elucidation of these mitomycins along with their *N*-methyl derivative porfiromycin **29**, which all contain the indolequinone structure[58] **30** (Figure 8).

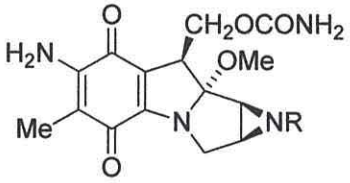

(28) R = H
(29) R = Me

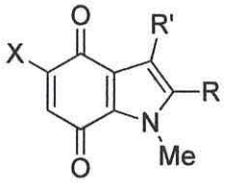

(30)

Figure 8. Structure of mitomycin C, porfiromycin and general structure of indolequinones

The total synthesis of these compounds was not reported until 1977 by Nakatsubo *et al.*[59-61] with improvements to these synthetic routes reported in the late 1980's by Fukuyama and Yang.[56, 62] Mitomycin C **28** was the first clinical agent designated as a hypoxia-TAP but was found to show only marginal hypoxic selectivity *in vitro*.[3] In comparison porfiromycin **29** showed superior hypoxic selectivity, both *in vitro* and *in vivo*.[63] However, clinical studies of mitomycin C **28** and porfiromycin **29** for radiation in head and neck cancer showed that they both had promising ability as an adjunct to radiation therapy.[64-66] Despite efforts to synthesise analogues[67-72] of these compounds, mitomycin C **28** remains the only member of this class of anti-cancer drug in routine clinical use.[73] Another structurally related compound to the mitomycins is *E*-3-(5-(aziridin-1-yl)-4,7-dioxo-3-hydroxymethyl-1-methylindol-2-yl)prop-2-en-1-ol (EO9) **31** (Figure 9), first synthesised by Speckamp and Oostveen in 1987[74] which contains the aziridinylbenzoquinone[58]

structure **32**. This required a synthesis containing over 20 steps, with the route later being improved in 1995 by Cotterill *et al.*[75] and in 2003 by Comer and Murphy.[76]

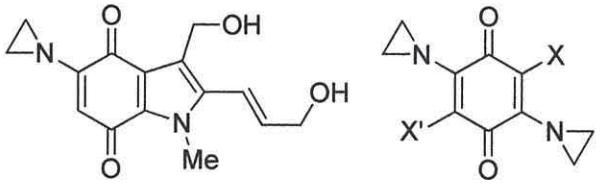

(31) **(32)**

Figure 9. Structure of EO9 and general structure of aziridinylbenzoquinones

EO9 **31** has been shown to have good hypoxia selectivity *in vitro* and *in vivo*. However, it failed to show activity in clinical phase II trials.[77] This can be attributed to its poor pharmacokinetic properties resulting in poor drug delivery.[78] Future work is focussed on developing more analogues of EO9 **31** which retain its desirable features but potentially have a better delivery system.[78-81]

3.0 Quinone reduction by hNQO1

3.1 Introduction

Of these three main classes of hypoxia-TAP our interest lies with the synthesis and bioactivation of quinones by hNQO1. This enzyme was first isolated in 1958 by Ernster and Navazio[82] and is also referred to as NAD(P)H: quinone oxidoreductase-1, EC 1.6.99.2, quinone reductase 1 (QR1) or DT-diaphorase. It exists as a *homo*-dimeric structure each subunit containing a non-covalently bound flavin adenine dinucleotide (FAD) cofactor.[50, 83] The structure of hNQO1 has been solved by X-ray crystallography (Figure 10).[58]

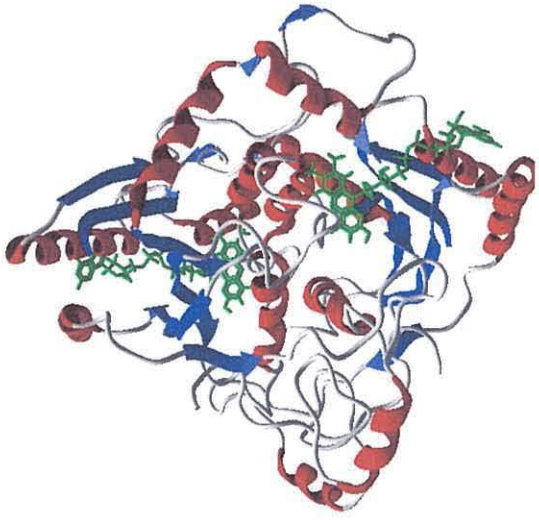

Figure 10. Crystal structure of dimeric hNQO1 showing two bound FAD (adapted from[58])

hNQO1 is a cytosolic flavoprotein that catalyses the two-electron reduction of a number of substrates using nicotinamide adenine dinucleotide (NADH) **35** or NADPH as electron donors (Scheme 6).[73, 84]

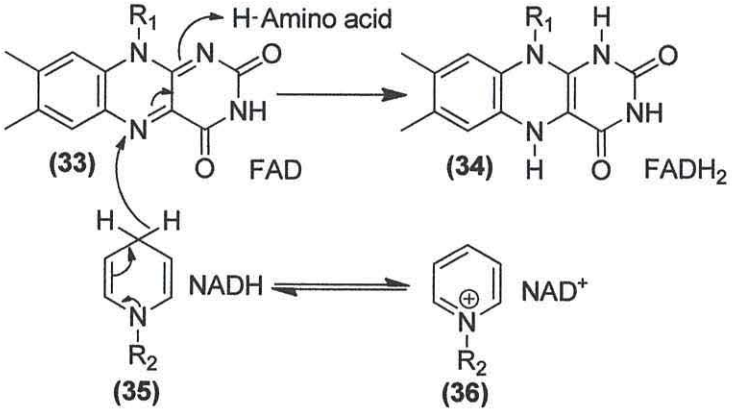

Scheme 6. Mechanism of two-electron reduction of FAD **33** to $FADH_2$ **34** utilising NADH **35**

Most importantly is its ability to bioactivate certain cancer chemotherapeutic quinones into a cytotoxic species. This, coupled with the fact that elevated levels of this enzyme have been discovered in several human solid tumours e.g. breast, colon, non-small-cell lung and ovarian[58] makes it an excellent target for enzyme-directed drug development.[58, 85]

3.2 Mechanisms of hNQO1 reduction

Several mechanisms have been proposed for the reduction of quinones by hNQO1. First to be postulated was the 'ping pong' mechanism in 1995 by Li *et al.*[86] suggesting that hydride transfer occurs directly to a carbonyl oxygen of the quinone **37** to form the intermediate anion **38**. This intermediate **38** is subsequently acidified to the hydroquinone **39** (Scheme 7).

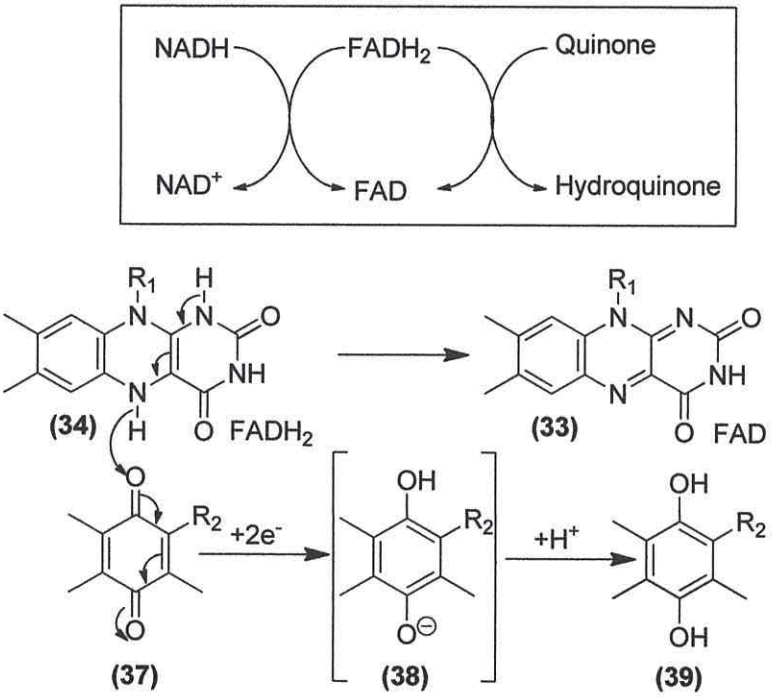

Scheme 7. Proposed mechanism one, hydride transfer from $FADH_2$ to a carbonyl oxygen

In 1998 Schlegal *et al.*[87] suggested that hydride transfer occurs directly to a carbonyl carbon of the quinone **37**. It was thought that mechanism one was not electronically feasible due to the electronegativity of the oxygen compared to the carbon.[88] This gives the intermediate anion **40** which is then acidified to the hydroquinone **39** (Scheme 8).

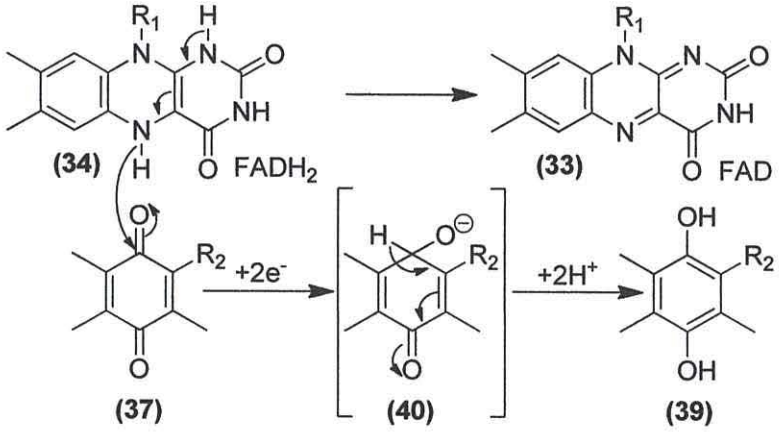

Scheme 8. Proposed mechanism two, hydride transfer from $FADH_2$ to a carbonyl carbon

Finally in 1999 a third mechanism was proposed by Faig *et al.*[89, 90] suggesting that hydride transfer occurs directly to an adjacent carbonyl carbon of the quinone **37**, a Michael-type addition reaction. This gives the anion intermediate **41** followed by tautomerisation to the hydroquinone **39** (Scheme 9).

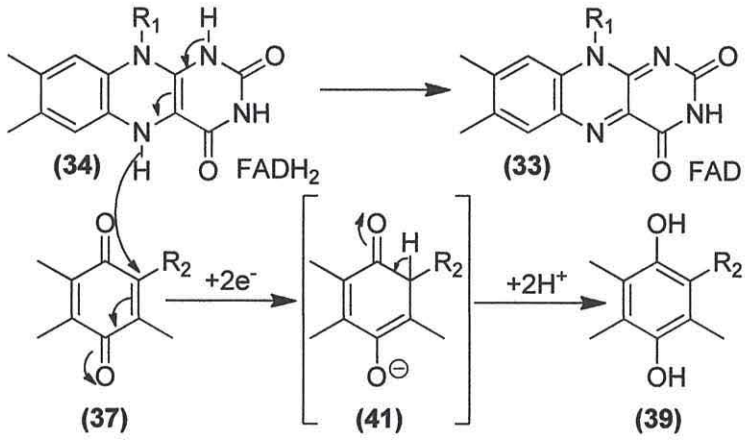

Scheme 9. Proposed mechanism three, hydride transfer from $FADH_2$ to an adjacent carbonyl carbon

4.0 Benzoquinone drug delivery system

4.1 Milstien and Cohen

It has been shown how quinones undergo a redox two-electron reduction by hNQO1 to form hydroquinones which can cyclise leading to the release of the therapeutic drug. One route that has been greatly studied as the gateway to this process is by using a benzoquinone delivery system. In 1972, Milstien and Cohen studied the kinetics of lactonisation of a series of *o*-hydroxyhydrocinnamic acids (Scheme 10).[91]

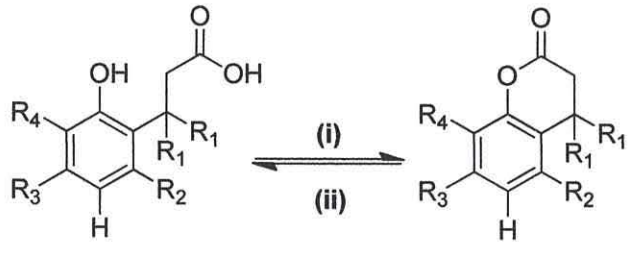

(a) $R_1 = R_2 = R_3 = R_4 = H$
(b) $R_1 = H$; $R_2 = R_3 = R_4 = CH_3$
(c) $R_2 = R_3 = R_4 = H$; $R_1 = CH_3$
(d) $R_1 = R_2 = R_3 = R_4 = CH_3$

Scheme 10. (i) $-H_2O$ (ii) H_2O

They investigated the effect of structural features on the reaction rate and found that increasing methyl substitution at the R_1 and R_2 side chain facilitated the rate of lactonisation by factors up to 10^{11} (Table 1).[92]

Compound 42	No. of methyl groups in trimethyl lock positions	Relative Rate	Lactone (%)*
a	0	1.0	3.6
b	1	6.7	38.3
c	2	4.4×10^3	96.2
d	3	3.4×10^{11}	>99.0

Table 1. Effect of the trimethyl lock on the relative rates of lactonisation

*At 30 °C, in 20% dioxane, $\mu = 0.3M$

As a result the amount of lactone at equilibrium was significantly increased from 3.6% of **43a** to >99.0% of **43d**.[91] The effect of this conformation, termed 'the trimethyl lock' was of great interest particularly regarding its comparability to enzymatic reactions.[93] It was proposed that severe steric repulsion between the three methyl groups in the trimethyl lock was responsible for this rapid lactonisation.[10] This was because the unique interlocking of these groups restricted the carboxylic acid **42d** on the side chain thus 'freezing' it into a conformation that was favourable to form the lactone **43d**.[91, 94] This is also a consequence of the g*em*-Thorpe-Ingold effect[95] first established back in 1915 by Beesley, Ingold and Thorpe. It was found that increasing the size of the substituents i.e. *gem*-alkyl substitution[96, 97] was effective in enhancing ring closure and retarding ring-opening reactions. This is believed to be caused by repulsion between the two *gem* substituents.[97] Since their discovery Cohen and co-workers[98-103] continued to research the facilitation of other, similar cyclisation reactions containing a trimethyl lock system. In the same year similar work carried out by Borchardt and Cohen[104] on the cyclisation of phenols found the presence of the trimethyl lock increased the rate of reaction by 10^5.

Work by Borchardt and Cohen[105] the same year on lactones **44** and **47** discovered that they can undergo aqueous degradation resulting in the formation of spirolactones **46** and **49** (Scheme 11). When lactone **44** reacted with *N*-bromosuccinimide (NBS) the carboxylic acid **45** was formed in 94% yield. Further stirring with sodium acetate buffer gave the spirolactone **46** in 82% yield. This reaction could be reversed using 5% sodium bicarbonate to reform the acid **45** in 86% yield. However, the conversion was so rapid for the bromine lactone **47** that the presumed brominated acid intermediate **48** could not even be detected. Addition of the NBS simply gave the spirolactone **49** in 60% yield.

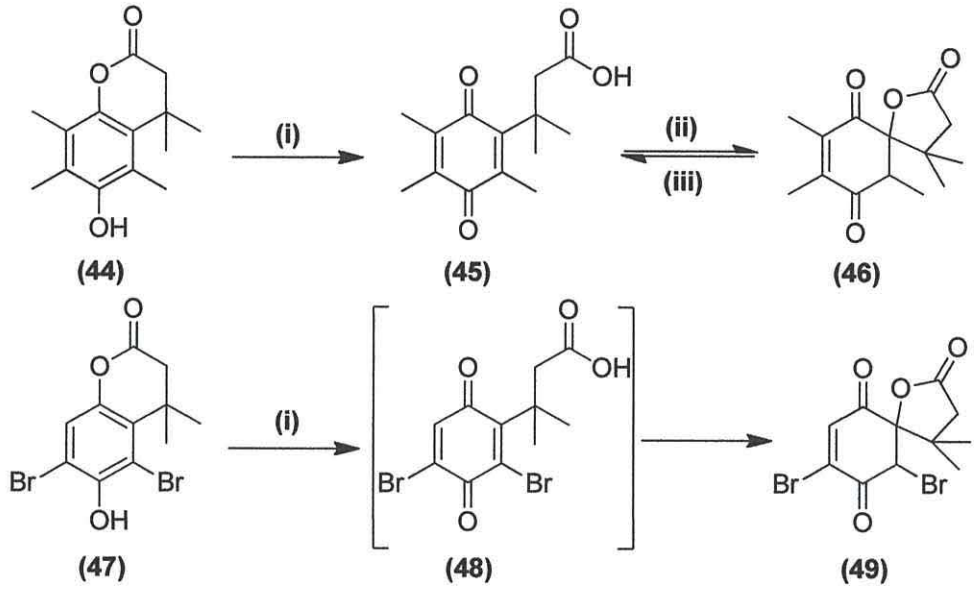

Scheme 11. (i) 1.1 equiv. NBS, acetonitrile/H_2O, 25 °C, 1 h (ii) 0.2M sodium acetate buffer (20% dioxane, pH 4.6), 25 °C, 24 h (iii) 5% $NaHCO_3$, acetonitrile, 25 °C, 3 h then H^+

The cause of these unique reactions can be attributed to the restricting ability of the lock. Although the bromine lactone **47** only contains two methyl groups and not three, the presence of the bulky bromine group attached resulted in the same effect.

4.2 Other redox benzoquinone drug delivery systems

Since this research on the trimethyl lock several redox-activated benzoquinone prodrug systems have been investigated utilising amines and amides,[106-111] alcohols,[111] esters,[106] coumarins[112] and peptide[113] groups. Additional work has been conducted on designing benzoquinone fluorophores activated by hNQO1 and based on the trimethyl lock.[114, 115]

4.2.1 Carpino *et al.*

In 1989 Carpino *et al.*[106] studied the cyclisation of esters and amides. They prepared a number of compounds **50a-f** by changing the functional group X which they reduced using sodium dithionite to give their respective hydroquinone intermediates **51a-f**. These were then cyclised to form the lactone **44** releasing XH in the process (Scheme 12).

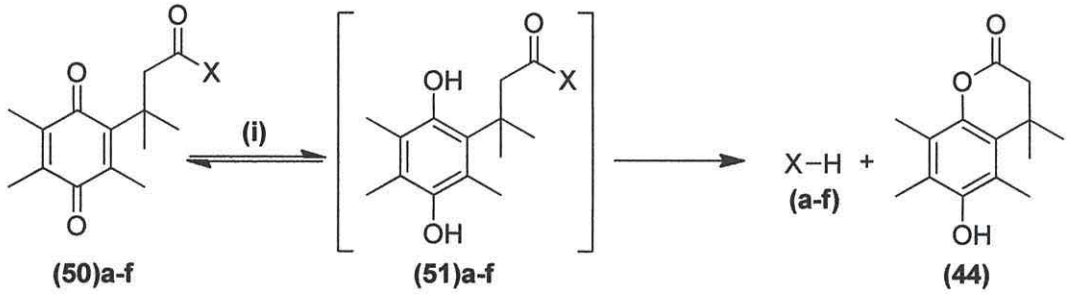

Scheme 12. (i) $Na_2S_2O_4$, CD_3OD-D_2O

50	X	$t_{1/2}$ (min)	50	X	$t_{1/2}$ (min)
a	-OMe	<3	**d**	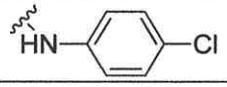	41
b	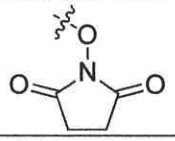	<3	**e**	$-NEt_2$	137
c	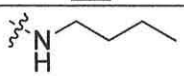	36	**f**	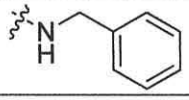	139

Table 2. Half-lives (min) for the cyclisation of a selection of quinones

Each quinone was found to have a short half-life of cyclisation ($t_{1/2}$) ranging from 3 minutes (min) for the methoxy **50a** and ester **50b** to 139 min for the amide **50f** (Table 2). This can be attributed to the presence of the trimethyl lock. If this were to be used as a benzoquinone drug delivery system (where X = drug) the rate of cyclisation could be tailored to either a fast acting or slow release rate depending on the substituents.

This work on amide-linked delivery systems associated with the trimethyl lock was continued by Amsberry and Borchardt in 1990[8] and 1991[107] and by Wang *et al.* in 1995.[109] In 1996 some similar acid and amide prodrugs were prepared by Wang *et al.*[93] and their X-ray crystallisation data studied. They concluded that the side chain X in these structures was not the predominant factor in the lactonisation rate but the presence of the trimethyl lock.

4.2.2 Wolfe *et al.*

In 1992 Wolfe *et al.*[108] synthesised another amide prodrug **52** following a method by Amsberry and Borchardt.[107] It was proposed that this compound would undergo the same reduction process as in scheme 12. However, stability studies in aqueous solution and in the absence of the reducing agent showed that it undergoes degradation instead. The amide prodrug **52** was found to equilibrate rapidly with the lactam **55** and undergo 1,2 conjugate addition to form the keto spirolactam **53**. This could then tautomerise to give the enol spirolactam **54** (Scheme 13).

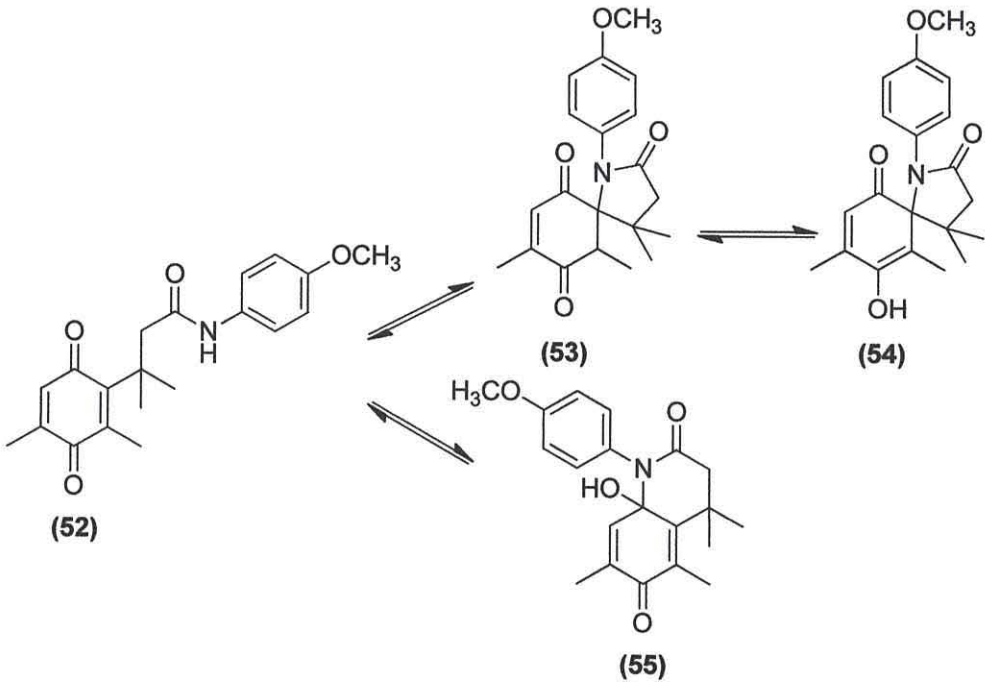

Scheme 13. Degradation of amide prodrug in aqueous solution

The formation of these lactams **53-55** highlights a problem with these reactions if they are to be used in prodrug therapy since they are unable to release the attached drug entity.

4.2.3 Liu *et al.*

In 1996, Liu *et al.*,[116] hoping to understand the reasons behind the formation of these spiro compounds further, prepared **56** and **57** (Figure 11), using the synthetic method described by Borchardt and Cohen.[105]

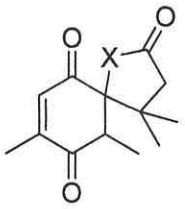

(56) X = O
(57) X = NR

Figure 11. Potential products of degradation

By structural analysis of the X-ray crystallisation data of **56** they concluded that a spirocyclisation reaction releases more steric congestion caused by the trimethyl lock than the normal lactonisation route. However, Liu *et al.*[116] also discovered that it only occurs readily under certain conditions and is susceptible to change by factors such as pH.

4.3 General redox benzoquinone drug delivery system

The release of a drug entity from this benzoquinone system has been represented by these numerous studies and is the basis for this research. Reduction of the key part of the structure **50**, the quinone centre by hNQO1 to the hydroquinone **51** results in cyclisation to form the lactone **44** which is non-toxic to cells[117] and the active drug (Scheme 14).

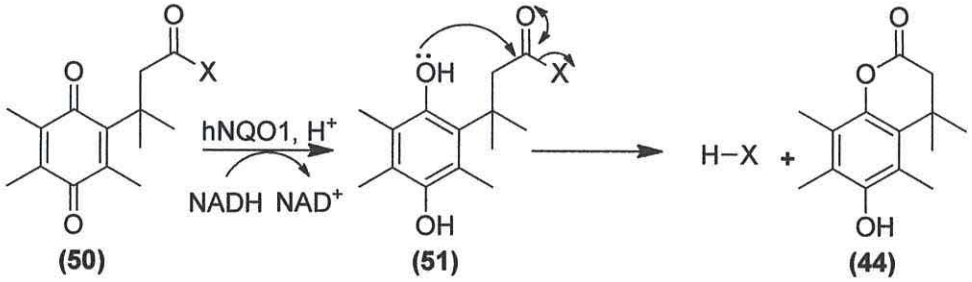

Scheme 14. General mechanism of benzoquinone drug delivery system

Since hNQO1 is overexpressed in hypoxic tumour tissues it is hoped that the drug will be selectively activated in these regions. However, it is also present in many normal cells including the kidneys, bone marrow and endothelial cells as well as stomach and bronchial epithelia. This redox benzoquinone drug delivery system was designed to improve the therapeutic index of a given compound and does not release the drug without reduction by a quinone-based 'trigger', the hydroquinone **51**. This increase in selectivity reduces toxicity and therefore the side effects.[73] Research has also been carried out developing

protease,[1] esterase[10, 11, 111, 118-122] and phosphatase[111, 123] activated prodrugs. However, this thesis will be focused on redox-activated delivery systems only. Although many different functional groups have been investigated our interest lies with mustard and guanidines as the X/drug substituents and these will be discussed in the following sections.

5.0 Nitrogen containing mustards

5.1 Introduction

Nitrogen mustards **58** were first introduced back in 1942 and are analogues of the sulfur mustard gas **59** which was implemented as a weapon in World War I (Figure 12).[124]

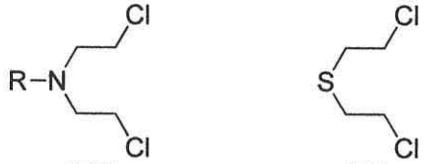

Figure 12. Structures of nitrogen and sulfur mustards

These mustards are DNA alkylating agents often used in chemotherapy[125] (Scheme 15).[126] Since chlorine is a good leaving group this facilitates nucleophilic attack of the nitrogen in the mustard **58**[127] which cyclises to form an aziridinium ion **61**.[125] This strained three-membered ring system readily alkylates preferentially at the N^7 position of guanine **60** to form the monoalkylation adduct **62**.[127] Minor alkylations can also occur at other sites such as the N^3 position of adenine.[125, 128] This process is then repeated with the cyclisation of the adduct **62** to form the aziridinium ion **63** which alkylates guanine **60** to give the crosslinked DNA **64**. These bifunctional adducts can generate an interstrand crosslink which is as much as 100 fold more cytotoxic than its monofunctional adduct.[129]

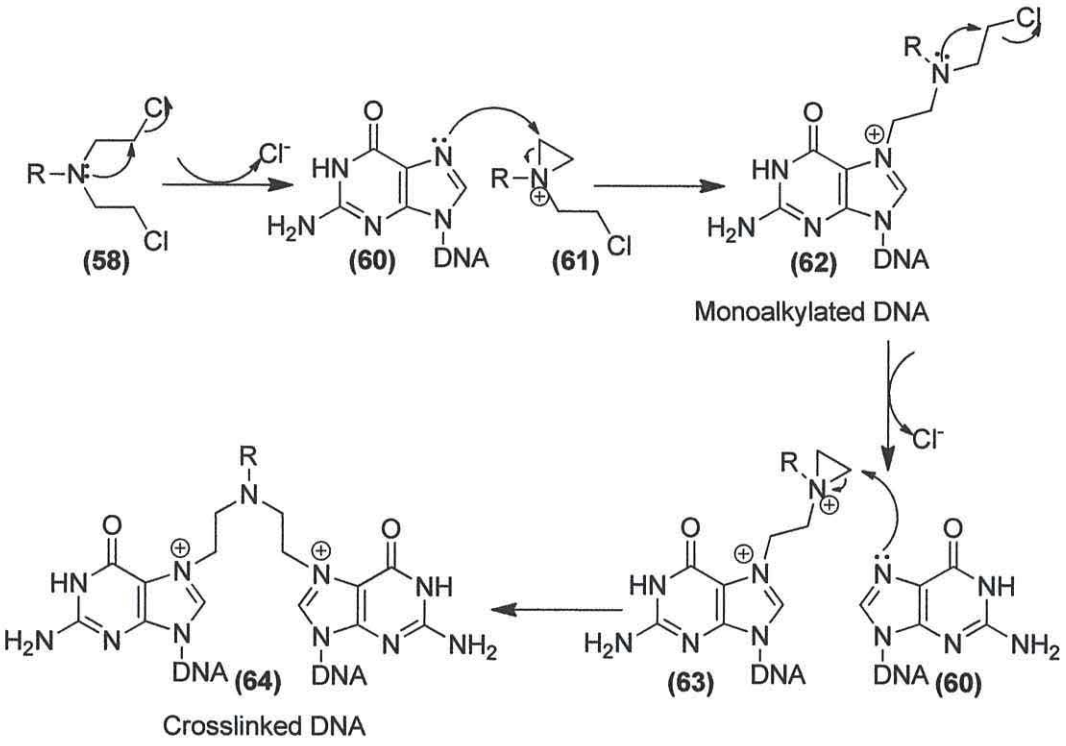

Scheme 15. Mechanism of DNA alkylation and interstrand crosslinking by nitrogen mustards

Crosslinking can occur between two complementary strands of DNA (interstrand) or on the same strand of DNA (intrastrand) (Figure 13).[127]

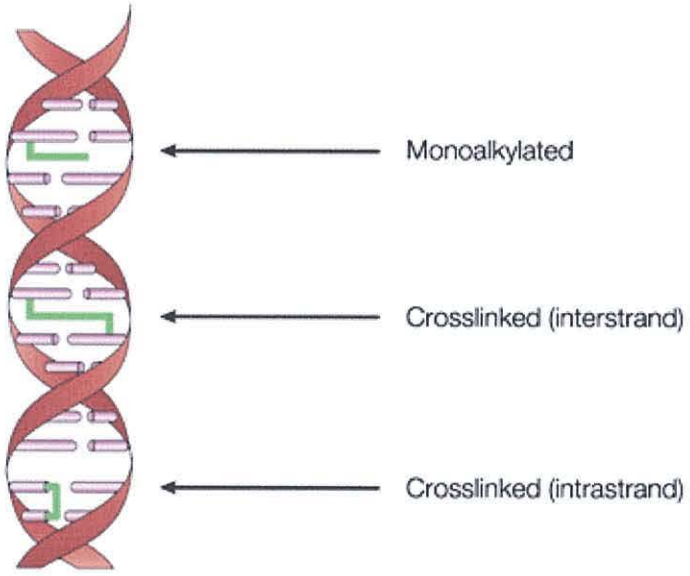

Figure 13. Types of DNA crosslinking

Interstrand crosslinks are essential for maximal cell killing[129] since they prevent two opposing strands in DNA from separating during replication or transcription. The end

result is inhibition of DNA synthesis. There has been found to be direct correlation between interstrand crosslinking and cytotoxicity.[130]

5.2 Examples of nitrogen mustards

The simplest member of the nitrogen mustard family is mechlorethamine **65** (Figure 14)[130, 131] which was the first clinically useful anti-tumour substance.[130]

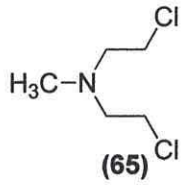

(65)

Figure 14. Structure of mechlorethamine

The problem is that mechlorethamine **65** reacts rapidly with biological material and water making it highly vesicant and chemically labile. To overcome these problems, the methyl group in **65** was replaced with an aromatic ring (Figure 15). This lowers its reactivity, to give more time for absorption and distribution before DNA alkylation allowing oral administration. However, the simplest aromatic mustard **66** is insoluble in water. Although its carboxylic acid analogue **67** is soluble, it is inactive.[126] To overcome this solubility issue a considerable amount of research has been carried out developing more water-soluble *N*-mustards.[132, 133] It was found that addition of CH_2 groups as spacers gave water-soluble active compounds such as chlorambucil **68** and melphalan **69** (Figure 15).[126]

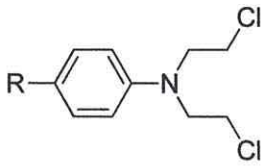

(66) R = H
(67) R = COOH
(68) R = $(CH_2)_3COOH$
(69) R = CH_2CHNH_2COOH

Figure 15. Structures of some aromatic nitrogen mustards

For over 50 years chlorambucil **68** has been used in the treatment of chronic lympocytic leukaemia.[134, 135] Melphalan **69** is used in certain types of bone marrow tumours, including multiple myeloma[136] and cancers such as ovarian, breast[137] and colorectal.[138, 139]

5.3 Strategies to improve the biological potential of mustards

Mustard compounds have a number of drawbacks for chemotherapy.[140] Their high reactivity means that they are chemically unstable.[141] This lowers their therapeutic efficacy since they react with other cellular components, such as proteins, inducing severe side effects.[142] One strategy has been to design and synthesise DNA-directed alkylating agents by linking the *N*-mustard residue to DNA-affinic molecules such as acridines **70**[143-145], 9-anilinoacridines **71**,[140-142, 145-147] quinolines **72**[148-150] or quinazolines **73**[151] (Figure 16).

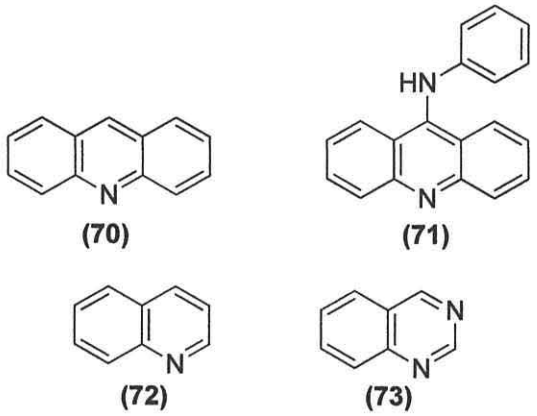

Figure 16. Structure of acridine, 9-anilinoacridine, quinoline and quinazoline

These conjugates have exhibited higher cytotoxicity and potency than their corresponding untargeted *N*-mustard derivatives.[142] The 9-anilinoacridine **74** (Figure 17) was found to possess potent therapeutic efficacy against human xenografts *in vivo* and has the capability to induce DNA interstrand crosslinking in tumour cells.[140, 149]

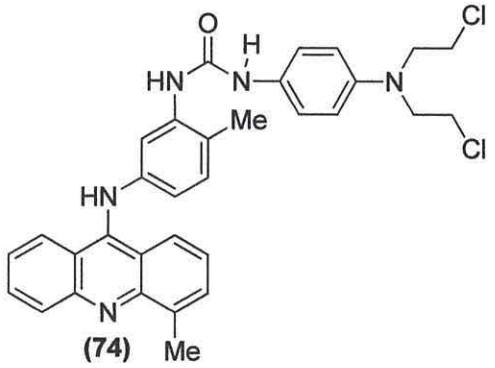

Figure 17. Structure of 9-anilinoacridine conjugate

Another strategy to minimise side effects is to prepare prodrugs of nitrogen mustards,[152-158] which can be activated selectively at the tumour site after enzymatic hydrolysis. Previous researchers[159] synthesised a methyl ester of melphalan attached *via* an amide linker to the quinone containing a trimethyl lock to give the prodrug **75**[117] (Figure 18).[160]

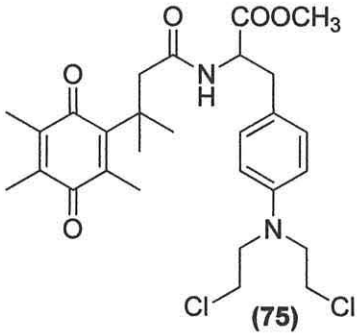

Figure 18. Structure of methyl ester of melphalan attached to a benzoquinone delivery system

This system was investigated as a method of increasing the oral absorption of the methyl ester melphalan across the intestine. The uptake, accumulation, activation and transport of the prodrug **75** was determined using Caco-2 cell monolayers and results showed potential for improving intestinal drug delivery.[161]

5.4 Volpato *et al.*

Another cytotoxic aromatic mustard studied is N^1,N^1-*bis*(2-chloroethyl)benzene-1,4-diamine **76** (Figure 19).[162]

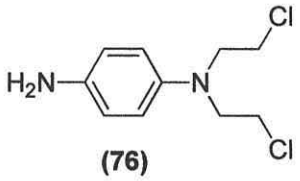

Figure 19. Structure of aniline mustard

In 2007 Volpato *et al.*[73] prepared a prodrug **78** using this aniline mustard **76** (Scheme 16). 2,3,5-trimethyl-1,4-hydroquinone **77** was reacted with methyl 3,3-dimethylacrylate and methanesulfonic acid to give the lactone **44** in 83% yield. This was stirred with NBS to give the carboxylic acid **45** in 97% yield and then with *N*-hydroxysuccinimide (NHS) and dicyclohexylcarbodiimide (DCC) to give the ester **50b** in 93% yield. In the final step, this precursor is treated with **76** to afford the mustard prodrug **78** in 57% yield.

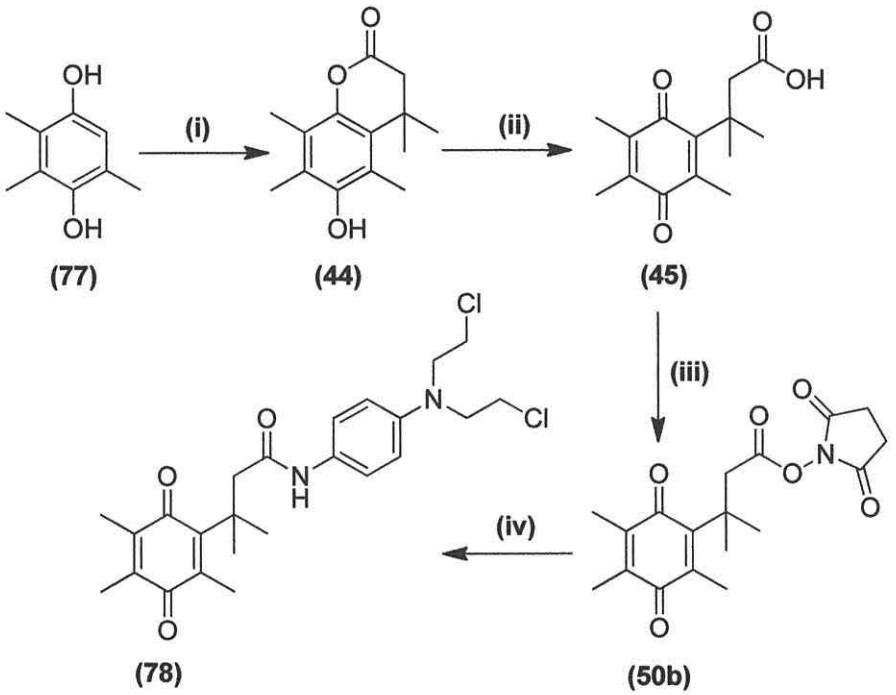

Scheme 16. (i) 1.2 equiv. methyl 3,3-dimethylacrylate, CH_3SO_3H, 70 °C, 3 h (ii) 1.4 equiv. NBS, acetonitrile/H_2O, r.t, >1.5 h (iii) 1.2 equiv. DCC, 1.1 equiv. NHS, THF, 0 °C then r.t, 20 h (iv) 3.8 equiv. *N*^{1},*N*^{1}-*bis*(2-chloroethyl)benzene-1,4-diamine, THF, N_2, dark, r.t, 72 h

The aim of their study was to provide mechanistic proof that the aniline mustard prodrug **78** could be reduced by hNQO1 to release an active therapeutic drug *via* the benzoquinone drug delivery system (Scheme 14, p.17). Using HPLC to monitor the progress of the reaction, the quinone **78** was reduced by hNQO1 to give the unstable hydroquinone **79** (Scheme 17). This intermediate **79** then underwent spontaneous cyclisation to form the non-toxic lactone **44** and free aniline mustard drug **76**. Volpato *et al.*[73] also reported the formation of an unwanted spirolactam compound **80** from aqueous degradation. This type of by-product has been previously reported[108] and is very problematic for drug systems since it prevents release of the active drug.

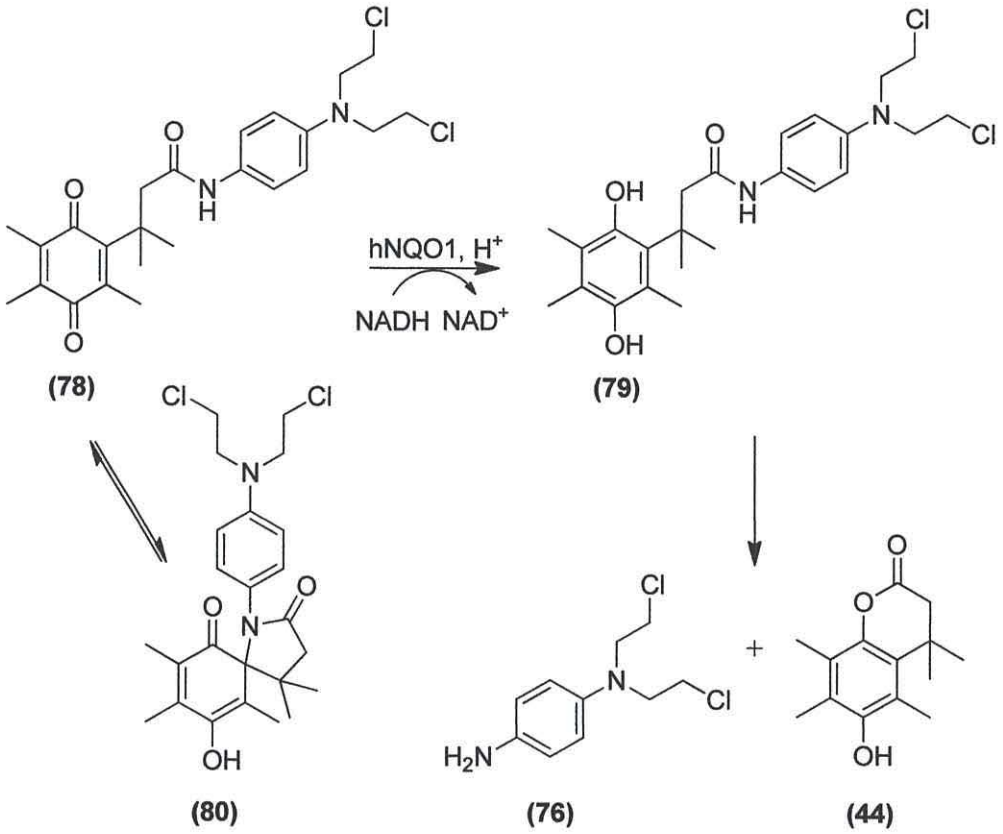

Scheme 17. Aniline mustard benzoquinone drug delivery system

Chemosensitivity studies also found the prodrug **78** to be selectively toxic to cells that overexpress hNQO1 under aerobic conditions. Further analysis also showed the presence of elevated interstrand crosslinks in hNQO1-rich compared to hNQO1-deficient cells. With this model quinone drug delivery system now proven to be effective and the release mechanism established, more potential candidates need to be prepared for future work.

6.0 Guanidine

6.1 Introduction

Guanidine **81** is a colourless crystalline solid readily soluble in both water and alcohol (Figure 20).

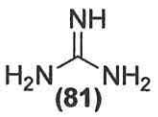

Figure 20. Structure of guanidine

An interesting property of guanidine **81** is that it is one of the strongest organic bases known with a pK_a of 13.6.[163] As a free base it is highly hygroscopic and lacks stability. However, protonation of guanidine **81** gives rise to a highly stable guanidinium cation **82** (Figure 21).[164]

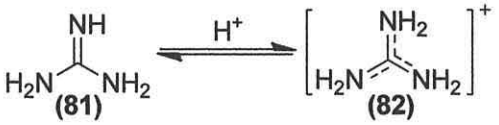

Figure 21. Formation of guanidinium ion

This stability can be attributed to delocalisation of the positive charge over the three nitrogen atoms represented by the resonance forms **83**, **84** and **85** (Figure 22).[165]

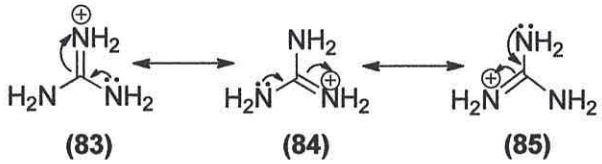

Figure 22. Equilibria of cationic resonance forms of guanidine

Guanidine **81** was first synthesised by Strecker[166] in 1861 by the degradation of aromatic natural product guanine **86** using hydrochloric acid and potassium chloride (Scheme 18).

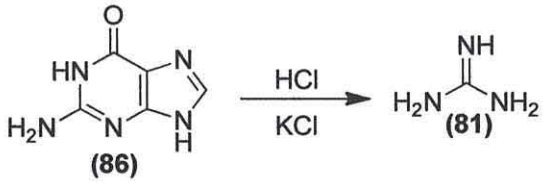

Scheme 18. Formation of guanidine **81** from guanine **86**

Despite its simplicity, the first single-crystal structure determination of the free base guanidine was first described 148 years later in 2009 by Yamada *et al.*[167] (Figure 23).

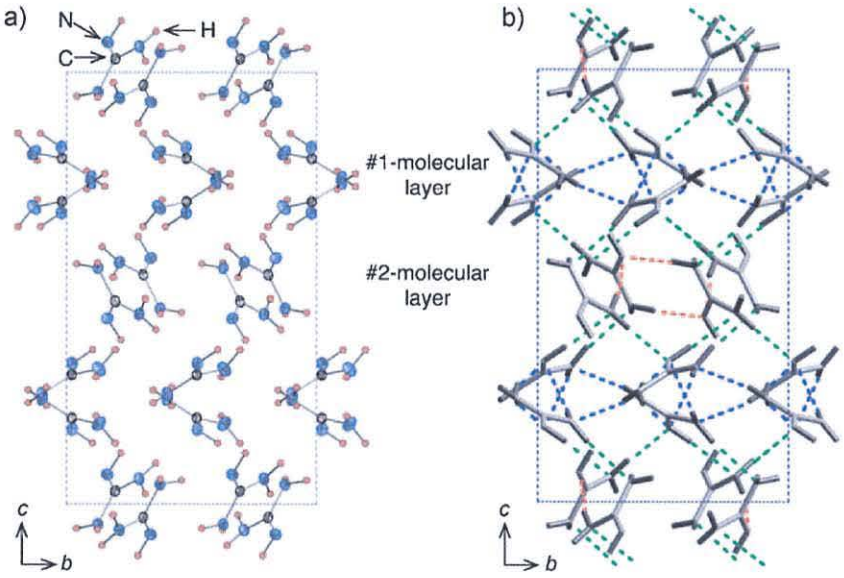

Figure 23. (a)-(b) Crystal structure of guanidine at 100 K with (b) highlighting the network of hydrogen-bonding

6.2. Guanidine in natural products

The guanidine moiety is of particular interest since it is incorporated into many biologically active natural products. It is a substructure of many important molecules such as arginine **87** (Figure 24),[168] one of the 20 common amino acids.

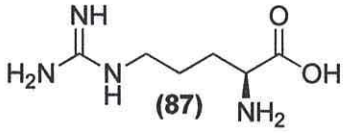

Figure 24. Structure of arginine

Arginine **87** was first isolated by Schultze and Steiger[169, 170] in 1886 from a lupin seedling extract. The presence of guanidine **81** results in it being positively charged over a wide pH range, existing as one of three zwitterionic forms **88**, **89** or **90** (Figure 25).

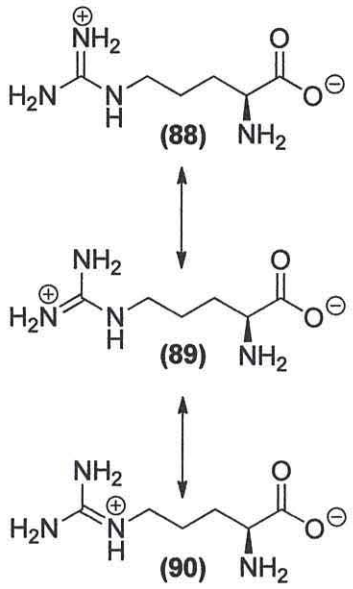

Figure 25. Zwitterionic forms of arginine

The presence of the guanidinium ion on the side chain of arginine **87** is ubiquitous in the active site of many enzymes that bind anionic substrates and is involved with stabilising protein tertiary structures.[171]

Guanidine is also present in a number of marine natural products such as ptilomycalin A **91** (Figure 26).[172]

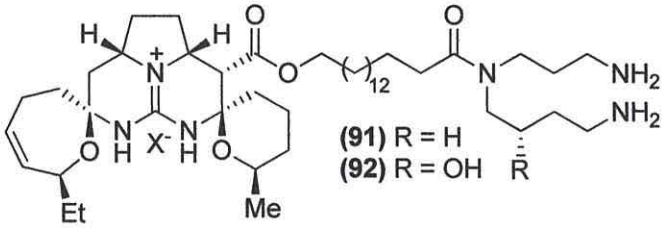

Figure 26. Structure of ptilomycalin A and crambescidin 800

First isolated in 1989[173] from the Caribbean sponge *Ptilocaulis spiculifer* and a red sea sponge of *Hemimycale sp* ptilomycalin A **91** was found to demonstrate high cytotoxic, anti-fungal and anti-viral activity.[174-178] It has since been discovered in the red Caribbean sponge *Batzella sp.* and starfishes *Fromia monilis* and *Celerina heffernani.*[176] Another series of related compounds with similar biological activity are the crambescidins, represented by crambescidin 800 **92** (Figure 26).[179, 180] These alkaloids were originally isolated in 1991[181] from the bright red sponge *Crambe crambe* along the Mediterranean

coast.[182-185] Both ptilomycalin A **91** and the crambescidins (e.g **92**) are characterised by a unique pentacyclic guanidine core.[174, 182, 186]

Another series of interesting polycyclic guanidine compounds, isolated from the red Caribbean sponge *Batzella sp.*[187, 188] (later found to be the same species as *Ptilocaulis spiculifer*)[187] were the batzelladine alkaloids represented by A-I **93-101** (Figure 27 and 28).[189] Patil, Faulkner and co-workers reported the isolation of batzelladines A-E **93-97** in 1995[187] and batzelladines F-I **98-101** in 1997.[188] This was followed by batzelladine J in 2005 by Gallimore *et al.*[190] and batzelladines K-N in 2007 by Hua *et al.*[191] isolated from the Caribbean sponge *Monanchora unguifera.*

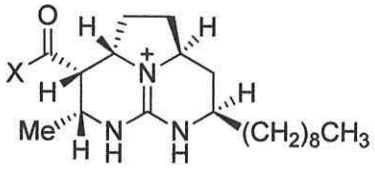

(93) X = R^2 Batzelladine A
(96) X = R^1 Batzelladine D
(99) X = R^4 Batzelladine G

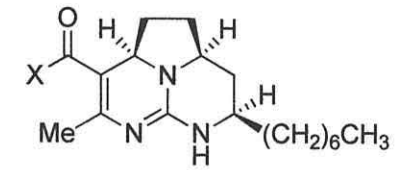

(94) X= R^2 Batzelladine B

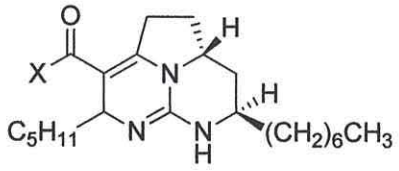

(95) X = R^1 Batzelladine C

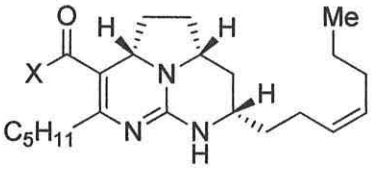

(97) X = R^1 Batzelladine E

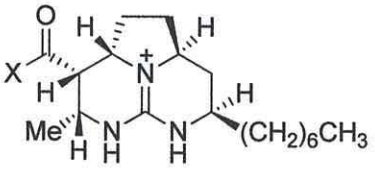

(98) X = R^3 Batzelladine F

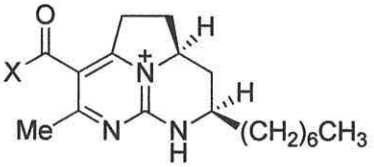

(100) X = R^5 Batzelladine H
(101) X = R^6 Batzelladine I

Figure 27. Structures of the batzelladine alkaloids A – I

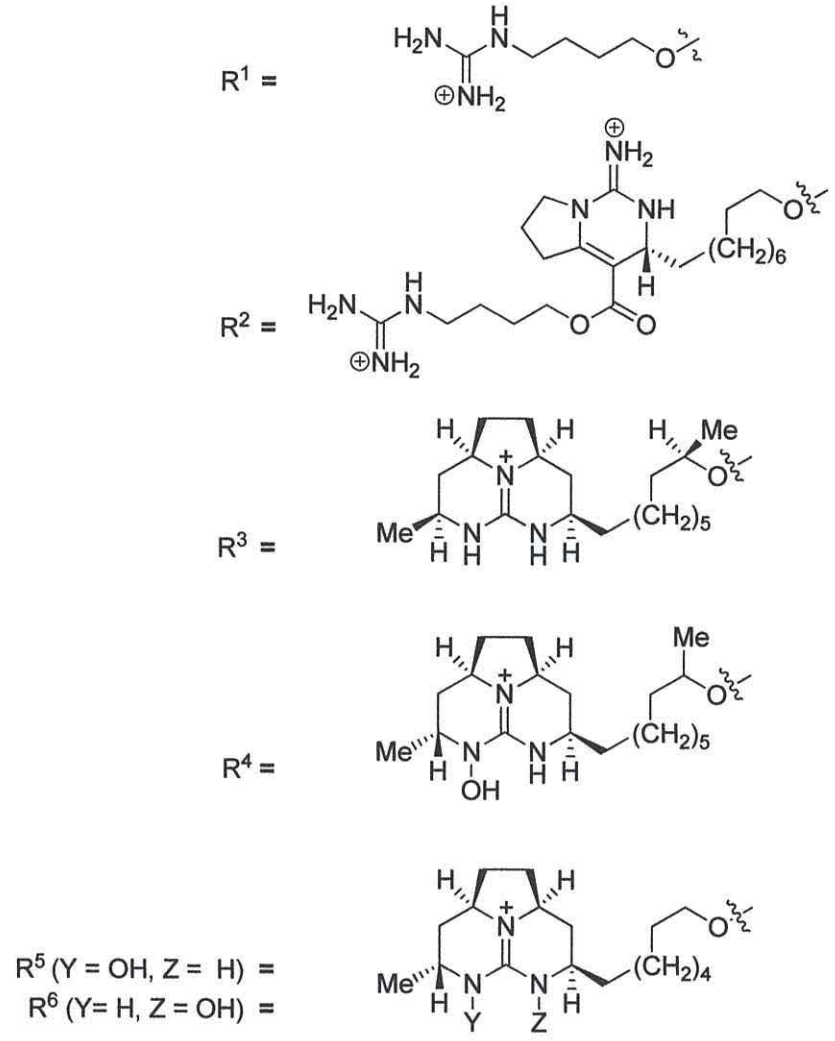

Figure 28. R groups of the batzelladine alkaloids A – I

All batzelladine alkaloids contain at least one stereochemically rich, fused tricyclic guanidine moiety.[179, 189, 192] Batzelladines A **93** and B **94** are micromolar inhibitors of binding of the HIV envelope gp120 to the human CD4 cell surface receptor protein on T-cells.[176, 187, 193] This means they have great potential for AIDS therapy.[176, 194] Batzelladines F-I **98-101** have shown high levels of activity in the dissociation of the protein tyrosine kinase $p56^{ick}$ from its complex with CD4.[172, 188, 189, 194] Compounds which prevent this binding have potential in the treatment of autoimmune diseases[188, 194, 195] such as murine lupus[188] and in allograft rejection.[188, 194] They also have the potential for powerful anti-cancer activity[196] and are important for immunological responses.[193, 197] Since their discovery they have attracted considerable interest from both a synthetic and biological perspective.[198, 199] A total synthesis of batzelladine E **97** was achieved in 1998 by Snider and Chen,[200] batzelladine D **96** in 1999[193] by Cohen *et al.*, batzelladine F **98** in 2001 by

Cohen and Overman[195] and batzelladine A **93** in 2004 by Shimokawa *et al.*[201] Since then a number of analogues have been synthesised and tested by the Murphy group in an attempt to increase biological activity over the natural batzaelladine alkaloids.[202-206]

Another example of a guanidine natural product is the alkaloid nitensidine E **102** (Figure 29), isolated in 2009 by Regasini *et al,*[207] from the leaves of *Pterogyne nitens*, a native tree common in South America. This compound was found to exhibit cytotoxicity for human myeloblastic leukemia and human glioblastoma cells.

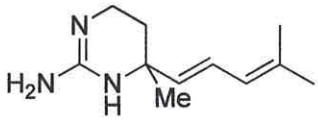

(102)

Figure 29. Structure of nitensidine E

Research has been carried out on guanidines as potential prodrugs for their role as anti-cancer agents,[208] however, they have not been explored using the benzoquinone drug delivery system. Other uses of guanidines include anti-protozoal agents[209, 210] and first-line treatment for type II diabetes.[211]

6.3 Synthetic routes to guanidines

Over the years many different strategies have been employed for the synthesis of guanidines.[212] The problem is that they are electron rich and strongly basic. Consequently many syntheses give protected products such as non-polar electron-withdrawing groups which are easily removed.[213] Their general synthesis has been outlined in Scheme 19 (adapted from[214]).

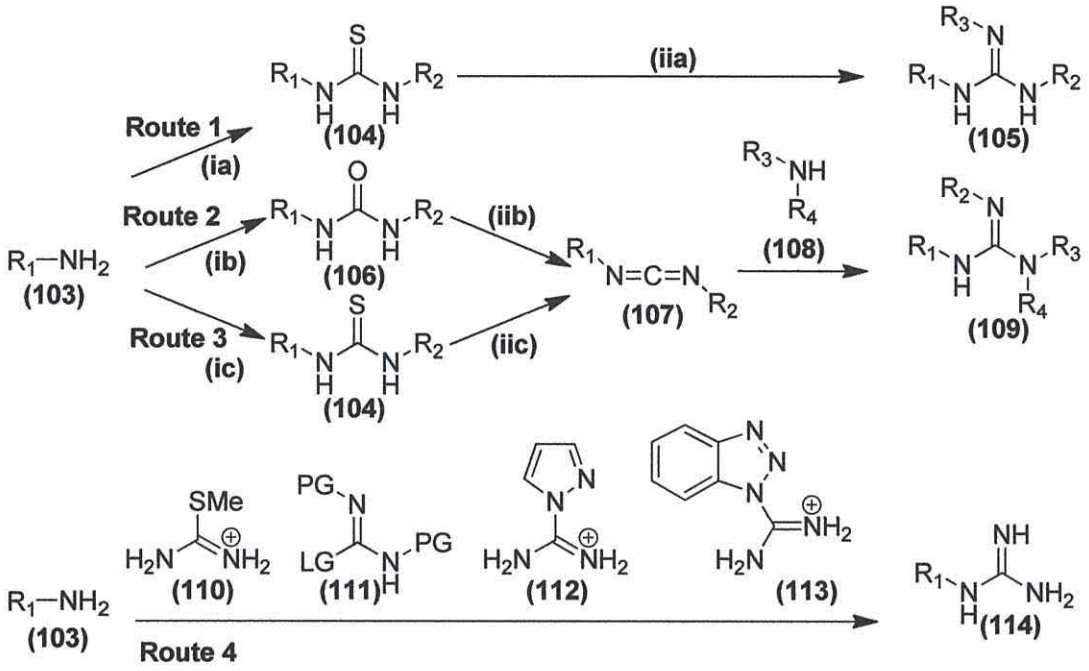

Scheme 19. (ia) R_2NCS (iia) S-alkylation then R_3NH_2 (ib) R_2NCO (iib) Br_2, PPh_3, Et_3N (ic) CS_2 then R_2NH_2 (iic) DIAD, PPh_3

All of these routes start with a primary amine **103**. Di-, tri- or tetrasubstituted acyclic guanidines are normally prepared through a thiourea **104** (Scheme 19, Route 1 or 3) or a urea **106** intermediate (Route 2) to give **105** or **109** respectively. Routes 2 and 3 also involve the formation of a carbodiimide **107**,[214] which can be reacted with primary or secondary amines, the reaction of which has been found to be catalysed by rare earth metal complexes.[215] Other reagents have also been used to synthesise guanidines including S-methylisothiourea **110**, protected guanidine **111** pyrazole-1-carboxamidine **112** and benzotriazole-1-carboxamidine **113** derivatives (Route 4) to give **114**. Monocyclic guanidines may also be prepared by application of routes 1-3.[214] Polysubstituted guanidines have more recently been found to be prepared by a bismuth-promoted synthesis using primary/secondary amines.[216]

In 2001 Orner and Hamilton[213] investigated the synthesis of a number of guanidines **117** from amines of varying reactivity **a** to **g** using ethoxycarbonyl isothiocyanate **115**, which proceed *via* the thiourea intermediates **116a-g** (Scheme 20).

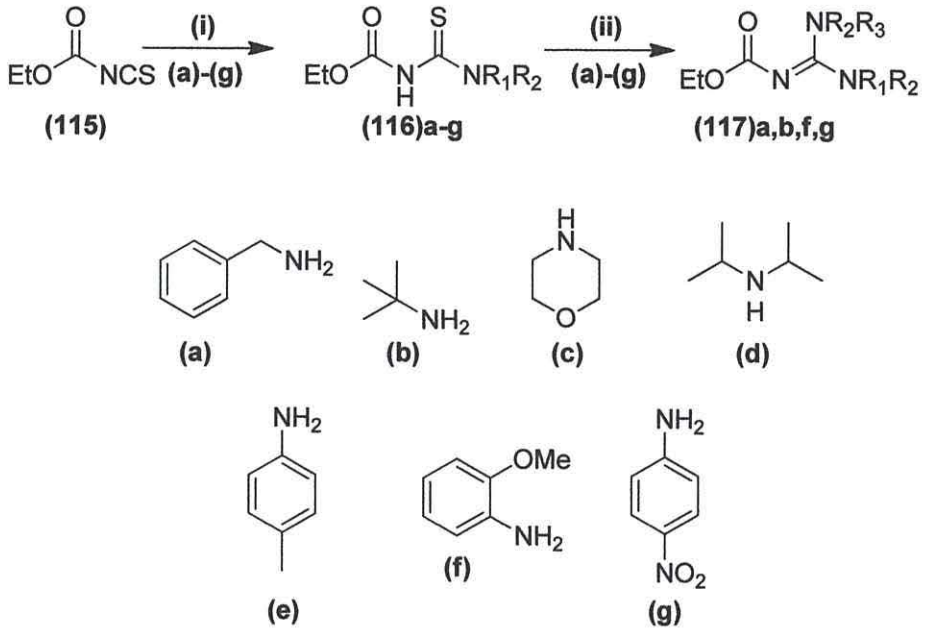

Scheme 20. (i) CH_2Cl_2/THF (ii) EDCI, CH_2Cl_2

The % yields of these reactions are summarised in Table 3.

Amine	% Yield of thiourea 116	% Yield of guanidine 117						
		a	b	c	d	e	f	g
a	99	99	99	95	76	92	82	85
b	99	99	74	59	55	99	99	65
c	99	0	0	0	0	0	0	0
d	99	0	0	0	0	0	0	0
e	92	99	87	99	81	95	97	34
f	77	96	99	61	84	98	67	39
g	72	85	76	99	42	35	34	0

Table 3. Synthesis of protected thioureas **116a-g** and guanidines **117a-g**

The results showed that thioureas derived from secondary amines **c** and **d** failed to form any detectable guanidine product. This highlights the steric limitations of these guanidines and poses a potential starting point for this thesis.

7.0 Aims

The aim of this project is to explore the prodrug benzoquinone delivery system (Scheme 21) which is able to deliver drugs *via* a reductive pathway. Our intention is to investigate release of aniline mustards and guanidines from this system and to assess the rate and efficiency of release as well as their capability as anti-cancer agents. The extensive medicinal properties of these compounds were discussed in the previous two sections.

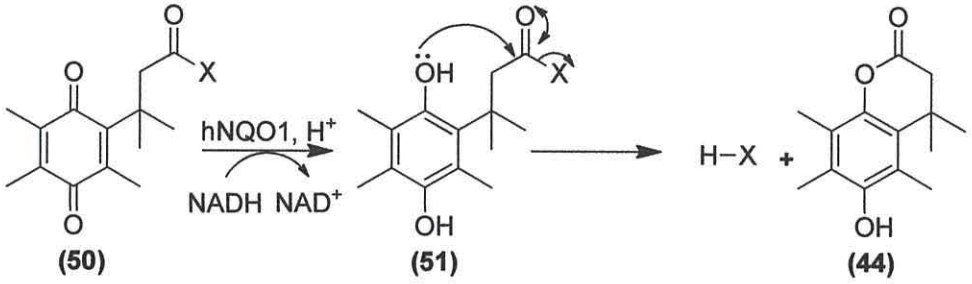

X = substituent/drug

Scheme 21. General mechanism of trimethyl-locked benzoquinone drug delivery system

Volpato *et al.*[73] have already proven this system to be effective for the release of an aniline mustard prodrug (Scheme 17, p.24). However, it is intended to determine if guanidines can also be substrates for hNQO1 following the same mechanistic pathway. This will begin by substituting some simple guanidines as X substituents. Synthesis of these compounds can be achieved by using the methodology described by Volpato *et al.*[73] (Scheme 22).

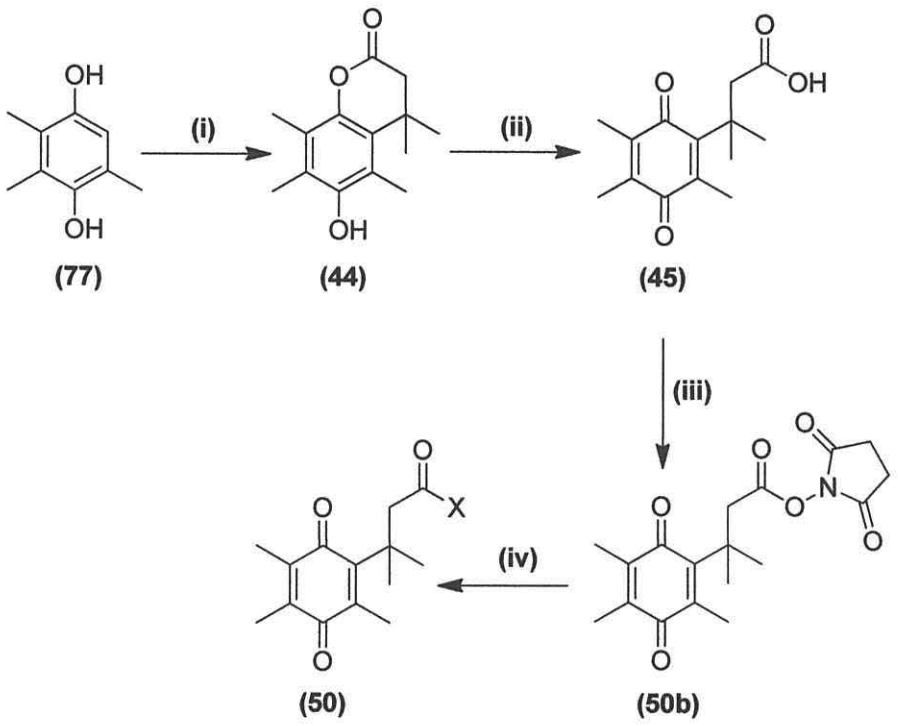

Scheme 22. (i) 1.2 equiv. methyl 3,3-dimethylacrylate, CH_3SO_3H, 70 °C, 3 h (ii) 1.4 equiv. NBS, acetonitrile/H_2O, r.t, >1.5 h (iii) 1.2 equiv. DCC, 1.1 equiv. NHS, THF, 0 °C then r.t, 20 h (iv) 3.8 equiv. X, THF, N_2, dark, r.t, 72 h

The limitations of forming guanidines from thioureas due to steric factors is well known in the literature (lit.).[213] It is hoped that by using the above substitution reaction using the ester precursor **50b** these problems can be avoided.

The second aim of this project is to determine the effect, if any, of replacing the two *gem*-methyls in structure **50** which behave as a conformational lock, accelerating the formation of the lactone **44** with an aromatic backbone such as that found in **118** (Scheme 23).

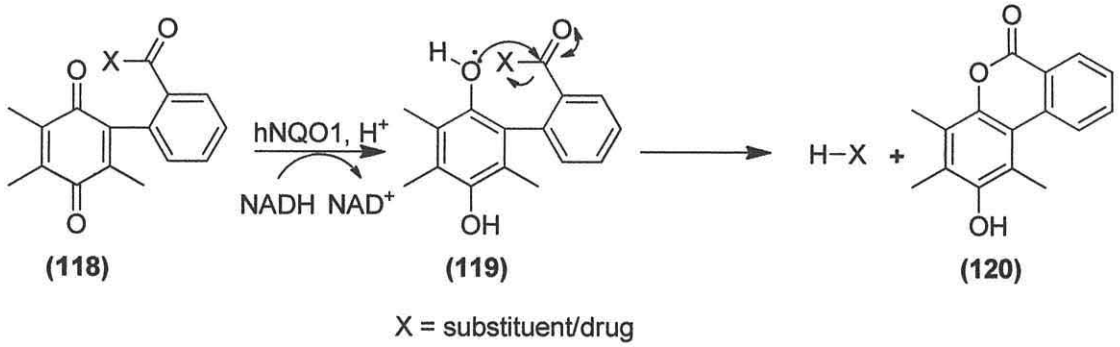

Scheme 23. General mechanism of phenyl benzoquinone drug delivery system

The lactonisation rate of the benzoquinones has been shown to be greatly enhanced by the presence of this trimethyl lock. It has previously been attributed to the close proximity of the three methyl groups leading to severe steric repulsion. It is anticipated that the addition of a phenyl group to the backbone will affect the reaction rate and thus allow the manipulation of the release rate of drugs as desired. The rate of release for the original trimethyl-locked and phenyl quinone backbones will then be compared.

Results and Discussion

8.0 Molecular modelling

8.1 Introduction

As previously discussed the main aim of this project was to investigate the efficiency of release of aniline mustards and guanidine substituents from the redox-actived benzoquinone delivery systems presented in scheme 24A (trimethyl lock system) and 24B (phenyl system) below.

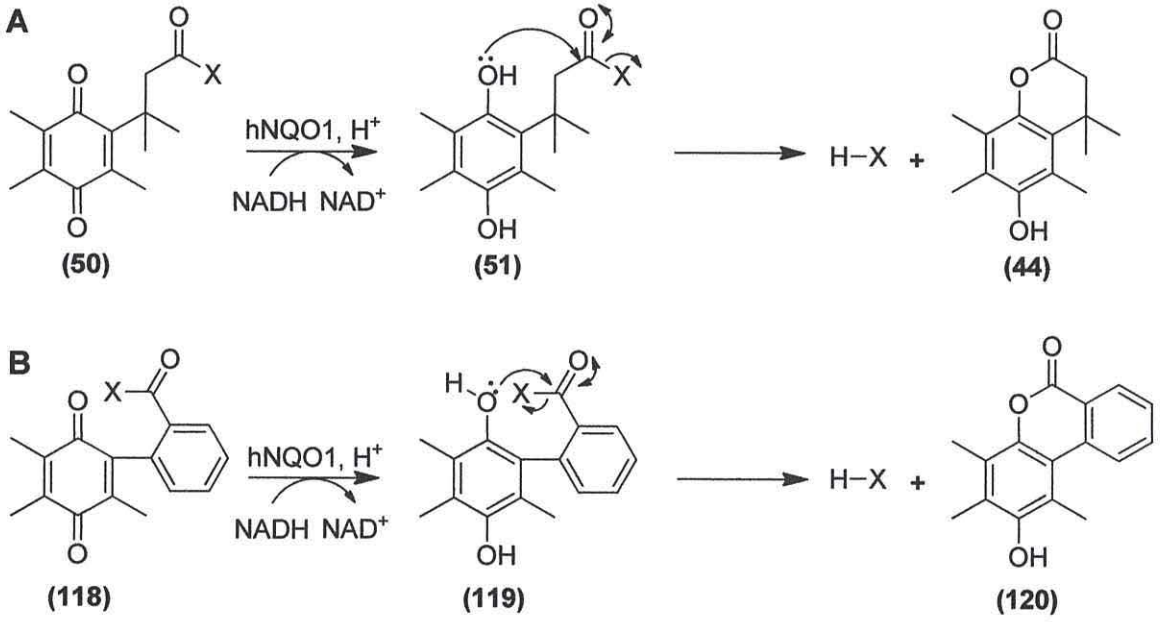

X = guanidine/aniline mustard substituent

Scheme 24. General mechanism of (A) trimethyl-locked and (B) phenyl benzoquinone drug delivery systems

As shown in scheme 24A and 24B mechanistically, the benzoquinone moieties **50** and **118** can undergo reduction *via* hNQO1 to afford the hydroquinone intermediates **51** and **119**. Due to the close proximity of the *ortho*-OH to the carbonyl group in these hydroquinones they can spontaneously undergo intramolecular cyclisation to release the free aniline/guanidine substituent X. The lactone **44** or **120** is formed as the by-product.

Pre-synthetic predictions using molecular modelling calculations were studied on hydroquinone intermediates utilising tetramethyl, dipiperidine, dimorpholine and aniline

mustard groups as X substituents to ensure that intramolecular cyclisation could occur. This is presented in the following section.

8.2 Hydroquinone cyclisation

8.2.1 Introduction

The intramolecular cyclisation step in scheme 24 was studied to ensure that the reaction could occur resulting in the release of the free substituents (aniline mustard or guanidine). A distance from the O^1 and C^5 of <4 Å is required for intramolecular cyclisation to occur (Figure 30), although it must be noted that these calculations are only a guide.

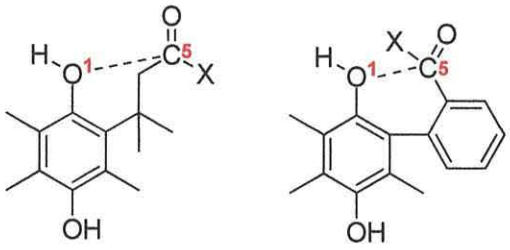

(51) **(119)**

X = guanidine/aniline mustard substituent

Figure 30. Distances (Å) between the *ortho*-O^1H and carbonyl carbon C^5

8.2.2 Determining the distances (Å) using Molegro Molecular Viewer

In order to obtain the distance (Å) from the O^1 to the C^5, 2-dimentional (2D) structures of the hydroquinone intermediates were constructed using ChemBioDraw Ultra 12.0 and saved (.cdx files). The 2D structures were then converted to 3D using Chem3D Pro12.0 and energy minimised with molecular dynamic calculations. These calculations were made using the MM2 minimisation facility which uses gas-phase calculations and ignores intermolecular interactions and many hydrogen-bonds. It is also important to note that the attacking nucleophile may be the phenoxide, and not the phenol, as shown in figure 30 and so this must be considered when viewing this data. The resulting 3D structures were saved (.mol2 files) and viewed using Molegro Molecular Viewer software (version 2.2). The distances (Å) between O^1 and C^5 for all the hydroquinones were measured. With the exception of compound **124**, which recorded a distance of 4.4 Å, all other compounds recorded a distance <4 Å (Figure 31, A, B, C and D). Overall, the data suggested that the hydroquinones can predictably undergo intramolecular cyclisation.

8.2.3 Molecular modelling of hydroquinones

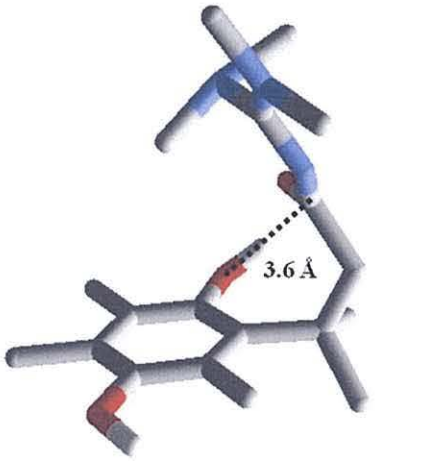

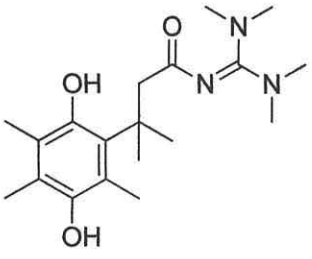

(121)

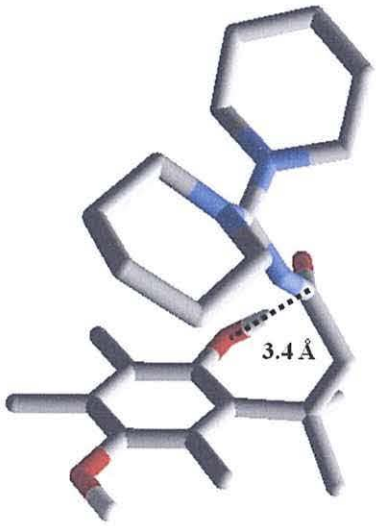

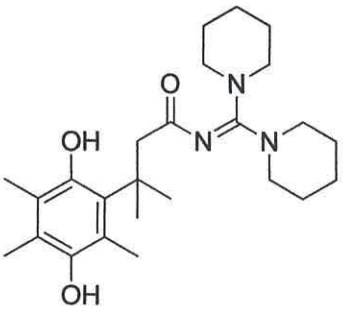

(122)

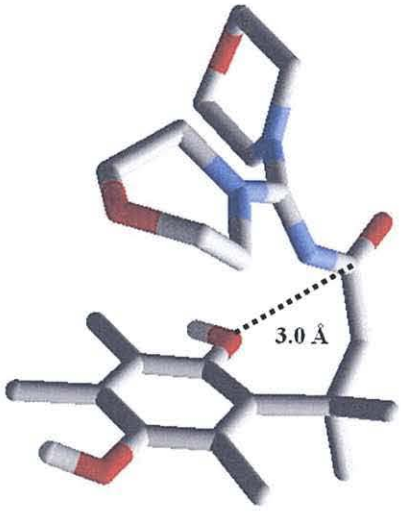

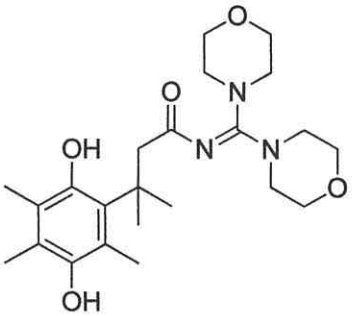

(123)

Figure 31. (A) Molecular modelling of the hydroquinone cyclisation intermediates **121**, **122** and **123**

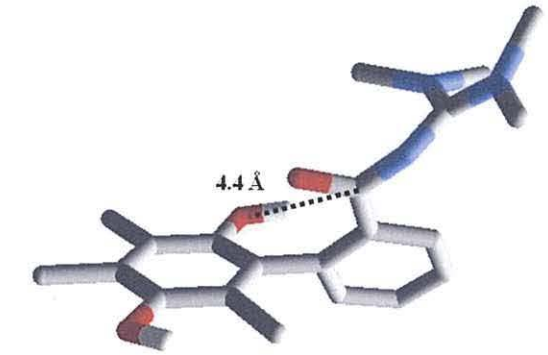

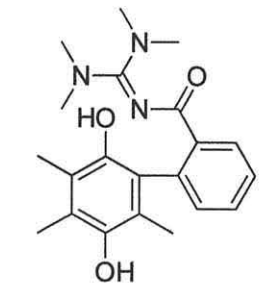

(124)

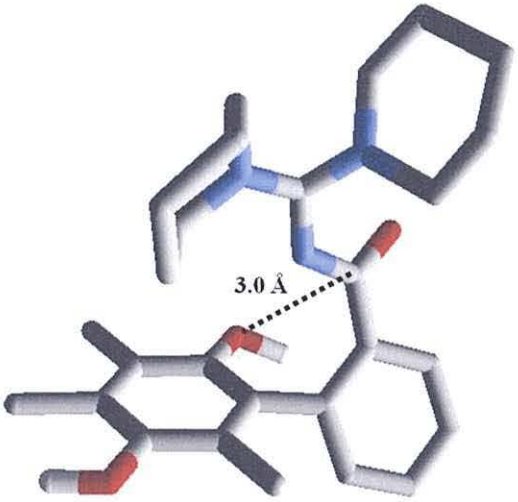

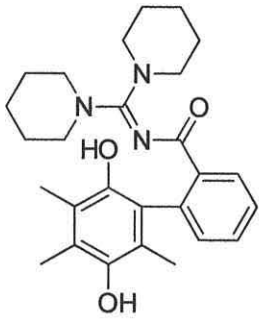

(125)

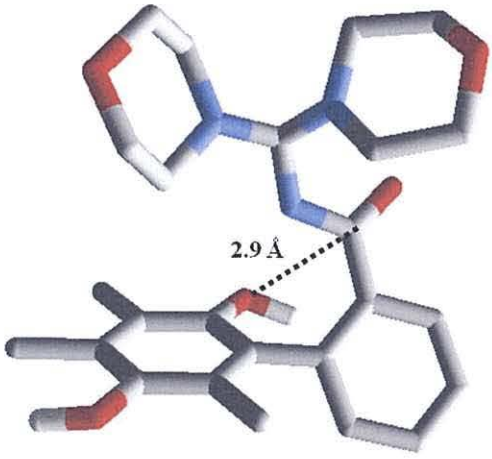

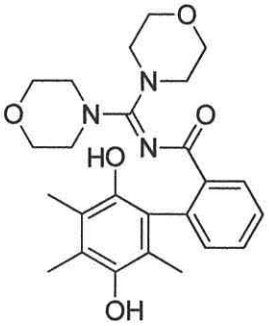

(126)

Figure 31. (B) Molecular modelling of the hydroquinone cyclisation intermediates **124**, **125** and **126**

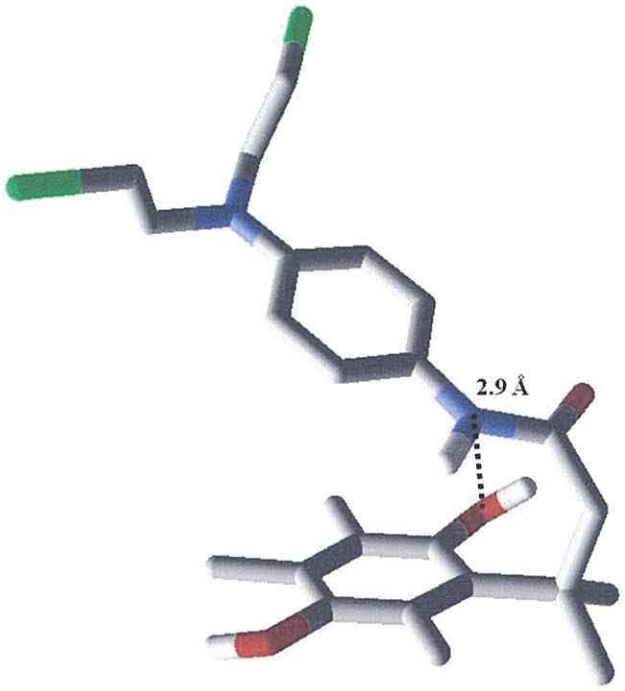

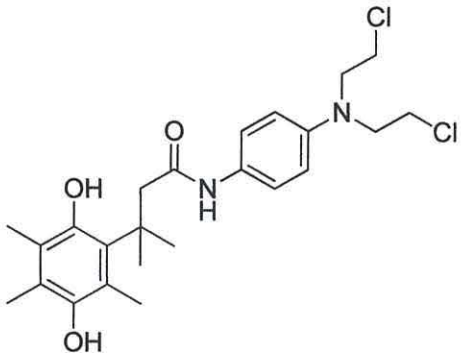

(79)

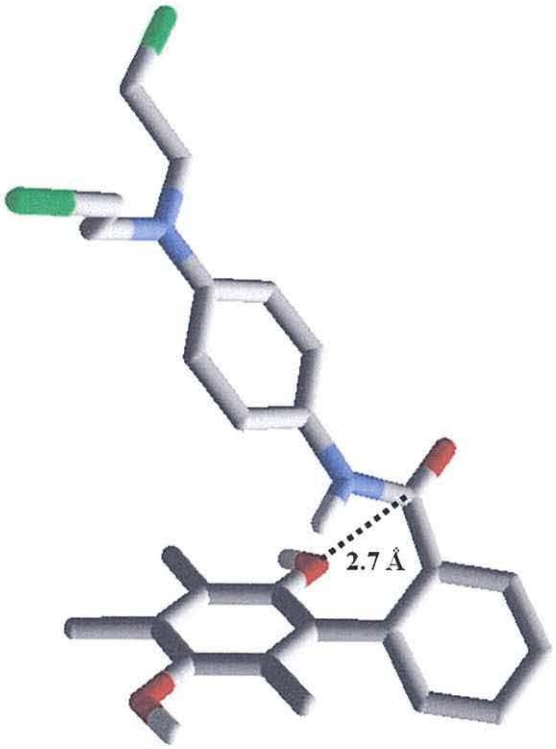

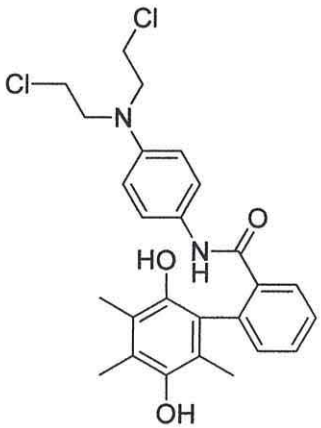

(127)

Figure 31. (C) Molecular modelling of the hydroquinone cyclisation intermediates **79** and **127**

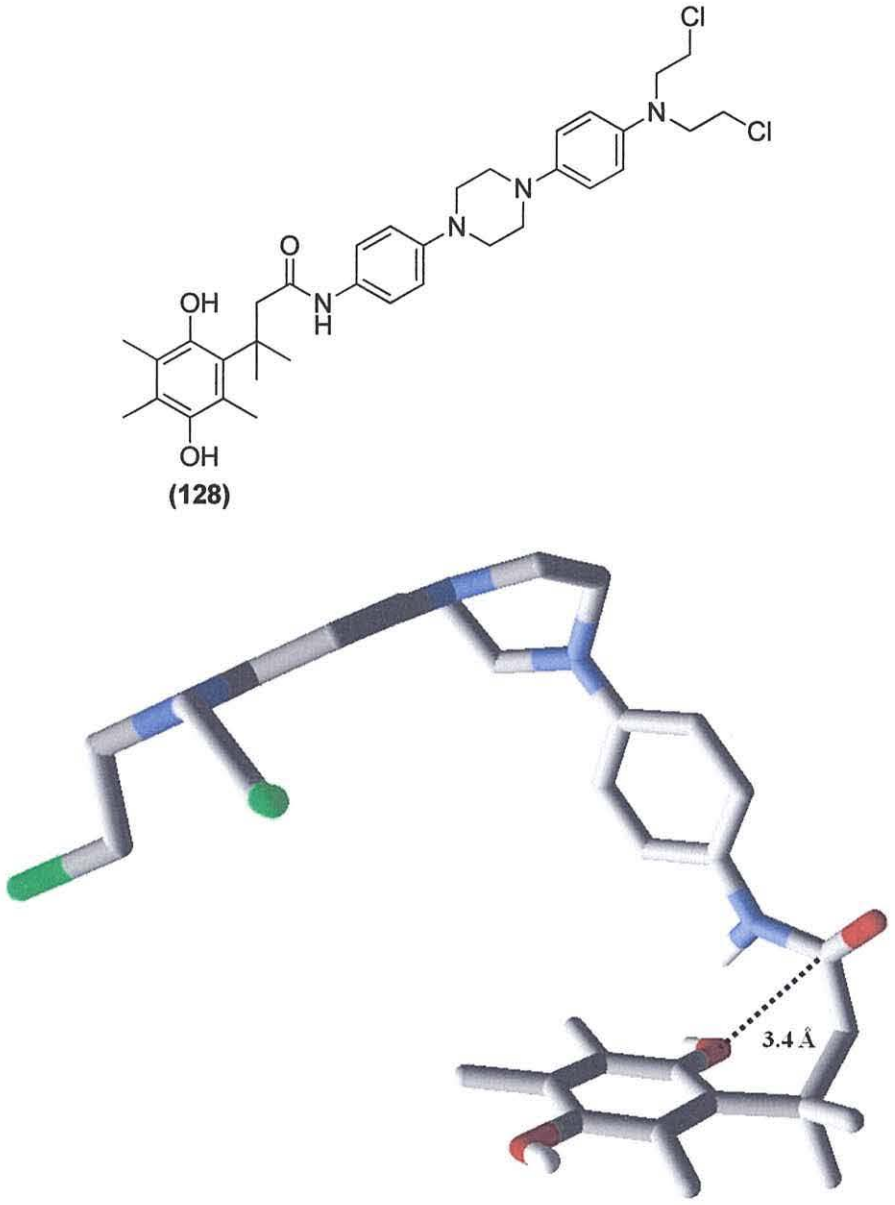

Figure 31. (D) Molecular modelling of the hydroquinone cyclisation intermediate **128**

8.3 Quinone reduction

8.3.1 Introduction

There are several reported mechanisms for the reduction of quinones by hNQO1. This section will concentrate on one of the mechanisms by which the bound reduced cofactor $FADH_2$ **34** donates a hydride to one of the quinone **37**'s carbonyls forming the hydroquinone species **39**. By virtue, the $FADH_2$ **34** is oxidised back to FAD **33** (Scheme 25).[86]

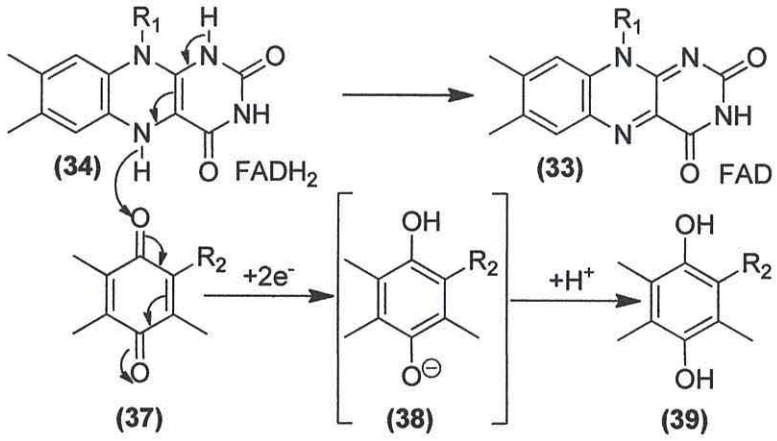

Scheme 25. Proposed mechanism one, hydride transfer from $FADH_2$ to a carbonyl oxygen

8.3.2 Considerations to determine if quinones act as substrates for hNQO1

Unlike the hydroquinone cyclisation there are two main considerations as to whether the quinones will be substrates for hNQO1. The first being the feasibility of the hydride transfer from the bound cofactor $FADH_2$ **34** and the second being the stabilisation and interaction of the ligand (compound) in the active site of the enzyme (protein). Both these considerations are discussed in the following sections.

8.3.2.1 Hydride transfer

(a) Ligand-$FADH_2$ distances (Å)

There are two important distances to consider, those between N^5 in the $FADH_2$ **34** to either O^1 or O^4 of the quinone **37** as shown in figure 32. If the measured distance is <4.0 Å then the hydride transfer reaction is likely to occur.

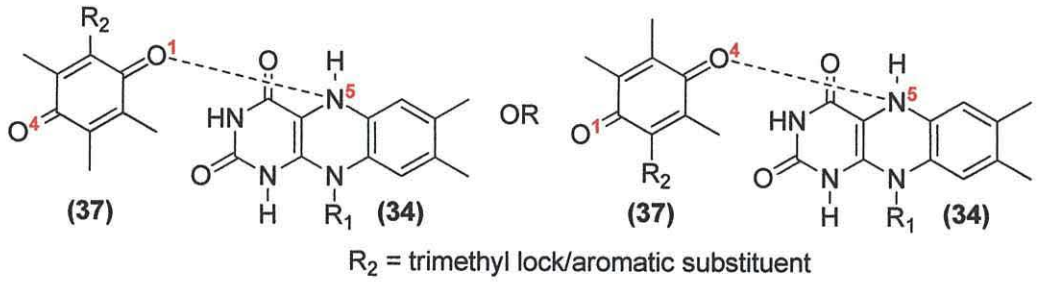

Figure 32. Distances determined between the quinone **37** and $FADH_2$ **34**

8.3.2.2 Other interactions between the substrate and protein

(a) Ligand-$FADH_2$ bonding interactions (Å)

In order for the hydride transfer process to occur the formation of hydrogen-bonds between the substrate **37** and the $FADH_2$ **34** must occur. Measurement of the inter-atomic distance (Å) between the N^5 and N^2 atoms in $FADH_2$ **34** to either O^1 or O^4 of the quinone **37**, acts as a guide to the potential for hydrogen-bonding between the substrate and the co-factor (Figure 33). Obviously closer distances suggests a viable substrate and the possibility of reaction and two possible orientations can be considered in which either O^4 (approach A) or O^1 (approach B) are in close proximity to the N^5 atom in $FADH_2$ **34**.

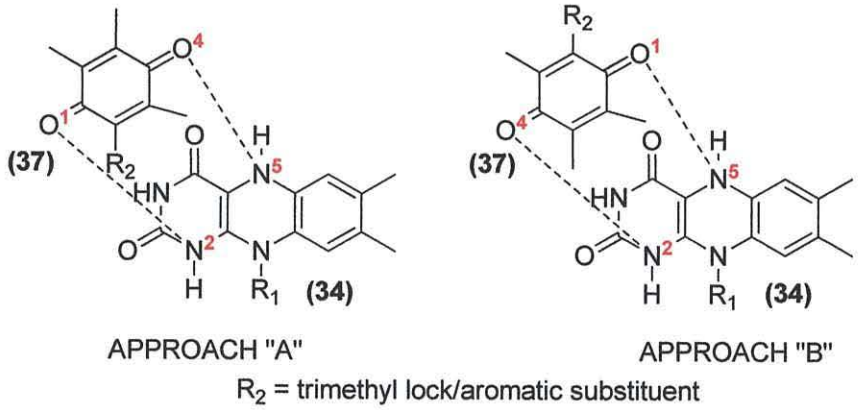

Figure 33. Potential bonding interactions between the quinone **37** and $FADH_2$ **34**

(b) Ligand-protein interactions

Favourable ligand-protein interactions may also occur between either of the quinone oxygens or the side chain R^2 with the amino acid residues of hNQO1. These side chain interactions should be more prevalent in approach A where the side chain R^2- is located within the active site of the enzyme. These interactions may be hydrogen-bonding or Van der Waals type interactions and will be reflected in inter-atomic distances of less than <5 Å between the ligand and the amino acid residues.

8.4 Docking experiments using Molegro Virtual Docker

8.4.1 Introduction

In order to design novel quinone delivery substrates for hNQO1, molecular docking experiments were performed using Molegro Virtual Docker (version 3). The X-ray crystal co-ordinates of hNQO1 was downloaded from the RCSB Protein Data Base (pdb code: 1H69, resolution 1.86 Å).[58] The structure was amended to provide a monomer of the protein and the bound cofactor, FAD **33** was altered to its reduced form ($FADH_2$) **34** (Figure 34).

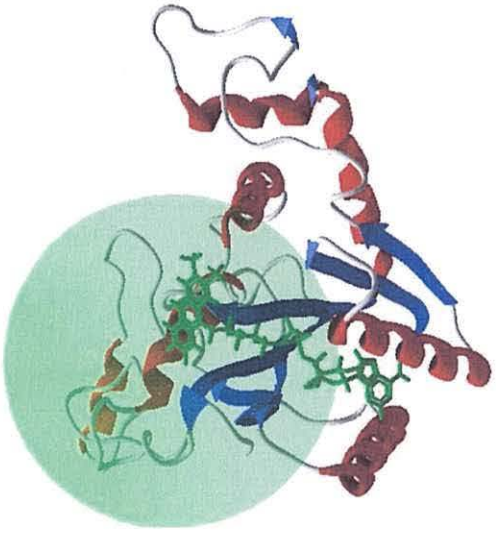

Figure 34. Crystal structure of monomeric hNQO1 showing one bound $FADH_2$ and area of the docking site

Molegro Virtual Docker can detect cavities (potential active sites) for hNQO1. For these experiments, the active site located/used was in close proximity to the $FADH_2$ **34**. Once the active site was detected the ligands were imported into the software and an initial randomised docking procedure was used called primary (1°) docking. A more specific secondary (2°) docking procedure was then used to fine-tune our docking results. This procedure is discussed in the following sections.

8.4.2 Primary (1°) docking procedure

The ligands were constructed as in section 8.2.2 (p.37), energy minimised and imported into the Molegro Virtual Docker along with the edited monomer (with the bound reduced $FADH_2$ **34**). The docking procedure was randomised using MolDock scoring function and the ligands were docked in a 15 Å radius around the bound $FADH_2$ **34** binding site. The

MolDock optimizer algorithms were used with a maximum of 10 runs and 10,000 iterations per ligand. A maximum of five poses (orientations) were returned in which similar poses were clustered and/or ignored (at root mean square deviation (RMSD)-threshold).

The docking procedure generated five top poses for each ligand. These poses were then analysed on their feasibility to perform a hydride transfer process with the reduced $FADH_2$ **34** (distances of <4 Å) and their interaction with the active site residues such as Van der Waals interactions (Appendix 1.1). The top ranked pose for each ligand was then selected for the secondary (2°) docking procedure.

8.4.3 Secondary (2°) docking procedure

As mentioned previously, secondary (2°) docking is more specific than primary (1°) docking as a template is created (Figure 35). This ensures that the quinone moiety remains in close proximity to the bound $FADH_2$ **34** during the simulation process whereas the remainder of the molecule can orientate freely within the active site. The template provides more accurate data with respect to ligand-active site interactions.

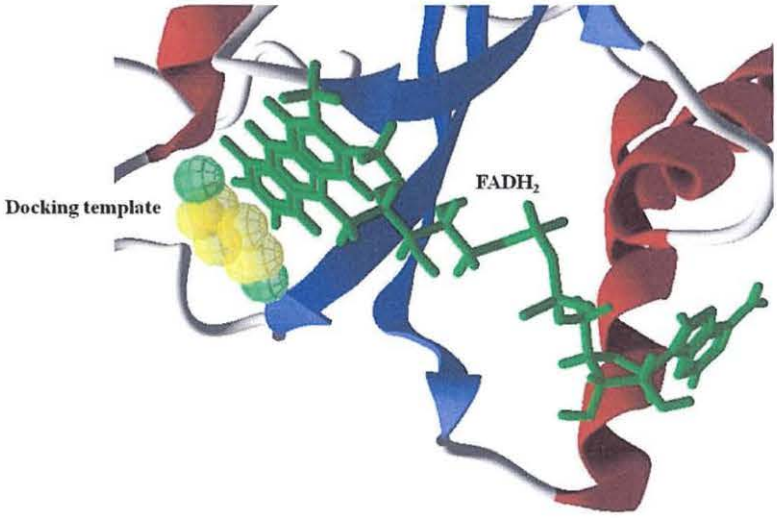

Figure 35. Docking template for quinones

The five top ranked poses for each ligand were returned and analysed (Appendix 1.2) based on the same criteria mentioned in section 8.4.2. A summary of the docking results of the top ranked poses for each ligand are provided in the following section.

8.5 Molecular modelling data of top ranked poses

8.5.1 Summary of secondary (2°) docking results of top ranked poses for 129

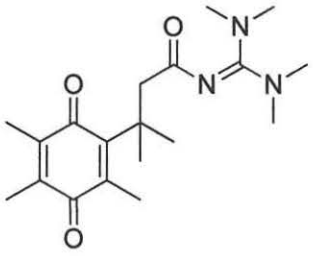

(129)

Returned Poses of Ligand	Interaction with $FADH_2$ (Å)	Ligand-$FADH_2$ distances (Å)		Ligand-Protein interactions	
		O^1----N^2	O^4----N^5	Inter-atomic distances (Å)	Van der Waals (<5 Å)
[00]	3.3 (O^4)	3.2	3.3	3.5 (Gly 193) 3.6 (Gly 150)..O^1	Gly 149, Gly 150, Gly 193, His 161, His 194, Ile 192, Leu 103, Met 154, Phe 106, Ser 191, Thr 147, Thr 148, Thr 195, Trp 105, Tyr 155
[01]	3.4 (O^4)	3.0	3.4		Gln 104, Gly 149, Gly 150, His 11, His 161, Met 154, Phe 106, Pro 102, Thr 148, Trp 105, Tyr 155
[03]	3.4 (O^4)	3.2	3.4	3.6 (Gly 150)..O^1	Gly 149, Gly 150, Gly 193, His 161, His 194, Ile 192, Met 154, Phe 106, Ser 191, Thr 148, Trp 105, Tyr 155

Table 4. Summary of distances (Å) and predicted bonding interactions (inter-atomic distances in Å) for top ranked poses in the hNQO1 active site

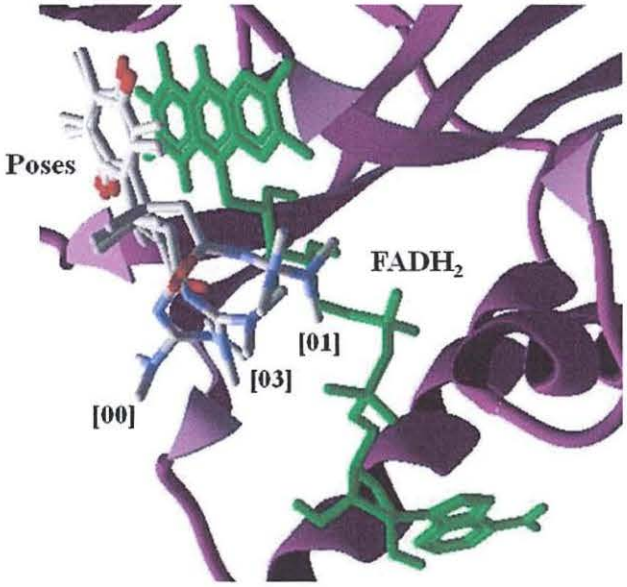

Figure 36. (A) Docking results of the top ranked poses in the hNQO1active site

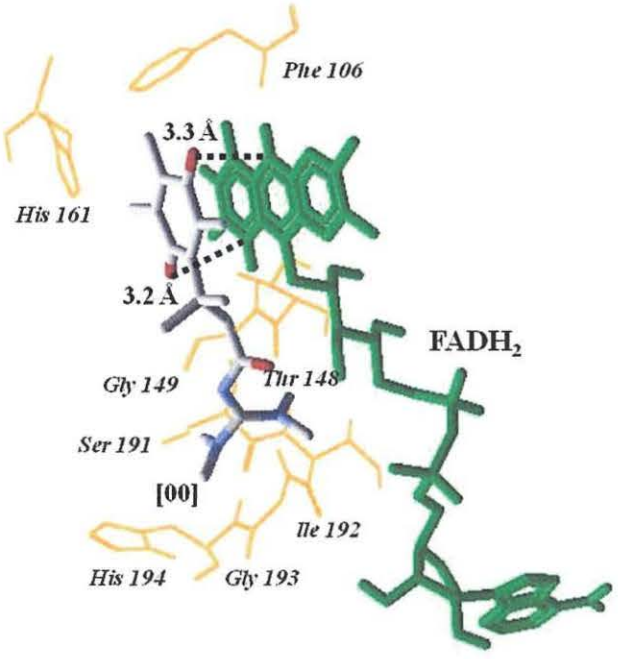

(B) Interaction of the best pose with the bound $FADH_2$

8.5.2 Summary of secondary (2°) docking results of top ranked poses for 130

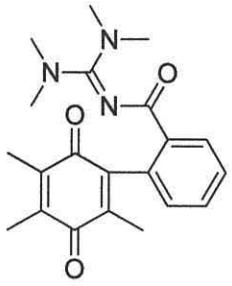

(130)

Returned Poses of Ligand	Interaction with $FADH_2$ (Å)	Ligand-$FADH_2$ distances (Å)		Ligand-Protein interactions	
		O^1----N^5	O^4----N^2	Inter-atomic distances (Å)	Van der Waals (<5 Å)
[01]	3.6 (O^1)		3.3		Gln 104, Gly 149, Gly 150, His 161, Met 154, Phe 106, Thr 148, Trp 105, Tyr 155
[03]	3.5 (O^1)	3.5	3.2	3.5 (Gly 150)..O^4	Gln 104, Gly 149, Gly 150, His 161, Leu 103, Met 154, Phe 106, Thr 148, Trp 105, Tyr 155

Table 5. Summary of distances (Å) and predicted bonding interactions (inter-atomic distances in Å) for top ranked poses in the hNQO1active site

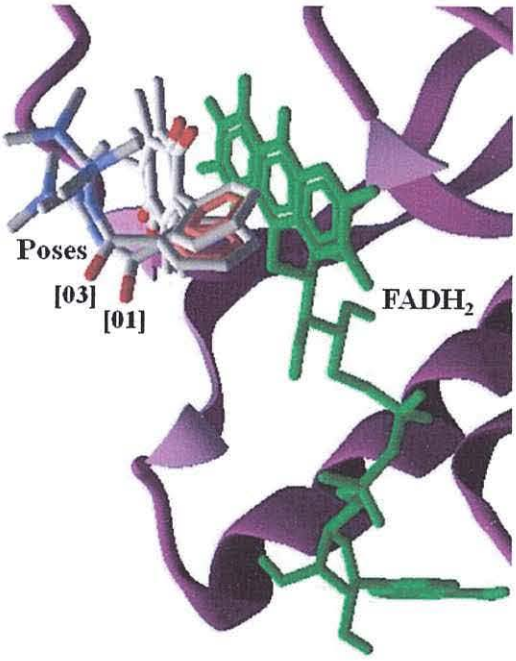

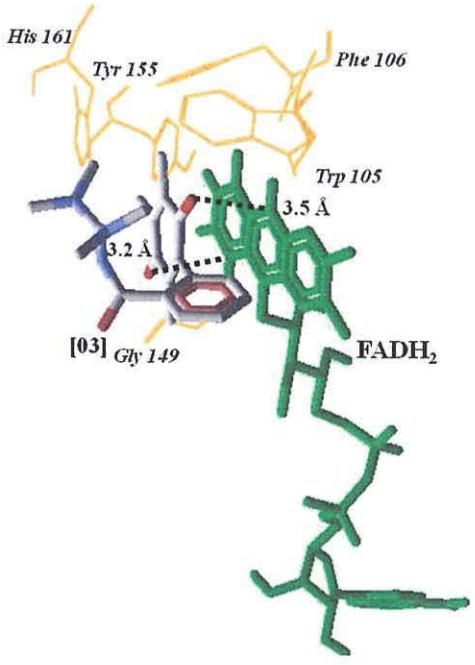

Figure 37. (A) Docking results of the top ranked poses in the hNQO1active site **(B)** Interaction of the best pose with the bound $FADH_2$.

8.5.3 Summary of secondary (2°) docking results of top ranked poses for 131

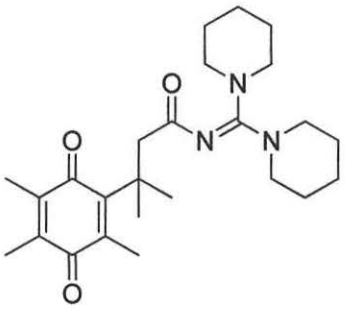

(131)

Returned Poses of Ligand	Interaction with $FADH_2$ (Å)	Ligand-$FADH_2$ distances (Å)		Ligand-Protein interactions
		O^1----N^2	O^4----N^5	Van der Waals (<5 Å)
[00]	3.4 (O^4)	3.0	3.4	Gly 149, Gly 150, His 161, Ile 160, Leu 103, Met 154, Phe 106, Ser 151, Ser 191, Thr 148, Trp 105, Tyr 155
[02]	3.6 (O^4)	2.8	3.6	Gly 149, Gly 150, His 161, Ile 160, Leu 103, Met 154, Phe 106, Thr 148, Trp 105, Tyr 155
[03]	3.1 (O^4)	3.2	3.1	Gly 149, Gly 150, His 161, Ile 160, Met 154, Phe 106, Ser 151, Thr 148, Trp 105, Tyr 155

Table 6. Summary of distances (Å) and predicted bonding interactions (inter-atomic distances in Å) for top ranked poses in the hNQO1 active site

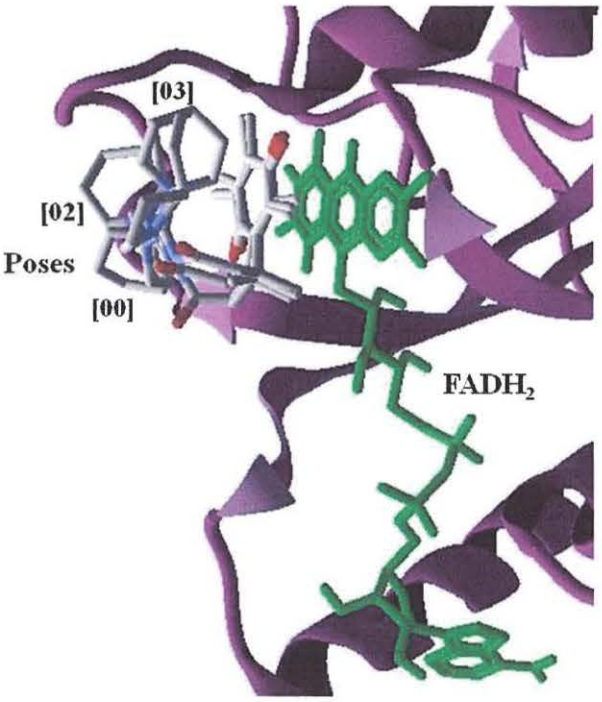

Figure 38. (A) Docking results of the top ranked poses in the hNQO1active site

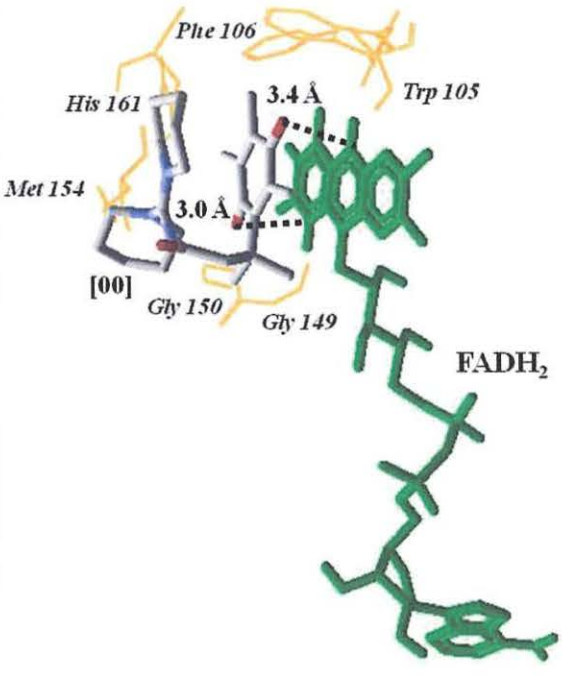

(B) Interaction of the best pose with the bound $FADH_2$

8.5.4 Summary of secondary (2°) docking results of top ranked poses for 132

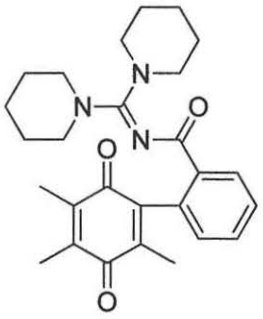

(132)

Returned Poses of Ligand	Interaction with $FADH_2$ (Å)	Ligand-$FADH_2$ distances (Å)		Ligand-Protein interactions
		O^1----N^5	O^4----N^2	Van der Waals (<5 Å)
[02]	3.4 (O^1)	3.4	3.4	Gln 104, Gly 149, Gly 150, His 161, Ile 160, Met 154, Phe 106, Thr 148, Trp 105, Tyr 155
[03]	3.2 (O^1)	3.2		Gln 104, Gly 149, Gly 150, His 161, Ile 160, Met 154, Phe 106, Thr 148, Trp 105, Tyr 155

Table 7. Summary of distances (Å) and predicted bonding interactions (inter-atomic distances in Å) for top ranked poses in the hNQO1 active site

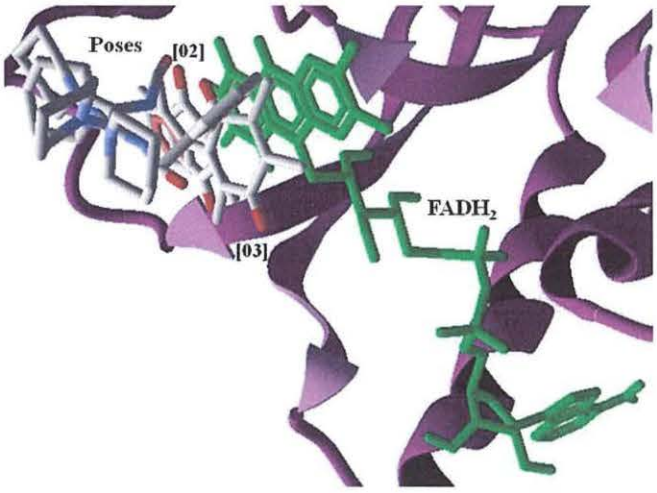

Figure 39. (A) Docking results of the top ranked poses in the hNQO1active site

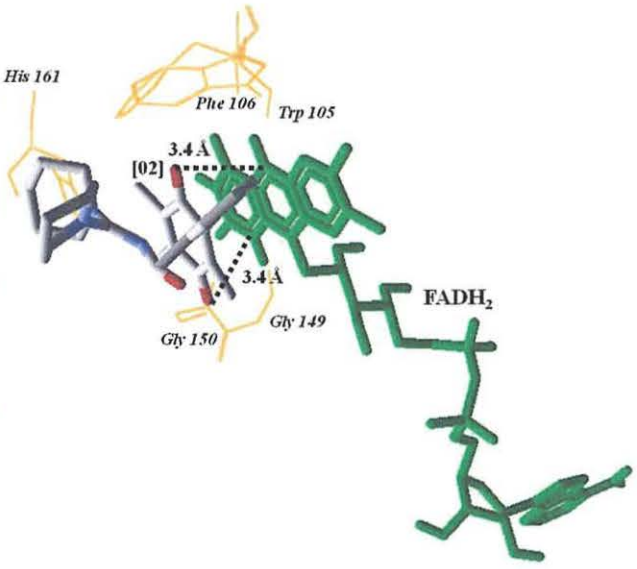

(B) Interaction of the best pose with the bound $FADH_2$

8.5.5 Summary of secondary (2°) docking results of top ranked poses for 133

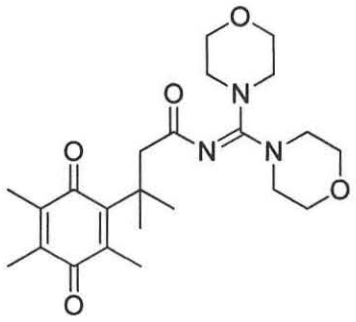

(133)

Returned Poses of Ligand	Interaction with $FADH_2$ (Å)	Ligand-$FADH_2$ distances (Å)		Ligand-Protein interactions
		O^1----N^2	O^4----N^5	Van der Waals (<5 Å)
[00]	3.1 (O^4)	3.1	3.1	Gly 149, Gly 150, His 161, Ile 160, Met 154, Phe 106, Ser 151, Thr 148, Trp 105, Tyr 155
[01]	3.3 (O^4)	3.0	3.3	Gly 149, Gly 150, His 161, Leu 103, Ile 160, Met 154, Phe 106, Ser 151, Thr 148, Trp 105, Tyr 155
[02]	3.2 (O^4)	3.2	3.2	Gly 149, Gly 150, His 161, Ile 160, Met 154, Phe 106, Thr 148, Trp 105, Tyr 155

Table 8. Summary of distances (Å) and predicted bonding interactions (inter-atomic distances in Å) for top ranked poses in the hNQO1 active site

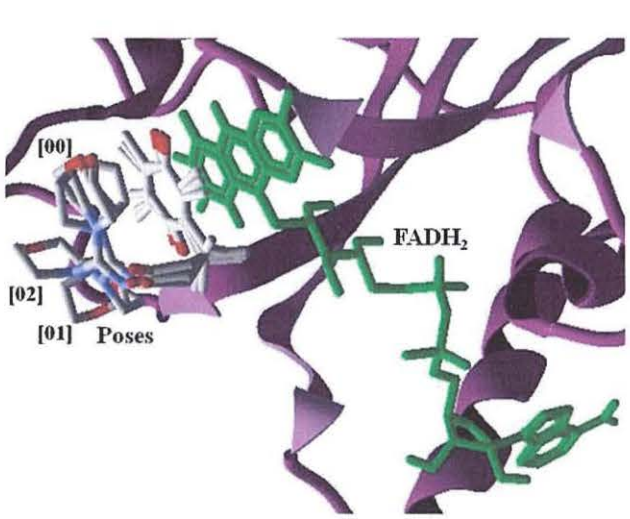

Figure 40. (A) Docking results of the top ranked poses in the hNQO1active site

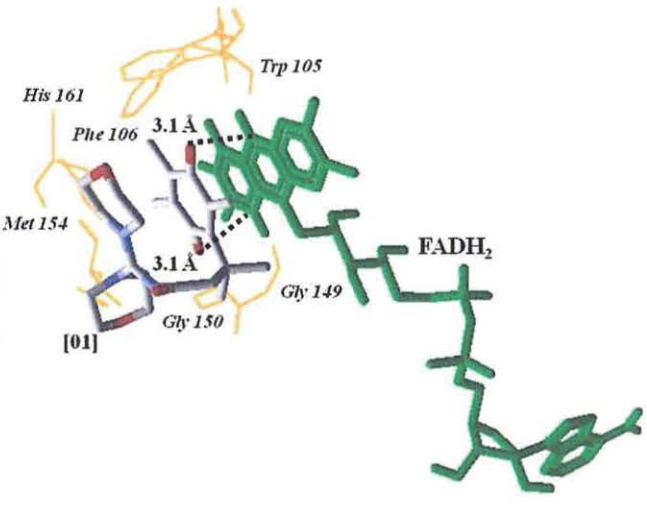

(B) Interaction of the best pose with the bound $FADH_2$

8.5.6 Summary of secondary (2°) docking results of top ranked poses for 134

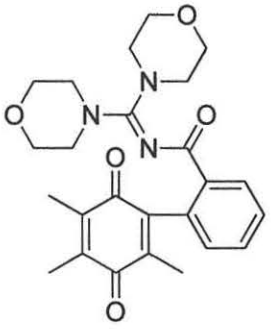

(134)

Returned Poses of Ligand	Interaction with $FADH_2$ (Å)	Ligand-$FADH_2$ distances (Å)				Ligand-Protein interactions
		O^1----N^2	O^1----N^5	O^4----N^2	O^4----N^5	Van der Waals (<5 Å)
[02]	3.5 (O^4)				3.5	Gly 149, Gly 150, Gly 193, His 161, His 194, Ile 160, Ile 192, Met 154, Phe 106, Ser 151, Ser 191, Thr 148, Trp 105, Tyr 155
[03]	3.4 (O^1)		3.4	3.4		Gln 104, Gly 149, Gly 150, His 161, Ile 160, Met 154, Phe 106, Thr 148, Trp 105, Tyr 155
[04]	3.9 (O^4)	3.5				Gly 149, Gly 150, Gly 193, His 161, His 194, Leu 103, Met 154, Phe 106, Ser 151, Ser 191, Thr 148, Trp 105, Tyr 155

Table 9. Summary of distances (Å) and predicted bonding interactions (inter-atomic distances in Å) for top ranked poses in the hNQO1 active site

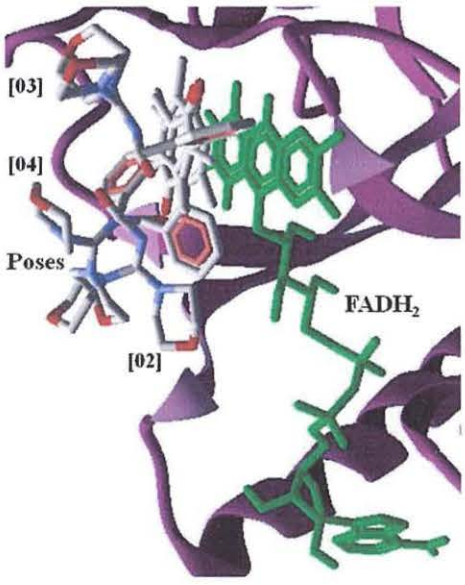

Figure 41. (A) Docking results of the top ranked poses in the hNQO1active site

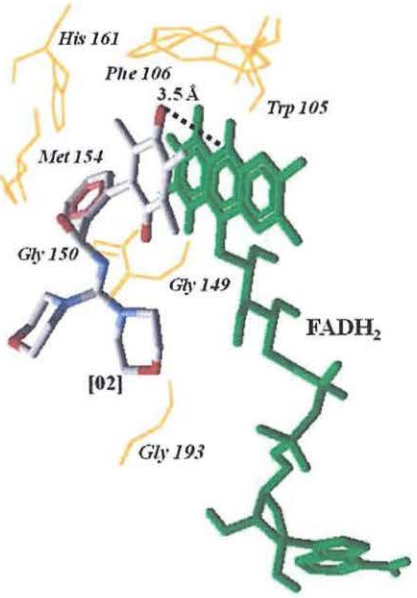

(B) Interaction of the best pose with the bound $FADH_2$

8.5.7 Summary of secondary (2°) docking results of top ranked poses for 78

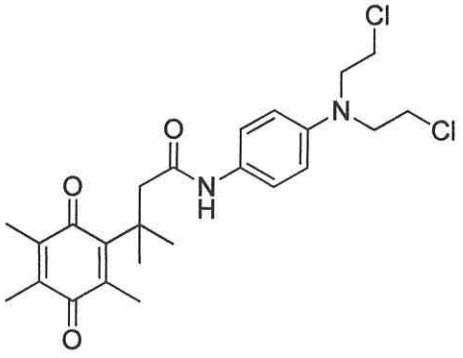

(78)

Returned Poses of Ligand	Interaction with $FADH_2$ (Å)	Ligand-$FADH_2$ distances (Å)		Ligand-Protein interactions
		O^1----N^5	O^4----N^2	Van der Waals (<5 Å)
[01]	3.6 (O^1)	3.6	3.6	Gln 104, Gly 149, Gly 150, His 161, Ile 160, Leu 103, Met 154, Phe 106, Ser 151, Thr 148, Trp 105, Tyr 155
[03]	3.5 (O^1)	3.5	3.5	Gln 104, Gly 149, Gly 150, His 161, Ile 160, Leu 103, Met 154, Phe 106, Thr 148, Trp 105, Tyr 155

Table 10. Summary of distances (Å) and predicted bonding interactions (inter-atomic distances in Å) for top ranked poses in the hNQO1 active site

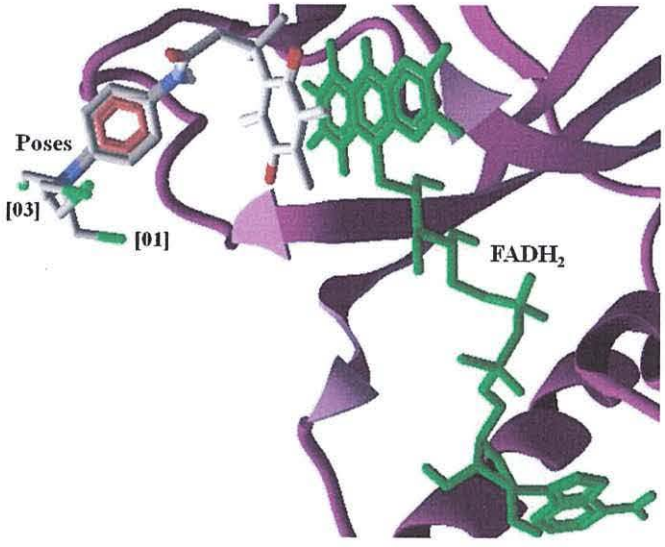

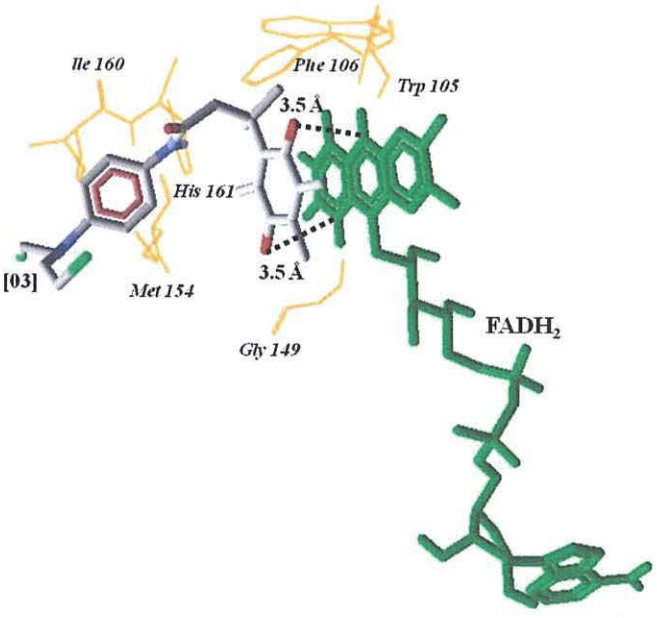

Figure 42. (A) Docking results of the top ranked poses in the hNQO1active site **(B)** Interaction of the best pose with the bound $FADH_2$.

8.5.8 Summary of secondary (2°) docking results of top ranked poses for 135

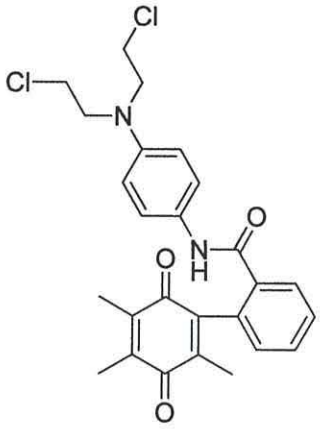

(135)

Returned Poses of Ligand	Interaction with $FADH_2$ (Å)	Ligand-$FADH_2$ distances (Å)	Ligand-Protein interactions	
		O^1----N^5	Inter-atomic distances (Å)	Van der Waals (<5 Å)
[00]	3.4 (O^1)	3.4	3.2 (Gly 150) 3.6 (Gly 149)	Gly 149, Gly 150, Gly 193, His 161, His 194, Met 154, Phe 106, Ser 151, Ser 191, Thr 148, Trp 105, Tyr 155
[01]	3.1 (O^1)	3.1	3.2 (Gly 150)	Gly 149, Gly 150, Gly 193, His 161, His 194, Ile 160, Met 154, Phe 106, Ser 151, Ser 191, Thr 148, Trp 105, Tyr 155
[03]	2.6 (O^1)	2.6		Gln 104, Gly 149, Gly 150, Gly 193, His 161, His 194, Ile 192, Met 154, Phe 106, Ser 191, Thr 148, Trp 105, Tyr 155

Table 11. Summary of distances (Å) and predicted bonding interactions (inter-atomic distances in Å) for top ranked poses in the hNQO1 active site

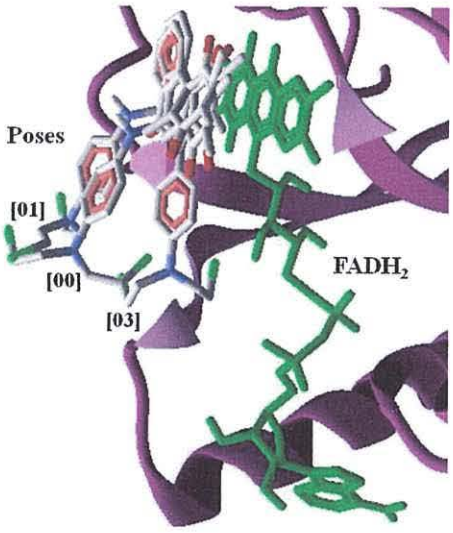

Figure 43. (A) Docking results of the top ranked poses in the hNQO1active site

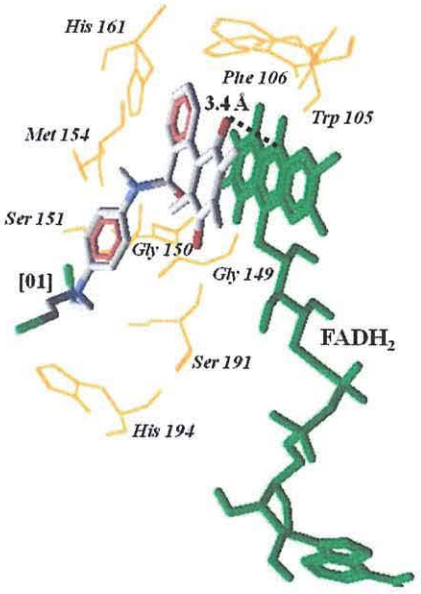

(B) Interaction of the best pose with the bound $FADH_2$

8.5.9 Summary of primary (1°) docking results of top ranked pose for 136

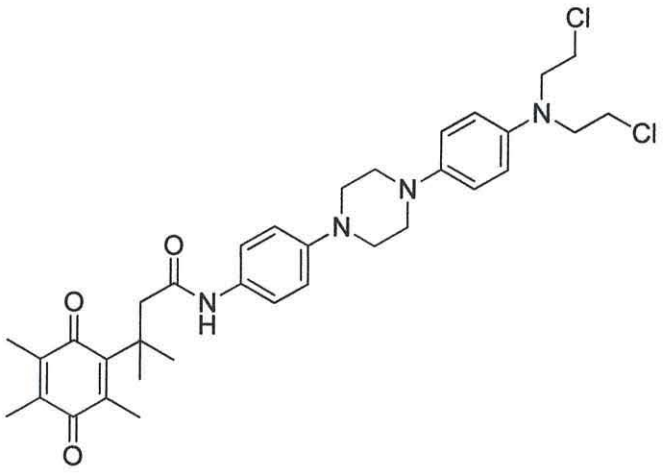

(136)

Returned Poses of Ligand	Interaction with $FADH_2$ (Å)	Ligand-$FADH_2$ distances (Å)	Ligand-Protein interactions
		O^1----N^5	Van der Waals (<5 Å)
[00]	3.0 (O^1)	3.0	Arg 200, Gln 104, Gly 149, Gly 150, Gly 193, Met 154, His 161, His 194, Ile 192, Phe 106, Ser 191, Trp 105, Thr 148, Thr 195, Tyr 155

Table 12. Summary of distances (Å) and predicted bonding interactions (inter-atomic distances in Å) for top ranked poses in the hNQO1 active site

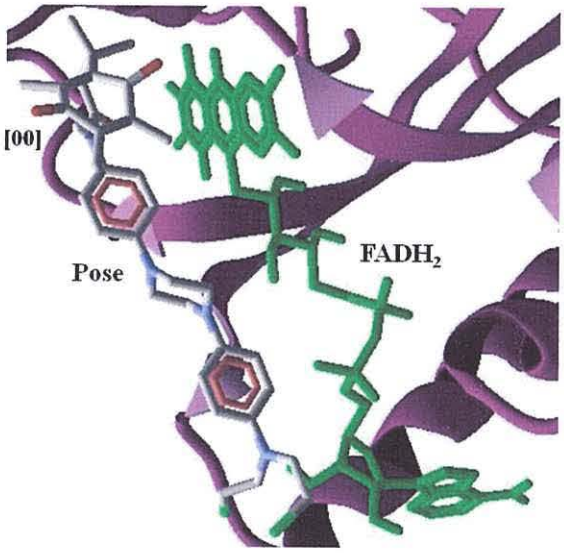

Figure 44. (A) Docking results of the top ranked poses in the hNQO1active site

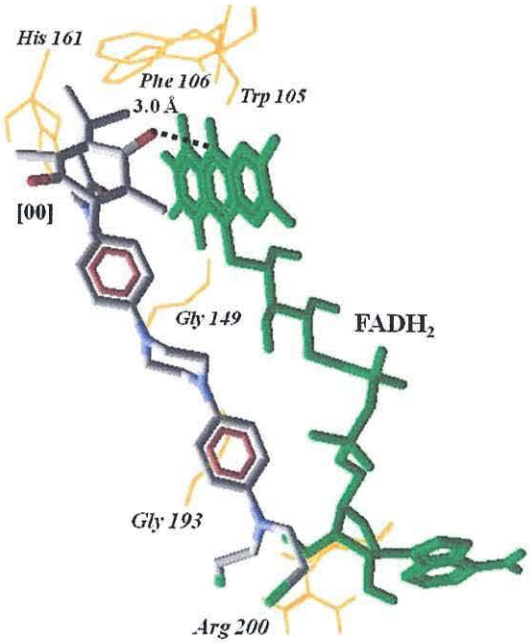

(B) Interaction of the best pose with the bound $FADH_2$

8.6 Primary (1°) docking for mechanisms two and three

The molecular modelling data suggest that hydride transfer occurs directly to a carbonyl oxygen of the quinone **37**, mechanism one (Scheme 25, p.42). To complete this section it is important to mention the two other potential mechanisms that have been discussed. Mechanism two suggests that hydride transfer occurs directly to the carbonyl carbon of the quinone **37** (refer to Scheme 8, p.11).[87, 88] There are two important distances (Å) from N^5 in the $FADH_2$ **34** to either C^1 or C^4 of the quinone **37** (Figure 45).

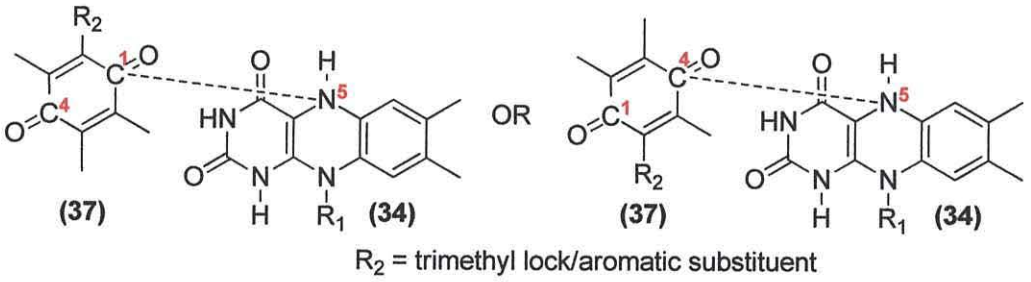

Figure 45. Distances (Å) determined between the quinone **37** and $FADH_2$ **34** for mechanism two

Mechanism three suggests that hydride transfer occurs directly to an adjacent carbonyl carbon (refer to Scheme 9, p.12).[89, 90] There are four important distances (Å) from N^5 in the $FADH_2$ **34** to C^2, C^3, C^5 or C^6 of the quinone **37** (Figure 46).

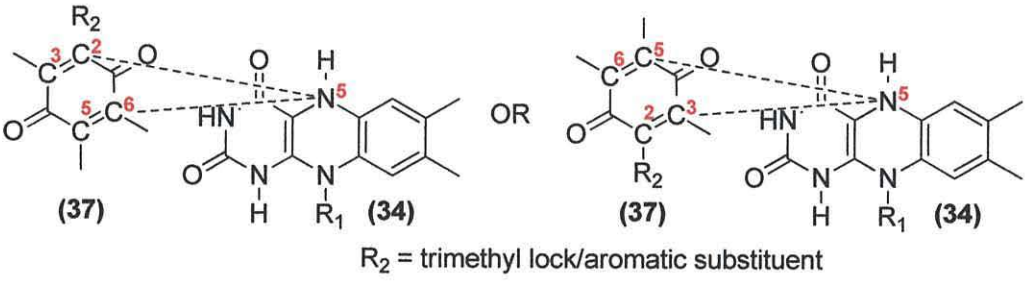

Figure 46. Distances (Å) determined between the quinone **37** and $FADH_2$ **34** for mechanism three

Using the previously obtained primary (1°) docking data these results could be modified to account for these two mechanisms, the only difference being their distances (Å) are now between different carbon atoms (Appendix 1.3 and 1.4). The next stage would be to submit their top ranked poses for secondary (2°) docking. This has already been determined for poses already selected for mechanism one. However, for the poses only selected for mechanism two and/or three these would have to be run on Molegro Virtual Docker before any further analysis can be undertaken.

8.7 Conclusion

Overall, the computational hNQO1 protein-ligand docking study suggests that hydride transfer from $FADH_2$ **34** to the quinone **37** is possible. In conclusion this has justified the synthesis of all of these compounds for their potential in a benzoquinone drug delivery system.

*All Molegro files for this section are provided in the supporting information

9.0 Synthetic method

9.1 Preparation of trimethyl-locked quinones

The initial synthetic objective was to prepare the ester precursor **50b** as reported by Volpato *et al.*[73] *via* a three-step synthesis (Scheme 26).

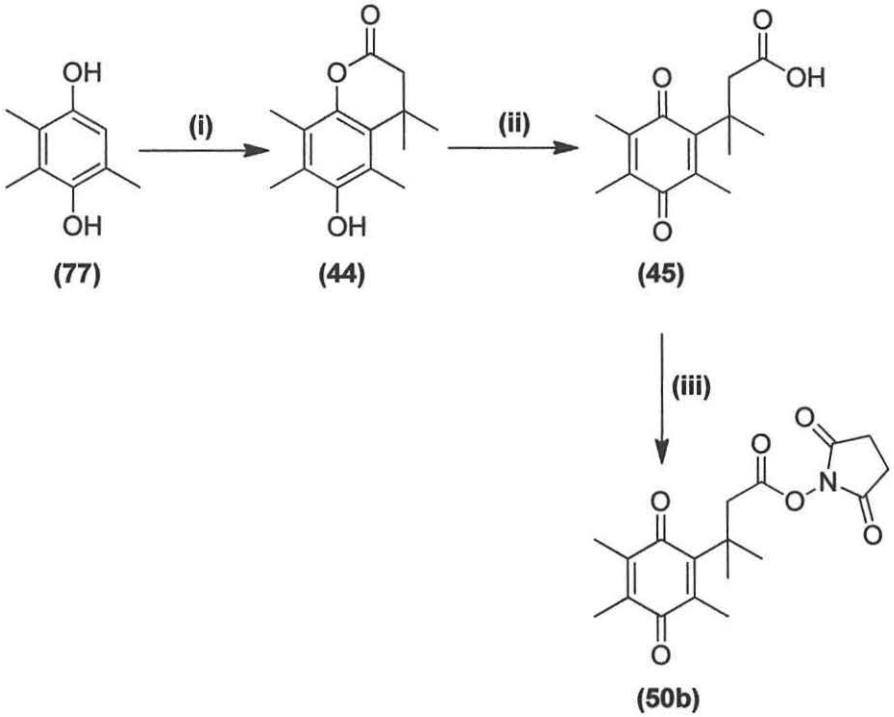

Scheme 26. (i) 1.2 equiv. methyl 3,3-dimethylacrylate, CH_3SO_3H, 70 °C, 3 h then r.t, 12 h (ii) 1.4 equiv. NBS, acetonitrile/H_2O, r.t, 1.5 h (iii) 1.2 equiv. DCC, 1.1 equiv. NHS, dry THF, 0 °C then r.t, 18 h

The first step in the synthesis of ester **50b** involved the addition of 2,3,5-trimethyl-1,4-hydroquinone **77** and methyl 3,3-dimethylacrylate to a solution of methanesulfonic acid. After 3 h at 70 °C and stirring at room temperature (r.t) overnight, work-up and recrystallisation from hexane/chloroform gave the lactone **44** as a white solid in 88% yield. The ^1H nuclear magnetic resonance (NMR) of **44** gave diagnostic signals at δ 1.46 (6H) for the two *geminal* CH_3 groups and 2.55 (2H) ppm for the CH_2 group. The ^{13}C NMR gave signals at δ 27.7 for the two *geminal* CH_3 groups, 35.5 for the $C(CH_3)_2$, 46.1 for the CH_2 and 168.8 ppm for the ester C=O. The remaining signals all correlated well to those expected for this structure. Finally a melting point (m.p.) of 183 – 185 °C (lit. 186 – 187 °C)[91] was found to be in accordance with the literature.

The second step was the oxidation of lactone **44** to the quinone acid **45**. This involved the drop-wise addition of NBS to a stirring solution of **44** over 1 h in acetonitrile/water. After work-up the crude product was re-dissolved in diethyl ether followed by subsequent cooling to 0 °C and the addition of petrol to give the quinone acid **45** as a yellow solid in 99% yield. The ^{1}H NMR had similar signals to **44**, however there was a slight downfield shift of the CH_2 group from δ 2.55 (2H) in **44** to 3.02 (2H) ppm in **45**. The ^{13}C NMR contained diagnostic signals at δ 178.4 for the acid C=O and 187.4 and 190.8 ppm for the quinone C=O groups. A melting point of 91 – 93 °C (lit. 101 – 103 °C)[105] was found to be slightly lower than expected with respect to the literature, however the acid **45** was felt to be of sufficient purity to progress to the next step.

The third step in the synthesis of the ester **50b** involved the addition of DCC to a solution of the quinone acid **45** and NHS in dry tetrahydrofuran (THF). After stirring for 18 h, work-up and recrystallisation from ethyl acetate this gave the ester **50b** as a yellow solid in >100% crude yield. The ^{1}H NMR was very similar to the acid **45**, however a diagnostic signal at δ 2.78 (4H) indicated the presence of the two succinimidyl CH_2 groups and corresponded to signals at 25.5 ppm in the ^{13}C NMR. This spectrum also contained diagnostic signals at δ 167.7 for the ester C=O and 168.9 ppm for the succinimidyl C=O groups. Finally, a melting point of 140 – 142 °C (lit. 145 °C)[106] was found to be in accordance with the literature.

During this work the yields obtained for the three steps were always higher than those reported.[73, 112] Whilst their approach was closely followed, slight changes in recrystallisation methods were employed which might explain the increased efficiency of each stage. The final product **50b** was judged to be of very high purity by NMR and of sufficient quality to be used in the next steps without further purification.

The next stage in the project was to investigate the reaction of this activated ester **50b** with substituted guanidines. Previous work carried out by Volpato *et al.*[73] employed an aniline mustard containing an amine acting as the nucleophile (Scheme 16, p.23). Our initial test reaction utilised commercially available 1,3-diphenylguanidine **137** as a substrate. Thus the ester **50b** was added to a solution of the guanidine **137** in dry THF and stirred in the dark for 23 h (Scheme 27). After aqueous work-up the crude reaction mixture was purified

by column chromatography using ethyl acetate/petrol. This proved to be an extremely complicated process resulting in the elution of several coloured bands. Very puzzling was the discovery of a deep purple solid isolated in some of the 20% ethyl acetate/petrol fractions, the identity of which is still unknown. Some of the more promising later fractions containing yellow solid provided mass spectrometry data concordant with those of the desired prodrug **138**. These fractions were purified for a second time by column chromatography. However, this led to the formation of several additional products as evidenced by thin layer chromatography (TLC) analysis.

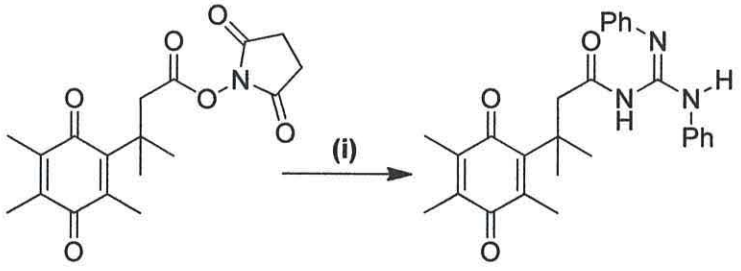

(50b) **(138)**

Scheme 27. (i) 2 equiv. **137**, dry CH_2Cl_2, N_2, dark, r.t, 46 h

The reaction was repeated using dry dichloromethane as the solvent and doubling the stirring time to 46 h. Once again the resulting crude reaction mixture was purified by column chromatography. Little change was observed on the outcome of the reaction and similar problems to those discussed previously were encountered with the isolation of multiple products.

With this lack of success it was proposed that the guanidine **138** may have undergone decomposition on silica during the purification process. Initial ^1H NMR analysis of the crude reaction mixture was in both cases promising, suggesting that the method itself was effective. To overcome these difficulties meant finding a new purification method. Thus repetition of the reaction in dry dichloromethane gave a crude product which was dissolved in diethyl ether and diluted with petrol to give a 50:50 ratio. Cooling to 0 °C led to the precipitation of a yellow solid in 16% yield which was identified as being the crude guanidine **138**. The ^1H NMR gave a multiplet at δ 6.89 – 7.65 (11H) for the aromatic CH's and one NH group and a broad (br.) singlet at 9.89 (1H) ppm for the other guanidine NH. The IR gave diagnostic bands at 1645 for the C=N and 1664 for the C=O groups together with bands at 3308 and 3401 cm^{-1} for the NH's. High resolution mass spectrometry

(HRMS) gave a mass of 444.2281 [$(M + H)^+$] Daltons which is in close agreement with the calculated mass of 444.2282. From the NMR data, it was apparent that the guanidine **138** was impure, however attempts to further purify by precipitation/recrystallisation led to considerable material losses.

During purification of the first reaction attempt a white solid was isolated in some of the earlier fractions (20 - 30% ethyl acetate/petrol). Since the ^{1}H NMR of the yellow solid correlated well with the desired diphenylguanidine **138**, this white solid was believed to be one of three isomers similar to those reported by Wolfe *et al.*[108] The potential structures were the spirolactams **139** and **140** and the six-membered lactam **141** (Scheme 28).

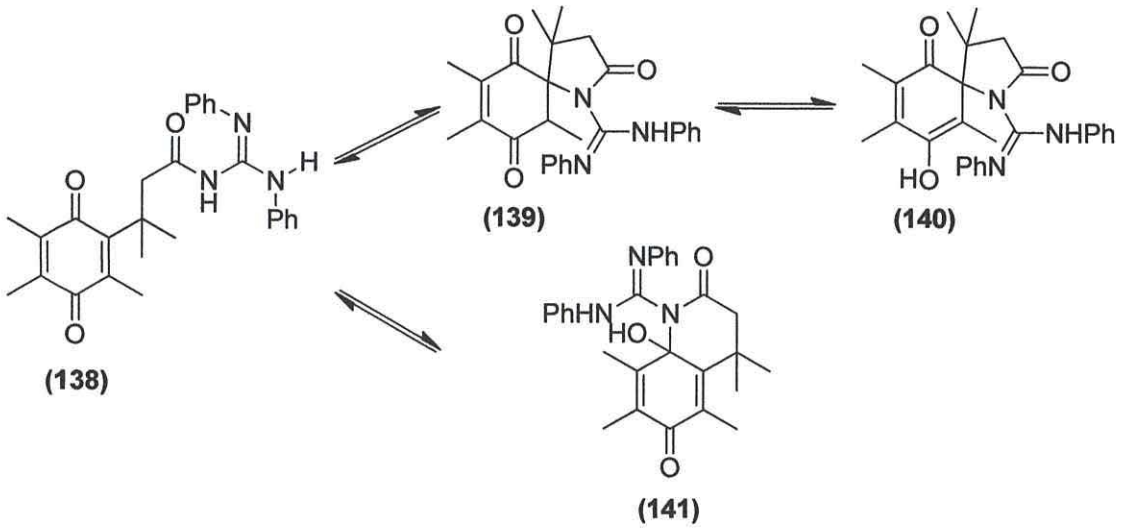

Scheme 28. Lactam isomers of compound **138**

The ^{1}H NMR of this white solid showed some similarities to **138**; however, with separate signals at δ 0.93 (3H) and 1.07 (3H) for the *geminal* CH_3 groups with the third methyl appearing as a doublet at 1.46 (3H, J = 6.5 Hz) ppm. This seemed to indicate the presence of a $CHCH_3$ in the molecule suggesting the ketolactam **139**. Further to this, the CH_2 was observed as a pair of doublets at δ 2.16 (1H, J = 17.5 Hz) and 2.75 (1H, J = 17.5 Hz) and a quartet at 5.31 (1H, J = 7.0 Hz) ppm for the CH. This again supported the ketolactam structure **139** as shown in figure 47.

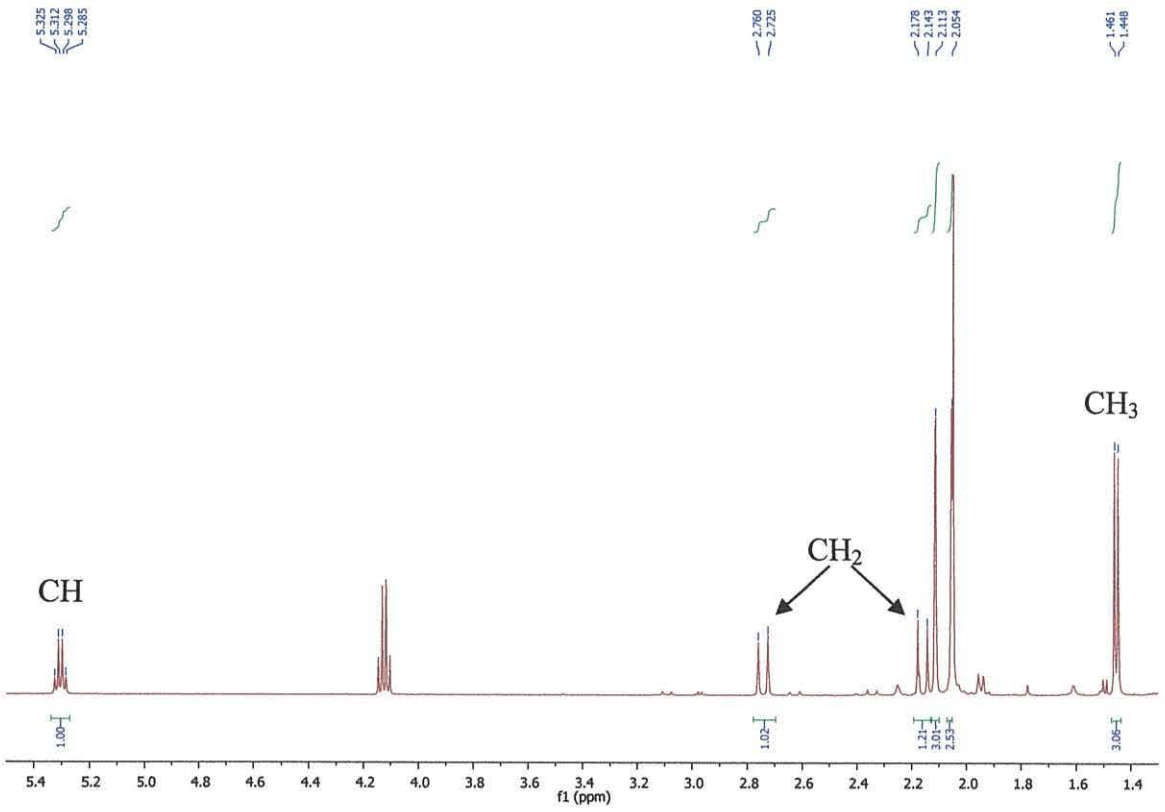

Figure 47. 500 MHz ^{1}H NMR spectrum expansion of **139**

Further signals at δ 6.67 (2H, d, J = 7.5 Hz), 6.77 (1H, t, J = 7.3 Hz), 6.90 (1H, t, J = 6.3 Hz) and 7.00 – 7.07 (6H, m) corresponded to ten aromatic CHs and a signal at 8.22 (1H) ppm for the NH group. Analysis of the ^{13}C NMR gave signals at δ 147.5 for the quaternary guanidine carbon, 174.9 for the amide C=O and at 192.8 and 197.4 ppm for the two ketone C=O. The IR gave bands at 1680 for the C=N, 1726 for the C=O groups and 3265 cm^{-1} for the NH group. High resolution mass spectrometry gave a mass of 444.2280 [(M + H)$^{+}$] Daltons which is in good agreement with the calculated value of 444.2282. This data seemed to support the ketolactam isomer **139** and was suggestive of a complex sequence of possible reactions for this process which is not desirable.

During purification of the second reaction attempt a further white crystalline solid was isolated in some of later fractions (60% ethyl acetate/petrol). The ^{1}H NMR of this solid showed some similarities to **138** and **139**. As in **139**, there were separate signals at δ 1.20 (3H) and 1.43 (3H) for the *geminal* CH_3 groups and two well separated doublets at 2.40 (1H, J = 14.8 Hz) and 3.99 (1H, J = 14.5 Hz) ppm for the CH_2 group. The spectrum also

contained ten aromatic CH signals and a signal at δ 5.83 (1H) ppm for an NH group. The two most distinguishing signals were a doublet at δ 1.18 (3H, J = 7.3 Hz) for a CH_3 and a quartet at 2.84 (1H, J = 7.0 Hz) ppm for a CH (Figure 48). This observation was puzzling since the ketolactam **139** which contains these two signals had already been identified.

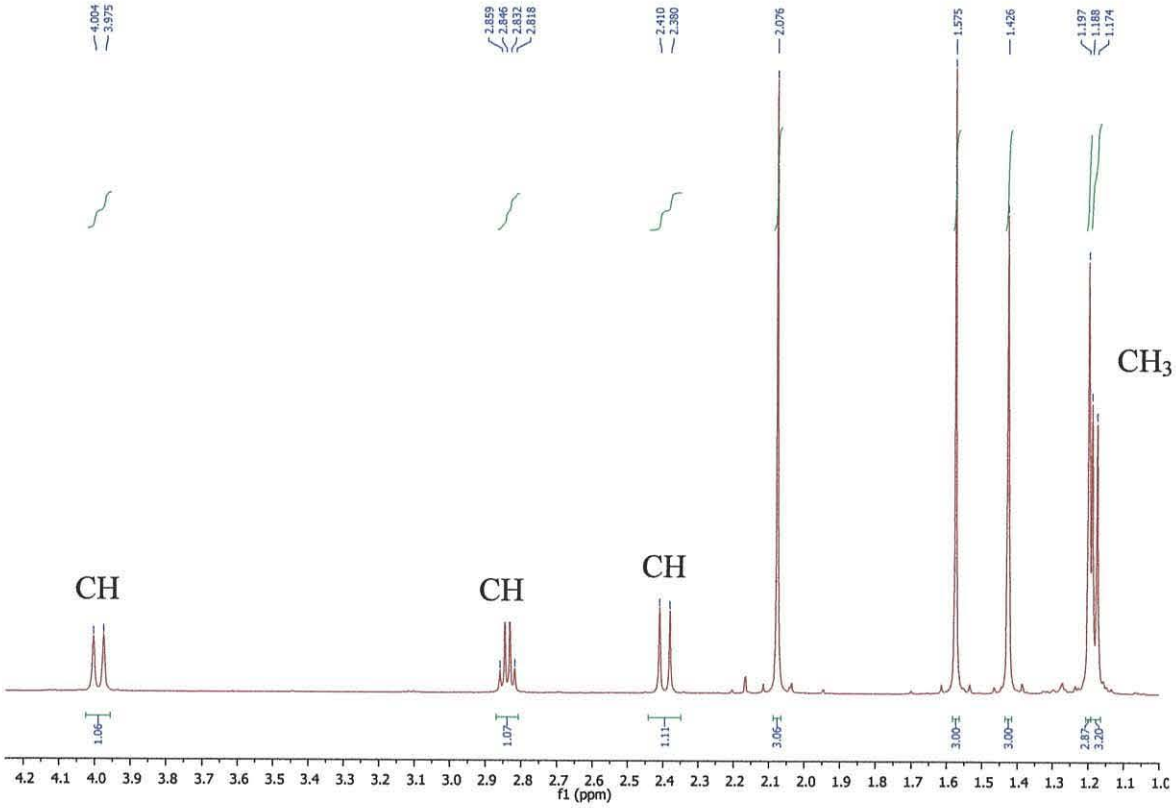

Figure 48. 500 MHz ^{1}H NMR spectrum expansion of **143**

The ^{13}C NMR was informative in that the quaternary carbonyl signals suggested the presence of only two different C=O environments. The first signal at δ 172.3 was indicative of a lactone/ester/lactam carbonyl whilst the second signal at 201.8 ppm was indicative of a ketone carbonyl. The IR gave bands at 1675 for a C=N, 1743 for C=O groups and 3330 cm^{-1} for an NH. High resolution mass spectrometry gave a mass of 444.2278 [(M + H)$^+$] Daltons which is in agreement with the calculated value of 444.2282 and confirmed that it was an isomer of the desired compound **138**.

Confirmation of structure was provided by X-ray crystallography (Scheme 29, Appendix 2.2.1) and gave evidence for an unreported reaction type in which the guanidine in **137** has undergone a 1,4-conjugate addition to the quinone system in **50b** followed by a 1,2-

addition to the carbonyl to give an intermediate oxyanion which then displaces the NHS to give a lactone **143** (Scheme 29).

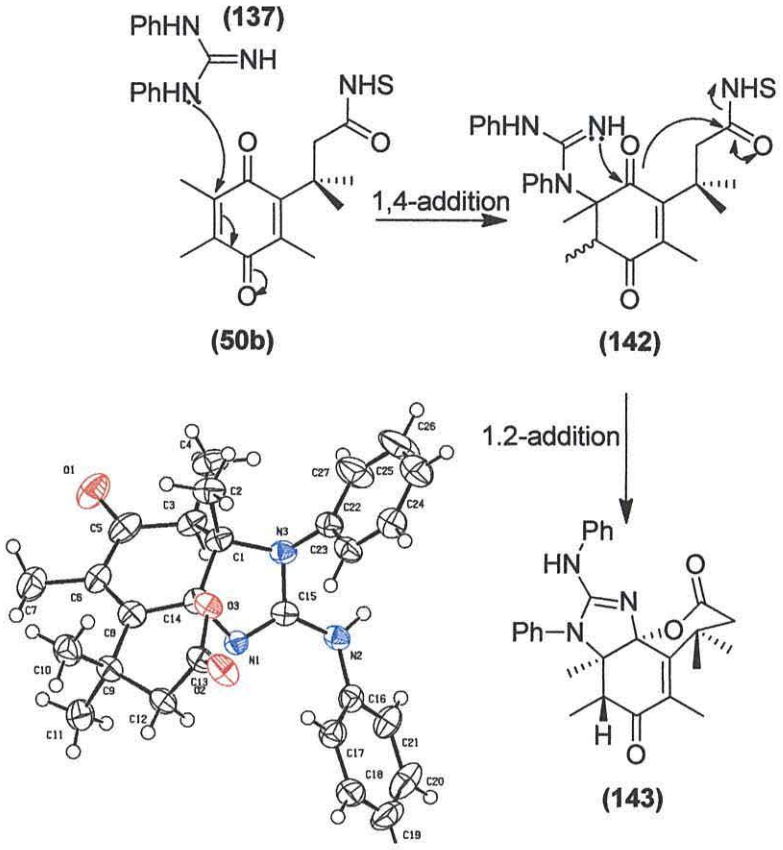

Scheme 29. Mechanism for the formation of **143** and X-ray crystal structure

Whilst this reaction produced a number of interesting compounds, it was decided that with all the problems encountered to conclude this work and to move on to guanidines with a higher number of substituents to eliminate the possibility for multiple addition reactions.

With this in mind, the commercially available 1,1,3,3-tetramethylguanidine **144** was added to a solution of the ester **50b** in dry dichloromethane and stirred in the dark for 46 h. After work-up the crude reaction mixture was purified by column chromatography which gave the desired tetramethylguanidine **129** as a yellow/orange oil in 63% yield (Scheme 30).

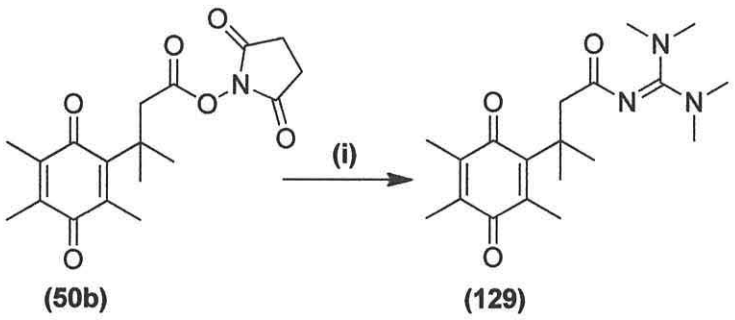

Scheme 30. (i) 1.1 equiv **144**, dry CH_2Cl_2, N_2, dark, r.t, 46 h

The ^1H NMR of **129** gave a diagnostic signal at δ 2.77 (12H) for the four guanidine CH_3 groups and correspondingly at 39.9 ppm in the ^{13}C NMR. This spectrum also contained signals at δ 166.6 for the quaternary guanidine carbon and 179.7 ppm for the amide C=O group. The IR gave a band at 1644 cm^{-1} for the C=O bonds. High resolution mass spectrometry data gave a mass of 348.2286 $[(M + H)^+]$ Daltons which is in agreement with the calculated mass of 348.2282. With this success our interest now turned to the preparation of other tetrasubstituted guanidines. Thus a reliable method for the formation of these guanidines in high yield was required.

Wu *et al.*[217] reported that it was possible to prepare guanidines by reaction of di(1*H*-imidazol-1-yl)methanimine **145** with amines in a two-stage process (Scheme 31).

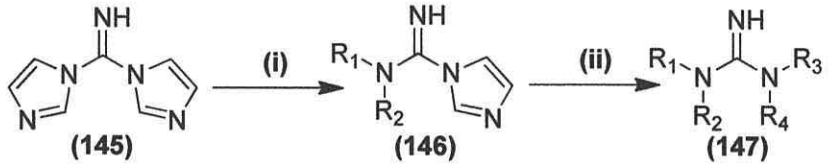

Scheme 31. (i) R_1R_2NH, THF, r.t/40 °C, 6 h (ii) R_3R_4NH, THF/DMF, 90 °C/Δ, 10 -18 h

Di(1*H*-imidazol-1-yl)methanimine **145** was easily prepared by the reaction of cyanogen bromide with imidazole in dichloromethane under reflux for 40 min. After work-up, the diimidazole **145** was obtained as a white solid in 93% yield and carried onto the next step without purification (Scheme 32).

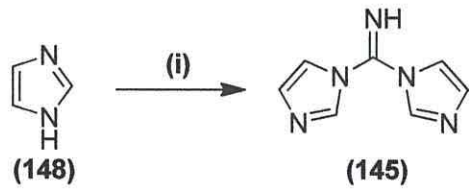

Scheme 32. (i) 0.3 equiv. cyanogen bromide, CH_2Cl_2, Δ, 40 min

The ^{1}H NMR of the imidazole **148** was very similar to **145**. However, the integration ratio of the CH signals doubled relative to the NH signal and were present at δ 7.16 (2H), 7.60 (2H) and 8.12 (2H) ppm respectively as broad singlets. Also present was a signal for the NH group at δ 10.26 (1H), slighty more upfield compared to the 12.31 ppm observed for imidazole **148**. The ^{13}C NMR contained three signals at δ 120.0, 130.7 and 138.4 for the CH's with an additional diagnostic signal at 141.8 ppm for the C=N group. Finally a melting point of 98 – 104 °C (lit. 103 °C)[218, 219] was found to be in accordance with the literature.

With di(1*H*-imidazol-1-yl)methanimine **145** in hand it was treated with piperidine to synthesise the dipiperidinylguanidine **150** which was reported by Wu *et al.*[217] They used a two-step synthesis to first substitute one imidazole with a piperidine to give **149** by stirring at r.t for 6 h and then again with excess piperidine at reflux for 12 h to give **150** (Scheme 33, (i) and (ii)).

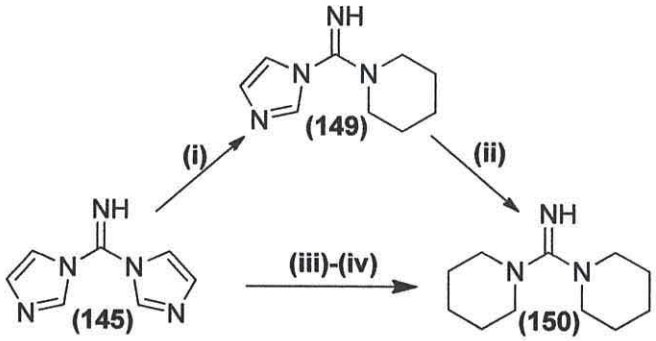

Scheme 33. (i) 1.2 equiv. piperidine, THF, r.t, 6 h (ii) 1.5 equiv. piperidine, THF, Δ, 12 h (iii) 5 equiv. piperidine, dry THF, N_2, Δ, 17 h (iv) aq. 2M NaOH, r.t

To save time and potentially improve on the yield it was decided to attempt this di-substitution in one step only. This meant refluxing the mixture for 9 h and adding an excess of the piperidine to the diimidazole **145** in dry THF. Purification of the product was attempted by column chromatography in methanol/dichloromethane rather than the work-up used by Wu *et al.*[217] However, this method proved to be unsuccessful.

The reaction was repeated but this time refluxed for 17 h and the original work-up was used. A TLC run beforehand had highlighted a distinctive spot, believed to be the dipiperidinylguanidine **150**. However after work-up this had now disappeared. The explanation was that it had been transferred into the aqueous layer by the saturated

ammonium chloride used to wash the organic layer. To confirm this theory the aqueous layer was back-extracted with dichloromethane and the guanidine **150** was isolated as a white hygroscopic solid in 33% yield. A third attempt at this reaction meant changing the work-up by washing with aqueous 2M sodium hydroxide only. This gave the guanidine **150** as a purple solid in 69% yield (Scheme 33, (iii) and (iv)), which was carried onto the next step without purification. On closer inspection of the work reported by Wu *et al.*,[217] it seemed there was an error in the procedure as a work-up employed in an earlier reaction used ammonium chloride and it was believed that this work-up was placed in the preparation of the guanidine **150** erroneously as other similar reactions seemed to employ a basic (NaOH) quench.

The crude ^{1}H NMR of **150** gave diagnostic signals at δ 1.41 (12H) and 3.06 (8H) ppm corresponding to the six CH_2 and four NCH_2 groups. The NH signal had also moved upfield from δ 10.26 (1H) in **145** to 6.96 (1H) ppm in **150**. In the ^{13}C NMR the CH_2 signals were observed at δ 23.6, 25.1 and 49.8 with a diagnostic quaternary guanidine signal at 162.3 ppm which is characteristic of this group of compounds. Finally high resolution mass spectrometry gave a mass of 196.1816 [$(M + H)^+$] Daltons which is in agreement with the calculated mass of 196.1814.

There was an improvement in the yields of both reactions, 93% compared to 81% for the preparation of the diimidazole **145** and 37% for the two stage preparation of guanidine **150** reported by Wu *et al.*[217] compared to 69% for the one step formation.

With a method for the preparation of the dipiperidinylguanidine **150** in hand the dimorpholinylguanidine analogue **151** was prepared. Thus an excess of morpholine was added to a solution of the diimidazole **145** in dry THF and the mixture boiled under reflux for 15 h. After work-up, the guanidine **151** was obtained as a purple solid in 60% crude yield (Scheme 34).

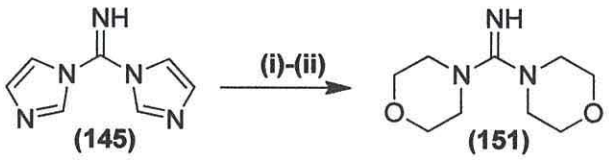

Scheme 34. (i) 5 equiv. morpholine, dry THF, N_2, Δ, 15 h (ii) aq. 2M NaOH, r.t

The crude ^{1}H NMR of **151** gave two triplets at δ 3.26 (8H, J = 4.9 Hz) and 3.76 (8H, J = 4.9 Hz) ppm each corresponding to four CH_2 groups. Their corresponding signals in the ^{13}C NMR were present at δ 47.9 and 66.1, respectively, along with a characteristic quaternary guanidine signal at 166.2 ppm. Unfortunately the guanidine **151** was impure with traces of morpholine which were difficult to remove by evaporation or washing and was thus used in this crude state in the next reaction. High resolution mass spectrometry gave a mass of 200.1392 [(M + H)$^+$] Daltons which is in good agreement with the calculated mass of 200.1394.

With the two tetrasubstituted guandines **150** and **151** now available they were reacted with the ester **50b** under the conditions previously employed. Thus the dipiperidinylguanidine **150** was treated with **50b** in dry dichloromethane over 65 h at r.t. TLC analysis over this period illustrated the reaction was slow and did not go to completion even on the addition of an excess of the guanidine **150**. After work-up, the crude reaction mixture was purified by column chromatography using methanol/ethyl acetate to give **131** as a yellow oil in 29% yield (Scheme 35).

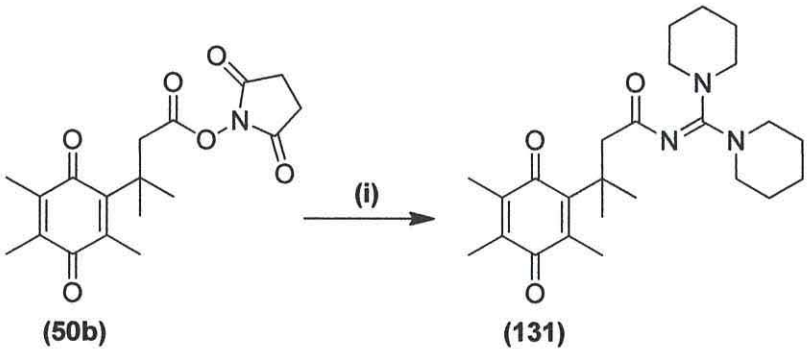

(50b) **(131)**

Scheme 35. (i) 1.5 equiv. **150**, dry CH_2Cl_2, N_2, dark, r.t, 65 h

The ^{1}H NMR of **131** gave diagnostic signals at δ 1.56 (12H, m) for the six CH_2 groups and at 3.12 – 3.15 (8H, m) for the four NCH_2 groups with their corresponding signals in the ^{13}C NMR at 24.1, 25.3 and at 49.8 ppm respectively. This spectrum also contained signals at δ 165.0 corresponding to the quaternary guanidine carbon and at 179.5, 187.6 and 190.5 ppm for the amide and quinone carbonyls respectively. The IR gave bands at 1641 for the C=N and at 1710 cm^{-1} for the carbonyl C=O groups. Finally, high resolution mass spectrometry gave a mass of 428.2908 [(M + H)$^+$] Daltons which is in exact agreement with the calculated mass of 428.2908.

Similarly the dimorpholinylguanidine **151** was reacted with the ester **50b** in dry dichloromethane and stirred in the dark for 46 h at r.t. After work-up and purification by column chromatography, this gave **133** as a yellow oil in 28% yield (Scheme 36).

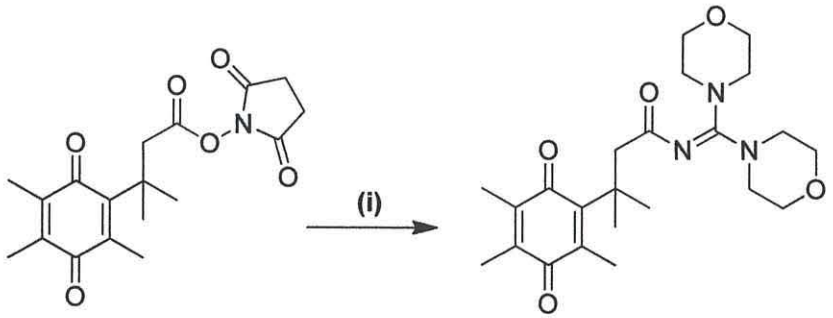

(50b) **(133)**

Scheme 36. (i) 1.5 equiv. **151**, dry CH_2Cl_2, N_2, dark, r.t, 46 h

Analysis by ^1H NMR of **133** gave two triplets at δ 3.22 (8H, J = 4.6 Hz) and at 3.68 (8H, J = 4.7 Hz) ppm each corresponding to four CH_2 groups. In the ^{13}C NMR the signals corresponding to these groups were present at δ 49.0 and 66.1 ppm, respectively. This spectrum also contained other diagnostic signals at δ 164.7 for the quaternary guanidine carbon and 181.2, 187.5 and 190.7 ppm corresponding to the amide and quinone carbonyls respectively. The IR gave bands at 1645 for the C=N and at 1711 cm^{-1} for the C=O bonds. Finally high resolution mass spectrometry gave a mass of 432.2486 $[(M + H)^+]$ Daltons which is in close agreement with the calculated mass of 432.2493.

Neither reaction to form **131** or **133** went to completion, leading to low percentage yields. However, problems have been previously reported[213] detailing the limitations of forming guanidines such as those with two morpholine groups, due to steric factors.

9.1.1 Conclusion

Despite all the problems encountered the methodology on the whole was successful and three candidate guanidine compounds were prepared **129**, **131** and **133** (Figure 49).

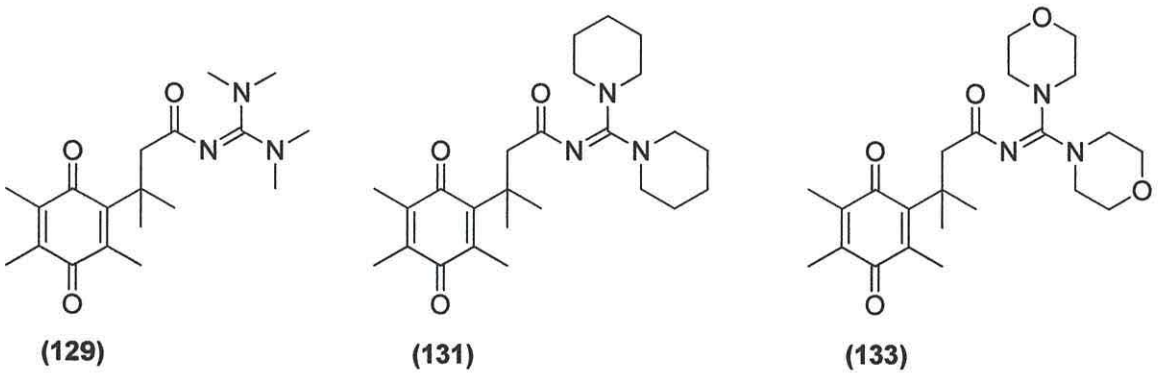

Figure 49. Structures of candidate compounds

9.2 Preparation of a new quinone-based delivery system

Our initial work focused on the preparation of guanidines based on the previously synthesised trimethyl-locked quinone backbone **50** (Scheme 37A) which, on reduction, delivers the drug and the associated lactone **44**. A major goal of the project was to investigate the preparation of a new quinone-based delivery system (Scheme 37B). It was envisaged that replacing the dimethyl section of **50** with a fused phenyl ring to give **118** would potentially offer a new system for delivering the drug which might have differing biological properties.

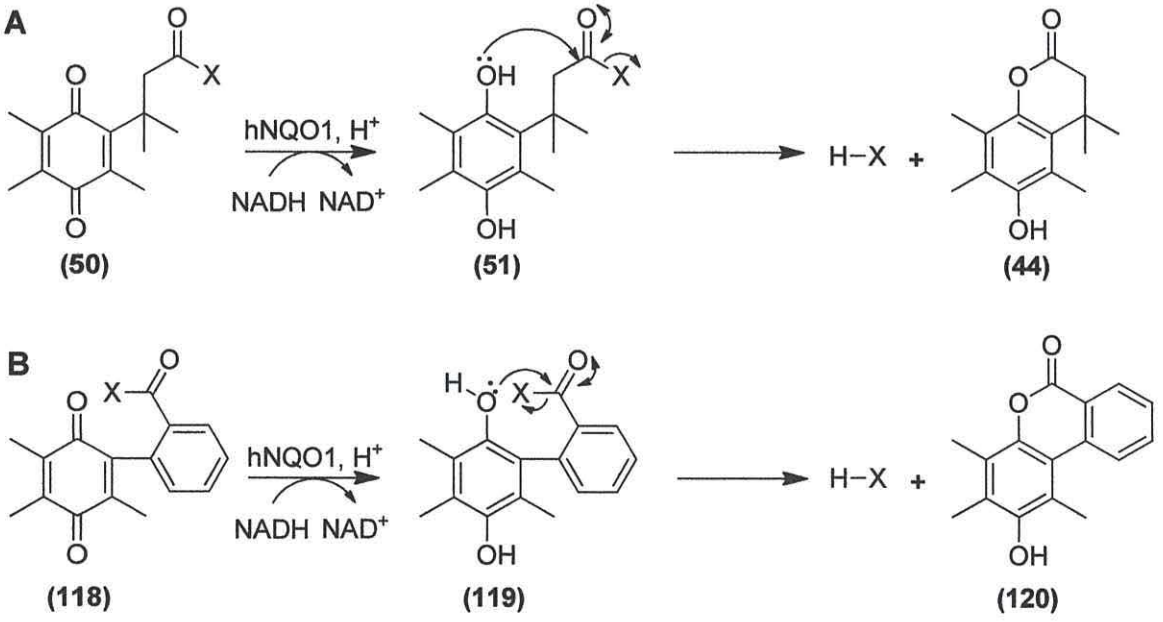

X = guanidine/aniline mustard substituent

Scheme 37. General mechanism of (A) trimethyl-locked and (B) phenyl benzoquinone drug delivery systems

Thus, in order to access the required lactone **120**, a different strategy was required. Investigation of the literature found that Hart *et al.*[220] reported the reaction of protected quinone **152** with lithiated *N*-phenylbenzamide **153** gave the spirolactone **154** which, on treatment with trifluoroacetic acid, trifluoroacetic anhydride and conc. H_2SO_4, gave the lactone **155** *via* a C-migration (Scheme 38). This ring-system is identical to the one required lacking only the methyl substituents. This rearrangment step was potentially a problem as they also reported an O-migration reaction to give the lactone **156** under acidic conditions so there appeared to be the necessity for some method development required to ensure the correct migration pattern.

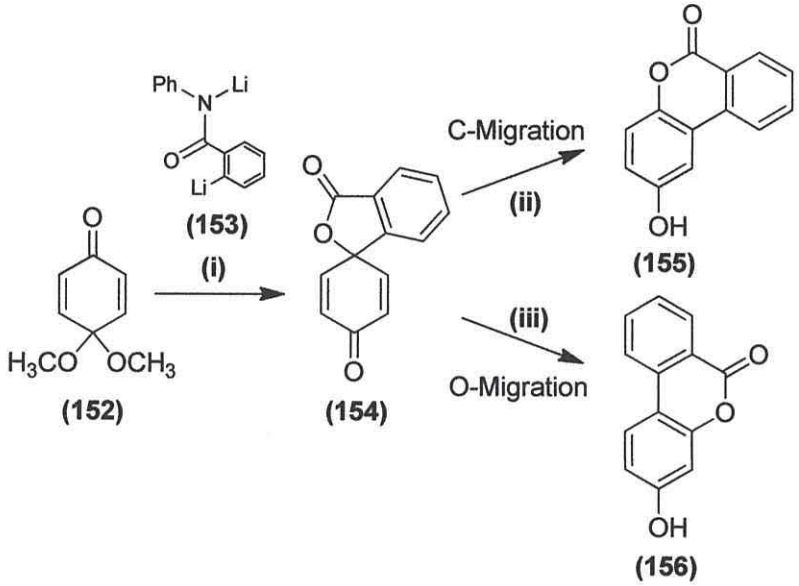

Scheme 38. (i) 0.6 equiv. *N*-phenylbenzamide, 1.5 equiv. *n*-BuLi (1.43M), dry THF, -78 °C, 30 min then 0 °C, 1.5 h then -78 °C, 4 h (ii) CF_3CO_2H, $(CF_3CO)_2O$, conc. H_2SO_4, Δ, 4.5 h (iii) 50% aq. H_2SO_4, Δ, 2 h[220]

In order to access this system, the method needed to be applied to the partially protected quinone **159**[221]. On inspection of the literature, it was found that **159** could be obtained by the selective deprotection of the tetramethylated intermediate **158**[222] which, in turn, could be accessed from the dimethoxybenzene **157**[223] which is easily prepared from the corresponding commercially available dihydroquinone **77** (Scheme 39).

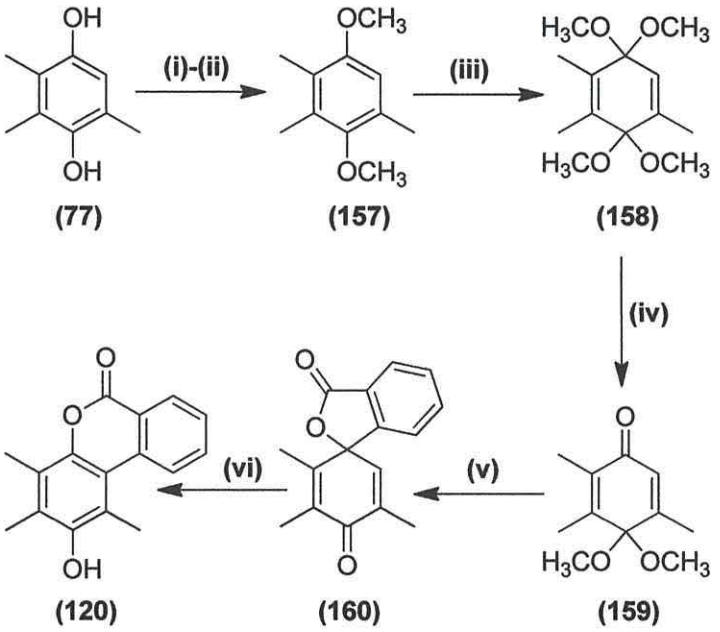

Scheme 39. (i) 5 equiv. K_2CO_3, butan-2-one, r.t, 30 min (ii) 4 equiv. MeI, 65 °C, 72 h (iii) 2% KOH, MeOH, <5 °C, 1 h, 1.6 Amp (iv) 2% aq. CH_3CO_2H, acetone, 0 °C, 25 min then r.t, 1.5 h (v) 0.6 equiv. *N*-phenylbenzamide, 1.5 equiv. *n*-BuLi (1.43M), dry THF, -78 °C, 30 min then 0 °C, 1.5 h then -78 °C, 4 h (vi) CF_3CO_2H, $(CF_3CO)_2O$, H_2SO_4, Δ, 4.5 h

Dimethoxybenzene **157** was prepared by the addition of K_2CO_3 to a stirring solution of 2,3,5-trimethyl-1,4-hydroquinone **77** in butan-2-one at r.t. After 30 min, methyl iodide was added to the mixture which was then heated at 65 °C for 16 h. After work-up and purification by column chromatography, this gave **157** as a clear/colourless oil in 62% yield. Also isolated in some of the later fractions was the quinone by-product **161** (*ca.* 7%) as a waxy yellow solid (Scheme 40) which contributed to the yield being lower than the 82% reported by Lipshutz *et al.*[223]

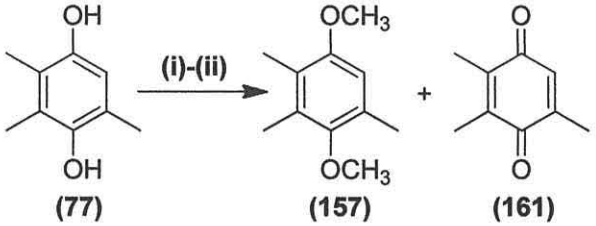

Scheme 40. (i) 5 equiv. K_2CO_3, butan-2-one, r.t, 30 min (ii) 4 equiv. MeI, 65 °C, 16 h

The ^1H NMR spectrum of **157** gave diagnostic signals at δ 3.69 (3H) and 3.81 (3H) corresponding to the two OCH_3 groups which were present at 55.7 and 60.1 ppm in the ^{13}C NMR. All other data were in accordance with the literature.[223]

The second synthetic step involved the electrochemical oxidation of **157** to give the *bis*-ketal **158**. Thus a solution of **157** in 2% methanolic potassium hydroxide was electrolysed in a cell containing a platinum cathode and a carbon felt anode at a current of 1 Amp for 3.5 h at <5 °C (Appendix 2.1). The reaction was monitored throughout by ultraviolet (UV) (first 2 h, Figure 50) and TLC analysis. After work-up, this yielded the *bis*-ketal **158** as a pale yellow solid in 91% yield (Scheme 41). This was a significant improvement in the yield of 63% reported by Henton *et al.*[222]

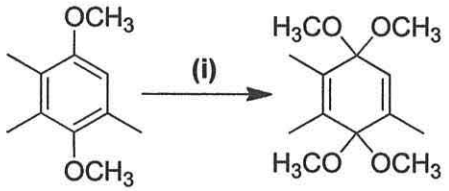

(157) **(158)**

Scheme 41. (i) 2% KOH, MeOH, <5 °C, 3.5 h, 1.0 Amp

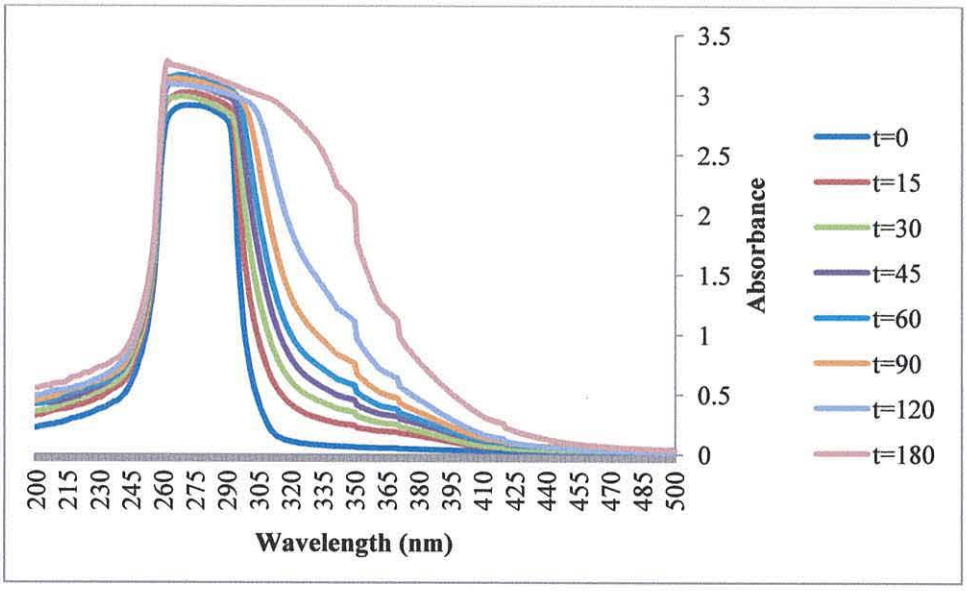

Figure 50. UV spectrum of reaction to form **158** from t = 0 min to t = 180 min

The ^{1}H NMR of **158** gave diagnostic signals at δ 2.96 (6H) and 3.17 (6H) for the four OCH_3 groups and their corresponding signals in the ^{13}C NMR were present at 50.6 and 50.7 ppm respectively. Finally, a melting point of 37 – 41 °C (lit. 34 - 42 °C)[222] was found to be in accordance with the literature.

Selective hydrolysis of the least hindered dimethylketal was achieved by dissolving **158** in acetone at 0 °C and adding a solution of 2% aqueous acetic acid. The resulting mixture was stirred for 25 min at 0 °C and a further 3 h at r.t. After work-up, this yielded the *mono*-

ketal **159** as a yellow solid in 94% yield (Scheme 42). A similar yield of 90% was reported by Henton *et al.*[221]

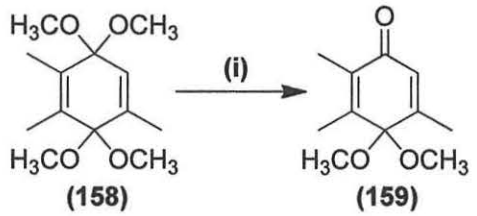

(158) (159)

Scheme 42. (i) 2% aq. CH_3CO_2H, acetone, 0 °C, 25 min then r.t, 3 h

The ^1H NMR of **159** showed the loss of the signal at δ 3.17 (6H) corresponding to two OCH_3 groups which was also apparent in the ^{13}C NMR as the signal at 50.7 was replaced by a signal at 184.7 ppm corresponding to the ketone carbonyl. Finally a melting point of 71 – 74 °C (lit. 74 – 75.5 °C)[221, 224] was found to be in close accordance with the literature.

With the *mono*-ketal **159** in hand the key stage in the synthesis was addressed *viz* the reaction of **159** with lithiated *N*-phenylbenzamide **153** using the method described by Hart *et al.*[220] Thus 2 equivalents (equiv.) of *n*-butyllithium were added to a solution of *N*-phenylbenzamide at -78 °C in dry THF. After stirring for 30 min followed by 1 h at 0 °C, the *mono*-ketal **159** dissolved in dry THF was added at -78 °C. The mixture was maintained at -78 °C for 4 h before warming to r.t. and stirred overnight. After an acidic work-up and column chromatography in diethyl ether/hexane, this gave the spirolactone **160** as white crystals in 22% yield (Scheme 43).

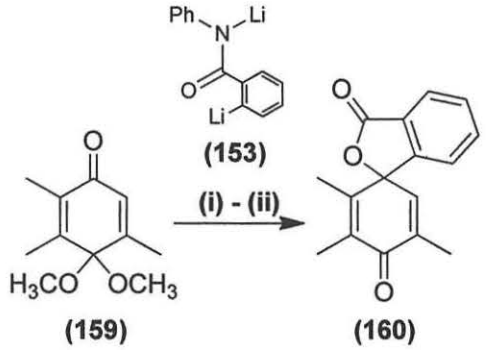

(159) (160)

Scheme 43. (i) 0.9 equiv. *N*-phenylbenzamide, 1.8 equiv. 2.2M *n*-BuLi, dry THF, -78 °C, 30 min then 0 °C, 1.5 h then -78 °C, 4 h then r.t, 12 h (ii) aq. 3M HCl

The initial yield for this step was low and one of the by-products observed in the reaction was 2,3,5-trimethylcyclohexa-2,5-diene-1,4-dione **161** (Figure 51). This had arrived from

direct hydrolysis of the methoxy groups in the *mono*-ketal **159** and would suggest an incomplete lithiation of the *N*-phenylbenzamide.

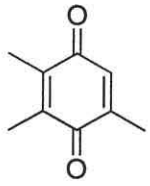

(161)

Figure 51. Structure of 2,3,5-trimethylcyclohexa-2,5-diene-1,4-dione by-product

There were also issues regarding the purification method. Poor solubility in diethyl ether/hexane caused the spirolactone **160** to precipitate out during the column chromatography and remain on the column. On repetition of the reaction chromatography using dichloromethane/petrol gave an improved yield of 49%.

One problem with the reaction was difficulties in separating the desired compound **160** from excess *N*-phenylbenzamide as their Rf values were very close. Thus the reaction was repeated using an excess of the *mono*-ketal **159** to avoid any un-reacted *N*-phenylbenzamide remaining. Using a large excess gave an improved yield of 66% but meant sacrificing a lot of the *mono*-ketal **159** as this underwent deprotection during acid work-up. It was found however by just using a slight excess of **159**, and recrystallising the crude product **160** from diethyl ether/methanol gave white crystals of **160** in 60% yield of very high purity. An X-ray crystal structure of **160** was obtained which confirmed that the proposed spirolactone had been formed (Figure 52, Appendix 2.2.2).

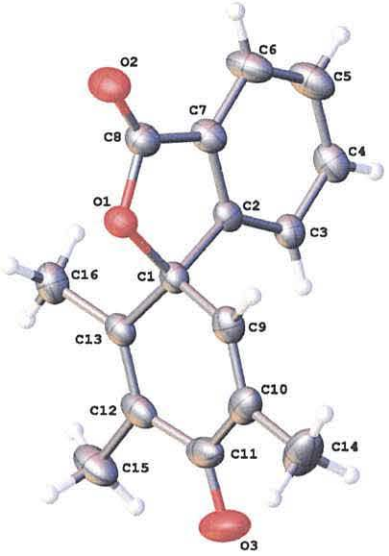

Figure 52. X-ray crystal structure of spirolactone **160**

The ^{1}H NMR of **160** displayed four diagnostic signals at δ 7.16 (1H, d, J = 7.9 Hz), 7.59 (1H, t, J = 7.4 Hz), 7.67 (1H, t, J = 7.6 Hz) and at 7.96 (1H, d, J = 7.6 Hz) ppm for the four aromatic CH groups. The ^{13}C NMR gave signals for the lactone and ketone carbonyls at δ 169.8 and 185.3 ppm, as well as bands at 1647 and 1773 cm^{-1} in the IR for the two carbonyl groups respectively. High resolution mass spectrometry gave a mass of 255.1016 [(M + H)$^{+}$] Daltons which is in exact agreement with the calculated mass of 255.1016.

With the spirolactone **160** in hand, its rearrangement to the desired six-membered lactone **120** was attempted using the method reported by Hart *et al.*[220] Thus spirolactone **160** was dissolved in a mixture of trifluoroacetic acid, trifluoroacetic anhydride and conc. H_2SO_4 and heated at reflux for 5.5 h. After the reaction was quenched with methanol and worked up, purification by column chromatography gave the white crystalline product **120** in 65% yield (Scheme 44), from which an X-ray crystal structure was obtained (Figure 53, Appendix 2.2.3).

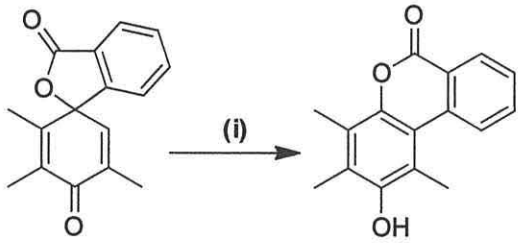

(160) (120)

Scheme 44. (i) CF_3CO_2H, $(CF_3CO)_2O$, conc. H_2SO_4, Δ, 7 h

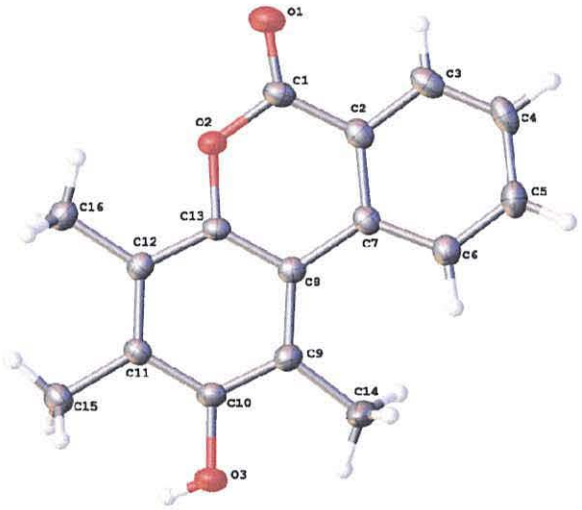

Figure 53. X-ray crystal structure of lactone **120**

This confirmed that the lactone **120** was formed *via* a C-migration process and none of the alternate O-migration product was formed. Repetition of the reaction by increasing the reflux time to 7 h gave a purer product after work-up, which on analysis by NMR was essentially one compound, the lactone **120** obtained in 99% yield.

The ^1H NMR of the lactone **120** was very similar to that of the spirolactone **160**; however, the peak at δ 4.75 (1H) ppm was diagnostic of the phenolic OH. In the ^{13}C NMR, as expected, the carbon signal at δ 83.3 in the spirolactone **160** had disappeared along with the carbonyl signal present at 185.3 ppm. The IR gave bands at 1698 for the ester C=O and 3433 cm^{-1} for the O-H stretch. High resolution mass spectrometry gave a mass of 255.1019 $[(M + H)^+]$ Daltons which is in close agreement with the calculated mass of 255.1016.

With the lactone **120** in hand, the conversion to the activated ester **163** was investigated and carried out in essentially the same manner as for the previously synthesised **50b** (Scheme 45).[73]

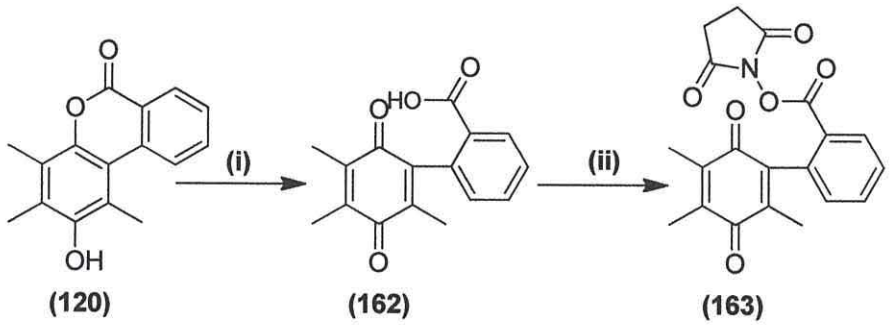

Scheme 45. (i) 1.4 equiv NBS, acetonitrile/H_2O, r.t, 1.5 h (ii) 1.2 equiv. DCC, 1.1 equiv. NHS, THF, 0 °C then r.t, 18 h

Thus addition of NBS to a stirring solution of the lactone **120** in acetonitrile/water after work-up and column chromatography gave the quinone acid **162** as a waxy yellow solid in 71% yield (Scheme 46).

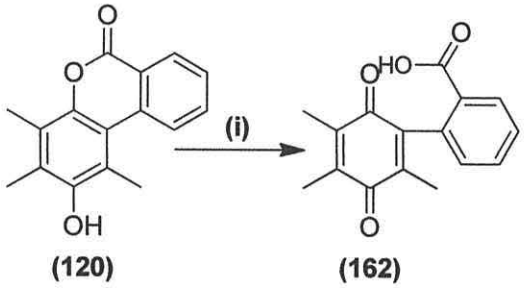

Scheme 46. (i) 1.4 equiv. NBS, acetonitrile/H_2O, r.t, 1.5 h

Analysis of the ^{13}C NMR of **162** gave diagnostic signals at δ 170.8, 186.2 and 187.9 ppm for the acid and two quinone carbonyls respectively. Similarly the IR spectrum gave bands at 1649, 1693 and 1721 for the three C=O groups, coupled with a band at 3263 cm^{-1} for the carboxylate OH bond. High resolution mass spectrometry gave a mass of 269.0817 [$(M - H)^+$] Daltons which is in good agreement with the calculated mass of 269.0819.

In this first attempt at the reaction it was apparent from the crude ^{1}H NMR that a second product was present which was also isolated by column chromatography as a white crystalline solid. The identity of the structure was determined by X-ray crystallography and was found to be a brominated spirolactone **164** (Figure 54, Appendix 2.2.4).

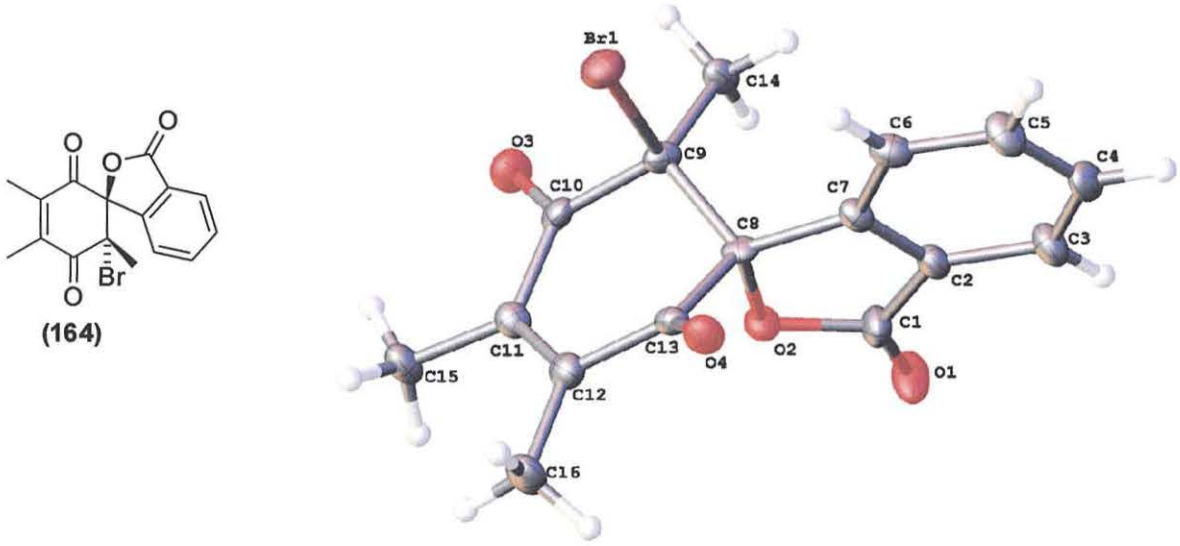

Figure 54. Chemical and X-ray crystal structure of brominated spirolactone **164**

This has obviously arisen from a bromolactonisation reaction and the structure was further confirmed by the presence of quaternary signals in the ^{13}C NMR spectrum at δ 61.5 and 90.4 ppm for the two non-aromatic ring carbons. High resolution mass spectrometry gave a mass of 349.0070 $[(M + H)^{+}]$ Daltons which is in exact agreement with the calculated mass of 349.0070. On repetition of the reaction the NBS used was freshly recrystallised[225] and this product was effectively eliminated and the reaction yield increased to 77%.

With the quinone acid **162** in hand the conversion to the ester **163** was investigated in a similar manner to the previously prepared **50b**.[73] Thus DCC was added to a solution of the quinone acid **162** and NHS in dry THF and after 18 h stirring followed by work-up gave the crude product **163** as a yellow gum (Scheme 47). Attempts to recrystallise the product were met with failure as did attempts to purify using column chromatography which gave the desired compound **163** in an impure form and in a very low yield of 28%.

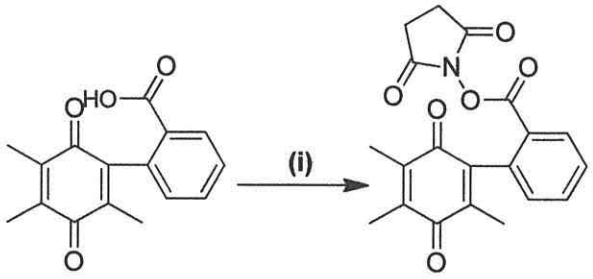

(162) (163)

Scheme 47. (i) 1.2 equiv. DCC, 1.1 equiv. NHS, dry THF, 0 °C then r.t, 18 h

Analysis of the ^{1}H NMR of the ester **163** gave a diagnostic signal at δ 2.81 (4H) for the two succinimidyl CH_2 groups which were also present in the ^{13}C NMR at 25.5 ppm. Other diagnostic signals in this spectrum were present at δ 161.5 for the ester C=O and 168.8 ppm for the two succinimidyl C=O groups. The IR gave bands at 1649, 1683, 1741 and 1772 cm^{-1} for the four C=O bonds. High resolution mass spectrometry gave a mass of 368.1130 $[(M + H)^{+}]$ Daltons which is in close agreement with the calculated mass of 368.1129. With the problems encountered in its purification it was decided to attempt to prepare and react the ester **163** *in situ*.

9.3 Preparation of phenyl quinones

Thus the reaction was repeated and on completion (TLC) the solution was filtered evaporated and re-dissolved in dry THF whereupon 1,1,3,3 tetramethylguanidine **144** was added and the reaction stirred in the dark for 46 h at r.t. After work-up and purification by column chromatography the tetramethylguanidine **130** was obtained as a yellow oil in 53% yield (Scheme 48).

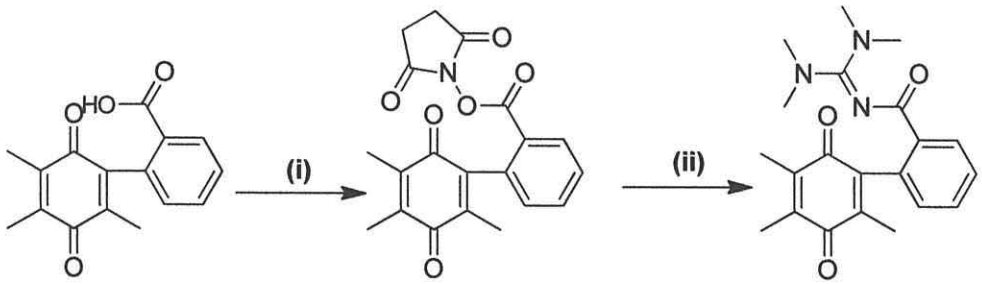

(162) (163) (130)

Scheme 48. (i) 1.2 equiv. DCC, 1.1 equiv. NHS, dry THF, 0 °C then r.t, 18 h (ii) 2 equiv. **144**, dry THF, N_2, dark, r.t, 46 h

The ^{1}H NMR of **130** gave diagnostic signals at δ 2.83 (12H) for the four guanidine CH_3 groups which were also present in the ^{13}C NMR at 40.1 ppm. Further diagnostic signals included the characteristic guanidine signal at δ 167.3 and amide carbonyl at 171.9 ppm. The IR displayed bands at 1648 for the C=N and 1727 cm^{-1} for the C=O groups. High resolution mass spectrometry data gave a mass of 368.1963 $[(M + H)^{+}]$ Daltons which is good agreement with the calculated mass of 368.1969.

The corresponding dipiperidinylguanidine **132** was prepared in a similar fashion and as before the ester **163** was prepared *in situ* and dissolved in dry THF, whereupon the guanidine **150** was added and the reaction stirred in the dark for 46 h at r.t. After work-up and purification by column chromatography the dipiperidinylguanidine **132** was obtained as a yellow oil in 21% yield (Scheme 49). Also recovered was the ester **163** as a yellow oil in 59% yield.

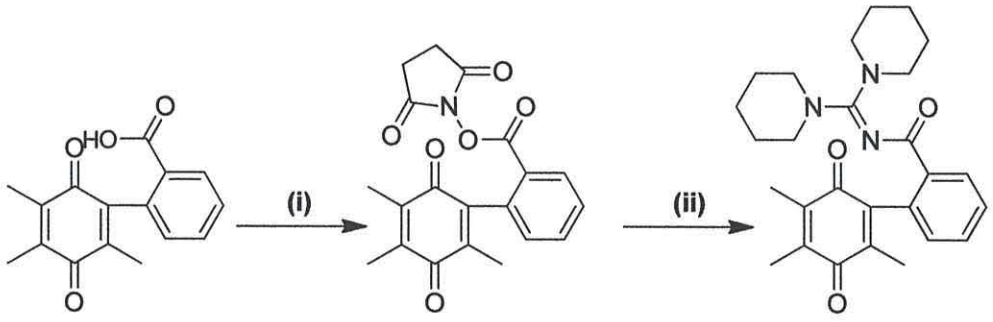

(162) **(163)** **(132)**

Scheme 49. (i) 1.2 equiv. DCC, 1.1 equiv. NHS, dry THF, 0 °C then r.t, 18 h (ii) 3 equiv. **150**, dry THF, N_2, dark, r.t, 46 h

The ^{1}H NMR of **132** gave diagnostic signals at δ 1.55 (12H) and 3.15 (8H) for the piperidinyl CH_2 groups which were also apparent at 24.4, 25.5 and 49.8 ppm in the ^{13}C NMR. In addition, the characteristic quaternary guanidine signal was present at δ 166.5 and amide carbonyl at 172.3 ppm. The IR displayed bands at 1647 for the C=N and 1732 cm^{-1} for the carbonyl groups. Finally, high resolution mass spectrometry gave a mass of 448.2592 $[(M + H)^{+}]$ Daltons which is in close agreement with the calculated mass of 448.2595.

The corresponding dimorpholinylguanidine analogue **134** was prepared from the ester **163** which was generated *in situ* and dissolved in dry THF, whereupon the guanidine **151** was added and the reaction stirred in the dark for 46 h at r.t. After work-up and purification by

column chromatography the guanidine **134** was obtained as a yellow oil in 42% yield (Scheme 50). Again the ester **163** was recovered as a yellow oil in 32% yield.

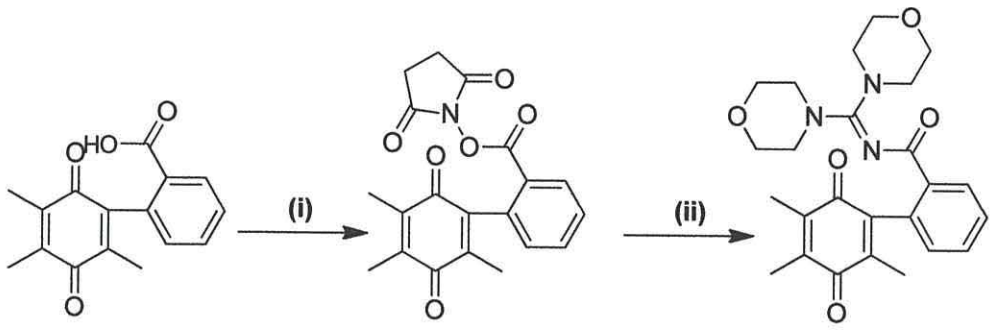

(162) **(163)** **(134)**

Scheme 50. (i) 1.2 equiv. DCC, 1.1 equiv. NHS, dry THF, 0 °C then r.t, 18 h (ii) 3 equiv. **151**, dry THF, N_2, dark, r.t, 46 h

The ^{1}H NMR of **134** gave diagnostic signals at δ 3.28 (8H) and 3.70 (8H) each corresponding to four morpholinyl CH_2 groups which were also present in the ^{13}C NMR at 49.1 and 66.1 ppm. The spectrum also contained a quaternary guanidine signal present at δ 164.7 and amide carbonyl at 173.2 ppm. The IR gave bands at 1646 for the C=N and 1726 cm^{-1} for the C=O groups and high resolution mass spectrometry gave a mass of 452.2180 $[(M + H)^+]$ Daltons which is in exact agreement with the calculated mass of 452.2180.

9.3.1 Conclusion

As with the trimethyl-locked dipiperidinyl **131** and dimorpholinyl **133** guanidines, the two corresponding reactions with the phenyl system did not go to completion. Interestingly, it was possible to isolate unreacted ester **163** as a by-product during the purification of guanidines **132** and **134**. This contrasts with attempts to isolate **163** when directly formed (Scheme 47). This is possibly due to excess guanidine in the reaction mixtures acting as a base to neutralise acidic sites on the silica, however this is a tenuous supposition. Despite these problems three candidate guanidine compounds were prepared **130**, **132** and **134** utilising the phenyl quinone backbone (Figure 55).

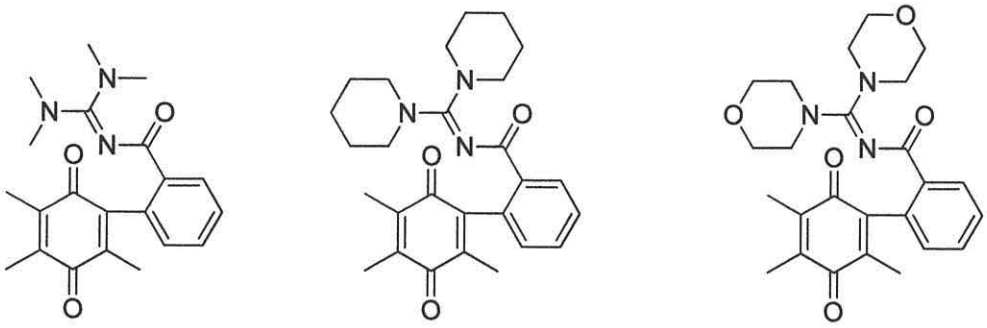

(130) (132) (134)

Figure 55. Structures of candidate compounds

9.4 Mustard reactions

With the successful preparation of the six guanidine derivatives, it was envisaged that the previously reported[73] aniline mustard prodrug **78** would be required as a standard for biological assays. Its preparation was thus investigated with the required aniline mustard starting material **76** prepared *via* a two-step synthesis[226, 227] from the available precursor **165** (Scheme 51).

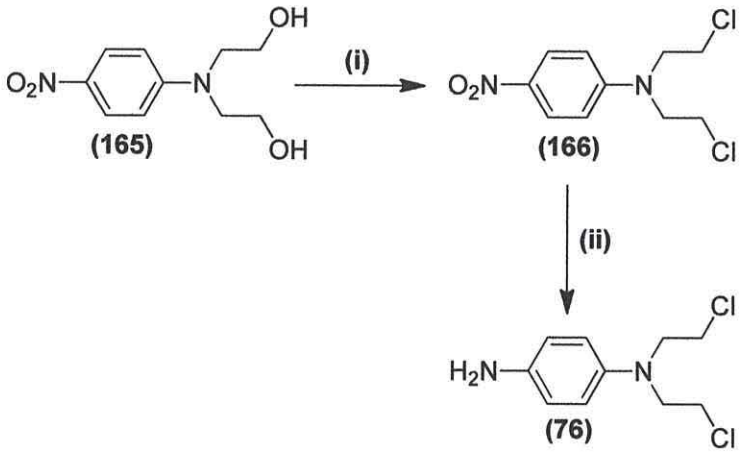

Scheme 51. (i) 1.8 equiv. pyridine, 2.3 equiv. $SOCl_2$, CH_2Cl_2, 0 °C then Δ, 1 h (ii) Pd (10%) on C, EtOH, H_2, r.t, 23 h

Thus the diol **165** was dissolved in dry dichloromethane and pyridine at 0 °C and treated with $SOCl_2$ and the mixture was boiled under reflux for 1 h. After work-up, the crude product was purified by column chromatography to yield **166** as yellow crystals in ~50% yield (Scheme 52).

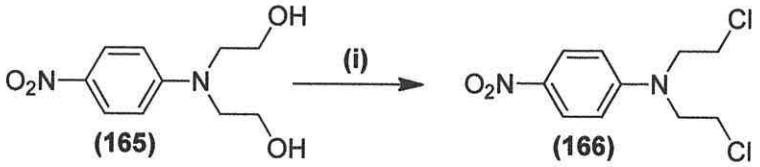

Scheme 52. (i) 1.8 equiv. pyridine, 2.3 equiv. $SOCl_2$, dry CH_2Cl_2, 0 °C then Δ, 1 h

The ^1H NMR of the nitromustard **166** gave two triplets at δ 3.70 (4H, J = 6.9 Hz) and 3.87 (4H, J = 6.9 Hz) for the four CH_2 groups and two doublets at 6.68 (2H, J = 9.5 Hz) and 8.15 (2H, J = 9.1 Hz) ppm corresponding to the AA'BB' pattern of the aromatic ring. In the ^{13}C NMR, signals for the four CH_2 groups were apparent at δ 39.9 and 53.3 and for the aromatic CH's at 110.7 and 126.4, with the remaining quaternary carbons present at 138.4 and 151.2 ppm respectively. High resolution mass spectrometry data gave a mass of 263.0355 [$(M + H)^+$] Daltons which is in close agreement with the calculated mass of 263.0349. Finally the melting point of 92 – 93 °C (lit. 95 - 96 °C)[228] was found to be in accordance with the literature.

Other fractions from the chromatography process demonstrated the presence of two further by-products (Figure 56). The first was found to be the monosubstituted compound **167** as a yellow solid (*ca.* 5%) which was identified from its ^1H NMR with the main diagnostic signals being a broad singlet at δ 1.71 (1H) for the OH group and a triplet at 3.90 (2H, J = 5.2 Hz) ppm for the CH_2-OH group. In the ^{13}C NMR there were four CH_2 signals present at δ 39.7, 53.4, 53.7 and 59.9 ppm respectively and the IR gave an O-H stretch at 3486 cm^{-1}. Finally high resolution mass spectrometry gave a mass of 245.0686 [$(M + H)^+$] Daltons which is in close agreement with the calculated mass of 245.0687. A second compound was isolated and, from the high resolution mass spectrometry, a mass of 273.0542 [$(M + H)^+$] Daltons was observed which corresponds to a chemical formula of $C_{10}H_{13}O_5N_2S$ which is calculated as 273.0540. It was thus proposed that the reaction had formed the 1,3,2,6-dioxathiazocane-2-oxide ring system and the structure was in fact **168**, isolated as a yellow solid in *ca.* 5% yield.

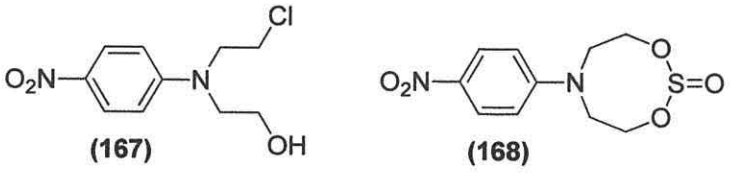

Figure 56. Structure of mono and sulfite by-products

Investigation of the literature indicated that this compound had not been reported previously, however its *m*-NO_2 isomer was reported in a similar reaction (Figure 57).[229]

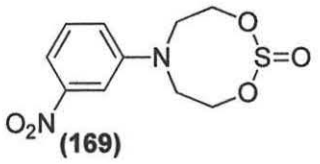

(169)

Figure 57. Structure of sulfite isomer of **168**

The initial yield for this reaction was 50% and it is likely that compounds **167** and **168** are possible intermediates in the synthesis of the desired product **166**. Repeating the reaction under reflux for 7 h and increasing the amount of pyridine gave an improved yield of 80% for the nitro mustard **166**. No sulfite **168** was found to be present and only a small amount, <1% of the mono compound **167** was isolated. It is apparent that the yield of 98% reported by the literature[227] was accomplished without additional purification since none of these by-products were mentioned.

The final stage in the preparation of **76** involved the hydrogenation of the nitro group in **166** which was accomplished by stirring a solution of **166** in ethanol with 5% Pd on carbon under an atmosphere of hydrogen for 17 h. After filtration through celite, the crude product was purified by column chromatography (isolated in 50% ethyl acetate/petrol) to yield the aniline mustard **76** as a brown oil in 68% yield (Scheme 53), the same yield as reported in the literature.[227]

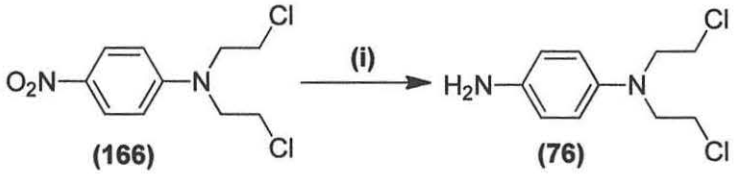

(166) **(76)**

Scheme 53. (i) Pd (5%) on C, EtOH, H_2, r.t, 17 h

Analysis of the ^{1}H NMR of **76** demonstrated the appearance of a broad singlet at δ 5.13 (2H) ppm corresponding to the aniline NH_2 whilst high resolution mass spectrometry gave a mass of 233.0609 $[(M + H)^+]$ Daltons which is in close agreement with the calculated mass of 233.0607. Further analysis of the higher running column fractions gave another compound which had an interesting set of signals in the ^{13}C NMR. These corresponded to four CH_2 environments at δ 42.3, 51.0, 51.6 and 53.6, four aromatic CH environments at

114.4, 115.7, 118.9 and 119.1 together with four quaternary carbon atoms at 141.1, 143.2, 143.3 and 144.1 ppm. On analysis by high resolution mass spectrometry a mass of 393.1609 [$(M + H)^+$] Daltons was obtained which is in close agreement with the formula $C_{20}H_{27}N_4Cl_2^{35}$ which requires 393.1607. In addition the isotope pattern is indicative of a dichloride with a pattern of 393.16 (100%), 395.16 (~64%) and 397.15 (~10%). Analysis of the ^1H NMR spectrum indicated the presence of two AA'BB' patterns at δ 6.56 (2H, d, J = 8.8 Hz), 6.74 (2H, d, J = 9.2 Hz), 6.78 (2H, d, J = 8.8 Hz) and 6.94 (2H, d, J = 9.1 Hz), ppm which suggested the presence of two aromatic ring systems. With this evidence in hand the structure **170** was proposed (Figure 58).

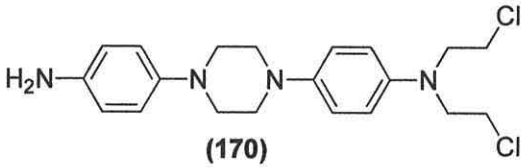

(170)

Figure 58. Structure of piperidine mustard

This mustard **170** has not been reported before and was isolated from the reaction mixture as a brown solid in 32% yield. Attempts to grow crystals suitable for X-ray analysis were unsuccessful as **170** appeared to be unstable and decomposed at room temperature on standing. Upon repeat of this reaction the required aniline mustard **76** was obtained in high yields (58 - 68%) but the by-product **170**, although always present, was only ever isolated in low yield (≤5%).

With the aniline mustard **76** in hand, it was coupled to the ester **50b** in dry THF over 21 h at r.t which after column chromatography gave the prodrug **78** as an orange solid in 65% yield (Scheme 54).

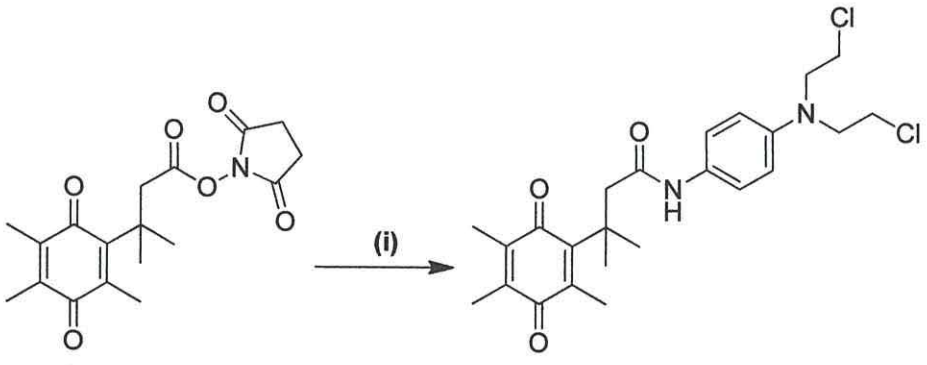

(50b) **(78)**

Scheme 54. (i) 2.8 equiv. **76**, dry THF, N_2, dark, r.t, 21 h

The ^{1}H NMR and ^{13}C NMR data of **78** was in excellent agreement with the reported values[73] and high resolution mass spectrometry gave a mass of 465.1705 $[(M + H)^{+}]$ Daltons which is in close agreement with the calculated mass of 465.1706. Finally a melting point of 80 – 84 °C (lit. 87 – 89 °C)[73] was found to be in accordance with the literature. There was a small improvement in the yield (57% to 65%) compared to that reported by Volpato *et al.*[73]

The next stage was to prepare the corresponding prodrug containing the phenyl quinone backbone **135**. Thus the ester **163** was added to a solution of the aniline mustard **76** in dry THF and stirred in the dark for 25 h at r.t. Upon work-up the crude product was purified by column chromatography to give a low yield of a compound which appeared to correspond to the desired product **135** on initial inspection of the NMR data (Scheme 55).

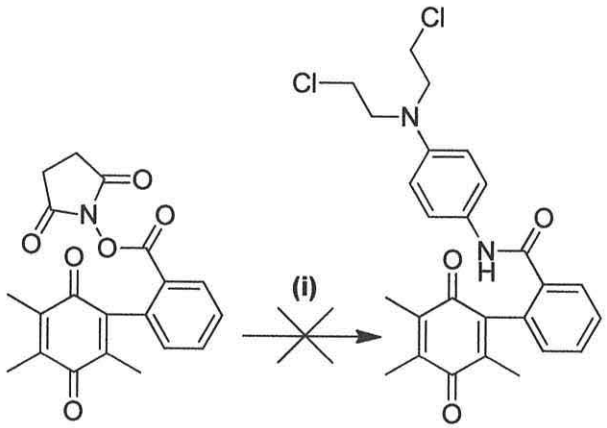

Scheme 55. (i) 3 equiv. **76**, dry THF, N_2, dark, r.t, 25 h

However on inspection of the high resolution mass spectrometry data, a mass of 600.1660 $[(M + H)^{+}]$ Daltons for the major ion was obtained which is considerably larger than the mass of 485.1393 calculated for **135** ($C_{26}H_{27}O_3N_2Cl_2^{35}$). On consideration of this mass it was apparent it corresponded to a formula $C_{30}H_{32}O_6N_3Cl_2^{35}$ $[(M + H)^{+}]$ which requires 600.1663. From this information it was possible to propose that the succinimidyl ester was still incorporated in the molecule. The proposed structure of this compound is **171** (Figure 59) and for this reaction outcome the amine nucleophile must have reacted at the imide carbonyl rather than displacing the NHS and forming an amide.

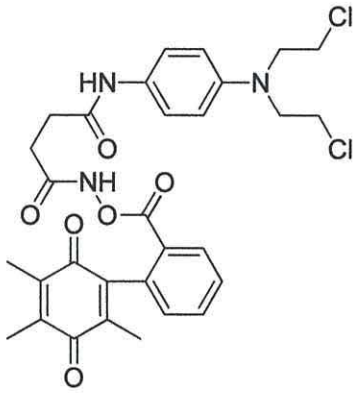

(171)

Figure 59. Structure of N^1-(4-(*bis*(2-chloroethyl)amino)phenyl)-N^4-((3',4',6'-trimethyl-2',5'-dioxo-2',5'-dihydro-[1,1'-biphenyl]-2-carbonyl)oxy)succinamide

Analysis of the ^{1}H NMR confirmed this by the presence of signals which might be expected for the desired product **135** but with the additional broad singlet at δ 2.69 (4H) ppm corresponding to the two succinimidyl CH_2 groups (Figure 60).

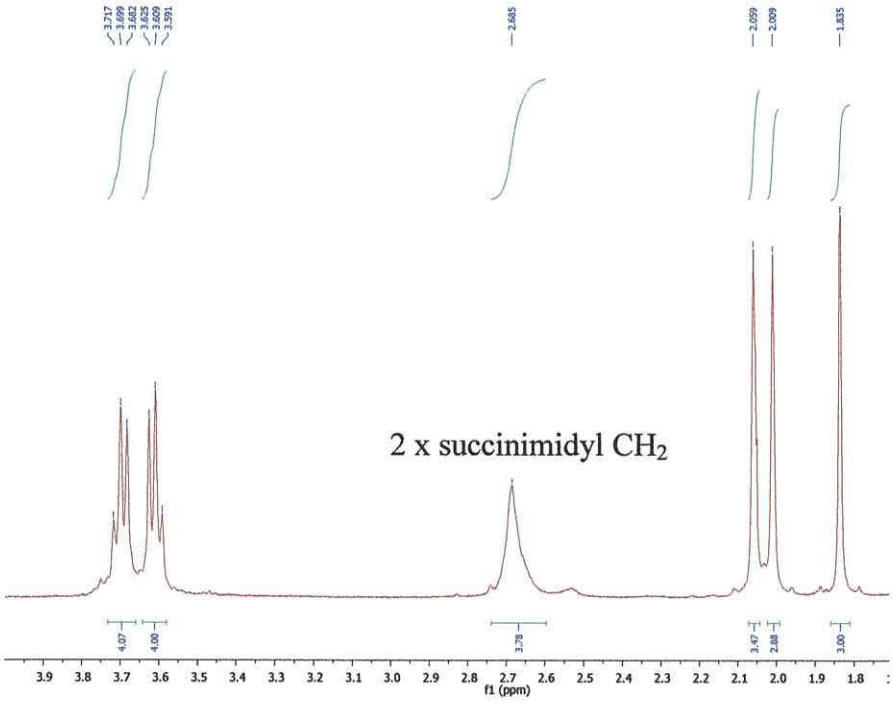

Figure 60. 400 MHz ^{1}H NMR spectrum expansion of **171**

In addition two NH signals were apparent at δ 7.57 (1H) and 9.86 (1H) ppm instead of the expected one signal. In the ^{13}C NMR, the succinimidyl CH_2 groups were present at δ 29.7 ppm. This mustard **171** was isolated in 24% yield and no other major products could be found. There appears to be no literature precedence for this type of reaction and time

constraints prevented further research on this reaction, however, this is an avenue that can be explored in the future.

9.5 Miscellaneous reactions

The preparation of two additional prodrugs was attempted, the first of which was derived from an interest in the by-product **170**, isolated during the reaction to form the aniline mustard **76** (Scheme 53, p.84). The reaction to form prodrug **136** was attempted by adding the ester **50b** to a solution of the mustard **170** in dry THF and stirring the mixture in the dark for 21 h at r.t (Scheme 56). After work-up attempts to purify the multi-spot mixture were unsuccessful. As the mustard **170** was only formed in trace amounts in subsequent reactions, a repeat of the reaction was not attempted.

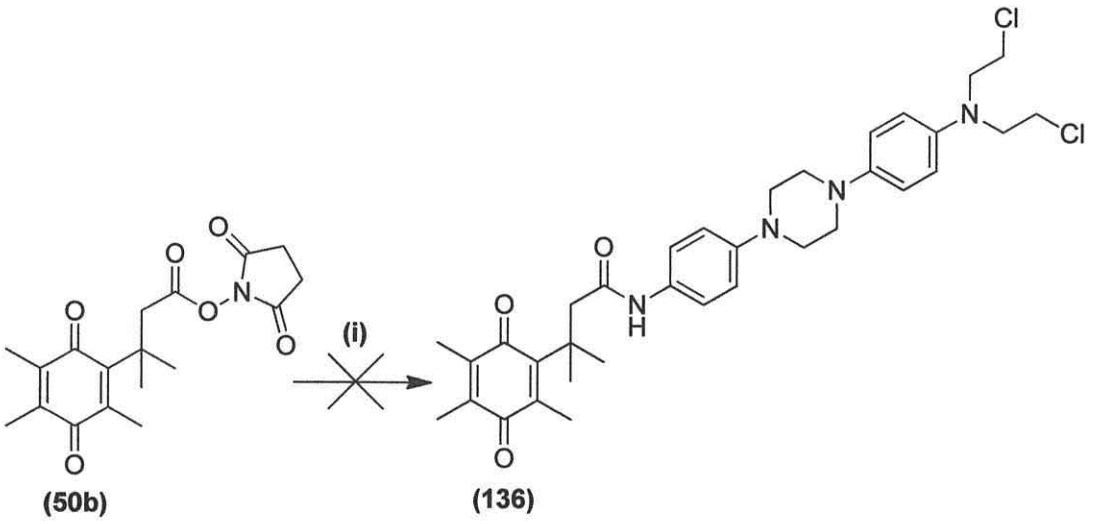

Scheme 56. (i) 0.7 equiv. **170**, dry THF, N_2, dark, r.t, 21 h

Despite this failure, the interesting mustard **170** might be worthy of further study and a method for optimising its formation could be sought.

In addition, an attempt was made to synthesise the prodrug **172** which incorporates tirapazamine **10** by adding the ester **50b** to a solution of tirapazamine **10** in dry *N*,*N*-dimethylformamide (DMF) and stirring for 72 h in the dark at r.t. (Scheme 57). However no reaction was apparent by TLC.

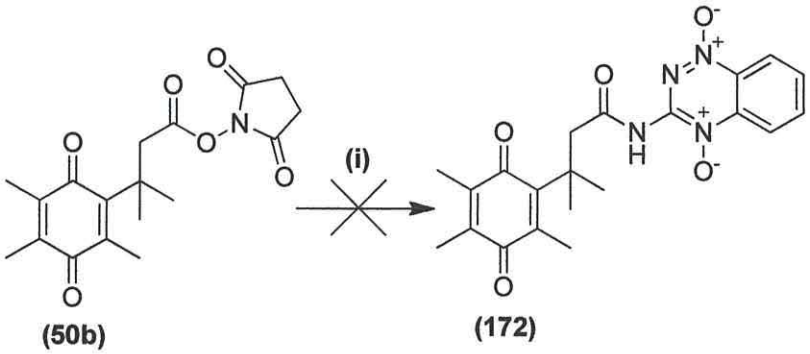

Scheme 57. (i) 1.5 equiv. **10**, dry DMF, N_2, dark, r.t, 72 h

One issue with this reaction was the poor solubility of the tirapazamine **10**, with DMF being the only solvent able to dissolve it. The presence of the two *N*-oxy functional groups also leads to a deactivation of the NH_2 group towards nucleophilic substitution. No further attempts at this reaction were undertaken.

10.0 Enzymatic evaluation

This section describes the enzymatic evaluation of the trimethyl-locked guanidine **129** and phenyl guanidine **130** as substrates for the enzyme hNQO1 using HPLC analysis.

10.1 Enzymatic evaluation of 129

The objective of this section is to provide mechanistic proof that the trimethyl-locked guanidine **129** can undergo two-electron reduction *via* the pathway shown in scheme 58.

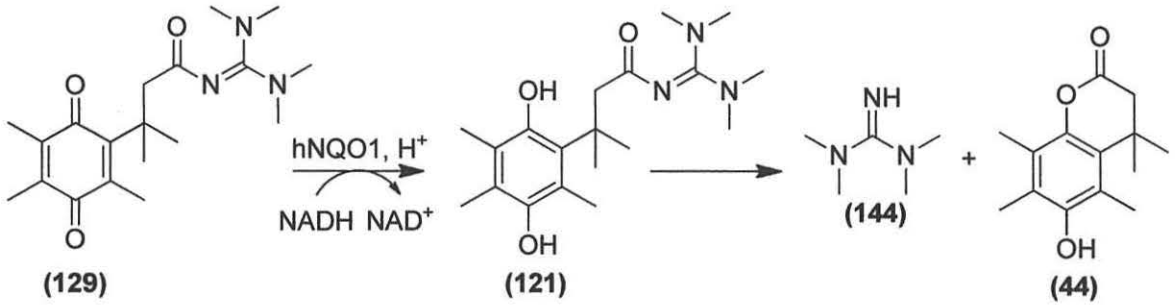

Scheme 58. Postulated enzymatic hNQO1 reaction of the guanidine in the presence of NADH

In the presence of NADH **35** and hNQO1, the substrate **129** can undergo a two-electron reduction process (Section 3.2, p.10-12) to afford the hydroquinone species **121**. This species **121** then performs an intramolecular cyclisation reaction to give the free guanidine **144** and the lactone **44** as the by-product.

10.2 Enzymatic activity of 129

A reaction containing the substrate **129** (100 μM) and NADH (500 μM) in phosphate buffer (10 mM, pH 7) was started by the addition of 0.5 μg hNQO1. The reaction was monitored using HPLC, eluting with a gradient of 10-99% acetonitrile/water and an injection volume of 2 μl. The temperature was maintained at 37 °C and the reaction was monitored over a period of 80 min (taking readings at every 10 min). The depletion of the substrate **129** and the formation of the lactone **44** was monitored at 240 nm. A control experiment was also included (same apart from a period of 77 min and readings every 7 min) in which no enzyme was added to the substrate. All other parameters were maintained the same, in effect this is also a stability experiment for the substrate **129** (Appendix 3.1). These enzymatic experiments were performed in triplicates whereby three independent experiments were carried out (Appendix 3.2). Chart 1 below illustrates the

depletion of the substrate **129** and formation of the lactone **44** over the 80 min period. In addition, the depletion of NADH **35** was also monitored at 340 nm (Chart 2).

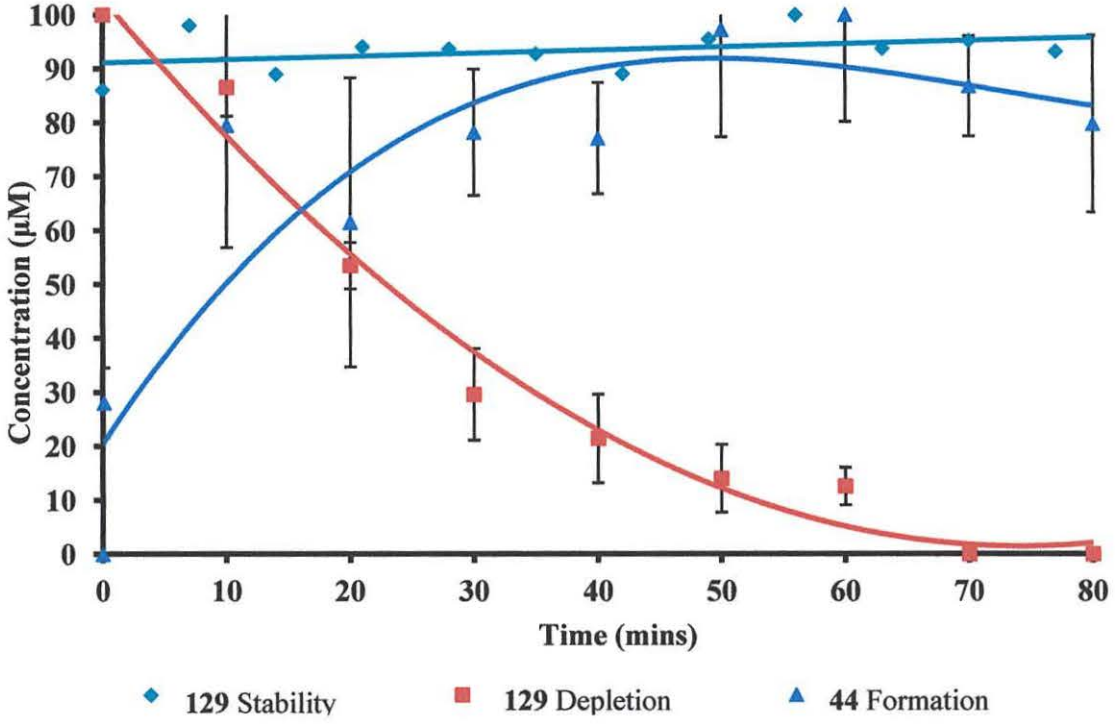

Chart 1. Concentration-time plot showing stability data of the guanidine **129** in the absence of hNQO1 and enzymatic data showing the depletion of the guanidine **129** and formation of the lactone **44** in the presence of hNQO1

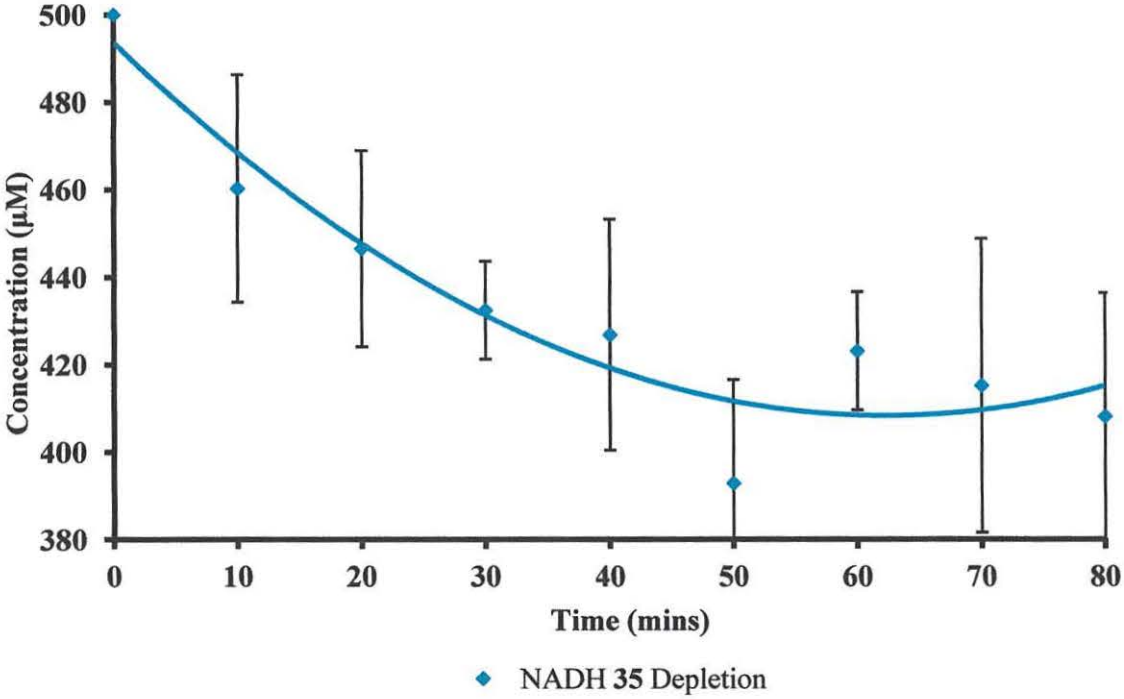

Chart 2. Concentration-time plot showing the depletion of the NADH **35** during the enzymatic study

Chart 1 shows that in the presence of the enzyme there is a correlation between the depletion of substrate **129** and formation of the lactone **44**, with their respective rates calculated as 2.74 and 2.41 μM/min.

10.3 Enzymatic evaluation of 130

The objective of this section is to provide mechanistic proof that the phenyl guanidine **130** can undergo two-electron reduction *via* the pathway shown in scheme 59 and outlined previously for guanidine **129** in scheme 58.

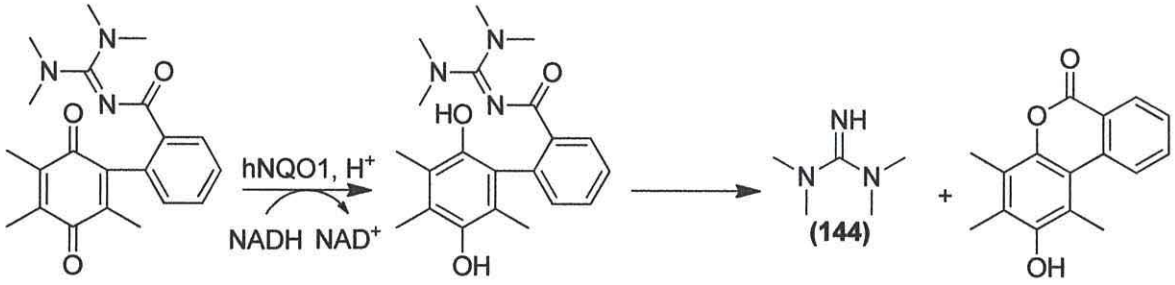

Scheme 59. Postulated enzymatic hNQO1 reaction of the guanidine in the presence of NADH

10.4 Enzymatic activity of 130

A reaction was carried out in the same manner as the previously analysed guanidine **129**; however this time a 2-99% acetonitrile/water gradient was used with an injection volume of 10 μl and readings every 20 min. The formation of the lactone **120** was monitored at 260 nm (Appendix 3.3 and 3.4). From these data, chart 3 and chart 4 were plotted.

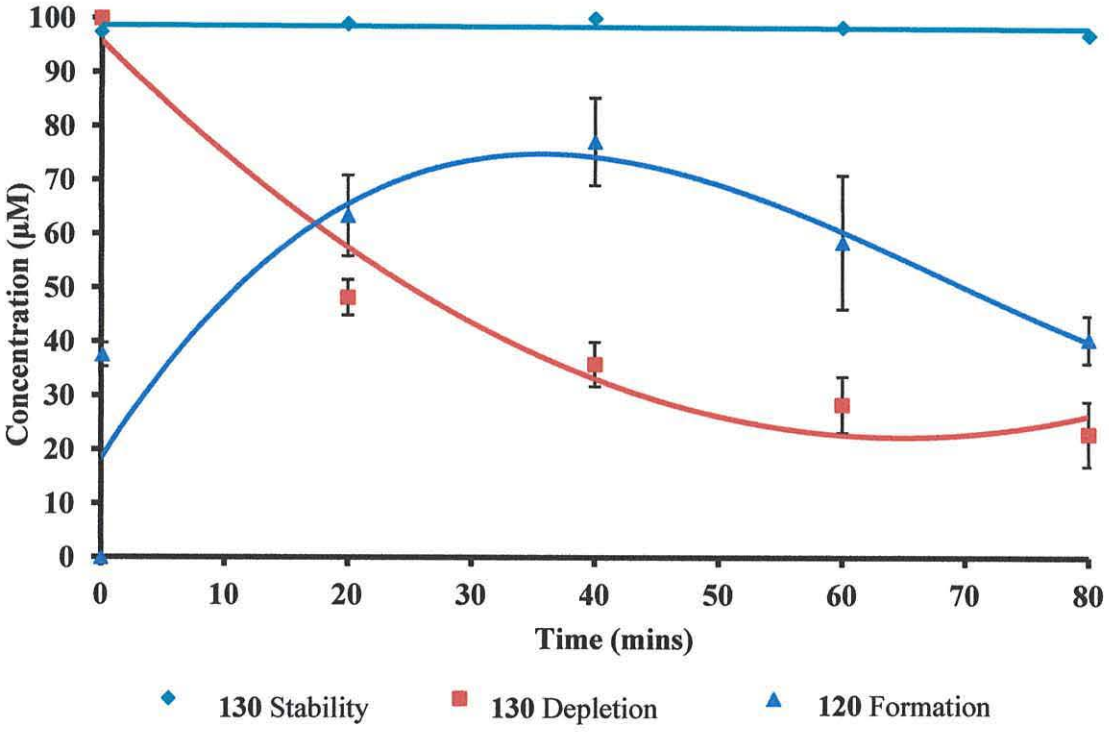

Chart 3. Concentration-time plot showing stability data of the guanidine **130** in the absence of hNQO1 and enzymatic data showing the depletion of the guanidine **130** and formation of the lactone **120** in the presence of hNQO1

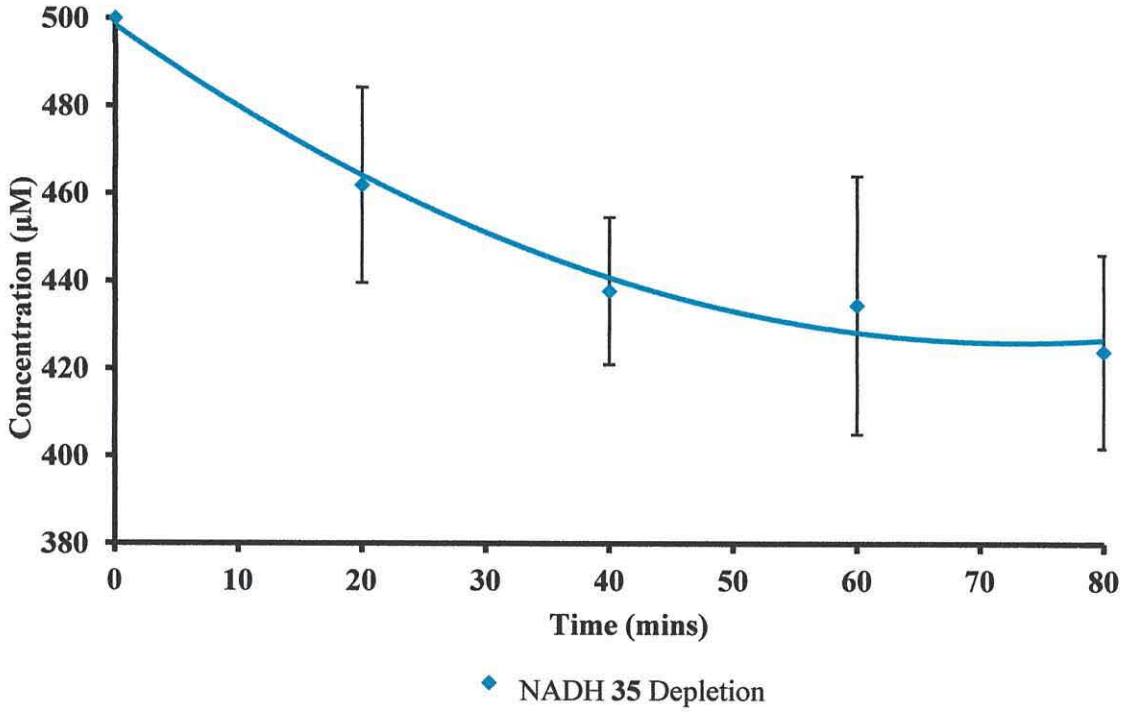

Chart 4. Concentration-time plot showing the depletion of the NADH **35** during the enzymatic study

Chart 3 indicates that the correlation between formation and depletion observed for **129/44** was not observed for **130/120** with the rates calculated as 2.26 and 3.59 μM/min respectively. In addition this reaction did not proceed to completion. The lactone **120** concentration (μM) was found to decrease after 40 min due to poor solubility in the phosphate buffer, even with an additional 5% dimethyl sulfoxide (DMSO) added to the solution.

10.5 Conclusion

In the absence of the enzyme, the substrates **129** and **130** are stable for up to 80 min (duration of the experiment). These results suggest that, as predicted by molecular modelling both **129** and **130** are good substrates for the enzyme hNQO1. It was not possible to monitor the formation of the free guanidine **144** due to its high polarity. Nevertheless, these experiments indicate that mechanistically, upon enzymatic activation, guanidines **129** and **130** undergo reduction to the hydroquinones **121** and **124**, which in turn undergo intramolecular cyclisation. These preliminary findings indicate that the trimethyl-locked guanidine **129** has a faster rate of depletion, 2.74 μM/min compared with the phenyl guanidine **130**'s 2.26 μM/min (see p.102 for further details on the method).

11.0 *In vitro* cytotoxicity evaluation

Compounds **129**, **131** and **133** were assayed against the cancer cell lines F179 and hDT7 as were the guanidines **144**, **150** and **151** (Table 13) (for method see p.103). F179 is a cloned cell line which does not contain hNQO1 whereas the cell line hDT7 does and thus a large difference in the IC_{50} values (μM) for these two cell lines would be expected.

Compound Number	Structure	F179 IC_{50} (μM)	hDT7 (hNQO1) IC_{50} (μM)
144	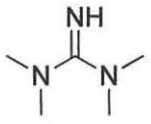	>100.0	>100.0
129	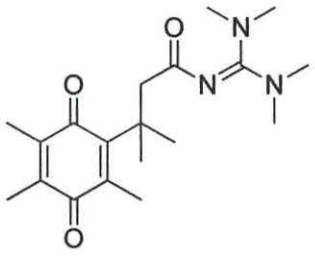	12.76	3.75
150	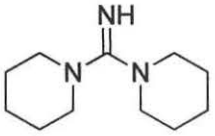	>100.0	>100.0
131	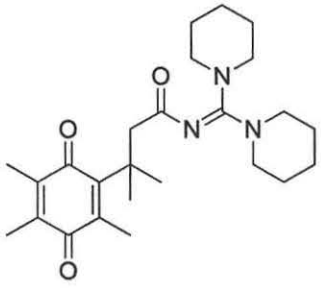	5.33	>100.0
151	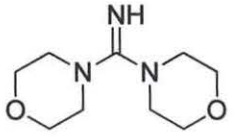	>100.0	>100.0

133	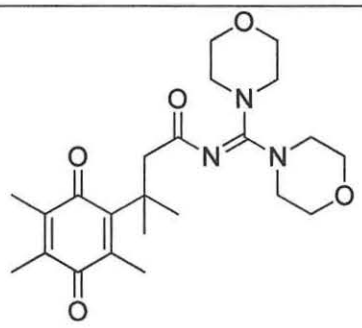	>100.0	39.56

Table 13. *In vitro* cytotoxicity evaluation (IC_{50} data) of guanidines

The IC_{50} data for the guanidines **144**, **150** and **151** for both cell lines showed values of >100 μM indicating no inhibition. However, **129** and **133** gave very encouraging results with IC_{50} values of 3.75 and 39.56 μM for the hDT7 cancer cell line. This suggests that these guanidines have activity against this cell line *via* hNQO1 activation. Suprisingly **131** gave an unusual result in that the inhibition was reversed and the F179 cell line gave an IC_{50} of 5.33 μM whilst against hDT7 was inactive. This result might imply a different mechanism is at work in this inhibition however the assay needs to be repeated to confirm these figures. Overall the study suggests that these substrates have some potential and confirm that the prodrug can be used for the delivery of guanidine based substrates. However, it must be noted that this data is subject to errors as there are no error bars (or +/-) values to give confidence that these results are statistically significant.

Conclusion

This thesis has explored the design and synthesis of novel guanidine and aniline mustard compounds for use in prodrug therapy. A series of compounds were synthesised (Figure 61) utilising quinone backbones **I, II** and **III**.

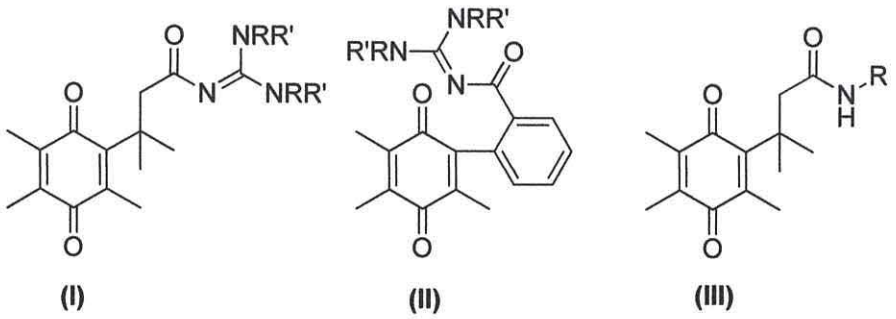

(I) R,R′ = Me **129**, -$(CH_2)_5$ **131**, -$(CH_2CH_2)_2O$ **133**

(II) R,R′ = Me **130**, -$(CH_2)_5$ **132**, -$(CH_2CH_2)_2O$ **134**

(III) R = $PhN(CH_2CH_2Cl)_2$ **78**

Figure 61. Structure of guanidine and aniline mustard quinone compounds

Molecular modelling provided the initial groundwork by determining the viability of these compounds to undergo quinone reduction by hNQO1 followed by hydroquinone cyclisation. Improvements were made to the synthetic methods reported, namely their % yields and compound purification. HPLC analysis proved the effectiveness of the trimethyl-locked drug system established by Volpato *et al.*[73] and phenyl system with guanidines by showing **129** and **130** to be good substrates. In theory the remaining compounds should follow the same mechanistic pathway in the presence of hNQO1 and NADH **35** and are currently being assessed for their enzymatic activity.

Continuation of this work would be to successfully prepare the aniline mustard prodrug **135** (Scheme 60). Reaction of the mustard **76** with the ester **163** resulted in substitution of the imide carbonyl and not the amide, which led to the formation of intermediate **171** (Figure 59, p.87). Directing this substitution at the desired site could possibly be achieved by reacting the mustard **76** directly with the quinone acid **162** instead thus bypassing this issue (Scheme 60).

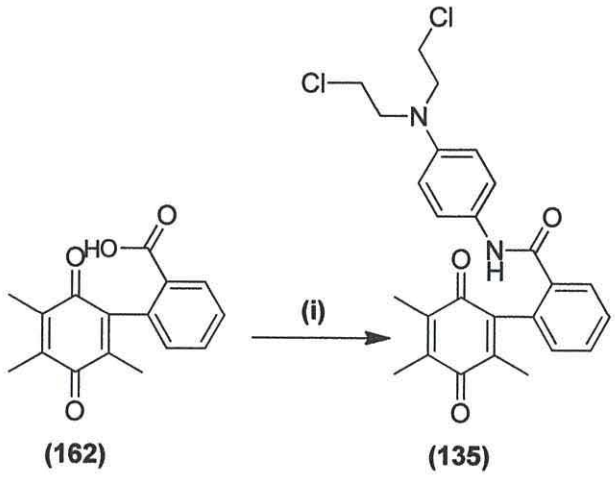

Scheme 60. (i) DCC, HOBT, **76**, dry THF, r.t

Another interesting reaction to reattempt is the synthesis of the prodrug **136** (Scheme 61) from the by-product of the aniline mustard reaction (Scheme 53, p.84). Whilst it is not absolutely clear how the piperidine mustard **170** was formed it is likely that it had arisen by reaction of the aniline mustard **76** undergoing self condensation or by reaction with the sulfite **168** which was proposed as a contaminant of a batch of the nitro mustard **166** and indeed was observed to be formed in the chlorination of the alcohol **165**. On repeating the synthesis of **76** using starting material purified by column chromatography only a small amount (≤5%) of the piperidine mustard **170** was produced and this was a limiting factor in its use in subsequent steps. In order to prepare **170**, optimisation of the preparation of sulfite **168** could be attempted which could then be reacted with the nitro compound **173** to form **174**. This substrate could then be chlorinated to afford **175** and reduced to give more appreciable amounts of **170** and thus enable the synthesis of the prodrug **136**.

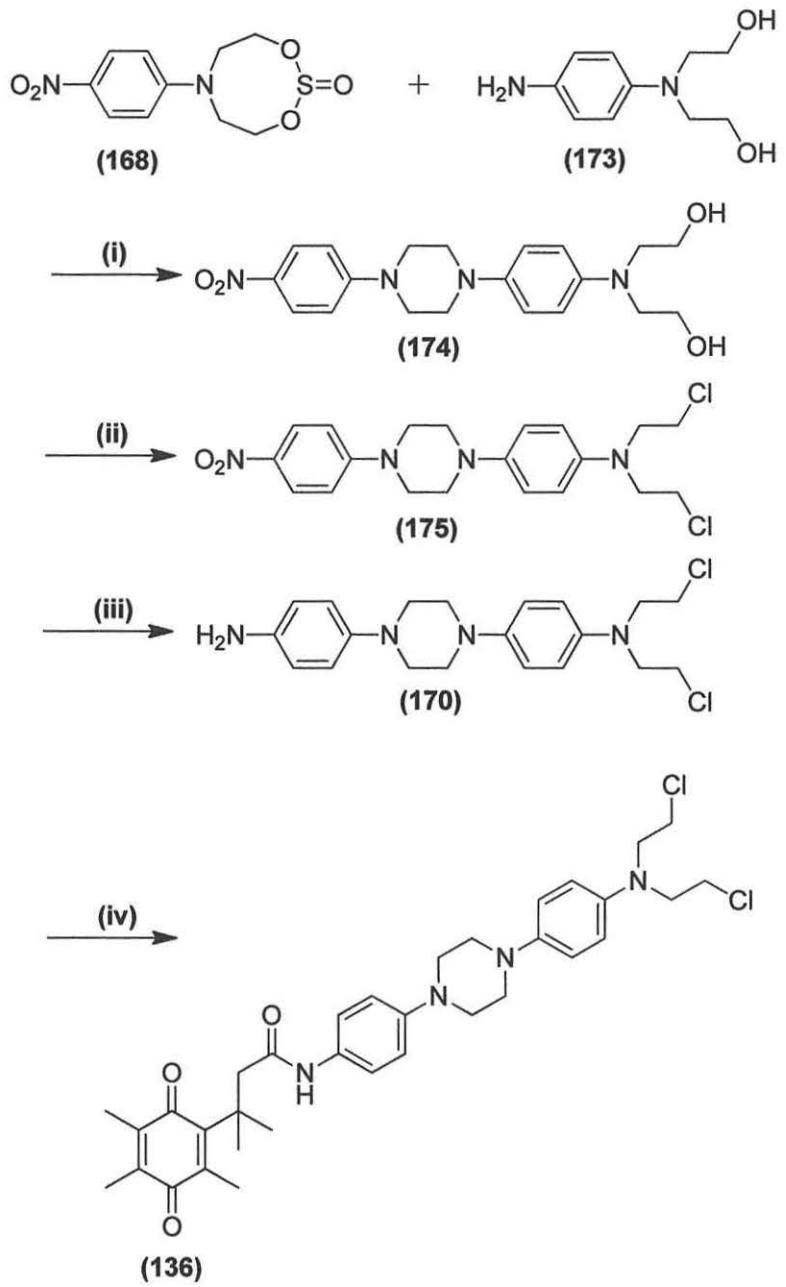

Scheme 61. (i) CH_2Cl_2, heat (ii) pyridine, $SOCl_2$, dry CH_2Cl_2, (iii) Pd (10%) on C, EtOH, H_2, r.t (iv) **170**, dry THF, N_2, dark, r.t

Other future work could be to progress the work on cytotoxic guanidines, by investigating the tirapazamine route in more detail. It was shown that substitution of tirapazamine **10** directly onto the ester **50b** proved unsuccessful (Scheme 62).

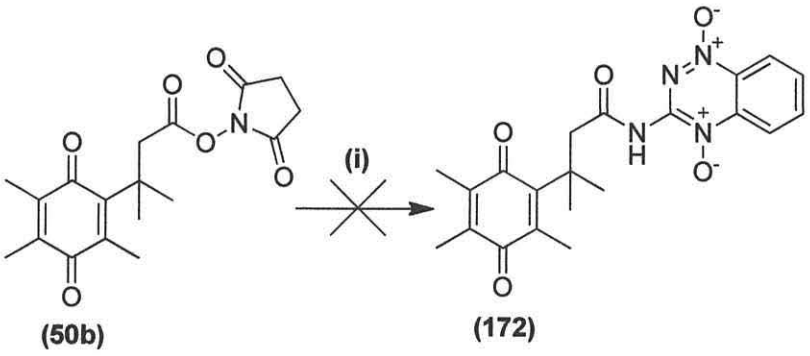

Scheme 62. (i) 1.5 equiv. tirapazamine **10**, dry DMF, N_2, dark, r.t, 72 h

Research has shown that it is the products of the one-electron reduction species that are believed to be the key radical intermediates in the cytotoxic action of tirapazamine **10**. The next step could be to attach 3-aminobenzo-1,2,4-triazine 1-*N*-oxide **15** to the ester **50b**, which contains only one NO group. The two routes to synthesising this compound have previously been discussed (Scheme 63) using either nitroaniline **11**[30-32] or hydroxybenzo-1,2,4-triazine 1-*N*-oxide **13**.[33, 34]

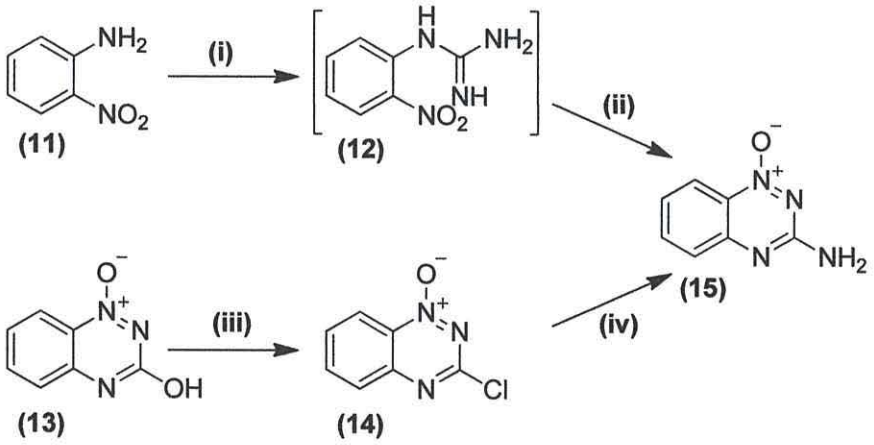

Scheme 63. (i) 0.5 equiv. cyanamide, 100 °C then r.t, HCl then 100 °C (ii) NaOH, r.t then 100 °C, 30 min (iii) DMA, $POCl_3$, Δ, 45 min (iv) NH_3, EtOH, Δ, 7 h

If substitution of this benzotriazine **15** is achieved onto the ester **50b** it may then be possible to add the second NO group directly onto this compound to give **172**.[32]

Experimental

General:

Chemicals

Chemicals were obtained from commercial suppliers Sigma Aldrich, Alfa Aesar and Thermo Fisher Scientific with no further purification. Reactions with *n*-butyllithium refer to the use of this reagent in hexane.

Melting point (m.p.)

Melting points in Degrees Celsius (°C) were determined using a Gallenkamp MF370 instrument and are uncorrected.

Nuclear magnetic resonance (NMR)

The ^{1}H and ^{13}C/distortionless enhancement by polarisation transfer (DEPT) (decoupled) spectra were recorded on a Bruker Avance 500 spectrometer at a frequency of 500 MHz (^{1}H) and 125 MHz (^{13}C/DEPT) in $CDCl_3$ unless otherwise stated. Some NMR were run on a Bruker 400 MHz spectrometer at Morvus Technology Ltd and this will be specified on these spectra. The chemical shifts are given as δ values (ppm) relative to the internal standard tetramethylsilane. Each spectrum has been calibrated using the solvent peak, $CDCl_3$ (^{1}H 7.27 ppm, ^{13}C 77.0 ppm) or DMSO-d_6 (^{1}H 2.54 ppm, ^{13}C 40.45 ppm). Also provided for the ^{1}H NMR are the *J* values (spin coupling constants) in hertz (Hz) and the multiplicity of the peaks. These are abbreviated as follows; s (singlet), d (doublet), t (triplet), ddd (doublet of doublets of doublets), q (quartet) and m (multiplet). Spectra were processed using MestReNova (version 6.0.2-5475) software.

Mass spectrometry (MS)

Samples were sent away to the EPSRC National Mass Spectrometry Service Centre in Swansea. Low resolution Chemical Ionisation (CI) and Electron Impact (EI) were recorded on a Quattro II triple quadrupole instrument. High resolution mass spectra were recorded on a Thermofisher LTQ Orbitrap XL spectrometer. High resolution Electrospray Ionisation (ESI) of compound **150** was recorded on a Bruker micro time of flight (TOF) instrument at

the School of Chemistry, Bangor University. Mass spectrometry measurements are reported in Daltons.

Infrared (IR)

IR spectra were obtained on a Bruker Tensor 27 machine either as a thin film (in chloroform or dichloromethane) or by using the KBr method for solids. Absorption frequencies are reported in wavenumber ν (cm^{-1}).

X-ray crystallography

Samples were sent away to the EPSRC National Crystallography Service at the School of Chemistry, University of Southampton. Tabulated data are provided on the following: (1) crystal data and structure refinement (2) atomic coordinates (x 10^4), equivalent isotropic displacement parameters ($Å^2$ x 10^3) and site occupancy factors (3) bond lengths (Å) and angles (°) (4) anisotropic displacement parameters ($Å^2$ x 10^3) (5) hydrogen coordinates (x 10^4) and isotropic displacement parameters ($Å^2$ x 10^3). Structures are present as 'wire' and/or 'ball and stick' images.

Chromatography

TLC was performed on precoated E.Merck silica gel 60 F254 glass plates. Compounds were visualised under UV light or by staining with phosphomolybdic acid (PMA), or iodine. Column chromatography was performed using Merck 7736 silica gel (particle size 40-63 μm) with the eluent specified in each case.

Enzymatic evaluation (cell-free assay)

Samples were analysed *via* HPLC at Morvus Technology Ltd using Thermo Separation Products SpectraSYSTEM HPLC system equipped with ChromQuest operating software using a specified acetonitrile/water gradient and a Waters SymmetryShield^{TM} RP18, 5 μm 3.9 x 150 mm column. Compounds were dissolved in DMSO to form a working stock (prepared fresh daily) of 10 mM and diluted to 100 μM in phosphate buffer pH 7. Statistical software Microsoft Office Excel 2007 was used for data analysis (including calculating reaction rates) and data were normalized to 100% (apart from the NADH **35**).

In vitro cytotoxicity evaluation (cellular assay)

Samples were sent away to Morvus Technology Ltd where growth inhibition was measured by the sulfo-rhodamine B (SRB) method as described by Skehan *et al.*[230] Isogenic clone of Chinese hamster cells in which one over-expressed hNQO1 (hDT7) and one that did not express (null) hNQO1 (F179) were used to determine the toxicity of the target compounds. In essence, cells were seeded into 96-well microplates in Eagle's minimum essential medium supplemented with non-essential amino acids, 2.0 mM glutamine and 10% (v/v) foetal bovine serum and incubated overnight. The test compounds were dissolved in DMSO, serially diluted in culture medium and added to the cells. After six days exposure the cells were stained with SRB and absorbance measured at 570 nm. The cytotoxicity of each compound was expressed as that concentration producing 50% inhibition of cell growth (IC_{50}) compared with cells incubated with medium only.

Ultraviolet (UV)

UV data to monitor the anodic oxidation of **157** was carried out on a Jasco V-550 UV-vis spectrophotometer at the School of Chemistry, Bangor University.

Miscellaneous

All anhydrous reactions were performed using oven dried glassware under a positive atmosphere of argon. *n*-Butyllithium in hexanes was titrated against diphenylacetic acid in THF immediately before use.[231] The term *in vacuo* refers to the reduced pressure of a Büchi rotary evaporator, at water pump pressure (14 mm Hg) at 30 - 50 °C. All chemical structures and reaction schemes were drawn using ChemBioDraw Ultra 12.0.

6-Hydroxy-4,4,5,7,8-pentamethylchroman-2-one 44[73, 112]

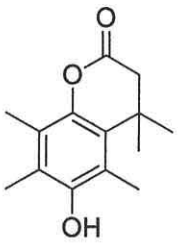

(44)

2,3,5-Trimethyl-1,4-hydroquinone **77** (5.07 g, 33.3 mmol) and methyl 3,3-dimethylacrylate (5.0 ml, 41 mmol) were added to methanesulfonic acid (50 ml). The resulting mixture was heated for 3 h at 70 °C under nitrogen and then left to stir at r.t overnight. The reaction mixture was added to water (200 ml) and extracted with ethyl acetate (3 x 150 ml). The organic layer was then washed with water (100 ml), saturated aqueous sodium hydrogen carbonate (100 ml) and brine (100 ml), dried ($MgSO_4$), filtered and the solvent removed *in vacuo* to give a grey solid (9.05 g). The crude product was recrystallised from hexane/chloroform (3:1) to yield the lactone **44** (6.88 g, 29.4 mmol, 88%) as a white solid (m.p. 183 – 185 °C, lit. 186 – 187 °C).[91]

^{1}H NMR: δ_H 1.46 (6H, s, 2 x *gem*-CH_3), 2.19 (3H, s, ring-CH_3), 2.23 (3H, s, ring-CH_3), 2.37 (3H, s, ring-CH_3), 2.55 (2H, s, CH_2), 4.70 (1H, s, OH)

^{13}C NMR: δ_C 12.3 (ring-CH_3), 12.5 (ring-CH_3), 14.4 (ring-CH_3), 27.7 (2 x *gem*-CH_3), 35.5 ($C(CH_3)_2$), 46.1 (CH_2), 118.9 (Ar-C), 121.8 (Ar-C), 123.4 (Ar-C), 128.2 (Ar-C), 143.5 (Ar-C), 148.8 (Ar-C), 168.8 (C=O)

Rf: 0.39 (50% diethyl ether/petrol)

3-Methyl-3-(2,4,5-trimethyl-3,6-dioxocyclohexa-1,4-dien-1-yl)butanoic acid 45[73, 112]

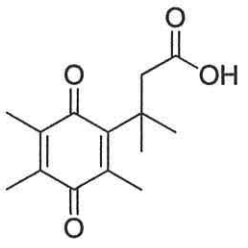

(45)

The lactone **44** (6.25 g, 26.7 mmol) was suspended in acetonitrile (aq. 15% v/v, 270 ml). A solution of *N*-bromosuccinimide (6.41 g, 36 mmol) in acetonitrile (aq. 40% v/v, 120 ml) was added drop-wise over 1 h to the suspension. The resulting mixture was stirred for a further 30 min, diluted with water (500 ml) and extracted with dichloromethane (3 x 100 ml). The organic layer was washed with water (2 x 100 ml) and brine (100 ml), then dried ($MgSO_4$), filtered and the solvent removed *in vacuo* to give a bright yellow solid (7.66 g). The crude product was re-dissolved in diethyl ether and, following small additions of petrol, cooled to 0 °C. The liquid was decanted to yield the quinone acid **45** (6.60 g, 26.4 mmol, 99%) as a bright yellow solid (m.p. 91 – 93 °C, lit. 101 – 103 °C).[105]

^{1}H NMR: δ_H	1.43 (6H, s, 2 x *gem*-CH_3), 1.92 (3H, s, ring-CH_3), 1.95 (3H, s, ring-CH_3), 2.14 (3H, s, ring-CH_3), 3.02 (2H, s, CH_2), 9.0-13.0 (1H, br. OH)
^{13}C NMR: δ_C	12.1 (ring-CH_3), 12.5 (ring-CH_3), 14.3 (ring-CH_3), 28.8 (2 x *gem*-CH_3), 37.9 ($C(CH_3)_2$), 47.2 (CH_2), 138.4 (C), 139.0 (C), 143.0 (C), 152.0 (C), 178.4 (acid C=O), 187.4 (quinone C=O), 190.8 (quinone C=O)
Rf:	0.17 (50% diethyl ether/petrol)

2,5-Dioxopyrrolidin-1-yl 3-methyl-3-(2,4,5-trimethyl-3,6-dioxocyclohexa-1,4-dien-1-yl)butanoate 50b[73]

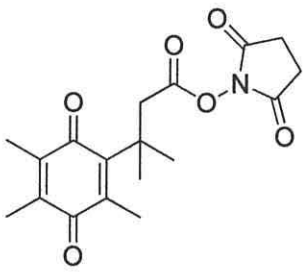

(50b)

Dicyclohexylcarbodiimide (1.80 g, 8.72 mmol) was added to a solution of quinone acid **45** (1.80 g, 7.19 mmol) and *N*-hydroxysuccinimide (0.91 g, 7.9 mmol) in dry THF (60 ml) at 0 °C under nitrogen. The mixture was stirred for 18 h at r.t and then filtered to remove dicyclohexylurea. The solvent was removed *in vacuo* from the resulting filtrate and the residue treated with ethyl acetate (30 ml) and filtered again. The solvent was removed *in vacuo* to give a yellow solid (3.09 g). The crude product was re-dissolved in ethyl acetate (11 ml) and cooled to 0 °C. The liquid was decanted to yield the *N*-hydroxysuccinimide ester **50b** (2.79 g, 8.03 mmol, >100%) as a yellow solid, without further purification (m.p. 140 – 142 °C, lit. 145 °C).[106]

^{1}H NMR: δ_H	1.53 (6H, s, 2 x *gem*-CH_3), 1.96 (6H, s, 2 x ring-CH_3), 2.17 (3H, s, ring-CH_3), 2.78 (4H, s, 2 x succinimidyl CH_2), 3.28 (2H, s, CH_2)
^{13}C NMR: δ_C	12.2 (ring-CH_3), 12.6 (ring-CH_3), 14.2 (ring-CH_3), 25.5 (2 x succinimidyl CH_2), 29.1 (2 x *gem*-CH_3), 38.8 ($C(CH_3)_2$), 44.1 (CH_2), 138.8 (C), 140.4 (C), 142.8 (C), 150.0 (C), 167.7 (ester C=O), 168.9 (2 x succinimidyl C=O), 187.4 (quinone C=O), 190.3 (quinone C=O)
Rf:	0.09 (25% ethyl acetate/hexane)

(*Z*)-*N*-(*N*,*N'*-Diphenylcarbamimidoyl)-3-methyl-3-(2,4,5-trimethyl-3,6-dioxocyclohexa-1,4-dien-1-yl)butanamide 138[73]

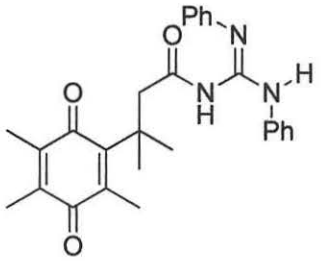

(138)

N-Hydroxysuccinimide ester **50b** (0.50 g, 1.4 mmol) was added to a solution of 1,3 diphenylguanidine **137** (0.61 g, 2.9 mmol) in dry dichloromethane (10 ml). After being stirred in the dark for 46 h at r.t under nitrogen, the mixture was extracted with ethyl acetate (2 x 200 ml) and the organic layer washed with water (2 x 200 ml). The organic extracts were dried ($MgSO_4$), filtered and the solvent was removed *in vacuo* to give a yellow/brown solid (0.75 g). The crude product was dissolved in a 50:50 diethyl ether/petrol mix. After cooling to 0 °C, the liquid was decanted to leave impure compound **138** (0.10 g, 0.23 mmol, 16%) as a yellow solid (m.p. 166 °C).

^{1}H NMR: δ_H	1.41 (6H, s, 2 x *gem*-CH_3), 1.95 (3H, s, ring-CH_3), 2.00 (3H, s, ring-CH_3), 2.15 (3H, s, ring-CH_3), 2.84 (2H, s, CH_2), 6.89 – 7.65 (11H, m, 10 x Ar-H, NH), 9.89 (1H, s, NH)
FTIR V_{max} ($CHCl_3$)	1590 (C=C), 1645 (C=N), 1664 (C=O), 2872, 2929, 2968 (C-H saturated), 3061, 3147, 3273 (C-H unsaturated), 3308, 3401 (N-H)
LRMS (EI):	444 (5%, $[M + H^+]$), 252 (100%)
HRMS $[(M + H)^+]$:	($C_{27}H_{30}O_3N_3$) Calculated: 444.2282 Found: 444.2281
Rf:	0.22 (15% ethyl acetate/petrol)

4,4,7,8,10-Pentamethyl-2,6,9-trioxo-*N*,*N'*-diphenyl-1-azaspiro[4.5]dec-7-ene-1-carboximidamide 139

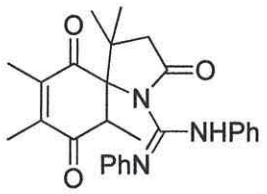

(139)

When purification of the reaction mixture was *via* column chromatography (10-50% ethyl acetate/petrol) and not decantation, fractions eluting in 20-30% ethyl acetate/petrol yielded the isomer by-product, ketolactam **139** as a white solid (m.p. 138 – 143 °C).

^{1}H NMR: δ_H	0.93 (3H, s, *gem*-CH_3), 1.07 (3H, s, *gem*-CH_3), 1.46 (3H, d, J = 6.5 Hz, ring-CH_3), 2.05 (3H, s, ring-CH_3), 2.11 (3H, s, ring-CH_3), 2.16 (1H, d, J = 17.5 Hz, CH), 2.75 (1H, d, J = 17.5 Hz, CH), 5.31 (1H, q, J = 7.0 Hz, CH), 6.67 (2H, d, J = 7.5 Hz, 2 x Ar-H), 6.77 (1H, t, J = 7.3 Hz, Ar-H), 6.90 (1H, t, J = 6.3 Hz, Ar-H), 7.00 – 7.07 (6H, m, 6 x Ar-H), 8.22 (1H, s, NH)
^{13}C NMR: δ_C	10.5 (CH_3), 13.0 (CH_3), 13.3 (CH_3), 22.8 (*gem*-CH_3), 29.9 (*gem*-CH_3), 40.1 ($C(CH_3)_2$), 47.6 (CH_2), 50.8 (CH), 81.5 (C), 121.3-128.5 (10 x Ar-CH), 138.0 (Ar-C), 143.3 (Ar-C), 145.2 (Ar-C), 146.2 (Ar-C), 147.5 (C=N), 174.9 (amide C=O), 192.8 (C=O), 197.4 (C=O)
FTIR V_{max} ($CHCl_3$)	1590 (C=C), 1680 (C=N), 1726 (C=O), 2869, 2970 (C-H saturated), 3058 (C-H unsaturated), 3265 (N-H)
HRMS [(M + H)$^+$]:	($C_{27}H_{30}O_3N_3$) Calculated: 444.2282 Found: 444.2280
Rf:	0.20 (20% ethyl acetate/petrol)

(3aR,4R,10aR)-3a,4,6,7,7-Pentamethyl-3-phenyl-2-(phenylamino)-3a,4,7,8-tetrahydro-3*H*-chromeno[8,8a-d]imidazole-5,9-dione 143

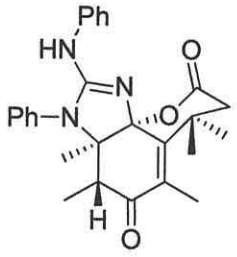

(143)

When purification of the reaction mixture was *via* column chromatography (20-60% ethyl acetate/petrol) and not decantation, fractions eluting in 60% ethyl acetate/petrol yielded the isomer by-product lactam **143** as white crystals (m.p. 199 – 203 °C).

^{1}H NMR: δ_H	1.18 (3H, d, J = 7.3 Hz, ring-CH_3), 1.20 (3H, s, *gem*-CH_3), 1.43 (3H, s, *gem*-CH_3), 1.58 (3H, s, ring-CH_3), 2.08 (3H, s, ring-CH_3), 2.40 (1H, d, J = 14.8 Hz, CH), 2.84 (1H, q, J = 7.0 Hz, CH), 3.99 (1H, d, J = 14.5 Hz, CH), 5.83 (1H, s, NH), 7.01 (1H, t, J = 7.4 Hz, Ar-H), 7.24 – 7.30 (4H, m, 4 x Ar-H), 7.39 – 7.43 (3H, m, 3 x Ar-H), 7.48 (2H, t, J = 7.4 Hz, 2 x Ar-H)
^{13}C NMR: δ_C	12.3 (CH_3), 14.0 (CH_3), 14.6 (CH_3), 27.8 (*gem*-CH_3), 28.4 (*gem*-CH_3), 36.1 ($C(CH_3)_2$), 46.8 (CH_2), 48.0 (CH), 72.3 (C), 101.6 (C), 118.6 (2 x Ar-CH), 123.0 (2 x Ar-CH), 128.7 (2 x Ar-CH), 128.8 (2 x Ar-CH), 129.4 (C), 129.9 (2 x Ar-CH), 136.0 (C), 138.5 (C), 150.4 (C), 156.7 (C=N), 172.3 (ester C=O), 201.8 (C=O)
FTIR V_{max} ($CHCl_3$)	1587 (C=C), 1675 (C=N), 1743 (C=O), 2879, 2939 (C-H saturated), 3010, 3143 (C-H unsaturated), 3330 (N-H)
HRMS [$(M + H)^+$]:	($C_{27}H_{30}O_3N_3$) Calculated: 444.2282 Found: 444.2278
Rf:	0.22 (35% ethyl acetate/hexane)
X-ray crystallography:	See Appendix 2.2.1

N-(*Bis*(dimethylamino)methylene)-3-methyl-3-(2,4,5-trimethyl-3,6-dioxocyclohexa-1,4-dien-1-yl)butanamide 129[73]

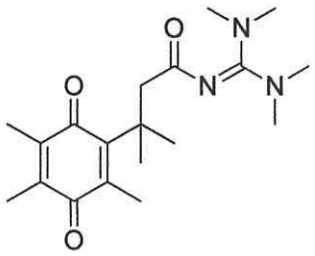

(129)

1,1,3,3-Tetramethylguanidine **144** (0.20 ml, 1.6 mmol) was added to a solution of *N*-hydroxysuccinimide ester **50b** (0.50 g, 1.4 mmol) in dry dichloromethane (9 ml). After being stirred in the dark for 46 h at r.t under nitrogen, the mixture was extracted with ethyl acetate (2 x 200 ml) and the organic layer washed with water (2 x 200 ml). The organic extracts were dried ($MgSO_4$), filtered and the solvent removed *in vacuo* to give a yellow/orange oil (0.45 g). The crude product was purified by column chromatography using a stepwise gradient of methanol/ethyl acetate (2-5%). Fractions eluting in 5% methanol/ethyl acetate yielded compound **129** as a yellow/orange oil (0.31 g, 0.91 mmol, 63%).

^{1}H NMR: δ_H	1.40 (6H, s, 2 x *gem*-CH_3), 1.88 (3H, s, ring-CH_3), 1.91 (3H, s, ring-CH_3), 2.06 (3H, s, ring-CH_3), 2.77 (12H, s, 4 x CH_3), 2.97 (2H, s, CH_2)
^{13}C NMR: δ_C	11.9 (ring-CH_3), 12.7 (ring-CH_3), 13.9 (ring-CH_3), 28.2 (2 x *gem*-CH_3), 37.9 ($C(CH_3)_2$), 39.9 (4 x CH_3), 52.1 (CH_2), 135.3 (C), 136.7 (C), 144.0 (C), 156.2 (C), 166.6 (C=N), 179.7 (amide C=O), 187.6 (quinone C=O), 190.6 (quinone C=O)
FTIR V_{max} ($CHCl_3$)	1595 (C=C), 1644 (C=O), 2956 (C-H saturated)
HRMS [(M + H)$^+$]:	($C_{19}H_{30}O_3N_3$) Calculated: 348.2282 Found: 348.2286
Rf:	0.26 (50% methanol/ethyl acetate)

Di(1*H*-imidazol-1-yl)methanimine 145[217]

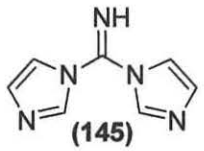

(145)

To a solution of imidazole **148** (6.87 g, 101 mmol) in dichloromethane (500 ml), cyanogen bromide (3.70 g, 34.9 mmol) was added. The mixture was heated at reflux for 40 min, then cooled to r.t and the white precipitate by-product removed by filtration. The filtrate was then concentrated to about 50 ml and cooled to 0 °C for 48 h. The crystallised solid was filtered, washed with chilled dichloromethane and the solvent removed under vacuum to yield impure compound **145** (5.23 g, 32.5 mmol, 93%) as a white solid (m.p. 98 – 104 °C, lit. 103 °C).[218, 219] This was used in the subsequent step without additional purification.

^{1}H NMR: δ_H (DMSO-d_6)	7.16 (2H, s, 2 x CH), 7.60 (2H, br. s, 2 x CH), 8.12 (2H, br. s, 2 x CH), 10.26 (1H, s, NH)
^{13}C NMR: δ_C (DMSO-d_6)	120.0 (2 x CH), 130.7 (2 x CH), 138.4 (2 x CH), 141.8 (C=N)

Di(piperidin-1-yl)methanimine 150[217]

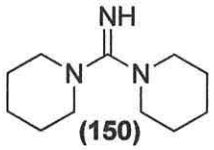

(150)

To a solution of di(1*H*-imidazol-1-yl)methanimine **145** (2.00 g, 12.4 mmol) in dry THF (40 ml), piperidine (6.1 ml, 62 mmol) was added and heated at reflux for 17 h under nitrogen. The resulting mixture was washed successively with aqueous 2M sodium hydroxide (3 x 50 ml) and the aqueous layer with dichloromethane (3 x 50 ml). The organic extracts were dried ($MgSO_4$), filtered and the solvent removed *in vacuo* to yield impure compound **150** (1.68 g, 8.60 mmol, 69%) as a purple solid. This was used in the subsequent step without additional purification.

^{1}H NMR: δ_H	1.41 (12H, s, 6 x CH_2), 3.06 (8H, s, 4 x CH_2), 6.96 (1H, s, NH)
^{13}C NMR: δ_C	23.6 (2 x CH_2), 25.1 (4 x CH_2), 48.9 (4 x CH_2), 162.3 (C=N)
HRMS [$(M + H)^+$]:	($C_{11}H_{22}N_3$) Calculated: 196.1814 Found: 196.1816

N-(Di(piperidin-1-yl)methylene)-3-methyl-3-(2,4,5-trimethyl-3,6-dioxocyclohexa-1,4-dien-1-yl)butanamide 131[73]

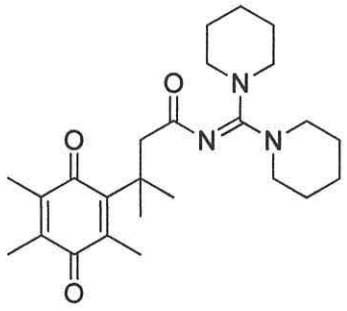

(131)

N-Hydroxysuccinimide ester **50b** (1.07 g, 3.08 mmol) was added to a solution of di(piperidin-1-yl)methanimine **150** (0.90 g, 4.6 mmol) in dry dichloromethane (25 ml). After being stirred in the dark for 65 h at r.t under nitrogen, the mixture was extracted with ethyl acetate (2 x 200 ml) and the organic layer washed with water (2 x 200 ml). The organic extracts were dried ($MgSO_4$), filtered and the solvent removed *in vacuo* to give a brown oil (1.35 g). The crude product was purified by column chromatography using a stepwise gradient of methanol/ethyl acetate (2-10%). Fractions eluting in 6-10% methanol/ethyl acetate yielded compound **131** as a yellow oil (0.38 g, 0.89 mmol, 29%).

^{1}H NMR: δ_H	1.40 (6H, s, 2 x *gem*-CH_3), 1.56 (12H, m, 6 x CH_2), 1.90 (3H, s, ring-CH_3), 1.92 (3H, s, ring-CH_3), 2.08 (3H, s, ring-CH_3), 3.02 (2H, s, CH_2), 3.12 – 3.15 (8H, m, 4 x CH_2)
^{13}C NMR: δ_C	12.0 (ring-CH_3), 12.7 (ring-CH_3), 14.0 (ring-CH_3), 24.1 (2 x CH_2), 25.3 (4 x CH_2), 28.2 (2 x *gem*-CH_3), 38.0 ($C(CH_3)_2$), 49.8 (4 x CH_2), 51.6 (CH_2), 135.9 (C), 137.1 (C), 143.7 (C), 155.7 (C), 165.0 (C=N), 179.5 (amide C=O), 187.6 (quinone C=O), 190.5 (quinone C=O)
FTIR V_{max} ($CHCl_3$)	1592 (C=C), 1641 (C=N), 1710 (C=O), 2857, 2938 (C-H saturated)
HRMS [$(M + H)^+$]:	($C_{25}H_{38}O_3N_3$) Calculated: 428.2908 Found: 428.2908
Rf:	0.21 (20% methanol/ethyl acetate)

Dimorpholinomethanimine 151[217]

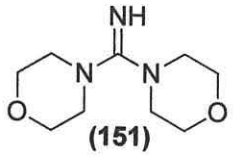

(151)

To a solution of di(1*H*-imidazol-1-yl)methanimine **145** (2.00 g, 12.4 mmol) in dry THF (40 ml), morpholine (5.4 g, 5.4 ml, 62 mmol) was added and heated at reflux for 15 h under nitrogen. The resulting mixture was washed successively with aqueous 2M sodium hydroxide (3 x 50 ml) and the aqueous layer with dichloromethane (3 x 50 ml). The organic extracts were dried ($MgSO_4$), filtered and the solvent removed *in vacuo* to yield impure compound **151** (1.48 g, 7.43 mmol, 60%) as a purple solid. This was used in the subsequent step without additional purification.

^{1}H NMR: δ_H	3.26 (8H, t, J = 4.9 Hz, 4 x CH_2), 3.76 (8H, t, J = 4.9 Hz, 4 x CH_2)
^{13}C NMR: δ_C	47.9 (4 x CH_2), 66.1 (4 x CH_2), 166.2 (C=N)
HRMS [(M + H)$^+$]:	($C_9H_{18}O_2N_3$) Calculated: 200.1394 Found: 200.1392

N-(Dimorpholinomethylene)-3-methyl-3-(2,4,5-trimethyl-3,6-dioxocyclohexa-1,4-dien-1-yl)butanamide 133[73]

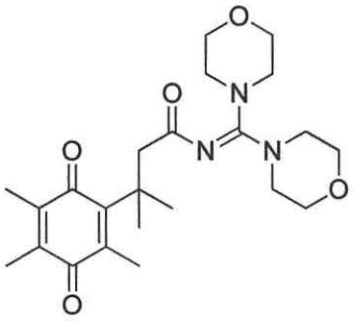

(133)

N-Hydroxysuccinimide ester **50b** (0.69 g, 2.0 mmol) was added to a solution of dimorpholinomethanimine **151** (0.59 g, 3.0 mmol) in dry dichloromethane (20 ml). After being stirred in the dark for 46 h at r.t under nitrogen, the mixture was extracted with ethyl acetate (2 x 150 ml) and the organic layer washed with water (2 x 150 ml). The organic extracts were dried ($MgSO_4$), filtered and the solvent removed in *vacuo* to give a yellow oil (0.88 g). The crude product was purified by column chromatography (5% methanol/ ethyl acetate) to yield compound **133** as a yellow oil (0.24 g, 0.55 mmol, 28%).

^{1}H NMR: δ_H	1.43 (6H, s, 2 x *gem*-CH_3), 1.95 (3H, s, ring-CH_3), 1.98 (3H, s, ring-CH_3), 2.12 (3H, s, ring-CH_3), 3.06 (2H, s, CH_2), 3.22 (8H, t, J = 4.6 Hz, 4 x CH_2), 3.68 (8H, t, J = 4.7 Hz, 4 x CH_2)
^{13}C NMR: δ_C	12.0 (ring-CH_3), 12.8 (ring-CH_3), 14.1 (ring-CH_3), 28.3 (2 x *gem*-CH_3), 38.1 ($C(CH_3)_2$), 49.0 (4 x CH_2), 52.2 (CH_2), 66.1 (4 x CH_2), 136.3 (C), 137.4 (C), 143.5 (C), 155.3 (C), 164.7 (C=N), 181.2 (amide C=O), 187.5 (quinone C=O), 190.7 (quinone C=O)
FTIR V_{max} ($CHCl_3$)	1598 (C=C), 1645 (C=N), 1711 (C=O), 2860, 2922, 2970 (C-H saturated)
HRMS [$(M + H)^+$]:	($C_{23}H_{34}O_5N_3$) Calculated: 432.2493 Found: 432.2486
Rf:	0.22 (15% methanol/ethyl acetate)

1,4-Dimethoxy-2,3,5-trimethylbenzene 157[223]

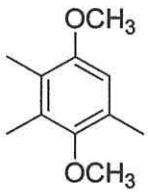

(157)

To a stirring solution of 2,3,5-trimethyl-1,4-hydroquinone **77** (10.02 g, 65.83 mmol) in butan-2-one (150 ml), K_2CO_3 (45.00 g, 325.6 mmol) was added at r.t. After 30 min, methyl iodide (16.2 ml, 261 mmol) was added to the mixture and stirred for a further 16 h at 65 °C. After cooling, the solvent was removed *in vacuo* and the resulting yellow precipitate extracted with diethyl ether (2 x 100 ml). The organic extracts were dried ($MgSO_4$), filtered and the solvent removed *in vacuo* to give a brown oil (11.69 g). The crude product was purified by column chromatography (5% diethyl ether/hexane) to yield compound **157** as a clear/colourless oil (7.29 g, 40.5 mmol, 62%). Also isolated in some of the later fractions was a quinone by-product **161** as a waxy yellow solid (*ca.* 7%).

^{1}H NMR: δ_H	2.15 (3H, s, ring-CH_3), 2.24 (3H, s, ring-CH_3), 2.32 (3H, s, ring-CH_3), 3.69 (3H, s, O-CH_3), 3.81 (3H, s, O-CH_3), 6.57 (1H, s, Ar-H)
^{13}C NMR: δ_C	11.8 (ring-CH_3), 12.6 (ring-CH_3), 16.2 (ring-CH_3), 55.7 (O-CH_3), 60.1 (O-CH_3), 110.3 (Ar-CH), 123.7 (Ar-C), 127.7 (Ar-C), 130.6 (Ar-C), 150.5 (Ar-C), 153.5 (Ar-C)
Rf:	0.33 (5% diethyl ether/hexane)

2,3,5-Trimethylcyclohexa-2,5-diene-1,4-dione 161

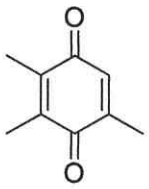

(161)

^{1}H NMR: δ_H 1.98 (3H, s, ring-CH_3), 2.00 (3H, s, ring-CH_3), 2.01 (3H, s, ring-CH_3), 6.53 (1H, q, J = 3.0 Hz, ring-CH)

^{13}C NMR: δ_C 12.0 (ring-CH_3), 12.3 (ring-CH_3), 15.8 (ring-CH_3), 133.0 (ring-CH), 140.7 (C), 140.8 (C), 145.3 (C), 187.4 (quinone C=O), 187.8 (quinone C=O)

Rf: 0.20 (10% diethyl ether/hexane)

3,3,6,6-Tetramethoxy-1,2,4-trimethylcyclohexa-1,4-diene 158[222]

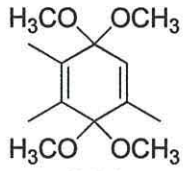

(158)

1,4-Dimethoxy-2,3,5-trimethylbenzene **157** (7.35 g, 40.8 mmol) in 2% methanolic potassium hydroxide (250 ml) was electrolysed for 3.5 h, the solution being stirred and maintained below 5 °C, maintaining the current at 1.0 Amp throughout. The solvent was removed *in vacuo* to yield a brown solid. The aqueous layer was extracted with diethyl ether (3 x 100 ml) and the organic layer washed with brine (2 x 100 ml). The organic extracts were dried over sodium carbonate, filtered and the solvent removed *in vacuo* to yield the *bis*-ketal **158** (8.98 g, 37.1 mmol, 91%) as a pale yellow solid (m.p. 37 – 41 °C, lit. 66 – 69 °C[221], lit. 34 – 42 °C).[222]

^{1}H NMR: δ_H	1.66 (3H, s, ring-CH_3), 1.73 (3H, s, ring-CH_3), 1.75 (3H, s, ring-CH_3), 2.96 (6H, s, 2 x O-CH_3), 3.17 (6H, s, 2 x O-CH_3), 6.00 (1H, s, ring-CH)
^{13}C NMR: δ_C	11.2 (ring-CH_3), 11.5 (ring-CH_3), 15.8 (ring-CH_3), 50.6 (2 x O-CH_3), 50.7 (2 x O-CH_3), 95.7 (C), 98.7 (C), 129.7 (ring-CH), 133.0 (C), 137.2 (C), 139.6 (C)
Rf:	0.21 (40% diethyl ether/hexane)

4,4-Dimethoxy-2,3,5-trimethylcyclohexa-2,5-dienone 159[221]

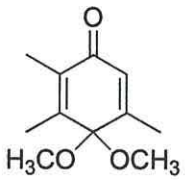

(159)

3,3,6,6-Tetramethoxy-1,2,4-trimethylcyclohexa-1,4-diene **158** (10.94 g, 45.15 mmol) was dissolved in acetone (50 ml) and cooled in ice to 0 °C and with vigorous stirring 2% chilled aqueous acetic acid (55 ml) was added slowly. The resulting mixture was stirred for 25 min at 0 °C and a further 3 h at r.t before being quenched by pouring into 5% bicarbonate solution (250 ml). The aqueous layer was then extracted with diethyl ether (4 x 100 ml), the organic layer washed with water (2 x 100 ml) and brine (100 ml). The organic extracts were dried ($MgSO_4$), filtered and the solvent removed *in vacuo* to yield the *mono*-ketal **159** (8.33 g, 45.5 mmol, 94%) as yellow solid (m.p. 71 – 74 °C, lit. 74 – 75.5 °C).[221, 224]

^{1}H NMR: δ_H	1.88 (3H, s, ring-CH_3), 1.89 (3H, s, ring-CH_3), 1.90 (3H, s, ring-CH_3), 2.98 (6H, s, 2 x O-CH_3), 6.32 (1H, s, ring-CH)
^{13}C NMR: δ_C	10.8 (ring-CH_3), 12.8 (ring-CH_3), 16.1 (ring-CH_3), 50.6 (2 x O-CH_3), 98.3 (C), 131.4 (ring-CH), 136.9 (C), 148.5 (C), 154.1 (C), 184.7 (C=O)
Rf:	0.21 (40% diethyl ether/hexane)

2,3,5-Trimethyl-3'*H*-spiro[cyclohexa[2,5]diene-1,1'-isobenzofuran]-3',4-dione 160[220]

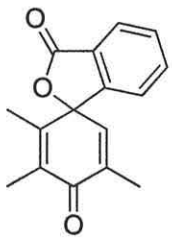

(160)

To a solution of *N*-phenylbenzamide (2.73 g, 13.8 mmol) in dry THF (33 ml), 2.2M *n*-butyllithium (12.6 ml, 27.6 mmol) was slowly added at -78 °C under argon. The resulting solution was stirred for 30 min at -78 °C, at 0 °C for 1 h, then cooled to -78 °C. A solution of the *mono*-ketal **159** (2.92 g, 14.9 mmol) in dry THF (10 ml) was added and the bright green solution stirred at -78 °C for 4 h, then left to stir at r.t overnight. The resulting mixture was diluted with diethyl ether (100 ml) and washed with aqueous 3M hydrochloric acid (3 x 100 ml). The combined aqueous layers were extracted with diethyl ether (3 x 50 ml) and the combined organic layers washed with brine (100 ml). The organic extracts were dried ($MgSO_4$), filtered and the solvent removed *in vacuo* to give a dark brown solid (4.30 g). The crude product was then recrystallised from diethyl ether/methanol to yield spirolactone **160** (2.10 g, 8.27 mmol, 60%) as white crystals (m.p. 167 – 168 °C).

^{1}H NMR: δ_H	1.55 (3H, s, ring-CH_3), 1.95 (3H, s, ring-CH_3), 1.97 (3H, s, ring-CH_3), 6.35 (1H, s, ring-CH), 7.16 (1H, d, J = 7.9 Hz, Ar-H), 7.59 (1H, t, J = 7.4 Hz, Ar-H), 7.67 (1H, t, J = 7.6 Hz, Ar-H), 7.96 (1H, d, J = 7.6 Hz, Ar-H)
^{13}C NMR: δ_C	11.6 (ring-CH_3), 14.0 (ring-CH_3), 15.9 (ring-CH_3), 83.3 (C), 121.8 (Ar-CH), 126.3 (Ar-CH), 130.1(Ar-CH), 133.9 (2 x C), 134.9 (Ar-CH), 135.9 (C), 138.9 (ring-CH), 146.3 (C), 148.4 (C), 169.8 (ester C=O), 185.3 (C=O)
FTIR V_{max} ($CHCl_3$)	1600 (C=C), 1647 (C=O), 1773 (C=O), 2923, 2955 (C-H saturated), 3028, 3062, 3090 (C-H unsaturated)
HRMS [(M + H)$^+$]:	($C_{16}H_{15}O_3$) Calculated: 255.1016 Found: 255.1016
X-ray crystallography:	See Appendix 2.2.2

2-Hydroxy-1,3,4-trimethyl-6*H*-benzo[c]chromen-6-one 120[220]

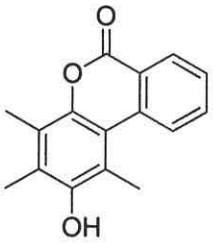

(120)

A mixture of the spirolactone **160** (0.50 g, 2.0 mmol), trifluoroacetic acid (5 ml), trifluoroacetic anhydride (10 ml) and conc. sulfuric acid (10 drops) was heated at reflux for 7 h. The solvent was removed *in vacuo* and the residue dissolved in methanol (25 ml) before being partitioned between dichloromethane (400 ml) and water (300 ml). The aqueous layer was then extracted with dichloromethane (3 x 200 ml), the combined organic extracts dried ($MgSO_4$), filtered and the solvent removed *in vacuo* to give a pale yellow solid. The crude product was recrystallised from dichloromethane/hexane to yield the lactone **120** (0.50 g, 2.0 mmol, 99%) as white crystals (m.p. 200 – 201 °C).

^{1}H NMR: δ_H	2.33 (3H, s, ring-CH_3), 2.44 (3H, s, ring-CH_3), 2.74 (3H, s, ring-CH_3), 4.75 (1H, s, OH), 7.57 (1H, t, J = 7.8 Hz, Ar-H), 7.79 (1H, t, J = 7.8 Hz, Ar-H), 8.28 (1H, d, J = 8.0 Hz, Ar-H), 8.47 (1H, d, J = 8.0 Hz, Ar-H)
^{13}C NMR: δ_C	12.4 (ring-CH_3), 12.9 (ring-CH_3), 16.2 (ring-CH_3), 116.0 (C), 117.4 (C), 122.2 (C), 123.5 (C), 125.3 (C), 126.5 (Ar-CH), 127.6 (Ar-CH), 130.5 (Ar-CH), 133.7 (Ar-CH), 136.4 (C), 144.4 (C), 148.9 (C), 161.7 (ester C=O)
FTIR V_{max} (KBr)	1607 (C=C), 1698 (ester C=O), 2855, 2926 (C-H saturated), 3008 (C-H unsaturated), 3433 (O-H)
HRMS [(M + H)$^+$]:	($C_{16}H_{15}O_3$) Calculated: 255.1016 Found: 255.1019
Rf:	0.21 (100% dichloromethane)
X-ray crystallography:	See Appendix 2.2.3

3',4',6'-Trimethyl-2',5'-dioxo-2',5'-dihydro-[1,1'-biphenyl]-2-carboxylic acid 162[73]

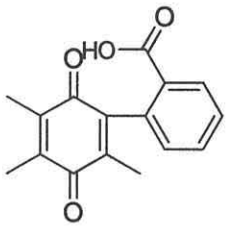

(162)

Lactone **120** (0.82 g, 3.2 mmol) was suspended in acetonitrile (aq. 15% v/v 40 ml). A solution of *N*-bromosuccinimide (0.78 g, 4.4 mmol) in acetonitrile (aq. 40% v/v 12 ml) was added drop-wise over 1 h to the suspension. The resulting mixture was stirred for a further 30 min, diluted with water (120 ml) and extracted with dichloromethane (3 x 50 ml). The organic layer was washed with water (2 x 50 ml) and brine (50 ml), then dried ($MgSO_4$), filtered and the solvent removed *in vacuo* to yield a yellow oil (1.03 g). The crude product was purified by column chromatography (dichloromethane followed by 20% ethyl acetate/petrol) to yield quinone acid **162** as a waxy yellow solid (0.67 g, 2.5 mmol, 77%). Also isolated was a brominated spirolactone by-product **164** as white crystals (m.p. 155 – 157 °C) in trace amounts (*ca.* 1%).

^{1}H NMR: δ_H	1.84 (3H, s, ring-CH_3), 2.03 (3H, s, ring-CH_3), 2.10 (3H, s, ring-CH_3), 7.15 (1H, d, J = 7.3 Hz, Ar-H), 7.50 (1H, t, J = 7.6 Hz, Ar-H), 7.63 (1H, t, J = 7.6 Hz, Ar-H), 8.19 (1H, d, J = 8.2 Hz, Ar-H), 8.50 - 11.50 (1H, br. OH)
^{13}C NMR: δ_C	12.3 (ring-CH_3), 12.5 (ring-CH_3), 13.7 (ring-CH_3), 128.4 (C), 128.7 (Ar-CH), 130.3 (Ar-CH), 131.5 (Ar-CH), 133.2 (Ar-CH), 136.3 (C), 138.7 (C), 140.8 (C), 140.9 (C), 145.0 (C), 170.8 (acid C=O), 186.2 (quinone C=O), 187.9 (quinone C=O)
FTIR V_{max} ($CHCl_3$)	1598 (C=C), 1649 (C=O), 1693 (C=O), 1721 (C=O), 2925, 2964 (C-H saturated), 3023, 3071 (C-H unsaturated), 3263 (O-H)
HRMS [$(M - H)^+$]:	($C_{16}H_{13}O_4$) Calculated: 269.0819 Found: 269.0817
Rf:	0.59 (5% methanol/ethyl acetate)

(1R,6S)-6-Bromo-3,4,6-trimethyl-3'*H*-spiro[cyclohex[3]ene-1,1'-isobenzofuran]-2,3',5-trione 164

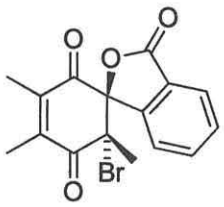

(164)

^{1}H NMR: δ_H	1.61 (3H, s, CH_3), 2.12 (3H, s, CH_3), 2.20 (3H, s, CH_3), 7.70 (1H, t, J = 7.6 Hz, Ar-H), 7.82 (1H, t, J = 7.6 Hz, Ar-H), 7.96 (1H, d, J = 7.6 Hz, Ar-H), 7.99 (1H, d, J = 7.9 Hz, Ar-H)
^{13}C NMR: δ_C	13.4 (CH_3), 14.0 (CH_3), 20.6 (CH_3), 61.5 (C), 90.4 (C), 125.9 (Ar-CH), 126.3 (Ar-CH), 126.5 (C), 131.1 (Ar-CH), 134.5 (Ar-CH), 143.4 (C), 143.6 (C), 143.9 (C), 167.5 (ester C=O), 188.1 (quinone C=O), 188.4 (quinone C=O)
FTIR V_{max} ($CHCl_3$)	1618 (C=C), 1693 (C=O), 1784 (C=O), 2850, 2920 (C-H saturated), 3080 (C-H unsaturated)
HRMS [(M + H)$^+$]:	($C_{16}H_{14}O_4Br$) Calculated: 349.0070 Found: 349.0070
Rf:	0.20 (45% dichloromethane/petrol)
X-ray crystallography:	See Appendix 2.2.4

2,5-Dioxopyrrolidin-1-yl 3',4',6'-trimethyl-2',5'-dioxo-2',5'-dihydro-[1,1'-biphenyl]-2-carboxylate 163[73]

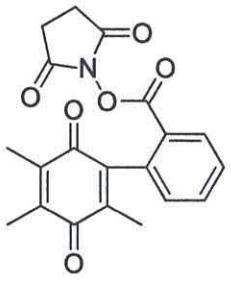

(163)

Dicyclohexylcarbodiimide (0.045 g, 0.22 mmol) was added to a solution of quinone acid **162** (0.047 g, 0.18 mmol) and *N*-hydroxysuccinimide (0.023 g, 0.20 mmol) in dry THF (2 ml) at 0 °C under nitrogen. The mixture was stirred for 18 h at r.t and then filtered to remove dicyclohexylurea. The solvent was removed *in vacuo* from the resulting filtrate and the residue treated with ethyl acetate (5 ml) and filtered again. The solvent was removed *in vacuo* to give a yellow solid (0.082 g). The crude product was purified by column chromatography using a stepwise gradient of ethyl acetate and petrol (10-40%). Fractions eluting in 20-25% ethyl acetate/petrol yielded the *N*-hydroxysuccinimide ester **163** as a yellow gum (0.018 g, 0.05 mmol, 28%).

^{1}H NMR: δ_H	1.86 (3H, s, ring-CH_3), 2.04 (3H, s, ring-CH_3), 2.07 (3H, s, ring-CH_3), 2.81 (4H, s, 2 x succinimidyl CH_2), 7.22 (1H, d, J = 7.5 Hz, Ar-H), 7.55 (1H, t, J = 7.8 Hz, Ar-H), 7.70 (1H, t, J = 7.6 Hz, Ar-H), 8.22 (1H, d, J = 7.8 Hz, Ar-H)
^{13}C NMR: δ_C	12.4 (ring-CH_3), 12.4 (ring-CH_3), 13.7 (ring-CH_3), 25.5 (2 x succinimidyl CH_2), 125.2 (C), 128.8 (Ar-CH), 130.6 (Ar-CH), 131.0 (Ar-CH), 133.9 (Ar-CH), 136.5 (C), 140.2 (C), 140.7 (C), 140.9 (C), 143.1 (C), 161.5 (ester C=O), 168.8 (2 x succinimidyl C=O), 185.6 (quinone C=O), 187.5 (quinone C=O)
FTIR V_{max} ($CHCl_3$)	1597 (C=C), 1649 (C=O), 1683 (C=O), 1741 (C=O), 1772 (C=O), 2855, 2932, 2994 (C-H saturated), 3070 (C-H unsaturated)
HRMS [$(M + NH_4)^+$]:	($C_{20}H_{21}O_6N_2$) Calculated: 385.1394 Found: 385.1398

HRMS [$(M + H)^+$]: ($C_{20}H_{18}O_6N$) Calculated: 368.1129 Found: 368.1130

Rf: 0.20 (40% ethyl acetate/petrol)

N-(*Bis*(dimethylamino)methylene)-3',4',6'-trimethyl-2',5'-dioxo-2',5'-dihydro-[1,1'-biphenyl]-2-carboxamide 130[73]

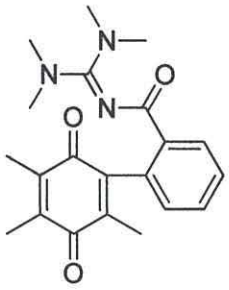

(130)

Dicyclohexylcarbodiimide (0.17 g, 0.82 mmol) was added to a solution of quinone acid **162** (0.18 g, 0.67 mmol) and *N*-hydroxysuccinimide (0.087 g, 0.76 mmol) in dry THF (8 ml) at 0 °C under nitrogen. The mixture was stirred for 18 h at r.t and then filtered to remove dicyclohexylurea. The solvent was removed *in vacuo* from the resulting filtrate and the residue treated with ethyl acetate (15 ml) and filtered again. The solvent was removed *in vacuo* to give a yellow solid which was re-dissolved in dry THF (8 ml). 1,1,3,3-Tetramethylguanidine **144** (0.18 ml, 1.4 mmol) was added and the mixture stirred in the dark for 46 h at r.t under nitrogen. Water (100 ml) was added and the mixture extracted with ethyl acetate (2 x 100 ml). The organic extracts were washed with water (2 x 100 ml), dried ($MgSO_4$), filtered and the solvent removed *in vacuo* to give a yellow oil (0.21 g). The crude product was purified by column chromatography (ethyl acetate) to yield compound **130** as a yellow oil (0.13 g, 0.35 mmol, 53%).

^{1}H NMR: δ_H	1.81 (3H, s, ring-CH_3), 2.01 (3H, s, ring-CH_3), 2.05 (3H, s, ring-CH_3), 2.83 (12H, s, 4 x CH_3), 7.06 (1H, d, J = 7.3 Hz, Ar-H), 7.40 – 7.46 (2H, m, 2 x Ar-H), 8.29 (1H, d, J = 7.6 Hz, Ar-H)
^{13}C NMR: δ_C	12.3 (ring-CH_3), 12.4 (ring-CH_3), 13.4 (ring-CH_3), 40.1 (4 x CH_3), 128.0 (Ar-CH), 129.5 (Ar-CH), 130.1 (Ar-CH), 130.6 (Ar-CH), 135.1 (C), 135.4 (C), 136.9 (C), 140.0 (C), 141.0 (C), 148.2 (C), 167.3 (C=N), 171.9 (amide C=O), 186.5 (quinone C=O), 188.3 (quinone C=O)
FTIR V_{max} ($CHCl_3$)	1585 (C=C), 1605 (C=C), 1648 (C=N), 1727 (C=O), 2795, 2928 (C-H saturated), 3059 (C-H unsaturated)
HRMS [$(M + H)^+$]:	($C_{21}H_{26}O_3N_3$) Calculated: 368.1969 Found: 368.1963

Rf: 0.19 (10% methanol/ethyl acetate)

N-(Di(piperidin-1-yl)methylene)-3',4',6'-trimethyl-2',5'-dioxo-2',5'-dihydro-[1,1'-biphenyl]-2-carboxamide 132[73]

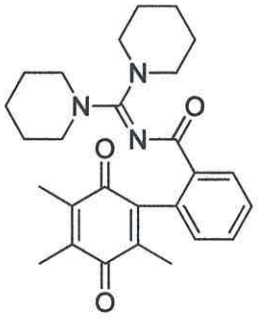

(132)

Dicyclohexylcarbodiimide (0.18 g, 0.87 mmol) was added to a solution of quinone acid **162** (0.20 g, 0.74 mmol) and *N*-hydroxysuccinimide (0.094 g, 0.82 mmol) in dry THF (8 ml) at 0 °C under nitrogen. The mixture was stirred for 18 h at r.t and then filtered to remove dicyclohexylurea. For the resulting filtrate the solvent was removed *in vacuo* and the residue dissolved in ethyl acetate (15 ml) and filtered again. The solvent was removed *in vacuo* to give a yellow solid which was re-dissolved in dry THF (8 ml). Di(piperidin-1-yl)methanimine **150** (0.44 g, 2.3 mmol) in dry THF (3 ml) was added and stirred in the dark for 46 h at r.t under nitrogen. Water (100 ml) was added and the mixture extracted with ethyl acetate (2 x 100 ml). The organic extracts were washed with water (2 x 100 ml), dried ($MgSO_4$), filtered and the solvent removed *in vacuo* to give a yellow oil (0.35 g). The crude product was purified by column chromatography (20% ethyl acetate/petrol) to yield un-reacted ester **163** (0.16 g, 0.44 mmol, 59%) as a yellow oil. This was followed by a stepwise gradient of methanol/ethyl acetate (20-70%). Fractions eluting in 25-65% methanol/ethyl acetate yielded compound **132** (0.071 g, 0.16 mmol, 21%) as a yellow oil.

^{1}H NMR: δ_H 1.55 (12H, s, 6 x CH_2), 1.81 (3H, s, ring-CH_3), 2.03 (3H, s, ring-CH_3), 2.06 (3H, s, ring-CH_3), 3.15 (8H, s, 4 x CH_2), 7.06 (1H, d, J = 6.9 Hz, Ar-H), 7.41 – 7.47 (2H, m, 2 x Ar-H), 8.32 (1H, d, J = 7.3 Hz, Ar-H)

^{13}C NMR: δ_C 12.4 (ring-CH_3), 12.4 (ring-CH_3), 13.4 (ring-CH_3), 24.4 (2 x CH_2), 25.5 (4 x CH_2), 49.8 (4 x CH_2), 128.1 (Ar-CH), 129.5 (Ar-CH), 130.2 (Ar-CH), 130.9 (Ar-CH), 135.1 (C), 135.3 (C), 136.5 (C), 140.0 (C), 141.0 (C), 148.3 (C), 166.5

	(C=N), 172.3 (amide C=O), 186.5 (quinone C=O), 188.4 (quinone C=O)
FTIR V_{max} ($CHCl_3$)	1586 (C=C), 1607 (C=C), 1647 (C=N), 1732 (C=O), 2855, 2935 (C-H saturated), 3061 (C-H unsaturated)
HRMS [$(M + H)^+$]:	($C_{27}H_{34}O_3N_3$) Calculated: 448.2595 Found: 448.2592
Rf:	0.18 (80% ethyl acetate/petrol)

N-(Dimorpholinomethylene)-3',4',6'-trimethyl-2',5'-dioxo-2',5'-dihydro-[1,1'-biphenyl]-2-carboxamide 134[73]

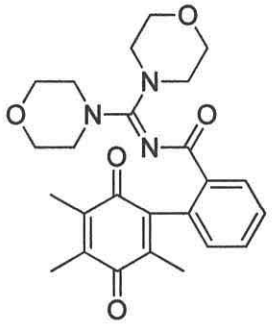

(134)

Dicyclohexylcarbodiimide (0.20 g, 0.97 mmol) was added to a solution of quinone acid **162** (0.22 g, 0.80 mmol) and *N*-hydroxysuccinimide (0.10 g, 0.87 mmol) in dry THF (8 ml) at 0 °C under nitrogen. The mixture was stirred for 18 h at r.t and then filtered to remove dicyclohexylurea. For the resulting filtrate the solvent was removed *in vacuo* and the residue dissolved with ethyl acetate (15 ml) and filtered again. The solvent was removed *in vacuo* to give a yellow solid which was re-dissolved in dry THF (8 ml). Dimorpholinomethanimine **151** (0.48 g, 2.4 mmol) in dry THF (6 ml) was added and stirred in the dark for 46 h at r.t under nitrogen. Water (100 ml) was added and the mixture extracted with ethyl acetate (2 x 100 ml). The organic extracts were washed with water (2 x 100 ml), dried ($MgSO_4$), filtered and the solvent removed *in vacuo* to give a brown oil (0.37 g). The crude product was purified by column chromatography (20% ethyl acetate/petrol) to yield un-reacted ester **163** (0.095 g, 0.26 mmol, 32%) as a yellow oil. This was followed by a stepwise gradient of ethyl acetate/petrol (20-100%). Fractions eluting in 50-80% ethyl acetate/petrol yielded compound **134** as a yellow oil (0.15 g, 0.34 mmol, 42%).

^{1}H NMR: δ_H 1.81 (3H, s, ring-CH_3), 2.04 (3H, s, ring-CH_3), 2.09 (3H, s, ring-CH_3), 3.28 (8H, s, 4 x CH_2), 3.70 (8H, s, 4 x CH_2), 7.09 (1H, d, J = 7.6 Hz, Ar-H), 7.44 – 7.53 (2H, m, 2 x Ar-H), 8.34 (1H, d, J = 7.2 Hz, Ar-H)

^{13}C NMR: δ_C 12.4 (2 x ring-CH_3), 13.5 (ring-CH_3), 49.1 (4 x CH_2), 66.1 (4 x CH_2), 128.2 (Ar-CH), 129.7 (Ar-CH), 130.9 (Ar-CH), 131.2 (Ar-CH), 135.4 (C), 135.5 (C), 135.8 (C), 140.4 (C),

	140.8 (C), 147.9 (C), 164.7 (C=N), 173.2 (amide C=O), 186.6 (quinone C=O), 188.1 (quinone C=O)
FTIR V_{max} (CH_2Cl_2)	1589 (C=C), 1616 (C=C), 1646 (C=N), 1726 (C=O), 2858, 2922, 2966 (C-H saturated), 3059 (C-H unsaturated)
HRMS [$(M + H)^+$]:	($C_{25}H_{30}O_5N_3$) Calculated: 452.2180 Found: 452.2180
Rf:	0.22 (5% methanol/ethyl acetate)

N,N-Bis(2-chloroethyl)-4-nitroaniline 166[226, 227]

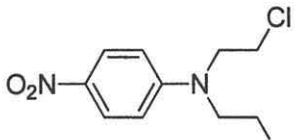

(166)

2,2'-((4-Nitrophenyl)azanediyl)diethanol **165** (0.80 g, 3.5 mmol) was suspended in dry dichloromethane (8 ml) and pyridine (1.0 ml, 12 mmol) and cooled to 0 °C. Thionyl chloride (1.2 ml, 16 mmol) was added slowly and the mixture stirred at reflux for 7 h. After cooling to r.t, the mixture was then extracted with dichloromethane (2 x 100 ml), the organic layer washed with water (2 x 100 ml), dried ($MgSO_4$), filtered and the solvent removed *in vacuo* to give a yellow solid (0.85 g). The crude product was then purified by column chromatography using a stepwise gradient of ethyl acetate and petrol (20-100%). Fractions eluting in 20% ethyl acetate/petrol yielded compound **166** (0.74 g, 2.8 mmol, 80%) as yellow crystals (m.p. 92 – 93 °C, lit. 95 - 96 °C).[228] Fractions eluting in 40% ethyl acetate/petrol yielded compound **167** (m.p. 99 – 101 °C) as a yellow solid in trace amounts (*ca.*1%).

^{1}H NMR: δ_H	3.70 (4H, t, J = 6.9 Hz, 2 x CH_2), 3.87 (4H, t, J = 6.9 Hz, 2 x CH_2), 6.68 (2H, d, J = 9.5 Hz, 2 x Ar-H), 8.15 (2H, d, J = 9.1 Hz, 2 x Ar-H)
^{13}C NMR: δ_C	39.9 (2 x CH_2), 53.3 (2 x CH_2), 110.7 (2 x Ar-CH), 126.4 (2 x Ar-CH), 138.4 (C), 151.2 (C)
HRMS [$(M + H)^+$]:	($C_{10}H_{13}O_2N_2Cl_2^{35}$) Calculated: 263.0349 Found: 263.0355
	($C_{10}H_{13}O_2N_2Cl^{35}Cl^{37}$) Calculated: 265.0319
	Found: 265.0324
	($C_{10}H_{13}O_2N_2Cl_2^{37}$) Calculated: 267.0290 Found: 267.0294
Rf:	0.15 (10% ethyl acetate/petrol)

2-((2-Chloroethyl)(4-nitrophenyl)amino)ethanol 167

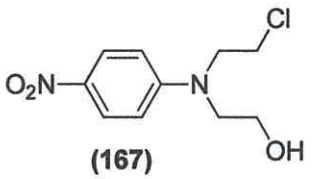

(167)

^{1}H NMR: δ_H 1.71 (1H, s, OH), 3.68 – 3.74 (4H, m, 2 x CH_2), 3.86 (4H, t, J = 7.2 Hz, CH_2), 3.90 (2H, t, J = 5.2 Hz, CH_2), 6.71 (2H, d, J = 9.6 Hz, 2 x Ar-H), 8.13 (2H, d, J = 9.6 Hz, 2 x Ar-H)

^{13}C NMR: δ_C 39.7 (CH_2), 53.4 (CH_2), 53.7 (CH_2), 59.9 (CH_2), 110.8 (2 x Ar-CH), 126.3 (2 x Ar-CH), 137.9 (C), 152.1 (C)

FTIR V_{max} (KBr) 1518 (N=O), 1598 (C=C), 2875, 2925, 2963 (C-H saturated), 3112 (C-H unsaturated), 3486 (O-H)

HRMS [$(M + H)^+$]: ($C_{10}H_{14}O_3N_2Cl^{35}$) Calculated: 245.0687 Found: 245.0686
($C_{10}H_{14}O_3N_2Cl^{37}$) Calculated: 247.0658 Found: 247.0654

Rf: 0.19 (40 % ethyl acetate/petrol)

Other possible by-product

6-(4-Nitrophenyl)-1,3,2,6-dioxathiazocane 2-oxide 168

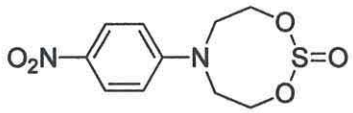

(168)

^{1}H NMR: δ_H	3.68 (2H, ddd, J = 2.2, 8.5, 16.0 Hz, 2 x CH), 3.94 (2H, ddd, J = 2.2, 5.0, 12.5 Hz, 2 x CH), 3.98 (2H, ddd, J = 2.0, 5.0, 16.0 Hz, 2 x CH), 4.69 (2H, ddd, J = 2.0, 8.5, 12.5 Hz, 2 x CH), 6.61 (2H, d, J = 9.5 Hz, 2 x Ar-H), 8.17 (2H, d, J = 9.5 Hz, 2 x Ar-H)
^{13}C NMR: δ_C	52.1 (2 x CH_2), 58.2 (2 x CH_2), 110.7 (2 x Ar-CH), 126.4 (2 x Ar-CH), 138.3 (C), 150.9 (C)
FTIR V_{max} (KBr)	1514 (N=O), 1598 (C=C), 2957, 3000 (C-H saturated), 3093 (C-H unsaturated),
LRMS:	273 (74%, [M + H^+]), 105 (100%)
HRMS [(M + H)$^+$]:	($C_{10}H_{13}O_5N_2S$) Calculated: 273.0540 Found: 273.0542
Melting point:	179 – 183 °C
Rf:	0.18 (30 % ethyl acetate/petrol)

N^1,N^1-*Bis*(2-chloroethyl)benzene-1,4-diamine 76[227]

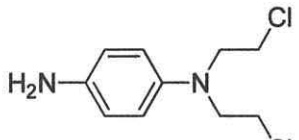

(76)

To *N,N-bis*(2-chloroethyl)-4-nitroaniline **166** (0.40 g, 1.5 mmol) in ethanol (35 ml) Pd (5% on C, 0.088 g) was added. The mixture was stirred in an atmosphere of hydrogen for 17 h, filtered through celite using a 2:1 ethyl acetate/hexane solvent mixture and the resulting solution concentrated *in vacuo* to give impure mustard as a brown solid **76** (0.99 g). The crude product was purified by column chromatography (50% ethyl acetate/petrol) to yield compound **76** (0.24 g, 1.0 mmol, 68%) as a brown oil which was used in the next reaction without additional purification. Also isolated in the later fractions was a by-product **170** (0.19 g, 0.48 mmol, 32%) as a brown solid (m.p. >280 °C).

^{1}H NMR: δ_H (DMSO-d_6)	3.57 – 3.58 (4H, m, 2 x CH_2), 3.66 (4H, t, J = 6.6 Hz, 2 x CH_2), 5.13 (2H, s, NH_2), 6.62 (4H, m, 4 x Ar-H)
^{13}C NMR: δ_C (DMSO-d_6)	42.5 (2 x CH_2), 54.5 (2 x CH_2), 116.6 (2 x Ar-CH), 117.0 (2 x Ar-CH) 139.2 (C), 140.5 (C)
HRMS [$(M + H)^+$]:	($C_{10}H_{15}N_2Cl_2^{35}$) Calculated: 233.0607 Found: 233.0609
	($C_{10}H_{15}N_2Cl^{35}Cl^{37}$) Calculated: 235.0577 Found: 235.0579
	($C_{10}H_{15}N_2Cl_2^{37}$) Calculated: 237.0548 Found: 237.0549
Rf:	0.16 (33% ethyl acetate/hexane)

4-(4-(4-Aminophenyl)piperazin-1-yl)-*N*,*N*-*bis*(2-chloroethyl)aniline 170

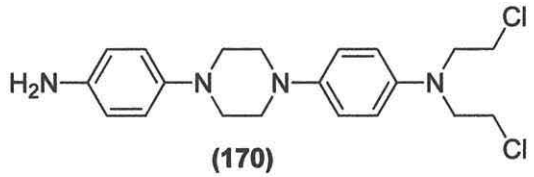

(170)

^{1}H NMR: δ_H (DMSO-d_6)	3.07 (4H, s, 2 x CH_2), 3.12 (4H, s, 2 x CH_2), 3.68 – 3.72 (8H, m, 4 x CH_2), 4.71 (2H, s, NH_2), 6.56 (2H, d, J = 8.8 Hz, 2 x Ar-H), 6.74 (2H, d, J = 9.2 Hz, 2 x Ar-H), 6.78 (2H, d, J = 8.8 Hz, 2 x Ar-H), 6.94 (2H, d, J = 9.1 Hz, 2 x Ar-H)
^{13}C NMR: δ_C (DMSO-d_6)	42.3 (2 x CH_2), 51.0 (2 x CH_2), 51.6 (2 x CH_2), 53.6 (2 x CH_2), 114.4 (2 x Ar-CH), 115.7 (2 x Ar-CH), 118.9 (2 x Ar-CH), 119.1 (2 x Ar-CH), 141.1 (C), 143.2 (C), 143.3 (C), 144.1 (C)
FTIR V_{max} (KBr)	1514 (C=C), 2756, 2819, 2875, 2973 (C-H saturated), 3055 (C-H unsaturated), 3371, 3455 (N-H)
HRMS [$(M + H)^+$]:	($C_{20}H_{27}N_4Cl_2^{35}$) Calculated: 393.1607 Found: 393.1609 ($C_{20}H_{27}N_4Cl^{35}Cl^{37}$) Calculated: 395.1578 Found: 395.1579 ($C_{20}H_{27}N_4Cl_2^{37}$) Calculated: 397.1549 Found: 397.1550
Rf:	0.15 (50% ethyl acetate/hexane)

N-(4-(*Bis*(2-chloroethyl)amino)phenyl)-3-methyl-3-(2,4,5-trimethyl-3,6-dioxocyclohexa-1,4-dien-1-yl)butanamide 78[73]

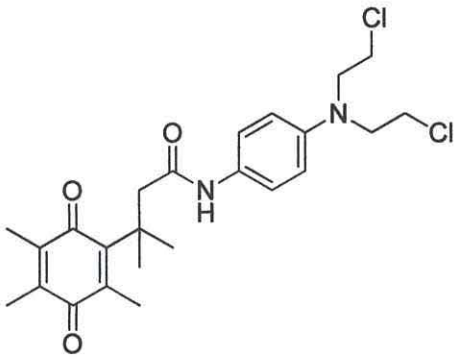

(78)

N-Hydroxysuccinimide ester **50b** (0.082 g, 0.23 mmol) in dry THF (1 ml) was added to a solution of N^1,N^1-*bis*(2-chloroethyl)benzene-1,4-diamine **76** (0.15 g, 0.64 mmol) in dry THF (2 ml). After being stirred in the dark for 21 h at r.t under nitrogen, the mixture was extracted with ethyl acetate (2 x 100 ml) and the organic layer washed with water (2 x 100 ml). The organic extracts were dried ($MgSO_4$), filtered and the solvent removed *in vacuo* to yield a brown oil (0.26 g). The crude product was then purified by column chromatography (20% ethyl acetate/petrol) to yield compound **78** (0.071 g, 0.15 mmol, 65%) as an orange solid (m.p. 80 – 84 °C, lit. 87 – 89 °C).[73]

^{1}H NMR: δ_H	1.50 (6H, s, 2 x *gem*-CH_3), 1.96 (3H, s, ring-CH_3), 1.97 (3H, s, ring-CH_3), 2.16 (3H, s, ring-CH_3), 2.98 (2H, s, CH_2), 3.60 (4H, t, J = 6.6 Hz, 2 x CH_2), 3.69 (4H, t, J = 6.8 Hz, 2 x CH_2), 6.61 (2H, d, J = 8.8 Hz, 2 x Ar-H), 6.94 (1H, s, NH), 7.25 (2H, d, J = 9.2 Hz, 2 x Ar-H)
^{13}C NMR: δ_C	12.1 (ring-CH_3), 12.7 (ring-CH_3), 14.2 (ring-CH_3), 29.2 (2 x *gem*-CH_3), 38.6 ($C(CH_3)_2$), 40.4 (2 x CH_2), 50.1 (CH_2), 53.7 (2 x CH_2), 112.5 (2 x Ar-H), 122.5 (2 x Ar-H), 128.2 (C), 138.2 (2 x C), 143.2 (2 x C), 153.0 (C), 170.0 (amide C=O), 187.5 (quinone C=O), 191.5 (quinone C=O)
FTIR V_{max} (CH_2Cl_2)	1596 (C=C), 1644 (C=O), 1733 (C=O), 2872, 2925, 2963 (C-H saturated), 3007, 3050, 3118, 3180 (C-H unsaturated), 3296 (N-H)
HRMS [(M + H)$^+$]:	($C_{24}H_{31}O_3N_2Cl_2^{35}$) Calculated: 465.1706 Found: 465.1705

($C_{24}H_{31}O_3N_2Cl^{35}Cl^{37}$) Calculated: 467.1677

Found: 467.1675

($C_{24}H_{31}O_3N_2Cl_2^{37}$) Calculated: 469.1648 Found: 469.1644

Rf: 0.18 (20% ethyl acetate/petrol)

N^1-(4-(*Bis*(2-chloroethyl)amino)phenyl)-N^4-((3',4',6'-trimethyl-2',5'-dioxo-2',5'-dihydro-[1,1'-biphenyl]-2-carbonyl)oxy)succinamide 171[73]

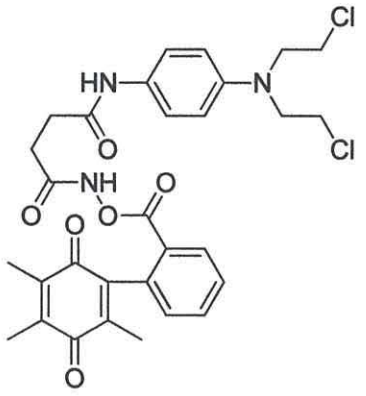

(171)

N-Hydroxysuccinimide ester **163** (0.077 g, 0.21 mmol) in dry THF (1.5 ml) was added to a solution of N^1,N^1-*bis*(2-chloroethyl)benzene-1,4-diamine **76** (0.15 g, 0.64 mmol) in dry THF (1.5 ml). After being stirred in the dark for 25 h at r.t under nitrogen, the mixture was extracted with ethyl acetate (2 x 50 ml) and the organic layer washed with water (2 x 50 ml). The organic extracts were dried ($MgSO_4$), filtered and the solvent removed *in vacuo* to yield a brown solid (0.17 g). The crude product was then purified by column chromatography (10 - 35% ethyl acetate/petrol) to yield the compound **171** (0.03 g, 0.05 mmol, 24%) as a light brown solid (m.p. 130 – 140 °C).

^{1}H NMR: δ_H 1.84 (3H, s, ring-CH_3), 2.01 (3H, s, ring-CH_3), 2.06 (3H, s, ring-CH_3), 2.69 (4H, s, 2 x succinimidyl CH_2), 3.61 (4H, t, J = 6.8 Hz, 2 x CH_2), 3.70 (4H, t, J = 7.0 Hz, 2 x CH_2), 6.62 (2H, d, J = 8.4 Hz, 2 x Ar-H), 7.19 (1H, d, J = 8.0 Hz, Ar-H), 7.30 (1H, d, J = 8.0 Hz, 2 x Ar-H), 7.51 (1H, t, J = 7.6 Hz, Ar-H), 7.57 (1H, s, NH), 7.66 (1H, t, J = 7.8 Hz, Ar-H), 8.19 (1H, d, J = 7.6 Hz, Ar-H), 9.86 (1H, s, NH)

^{13}C NMR: δ_C (partial) 12.4 (ring-CH_3), 12.5 (ring-CH_3), 13.8 (ring-CH_3), 29.7 (2 x succinimidyl CH_2), 40.5 (2 x CH_2), 53.6 (2 x CH_2), 112.4 (2 x Ar-H), 122.7 (2 x Ar-H), 128.8 (2 x Ar-H), 130.5 (2 x Ar-H), 136.3 (C), 140.7 (C), 164.1 (2 x amide C=O), 186.1 (quinone C=O), 187.7 (quinone C=O)

FTIR V_{max} (KBr)	1598 (C=C), 1650 (C=O), 1697 (C=O), 1739 (C=O), 1773 (C=O), 2982 (C-H saturated), 3212, 3334 (C-H unsaturated), 3440, 3525 (N-H)
HRMS [(M + H)$^+$]:	($C_{30}H_{32}O_6N_3Cl_2^{35}$) Calculated: 600.1663 Found: 600.1660
	($C_{30}H_{32}O_6N_3Cl^{35}Cl^{37}$) Calculated: 602.1633 Found: 602.1631
	($C_{30}H_{32}O_6N_3Cl_2^{37}$) Calculated: 604.1604 Found: 604.1604
Rf:	0.19 (55% ethyl acetate/hexane)

References

1 K. Achilles, *Arch. Pharm. Pharm. Med. Chem.*, 2001, **334**, 209.

2 P. L. Carl, P. K. Chakravarty, J. A. Katzenellenbogen, and M. J. Weber, *Proc. Natl. Acad. Sci.*, 1980, **77**, 2224.

3 W. A. Denny, *Eur. J. Med. Chem.*, 2001, **36**, 577.

4 S. Jaracz, J. Chen, L. V. Kuznetsova, and I. Ojima, *Bioorg. Med. Chem.*, 2005, **13**, 5043.

5 A. Albert, *Nature*, 1958, **182**, 421.

6 N. J. Harper, *J. Med. Pharmaceut. Chem.*, 1959, **1**, 467.

7 W. A. Denny, *Lancet Oncol.*, 2000, **1**, 25.

8 K. L. Amsberry and R. T. Borchardt, *J. Org. Chem.*, 1990, **55**, 5867.

9 A. K. Sinhababu and D. R. Thakker, *Adv. Drug. Deliver. Rev.*, 1996, **19**, 241.

10 M. N. Levine, L. D. Lavis, and R. T. Raines, *Molecules*, 2008, **13**, 204.

11 B. Wang, H. Zhang, and W. Wang, *Bioorg. Med. Chem. Lett.*, 1996, **6**, 945.

12 S. Padmanabhan, J. E. Coughlin, G. Zhang, C. J. Kirk, and R. P. Iyer, *Bioorg. Med. Chem. Lett.*, 2006, **16**, 1491.

13 M. Höckel and P. Vaupel, *J. Natl. Cancer Inst.*, 2001, **93**, 266.

14 J. M. Brown and A. J. Giaccia, *Cancer Res.*, 1998, **58**, 1408.

15 J. M. Brown, *Mol. Med. Today*, 2000, **6**, 157.

16 D. P. Naughton, *Adv. Drug. Deliver. Rev.*, 2001, **53**, 229.

17 M. Jaffar, K. J. Williams, and I. J. Stratford, *Adv. Drug. Deliver. Rev.*, 2001, **53**, 217.

18 A. C. Sartorelli, *Cancer Res.*, 1988, **48**, 775.

19 M. Stubbs, P. M. J. McSheehy, J. R. Griffiths, and C. L. Bashford, *Mol. Med. Today*, 2000, **6**, 15.

20 J. W. Baish, P. A. Netti, and R. K. Jain, *Microvasc. Res.*, 1997, **53**, 128.

21 C. P. Guise, A. T. Wang, A. Theil, D. J. Bridewell, W. R. Wilson, and A. V. Patterson, *Biochem. Pharmacol.*, 2007, **74**, 810.

22 J. M. Brown and A. Koong, *J. Natl. Cancer Inst.*, 1991, **83**, 178.

23 M. P. Hay, B. M. Sykes, W. A. Denny, and W. R. Wilson, *Bioorg. Med. Chem. Lett.*, 1999, **9**, 2237.

[24] B. Palcic, B. Faddegon, and L. D. Skarsgard, *Radiat. Res.*, 1984, **100**, 340.

[25] S. Cole, I. J. Stratford, G. E. Adams, E. M. Fielden, and T. C. Jenkins, *Radiat. Res.*, 1990, **124**, S38.

[26] C. Jin, L. Bai, H. Wu, F. Tian, and G. Guo, *Biomaterials*, 2007, **28**, 3724.

[27] R. J. Knox, T. C. Jenkins, S. M. Hobbs, S. Chen, R. G. Melton, and P. J. Burke, *Cancer Res.*, 2000, **60**, 4179.

[28] A. Christofferson and J. Wilkie, *Biochem. Soc. Trans.*, 2009, **37**, 413.

[29] T. Fuchs, G. Chowdhury, C. L. Barnes, and K. S. Gates, *J. Org. Chem.*, 2001, **66**, 107.

[30] F. Arndt, *Ber. Deut. Chem. Ges.*, 1913, **46**, 3522.

[31] F. J. Wolf, K. Pfister 3rd, R. M. Wilson Jr, and C. A. Robinson, *J. Am. Chem. Soc.*, 1954, **76**, 3551.

[32] J. C. Mason and G. Tennant, *J. Chem. Soc. B.*, 1970, 911.

[33] F. Arndt and B. Rosenau, *Ber. Deut. Chem. Ges.*, 1917, **50**, 1248.

[34] R. F. Robbins and K. Schofield, *J. Chem. Soc.*, 1957, 3186.

[35] R. F. Anderson, S. S. Shinde, M. P. Hay, S. A. Gamage, and W. A. Denny, *J. Am. Chem. Soc.*, 2003, **125**, 748.

[36] J. S. Daniels and K. S. Gates, *J. Am. Chem. Soc.*, 1996, **118**, 3380.

[37] S. S. Shinde, R. F. Anderson, M. P. Hay, S. A. Gamage, and W. A. Denny, *J. Am. Chem. Soc.*, 2004, **126**, 7865.

[38] R. F. Anderson, S. S. Shinde, M. P. Hay, S. A. Gamage, and W. A. Denny, *Org. Biomol. Chem.*, 2005, **3**, 2167.

[39] S. S. Shinde, M. P. Hay, A. V. Patterson, W. A. Denny, and R. F. Anderson, *J. Am. Chem. Soc.*, 2009, **131**, 14220.

[40] S. A. Fitzsimmons, A. D. Lewis, R. J. Riley, and P. Workman, *Carcinogenesis*, 1994, **15**, 1503.

[41] V. Junnotula, A. Rajapakse, L. Arbillaga, A. López de Cerain, B. Solano, R. Villar, A. Monge, and K. S. Gates, *Bioorg. Med. Chem.*, 2010, **18**, 3125.

[42] X. Shi, S. M. Mandel, and M. S. Platz, *J. Am. Chem. Soc.*, 2007, **129**, 4542.

[43] D. Rischin, L. Peters, R. Hicks, P. Hughes, R. Fisher, R. Hart, M. Sexton, I. D'Costa, and R. von Roemeling, *J. Clin. Oncol.*, 2001, **19**, 535.

[44] D.-J. Lee, A. Trotti, S. Spencer, R. Rostock, C. Fisher, R. von Roemeling, E. Harvey, and E. Groves., *Int. J. Radiat. Oncol.*, 1998, **42**, 811.

[45] D. Rischin, L. J. Peters, B. O'Sullivan, J. Giralt, R. Fisher, K. Yuen, A. Trotti, J. Bernier, J. Bourhis, J. Ringash, M. Henke, and L. Kenny, *J. Clin. Oncol.*, 2010, **28**, 2989.

[46] M. P. Hay, K. O. Hicks, F. B. Pruijn, K. Pchalek, B. G. Siim, W. R. Wilson, and W. A. Denny, *J. Med. Chem.*, 2007, **50**, 6392.

[47] M. P. Hay, K. O. Hicks, K. Pchalek, H. H. Lee, A. Blaser, F. B. Pruijn, R. F. Anderson, S. S. Shinde, W. R. Wilson, and W. A. Denny, *J. Med. Chem.*, 2008, **51**, 6853.

[48] A. Monge, J. A. Palop, A. López de Ceráin, V. Senador, F. J. Martínez-Crespo, Y. Sainz, S. Narro, E. García, C. de Miguel, M. González, E. Hamilton, A. J. Barker, E. D. Clarke, and D. T. Greenhow, *J. Med. Chem.*, 1995, **38**, 1786.

[49] E. Vincente, R. Villar, S. Pérez-Silanes, I. Aldana, R. C. Goldman, and A. Mong, *Infect. Disord. Drug. Targets*, 2011, **2**, 196.

[50] M. A. Colucci, C. J. Moody, and G. D. Couch, *Org. Biomol. Chem.*, 2008, **6**, 637.

[51] S. A. Everett, E. Swann, M. A. Naylor, M. R. L. Stratford, K. B. Patel, N. Tian, R. G. Newman, B. Vojnovic, C. J. Moody, and P. Wardman, *Biochem. Pharmacol.*, 2002, **63**, 1629.

[52] T. Hata, Y. Sano, A. Sugawara, R. Matsumae, K. Kanamori, T. Shima, and T. Hoshi, *J. Antibiot.*, 1956, **9**, 141.

[53] S. K. Arora, M. B. Cox, and P. Arjunan, *J. Med. Chem.*, 1990, **33**, 3000.

[54] S. Wakaki, H. Marumo, K. Tomioka, G. Shimizu, E. Kato, H. Kamada, S. Kudo, and Y. Fujimoto, *Antibiot. Chemother.*, 1958, **8**, 228.

[55] Y. Kishi, *J. Nat. Prod.*, 1979, **42**, 549.

[56] T. Fukuyama and L. Yang, *J. Am. Chem. Soc.*, 1989, **111**, 8303.

[57] J. S. Webb, D. B. Cosulich, J. H. Mowat, J. B. Patrick, R. W. Broschard, W. E. Meyer, R. P. Williams, C. F. Wolf, W. Fulmor, and C. Pidacks, *J. Am. Chem. Soc.*, 1962, **84**, 3185.

[58] M. Faig, M. A. Bianchet, S. Winski, R. Hargreaves, C. J. Moody, A. R. Hudnott, D. Ross, and L. M. Amzel, *Structure*, 2001, **9**, 659.

[59] F. Nakatsubo, A. J. Cocuzza, D. E. Keeley, and Y. Kishi, *J. Am. Chem. Soc.*, 1977, **99**, 4835.

[60] F. Nakatsubo, T. Fukuyama, A. J. Cocuzza, and Y. Kishi, *J. Am. Chem. Soc.*, 1977, **99**, 8115.

[61] T. Fukuyama, F. Nakatsubo, A. J. Cocuzza, and Y. Kishi, *Tetrahedron Lett.*, 1977, **18**, 4295.

[62] T. Fukuyama and L. Yang, *J. Am. Chem. Soc.*, 1987, **109**, 7881.

[63] S. R. Keyes, S. Rockwell, and A. C. Sartorelli, *Cancer Res.*, 1985, **45**, 3642.

[64] S. Rockwell, S. R. Keyes, and A. C. Sartorelli, *Cancer Res.*, 1988, **48**, 5471.

[65] J. B. Weissberg, Y. H. Son, R. J. Papac, C. Sasaki, D. B. Fischer, R. Lawrence, S. Rockwell, A. C. Sartorelli, and J. J. Fischer, *Int. J. Radiat. Oncol.*, 1989, **17**, 3.

[66] M. F. Belcourt, W. F. Hodnick, S. Rockwell, and A. C. Sartorelli, *Adv. Enzyme Regul.*, 1998, **38**, 111.

[67] B. S. Lyengar, H.-J. Lin, L. Cheng, and W. A. Remers, *J. Med. Chem.*, 1981, **24**, 975.

[68] B. S. Lyengar, S. M. Sami, S. E. Tarnow, W. A. Remers, W. T. Bradner, and J. E. Schurig, *J. Med. Chem.*, 1983, **26**, 1453.

[69] S. M. Sami, B. S. Lyengar, S. E. Tarnow, W. A. Remers, W. T. Bradner, and J. E. Schurig, *J. Med. Chem.*, 1984, **27**, 701.

[70] H. D. Beall, S. Winski, E. Swann, A. R. Hudnott, A. S. Cotterill, N. O'Sullivan, S. J. Green, R. Bien, D. Siegel, D. Ross, and C. J. Moody, *J. Med. Chem.*, 1998, **41**, 4755.

[71] E. Swann, P. Barraja, A. M. Oberlander, W. T. Gardipee, A. R. Hudnott, H. D. Beall, and C. J. Moody, *J. Med. Chem.*, 2001, **44**, 3311.

[72] M. Jaffar, R. M. Phillips, K. J. Williams, I. Mrema, C. Cole, N. S. Wind, T. H. Ward, I. J. Stratford, and A. V. Patterson, *Biochem. Pharmacol.*, 2003, **66**, 1199.

[73] M. Volpato, N. Abou-Zeid, R. W. Tanner, L. T. Glassbrook, J. Taylor, I. Stratford, P. M. Loadman, M. Jaffar, and R. M. Phillips, *Mol. Cancer Ther.*, 2007, **6**, 3122.

[74] E. A. Oostveen and W. N. Speckamp, *Tetrahedron*, 1987, **43**, 255.

[75] A. S. Cotterill, C. J. Moody, and J. R. A. Roffey, *Tetrahedron*, 1995, **51**, 7223.

[76] E. Comer and W. S. Murphy, *ARKIVOC*, 2003, 286.

[77] L. Y. Dirix, F. Tonnesen, J. Cassidy, R. Epelbaum, W. W. ten Bokkel Huinink, N. Pavlidis, R. Sorio, T. Gamucci, I. Wolff, A. T. Velde, J. Lan, and J. Verweij, *Eur. J. Cancer*, 1996, **32**, 2019.

[78] R. M. Philips, M. Jaffar, D. J. Maitland, P. M. Loadman, S. D. Shnyder, G. Steans, P. A. Cooper, A. Race, A. V. Patterson, and I. J. Stratford, *Biochem. Pharmacol.*, 2004, **68**, 2107.

[79] R. M. Phillips, *Biochem. Pharmacol.*, 1996, **52**, 1711.

[80] M. Jaffar, M. A. Naylor, N. Robertson, S. Lockyer, R. M. Phillips, S. A. Everett, G. E. Adams, and I. Stratford, *Anticancer Drug. Des.*, 1998, **13**, 105.

[81] P. M. Loadman, M. C. Bibby, and R. M. Philips, *Brit. J. Pharmacol.*, 2002, **137**, 701.

[82] L. Ernster and F. Navazio, *Acta Chem. Scand.*, 1958, **12**, 595.

[83] H. D. Beall, A. R. Hudnott, S. Winski, D. Siegel, E. Swann, D. Ross, and C. J. Moody, *Bioorg. Med. Chem. Lett.*, 1998, **8**, 545.

[84] S. Chen, K. Wu, and R. Knox, *Free Rad. Biol. Med.*, 2000, **29**, 276.

[85] G. Cavelier and L. M. Amzel, *Proteins*, 2001, **43**, 420.

[86] R. Li, M. A. Bianchet, P. Talalay, and L. M. Amzel, *Proc. Natl. Acad. Sci. USA.*, 1995, **92**, 8846.

[87] B. P. Schlegal, K. Ratnam, and T. M. Penning, *Biochemistry*, 1998, **37**, 11003.

[88] A. Suleman and E. B. Skibo, *J. Med. Chem.*, 2002, **45**, 1211.

[89] M. A. Bianchet, C. Foster, M. Faig, P. Talalay, and L. M. Amzel, *Biochem. Soc. T.*, 1999, **27**, 610.

[90] M. Faig, M. A. Bianchet, P. Talalay, S. Chen, S. Winski, D. Ross, and L. M. Amzel, *Proc. Natl. Acad. Sci. USA*, 2000, **97**, 3177.

[91] S. Milstien and L. A. Cohen, *J. Am. Chem. Soc.*, 1972, **94**, 9158.

[92] J. M. Karle and I. L. Karle, *J. Am. Chem. Soc.*, 1972, **94**, 9182.

[93] B. Wang, M. G. Nicolaou, S. Liu, and R. T. Borchardt, *Bioorg. Chem.*, 1996, **24**, 39.

[94] R. E. Winans and C. F. Wilcox Jr, *J. Am. Chem. Soc.*, 1976, **98**, 4281.

[95] R. M. Beesley, C. K. Ingold, and J. F. Thorpe, *J. Chem. Soc. Trans.*, 1915, **107**, 1080.

[96] C. Danforth, A. W. Nicholson, J. C. James, and G. M. Loudon, *J. Am. Chem. Soc.*, 1976, **98**, 4275.

[97] F. C. Lightstone and T. C. Bruice, *J. Am. Chem. Soc.*, 1994, **116**, 10789.

[98] R. T. Borchardt and L. A. Cohen, *J. Am. Chem. Soc.*, 1973, **95**, 8308.

[99] R. T. Borchardt and L. A. Cohen, *J. Am. Chem. Soc.*, 1973, **95**, 8313.

[100] R. T. Borchardt and L. A. Cohen, *J. Am. Chem. Soc.*, 1973, **95**, 8319.

[101] M. M. King and L. A. Cohen, *J. Am. Chem. Soc.*, 1983, **105**, 2752.

[102] P. S. Hillery and L. A. Cohen, *J. Am. Chem. Soc.*, 1983, **105**, 2760.

[103] P. S. Hillery and L. A. Cohen, *J. Org. Chem.*, 1983, **48**, 3465.

[104] R. T. Borchardt and L. A. Cohen, *J. Am. Chem. Soc.*, 1972, **94**, 9166.

[105] R. T. Borchardt and L. A. Cohen, *J. Am. Chem. Soc.*, 1972, **94**, 9175.

[106] L. A. Carpino, S. A. Triolo, and R. A. Berglund, *J. Org. Chem.*, 1989, **54**, 3303.

[107] K. L. Amsberry and R. T. Borchardt, *Pharmaceut. Res.*, 1991, **8**, 323.

[108] J. L. Wolfe, D. V. Velde, and R. T. Borchardt, *J. Org. Chem.*, 1992, **57**, 6138.

[109] B. Wang, S. Liu, and R. T. Borchardt, *J. Org. Chem.*, 1995, **60**, 539.

[110] M. G. Nicolaou, J. L. Wolfe, R. L. Schowen, and R. T. Borchardt, *J. Org. Chem.*, 1996, **61**, 6633.

[111] D. Shan, M. G. Nicolaou, R. T. Borchard, and B. Wang, *J. Pharm. Sci.*, 1997, **86**, 765.

[112] S. Passmore, 'Synthesis and Evaluation of Redox-activated Prodrug Delivery Systems as Biological Markers', PhD Thesis, University of Manchester, 2009.

[113] A. Zheng, D. Shan, X. Shi, and B. Wang, *J. Org. Chem.*, 1999, **64**, 7459.

[114] S.-T. Huang and Y.-L. Lin, *Org. Lett.*, 2006, **8**, 265.

[115] S.-T. Huang, Y.-X. Peng, and K.-L. Wang, *Biosens. Bioelectron.*, 2008, **23**, 1793.

[116] S. Liu, B. Wang, M. G. Nicolaou, and R. T. Borchardt, *J. Chem. Crystallogr.*, 1996, **26**, 209.

[117] N. Weerapreeyakul, R. Anorach, T. Khuansawad, C. Yenjai, and M. Isaka, *Chem. Pharm. Bull.*, 2007, **55**, 930.

[118] K. L. Amsberry, A. E. Gerstenberger, and R. T. Borchardt, *Pharmaceut. Res.*, 1991, **8**, 455.

[119] B. Wang, S. Gangwar, G. M. Pauletti, T. J. Siahaan, and R. T. Borchardt, *J. Org. Chem.*, 1997, **62**, 1363.

[120] G. M. Pauletti, S. Gangwar, B. Wang, and R. T. Borchardt, *Pharmaceut. Res.*, 1997, **14**, 11.

[121] Y. Liao and B. Wang, *Bioorg. Med. Chem. Lett.*, 1999, **9**, 1795.

[122] Y. Liao, S. Hendrata, S. Y. Bae, and B. Wang, *Chem. Pharm. Bull.*, 2000, **48**, 1138.

[123] Y. Ueda, A. B. Mikkilineni, J. O. Knipe, W. C. Rose, A. M. Casazza, and D. M. Vyas, *Bioorg. Med. Chem. Lett.*, 1993, **3**, 1761.

[124] A. Gilman and F. S. Philips, *Science*, 1946, **103**, 409.

[125] W. B. Mattes, C.-S. Lee, J. Laval, and T. R. O'Connor, *Carcinogenesis*, 1996, **17**, 643.

[126] C. Avendaño and J. C. Menéndez, 'Medicinal Chemistry of Anticancer Drugs, First Ed.' Elsevier Science, 2008.

[127] L. H. Hurley, *Nature Rev. Cancer*, 2002, **2**, 188.

[128] A. Masta, P. J. Gray, and D. R. Philips, *Nucleic Acids Res.*, 1995, **23**, 3508.

[129] Z. H. Siddik, 'The Cancer Handbook First Ed.' John Wiley & Sons, 2002.

[130] S. M. Rink, M. S. Solomon, M. J. Taylor, S. B. Rajur, L. W. McLaughlin, and P. B. Hopkins, *J. Am. Chem. Soc.*, 1993, **115**, 2551.

[131] M. R. Osborne, D. E. V. Wilman, and P. D. Lawley, *Chem. Res. Toxicol.*, 1995, **8**, 316.

[132] B. D. Palmer, W. R. Wilson , S. Cliffe, and W. A. Denny, *J. Med. Chem.*, 1992, **35**, 3214.

[133] N. Kapuriya, R. Kakadiya, H. Dong, A. Kumar, P.-C. Lee, X. Zhang, T.-C. Chou, T.-C. Lee, C.-H. Chen, K. Lam, B. Marvania, A. Shah, and T.-L. Su, *Bioorg. Med. Chem.*, 2011, **19**, 471.

[134] A. Begleiter, M. Mowat, L. G. Israels, and J. B. Johnston, *Leuk. Lymphoma*, 1996, **23**, 187.

[135] K. R. Rai, B. L. Peterson, F. R. Appelbaum, J. Kolitz, L. Elias, L. Shepherd, J. Hines, G. A. Threatte, R. A. Larson, B. D. Cheson, and C. A. Schiffer, *N. Engl. J. Med.*, 2000, **343**, 1750.

[136] D. Cunningham, L. Paz-Arez, M. E. Gore, J. Malpas, T. Hickish, M. Nicolson, M. Meldrum, C. Viner, S. Milan, and P. J. Selby, *J. Clin. Oncol.*, 1994, **12**, 764.

[137] J. A. Moscow, C. A. Swanson, and K. H. Cowan, *Br. J. Cancer*, 1993, **68**, 732.

[138] R. S. Leff, J. M. Tompson, D. B. Johnson, K. R. Mosley, M. B. Daly, W. A. Knight 3rd, R. L. Ruxer, and G. L. Messerschmidt, *J. Clin. Oncol.*, 1986, **4**, 1586.

[139] J. Rothbarth, C. Koevoets, R. A. E. M. Tollenaar, M. J. Tilby, C. J. H. van de Velde, G. J. Mulder, and P. J. K. Kuppen, *Biochem. Pharmacol.*, 2004, **67**, 1771.

[140] N. Kapuriya, K. Kapuriya, H. Dong, X. Zhang, T.-C. Chou, Y.-T. Chen, T.-C. Lee, W.-C. Lee, T.-H. Tsai, Y. Naliapara, and T.-L. Su, *Bioorg. Med. Chem.*, 2009, **17**, 1264.

[141] C.-H. Chen, Y.-W. Lin, X. Zhang, T.-C. Chou, T.-J. Tsai, N. Kapuriya, R. Kakadiya, and T.-L. Su, *Eur. J. Med. Chem.*, 2009, **44**, 3056.

[142] N. Kapuriya, K. Kapuriya, X. Zhang, T.-C. Chou, R. Kakadiya, Y.-T. Wu, T.-H. Tsai, Y.-T. Chen, T.-C. Lee, A. Shah, Y. Naliapara, and T.-L. Su, *Bioorg. Med. Chem.*, 2008, **16**, 5413.

[143] T. A. Gourdie, K. K. Valu, G. L. Gravatt, T. J. Boritzki, B. C. Baguley, L. P. G. Wakelin, W. R. Wilson, P. D. Woodgate, and W. A. Denny, *J. Med. Chem.*, 1990, **33**, 1177.

[144] K. K. Valu, T. A. Gourdie, T. J. Boritzki, G. L. Gravatt, B. C. Baguley, W. R. Wilson, L. P. G. Wakelin, P. D. Woodgate, and W. A. Denny, *J. Med. Chem.*, 1990, **33**, 3014.

[145] T.-L. Su, Y.-W. Lin, T.-C. Chou, X. Zhang, V. A. Bacherikov, C.-H. Chen, L. F. Liu, and T.-J. Tsai, *J. Med. Chem.*, 2006, **49**, 3710.

[146] V. A. Bacherikov, T.-C. Chou, H.-J. Dong, C.-H. Chen, Y.-W. Lin, T.-J. Tsai, and T.-L. Su, *Bioorg. Med. Chem. Lett.*, 2004, **14**, 4719.

[147] V. A. Bacherikov, T.-C. Chou, H.-J. Dong, X. Zhang, C.-H. Chen, Y.-W. Lin, T.-J. Tsai, R.-Z. Lee, L. F. Liu, and T.-L. Su, *Bioorg. Med. Chem.*, 2005, **13**, 3993.

[148] G. L. Gravatt, B. C. Baguley, W. R. Wilson, and W. A. Denny, *J. Med. Chem.*, 1991, **34**, 1552.

[149] R. Kakadiya, H. Dong, A. Kumar, D. Narsinh, X. Zhang, T.-C. Chou, T.-C. Lee, A. Shah, and T.-L. Su, *Bioorg. Med. Chem.*, 2010, **18**, 2285.

[150] M. G. Ferlin, L. D. Via, and O. M. Gia, *Bioorg. Med. Chem.*, 2004, **12**, 771.

[151] B. Marvania, P.-C. Lee, R. Chaniyara, H. Dong, S. Suman, R. Kakadiya, T.-C. Chou, T.-C. Lee, A. Shah, and T.-L. Su, *Bioorg. Med. Chem.*, 2011, **19**, 1987.

[152] N. H. Greig, S. Genka, E. M. Daly, D. J. Sweeney, and S. I. Rapoport, *Cancer Chemother. Pharmacol.*, 1990, **25**, 311.

[153] D. E. Kerr, Z. Li, N. O. Siemers, P. D. Senter, and V. M. Vrudhula, *Bioconjugate Chem.*, 1998, **9**, 255.

[154] M. Wickström, J. I. Johnsen, F. Ponthan, L. Segerström, B. Sveinbjörnsson, M. Lindskog, H. Lövborg, K. Viktorsson, R. Lewensohn, P. Kogner, R. Larsson, and J. Gullbo, *Mol. Cancer Ther.*, 2007, **6**, 2409.

[155] S. Mittal, Y. Tsume, C. P. Landowski, K.-D. Lee, J. M. Hilfinger, and G. L. Amidon, *Eur. J. Pharm. Biopharm.*, 2007, **67**, 752.

[156] S. Mittal, X. Song, B. S. Vig, and G. L. Amidon, *Pharmaceut. Res.*, 2007, **24**, 1290.

[157] T. Kryczka, Z. Kazimierczuk, M. Kozlowska, S. J. Chrapusta, L. Vilpo, J. Vilpo, K. Stachnik, M. Janisz, and P. Grieb, *Anticancer Drugs*, 2007, **18**, 301.

[158] P. J. Pedersen, M. S. Christensen, T. Ruysschaert, L. Linderoth, T. L. Andresen, F. Melander, O. G. Mouritsen, R. Madsen, and M. H. Clausen., *J. Med. Chem.*, 2009, **52**, 3408.

[159] L. Gharat, P. Visser, M. Brummelhuis, R. Guiles, and P. J. Chikhale, *Med. Chem. Res.*, 1998, **8**, 444.

[160] N. Weerapreeyakul, R. G. Hollenbeck, and P. J. Chikhale, *Bioorg. Med. Chem. Lett.*, 2000, **10**, 2391.

[161] L. Gharat, R. Taneji, N. Weerapreeyakul, B. Rege, J. Polli, and P. J. Chikhale, *Int. J. Pharm.*, 2001, **219**, 1.

[162] P. D. Edwards, D. L. D. Foster, L. N. Owen, and M. J. Pringle, *J. Chem. Soc. Perk. T.1.*, 1973, 2397.

[163] S. J. Angyal and W. K. Warburton, *J. Chem. Soc.*, 1951, 2492.

[164] P. Gund, *J. Chem. Educ.*, 1972, **49**, 100.

[165] E. D. Raczynska, M. K. Cyranski, M. Gutowski, J. Rak, J.-F. Gal, P.-C. Maria, M. Darowska, and K. Duczmal, *J. Phys. Org. Chem.*, 2003, **16**, 91.

[166] A. Strecker, *Liebigs Ann. Chem.*, 1861, **118**, 151.

[167] T. Yamada, X. Liu, U. Englert, H. Yamane, and R. Dronskowski, *Chem. Eur. J.*, 2009, **15**, 5651.

[168] J. Sun, J. M. Miller, A. Beig, L. Rozen, G. L. Amidon, and A. Dahan., *Expert Opin. Drug Metab. Toxicol.*, 2011, **7**, 313.

[169] E. Schulze and E. Steiger, *Ber. Dtsch. Chem. Ges.*, 1886, **19**, 1177.

[170] E. Schulze and E. Steiger, *Z. Physiol. Chem.*, 1886, **11**, 43.

[171] F. P. Schmidtchen and M. Berger, *Chem. Rev.*, 1997, **97**, 1609.

[172] Z. D. Aron and L. E. Overman, *Chem. Commun.*, 2004, 253.

[173] Y. Kashman and S. Hirsh, *J. Am. Chem. Soc.*, 1989, **111**, 8925.

[174] B. B. Snider and Z. Shi, *J. Am. Chem. Soc.*, 1994, **116**, 549.

[175] G. P. Black, P. J. Murphy, N. D. A. Walshe, D. E. Hibbs, M. B. Hursthouse, and K. M. A. Malik, *Tetrahedron Lett.*, 1996, **37**, 6943.

[176] L. Heys, C. G. Moore, and P. J. Murphy, *Chem. Soc. Rev.*, 2000, **29**, 57.

[177] I. Ohtani, T. Kusumi, and H. Kakisawa, *Tetrahedron Lett.*, 1992, **33**, 2525.

[178] I. Ohtani, T. Kusumi, H. Kakisawa, Y. Kashman, and S. Hirsh, *J. Am. Chem. Soc.*, 1992, **114**, 8472.

[179] C. A. Bewley, S. Ray, F. Cohen, S. K. Collins, and L. E. Overman, *J. Nat. Prod.*, 2004, **67**, 1319.

[180] Z. D. Aron, H. Pietraszkiewicz, L. E. Overman, F. Valeriote, and C. Cuevas, *Bioorg. Med. Chem. Lett.*, 2004, **14**, 3445.

[181] E. A. Jares-Erijman, R. Sakai, and K. L. Rinehart, *J. Org. Chem.*, 1991, **56**, 5712.

[182] E. A. Jares-Erijman, A. L. Ingrum, J. R. Carney, K. L. Rinehart, and R. Sakai, *J. Org. Chem.*, 1993, **58**, 4805.

[183] R. G. S. Berlinck, J. C. Braekman, and D. Daloze, *J. Nat. Prod.*, 1993, **56**, 1007.

[184] D. S. Coffey, A. I. Mcdonald, L. E. Overman, and F. Stappenbeck, *J. Am. Chem. Soc.*, 1999, **121**, 6944.

[185] D. S. Coffey, A. I. McDonald, L. E. Overman, M. H. Rabinowitz, and P. A. Renhowe, *J. Am. Chem. Soc.*, 2000, **122**, 4893.

[186] D. S. Coffey, L. E. Overman, and F. Stappenbeck, *J. Am. Chem. Soc.*, 2000, **122**, 4904.

[187] A. D. Patil, N. V. Kumar, W. C. Kokke, M. F. Bean, A. J. Freyer, C. D. Brosse, S. Mai, A. Truneh, D. J. Faulkner, B. Carte, A. L. Breen, R. P. Hertzberg, R. K. Johnson, J. W. Westley, and B. C. M. Potts, *J. Org. Chem.*, 1995, **60**, 1182.

[188] A. D. Patil, A. J. Freyer, P. B. Taylor, B. Carté, G. Zuber, R. K. Johnson, and D. J. Faulkner, *J. Org. Chem.*, 1997, **62**, 1814.

[189] M. A. Arnold, K. A. Day, S. G. Durón, and D. Y. Gin, *J. Am. Chem. Soc.*, 2006, **128**, 13255.

[190] W. A. Gallimore, M. Kelly, and P. J. Scheuer, *J. Nat. Prod.*, 2005, **68**, 1420.

[191] H.-M. Hua, J. Peng, D. C. Dunbar, R. F. Schinazi, A. G. de Castro Andrews, C. Cuevas, L. F. Garcia-Fernandez, M. Kelly, and M. T. Hamann, *Tetrahedron*, 2007, **63**, 11179.

[192] S. G. Duron and D. Y. Gin, *Org. Lett.*, 2001, **3**, 1551.

[193] F. Cohen, L. E. Overman, and S. K. L. Sakata, *Org. Lett.*, 1999, **1**, 2169.

[194] A. S. Franklin, S. K. Ly, G. H. Mackin, L. E. Overman, and A. J. Shaka, *J. Org. Chem.*, 1999, **64**, 1512.

[195] F. Cohen and L. E. Overman, *J. Am. Chem. Soc.*, 2001, **123**, 10782.

[196] L. E. Overman and J. P. Wolfe, *J. Org. Chem.*, 2001, **66**, 3167.

[197] A. I. McDonald and L. E. Overman, *J. Org. Chem.*, 1999, **64**, 1520.

[198] M. C. Elliot and M. S. Long, *Tetrahdedron Lett.*, 2002, **43**, 9191.

[199] M. C. Elliott and M. S. Long, *Org. Biomol. Chem.*, 2004, **2**, 2003.

[200] B. B. Snider and J. Chen, *Tetrahedron Lett.*, 1998, **39**, 5697.

[201] J. Shimokawa, K. Shirai, A. Tanatani, Y. Hashimoto, and K. Nagasawa, *Angew. Chem. Int. Ed.*, 2004, **43**, 1559.

[202] S. Vale, 'Synthesis of an Analogue of Batzelladine A', MChem Project, University of Wales, Bangor, 2005.

[203] T. Roberts, 'Synthesis of Analogues of Batzelladine A', MChem Project, University of Wales, Bangor, 2007.

[204] C. M. Martin, 'Synthesis of Analogues of the Batzelladine Alkaoloids', MChem Project, Bangor University, 2008.

[205] E. L. Bennett, 'Synthesis of Analogues of the Batzelladine Alkaloid A', MChem Thesis, Bangor University, 2009.

[206] J. P. Leyland, 'Synthesis and Biological Activity of Analogues of Batzelladine F', MChem Thesis, Bangor University, 2011.

[207] L. O. Regasini, I. Castro-Gamboa, D. H. S. Silva, M. Furlan, E. J. Barreiro, P. M. P. Ferreira, C. Pessoa, L. V. C. Lutufo, M. O. de Moraes, M. C. M. Young, and V. da Silva Bolzani, *J. Nat. Prod.*, 2009, **72**, 473.

[208] M. G. Saulnier, D. B. Frennesson, M. S. Deshpande, S. B. Hansel, and D. M. Vyas, *Bioorg. Med. Chem. Lett.*, 1994, **4**, 1985.

[209] R. K. Arafa, R. Brun, T. Wenzler, F. A. Tanious, W. D. Wilson, C. E. Stephens, and D. W. Boykin, *J. Med. Chem.*, 2005, **48**, 5480.

[210] R. K. Arafa, M. A. Ismail, M. Munde, W. D. Wilson, T. Wenzler, R. Brun, and D. W. Boykin, *Eur. J. Med. Chem.*, 2008, **43**, 2901.

[211] K. M. Huttunen, A. Mannila, K. Laine, E. Kemppainen, J. Leppanen, J. Vepsalainen, T. Jarvinen, and J. Rautio, *J. Med. Chem.*, 2009, **52**, 4142.

[212] A. R. Katritzky and B. V. Rogovoy, *Chem. Inform.*, 2005, **36**, 49.

[213] B. P. Orner and A. D. Hamilton, *J. Incl. Phenom. Macro.*, 2001, **41**, 141.

[214] T. R. M. Rauws and B. U. W. Maes, *Chem. Soc. Rev.*, 2012, **41**, 2463.

[215] W.-X. Zhang, M. Nishiura, and Z. Hou, *Chem. Eur. J.*, 2007, **13**, 4037.

[216] S. Cunha and M. T. Rodrigues Jr, *Tetrahedron Lett.*, 2006, **47**, 6955.

[217] Y.-Q. Wu, S. K. Hamilton, D. E. Wilkinson, and G. S. Hamilton, *J. Org. Chem.*, 2002, **67**, 7553.

[218] J. P. Ferris, C. H. Huang, and W. J. Hagan Jr, *Nucleos. Nucleot.*, 1989, **8**, 407.

[219] V. D. Jadhav and F. P. Schmidtchen, *J. Org. Chem.*, 2008, **73**, 1077.

[220] D. J. Hart, A. Kim, R. Krishnamurthy, G. H. Merriman, and A.-M. Waltos, *Tetrahedron*, 1992, **48**, 8179.

[221] D. R. Henton, K. Anderson, M. J. Manning, and J. S. Swenton, *J. Org. Chem.*, 1980, **45**, 3422.

[222] D. R. Henton, R. L. McCreery, and J. S. Swenton, *J. Org. Chem.*, 1980, **45**, 369.

[223] B. H. Lipshutz, S.-K. Kim, P. Mollard, and K. L. Stevens, *Tetrahedron*, 1998, **54**, 1241.

[224] G. Andersson, *Acta Chem. Scand. B*, 1976, **30**, 64.

[225] H. J. Dauben Jr and L. L. McCoy, *J. Am. Chem. Soc.*, 1959, **81**, 4863.

[226] A. M. Jordan, T. H. Khan, H. Malkin, and H. M. I. Osborn, *Bioorg. Med. Chem.*, 2002, **10**, 2625.

[227] N. Abou-Zeid, 'Design and Synthesis of Quinone Bioreductive Prodrugs as Anti-tumour Agents', PhD Thesis, University of Manchester, 2004.

[228] B. D. Palmer, W. R. Wilson, S. M. Pullen, and W. A. Denny, *J. Med. Chem.*, 1990, **33**, 112.

[229] B. Degutis, *Chemija ir Chemine Technologija*, 1964, **4**, 59.

[230] P. Skehan, R. Storeng, D. Scudiero, A. Monks, J. McMahon, D. Vistica, J. T. Warren, H. Bokesch, S. Kenney, and M. R. Boyd, *J. Natl. Cancer Inst.*, 1990, **82**, 1107.

[231] W. G. Kofron and L. M. Baclawski, *J. Org. Chem.*, 1976, **41**, 1879.

Appendices

1.0 Molecular modelling

1.1 Primary (1°) docking for mechanism one

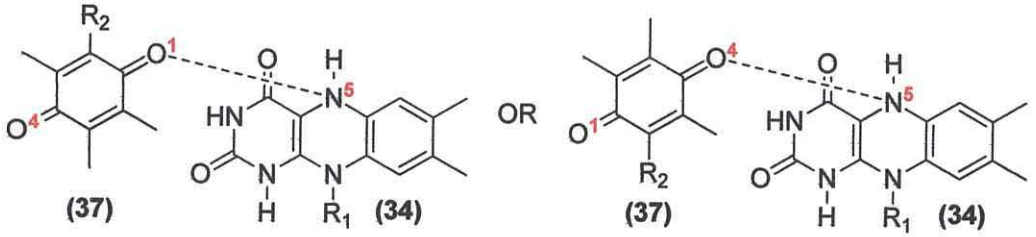

R_2 = trimethyl lock/aromatic substituent

	Interaction with $FADH_2$ (Å)								
Poses	**129**	**130**	**131**	**132***	**133**	**134***	**78**	**135**	**136**
[00]	3.3(O^4)	5.0 (O^4)	4.5 (O^1)	5.0 (O^1)	4.7 (O^4)	7.3 (O^1)	11.3 (O^1)	11.0 (O^4)	3.0 (O^1)
[01]	4.9 (O^4)	4.6 (O^1)	4.6 (O^4)	5.0 (O^4)	6.8 (O^4)	6.5 (O^1)	10.9 (O^1)	10.9 (O^4)	11.1 (O^1)
[02]	3.3 (O^4)	3.2 (O^4)	9.7 (O^1)	8.2 (O^4)	3.3 (O^4)	4.6 (O^1)	11.4 (O^4)	10.7 (O^1)	10.6 (O^1)
[03]	3.7 (O^4)	3.3 (O^4)	3.4 (O^4)	5.9 (O^1)	4.7 (O^1)	5.1 (O^1)	3.8 (O^4)	8.2 (O^4)	11.6 (O^1)
[04]	3.3 (O^1)	5.6 (O^4)	4.4 (O^1)	4.6 (O^1)	4.2 (O^4)	9.7 (O^4)	11.0 (O^1)	3.5 (O^4)	10.0 (O^1)

Appendix 1.1.1 Primary (1°) docking distances (Å) between the N^5 of $FADH_2$ and either O^1 or O^4 of the quinone. Distances <4 Å are shown in yellow

*Original structures submitted for primary (1°) docking contained errors converting from 2D to 3D. Corrected structures were submitted for secondary (2°) docking

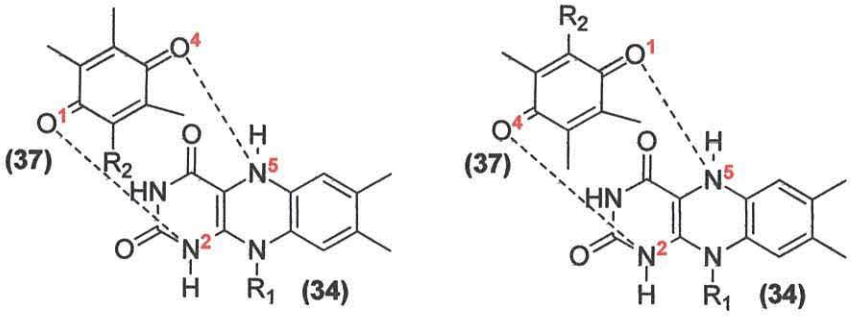

APPROACH "A" APPROACH "B"

R_2 = trimethyl lock/aromatic substituent

Appendix 1.1.2 (see table overleaf)

Ligands	Returned Poses of Ligands	Ligand-$FADH_2$ distances (Å)				Ligand-Protein interactions	
		O^1------N^2	O^1------N^5	O^4------N^2	O^4------N^5	Inter-atomic distances (Å)	Van der Waals (<5 Å)
129	[00]	3.4			3.3	3.3 (Gly 193) 3.3 (Gly 150)..O^1	Gly 149, Gly 150, Gly 193, His 161, His 194, lle 192, Met 154, Phe 106, Ser 191, Thr 147, Thr 148, Thr 195, Trp 105, Tyr 155
129	[02]	3.3			3.3		Gly 149, Gly 150, Gly 193, His 11, His 161, lle 192, Phe 106, Pro 102, Met 154, Thr 148, Trp 105, Tyr 155
129	[03]	3.2				3.5 (Gly 193)	Gly 149, Gly 150, Gly 193, His 161, His 194, lle 192, Met 154, Phe 106, Ser 191, Thr 148, Trp 105, Tyr 155
129	[04]		3.3	3.4			Gln 104, Gly 149, Gly 150, His 161, Met 154, Phe 106, Thr 148, Trp 105, Tyr 155
130	[02]				3.2		Gly 149, Gly 150, Gly 193, His 161, His 194, lle 192, Met 154, Phe 106, Ser 191, Thr 148, Trp 105, Tyr 155
130	[03]				3.3		Gln 104, Gly 149, Gly 150, Gly 193, His 161, Met 154, Phe 106, Thr 148, Trp 105, Tyr 155
131	[03]	3.2			3.4		Gly 149, Gly 150, Gly 193, His 161, His 194, lle 192, Met 154, Phe 106, Ser 191, Thr 148, Thr 195, Trp 105, Tyr 155
133	[02]	3.2			3.3		Gln 104, Gly 149, Gly 150, His 11, His 161, Met 154, Phe 106, Pro 102, Thr 148, Trp 105, Tyr 155
78	[03]				3.8 (Manually)		Gln 104, Gly 149, Gly 150, Gly 152, His 161, His 194, lle 160, Met 154, Phe 106, Ser 151, Ser 191, Thr 148, Thr 195, Trp 105, Tyr 155
135	[04]				3.5		Gln 104, Gly 149, Gly 150, Gly 193, His 161, His 194, lle 160, lle 192, Met 154, Phe 106, Ser 191, Thr 148, Trp 105
136	[00]		3.0				Arg 200, Gln 104, Gly 149, Gly 150, Gly 193, Met 154, His 161, His 194, lle 192, Phe 106, Ser 191, Trp 105, Thr 148, Thr 195, Tyr 155

Appendix 1.1.2 Summary for primary (1°) docking of predicted bonding interactions in the hNQO1 active site (inter-atomic distances in Å)

1.2 Secondary (2°) docking for mechanism one

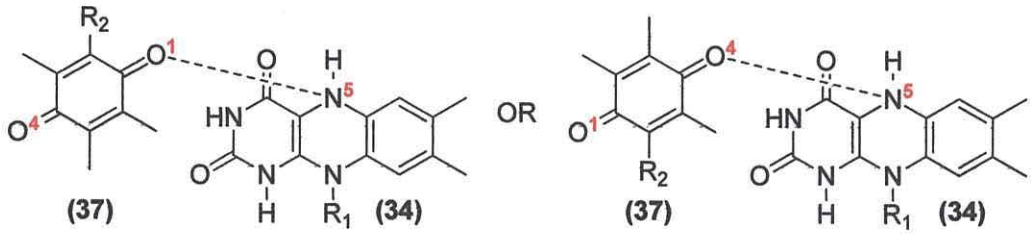

R_2 = trimethyl lock/aromatic substituent

	Interaction with $FADH_2$ (Å)								
Poses	**129**	**130**	**131**	**132**	**133**	**134**	**78**	**135**	**136**
[00]	3.3 (O^4)	5.1 (O^4)	3.4 (O^4)	5.3 (O^4)	3.1 (O^4)	5.3 (O^4)	3.4 (O^1)	3.4 (O^1)	10.1 (O^1)
[01]	3.4 (O^4)	3.6 (O^1)	2.4 (O^4)	5.1 (O^4)	3.3 (O^4)	5.0 (O^4)	3.6 (O^1)	3.1 (O^1)	10.3 (O^1)
[02]	3.4 (O^4)	3.9 (O^4)	3.6 (O^4)	3.4 (O^1)	3.2 (O^4)	3.5 (O^4)	3.7 (O^1)	3.5 (O^4)	10.7 (O^1)
[03]	3.4 (O^4)	3.5 (O^1)	3.1 (O^4)	3.2 (O^1)	7.1 (O^4)	3.4 (O^1)	3.5 (O^1)	2.6 (O^1)	10.3 (O^1)
[04]	3.2 (O^1)	3.4 (O^4)	3.2 (O^1)	3.2 (O^1)	3.5 (O^4)	3.9 (O^4)	3.5 (O^1)	5.3 (O^4)	10.9 (O^1)

Appendix 1.2.1 Secondary (2°) docking distances (Å) between the N^5 of $FADH_2$ and either O^1 or O^4 of the quinone. Distances <4 Å are shown in yellow

Additional parameters for secondary (2°) docking

Population Size = 200, Scaling Factor = 0.5, Turnover rate = 0.9, Terminate = RMSD-based, RMS gradient = 0.1

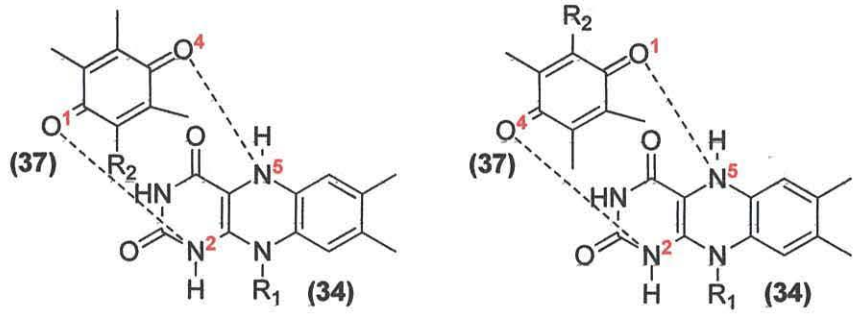

APPROACH "A" APPROACH "B"

R_2 = trimethyl lock/aromatic substituent

Appendix 1.2.2 (see table p.157-159)

Ligands	Returned Poses of Ligands	Ligand-$FADH_2$ distances (Å)				Ligand-Protein interactions	
		O^1------N^2	O^1------N^5	O^4------N^2	O^4------N^5	Inter-atomic distances (Å)	Van der Waals (<5 Å)
129	[00]	3.2			3.3	3.5 (Gly 193) 3.6 (Gly 150)..O^1	Gly 149, Gly 150, Gly 193, His 161, His 194, lle 192, Leu 103, Met 154, Phe 106, Ser 191, Thr 147, Thr 148, Thr 195, Trp 105, Tyr 155
129	[01]	3.0			3.4		Gln 104, Gly 149, Gly 150, His 11, His 161, Met 154, Phe 106, Pro 102, Thr 148, Trp 105, Tyr 155
129	[02]	3.3			3.4		Gly 149, Gly 150, Gly 193, His 161, His 194, lle 192, Met 154, Phe 106, Ser 191, Thr 148, Trp 105, Tyr 155
129	[03]	3.2			3.4	3.6 (Gly 150)..O^1	Gly 149, Gly 150, Gly 193, His 161, His 194, lle 192, Met 154, Phe 106, Ser 191, Thr 148, Trp 105, Tyr 155
129	[04]		3.2	3.3			Gln 104, Gly 149, Gly 150, His 161, Met 154, Phe 106, Thr 148, Trp 105, Tyr 155
130	[01]			3.3			Gln 104, Gly 149, Gly 150, His 161, Met 154, Phe 106, Thr 148, Trp 105, Tyr 155
130	[02]	3.2					Gly 149, Gly 150, His 161, Leu 103, Met 154, Phe 106, Thr 148, Trp 105, Tyr 155
130	[03]		3.5	3.2		3.5 (Gly 150)..O^4	Gln 104, Gly 149, Gly 150, His 161, Leu 103, Met 154, Phe 106, Thr 148, Trp 105, Tyr 155
130	[04]				3.4		Gln 104, Gly 149, Gly 150, Gly 193, His 161, Met 154, Phe 106, Thr 148, Trp 105, Tyr 155
131	[00]	3.0			3.4		Gly 149, Gly 150, His 161, lle 160, Leu 103, Met 154, Phe 106, Ser 151, Ser 191, Thr 148, Trp 105, Tyr 155
131	[01]				2.4	2.6 (Tyr 155) 3.5 (Gly 150)	Gln 104, Gly 149, Gly 150, His 161, lle 160, Leu 103, Met 154, Phe 106, Ser 151, Ser 191, Thr 148, Trp 105, Tyr 155
131	[02]	2.8			3.6		Gly 149, Gly 150, His 161, lle 160, Leu 103, Met 154, Phe 106, Thr 148, Trp 105, Tyr 155
131	[03]	3.2			3.1		Gly 149, Gly 150, His 161, lle 160, Met 154, Phe 106, Ser 151, Thr 148, Trp 105, Tyr 155
131	[04]		3.2	3.1		3.6 (Gly 150)..O^4	Gly 149, Gly 150, His 161, lle 160, Met 154, Phe 106, Ser 151, Thr 148, Trp 105, Tyr 155

Ligands	Returned Poses of Ligands	Ligand-$FADH_2$ distances (Å)				Ligand-Protein interactions	
		O^1------N^2	O^1------N^5	O^4------N^2	O^4------N^5	Inter-atomic distances (Å)	Van der Waals (<5 Å)
132	[02]		3.4	3.4			Gln 104, Gly 149, Gly 150, His 161, Ile 160, Met 154, Phe 106, Thr 148, Trp 105, Tyr 155
132	[03]		3.2				Gln 104, Gly 149, Gly 150, His 161, Ile 160, Met 154, Phe 106, Thr 148, Trp 105, Tyr 155
132	[04]		3.2				Gly 149, Gly 150, Gly 193, His 161, His 194, Ile 192, Met 154, Phe 106, Ser 191, Thr 148, Trp 105, Tyr 155
133	[00]	3.1			3.1		Gly 149, Gly 150, His 161, Ile 160, Met 154, Phe 106, Ser 151, Trp 105, Thr 148, Tyr 155
133	[01]	3.0			3.3		Gly 149, Gly 150, His 161, Leu 103, Ile 160, Met 154, Phe 106, Ser 151, Thr 148, Trp 105, Tyr 155
133	[02]	3.2			3.2		Gly 149, Gly 150, His 161, Ile 160, Met 154, Phe 106, Thr 148, Trp 105, Tyr 155
133	[04]	3.1			3.5	3.0 (His 194) 3.2 (Gly 193)	Gly 149, Gly 150, Gly 193, His 161, His 194, Ile 192, Met 154, Phe 106, Ser 191, Thr 148, Trp 105, Tyr 155, Tyr 190
134	[02]				3.5		Gly 149, Gly 150, Gly 193, His 161, His 194, Ile 160, Ile 192, Met 154, Phe 106, Ser 151, Ser 191, Thr 148, Trp 105, Tyr 155
134	[03]		3.4	3.4			Gln 104, Gly 149, Gly 150, His 161, Ile 160, Met 154, Phe 106, Thr 148, Trp 105, Tyr 155
134	[04]	3.5					Gly 149, Gly 150, Gly 193, His 161, His 194, Leu 103, Met 154, Phe 106, Ser 151, Ser 191, Thr 148, Trp 105, Tyr 155
78	[00]		3.4				Gln 104, Gly 149, Gly 150, His 161, Ile 160, Leu 103, Met 154, Phe 106, Thr 148, Trp 105, Tyr 155
78	[01]		3.6	3.6			Gln 104, Gly 149, Gly 150, His 161, Ile 160, Leu 103, Met 154, Phe 106, Ser 151, Thr 148, Trp 105, Tyr 155
78	[02]			3.5			Gly 149, Gly 150, His 161, Ile 160, Leu 103, Met 154, Phe 106, Ser 151, Thr 148, Trp 105, Tyr 155
78	[03]		3.5	3.5			Gln 104, Gly 149, Gly 150, His 161, Ile 160, Leu 103, Met 154, Phe 106, Thr 148, Trp 105, Tyr 155

Ligands	Returned Poses of Ligands	Ligand-$FADH_2$ distances (Å)				Ligand-Protein interactions	
		O^1------N^2	O^1------N^5	O^4------N^2	O^4------N^5	Inter-atomic distances (Å)	Van der Waals (<5 Å)
78	[04]		3.5	3.4			Gln 104, Gly 149, Gly 150, His 161, Ile 160, Leu 103, Met 154, Phe 106, Ser 151, Thr 148, Trp 105, Tyr 155
135	[00]		3.4			3.2 (Gly 150) 3.6 (Gly 149)	Gly 149, Gly 150, Gly 193, His 161, His 194, Met 154, Phe 106, Ser 151, Ser 191, Thr 148, Trp 105, Tyr 155
135	[01]		3.1			3.2 (Gly 150)	Gly 149, Gly 150, Gly 193, His 161, His 194, Ile 160, Met 154, Phe 106, Ser 151, Ser 191, Thr 148, Trp 105, Tyr 155
135	[02]	3.0			3.5		Gly 149, Gly 150, Gly 193, His 161, Met 154, Ile 160, Phe 106, Trp 105, Tyr 155
135	[03]		2.6				Gln 104, Gly 149, Gly 150, Gly 193, His 161, His 194, Ile 192, Met 154, Phe 106, Ser 191, Thr 148, Trp 105, Tyr 155

Appendix 1.2.2 Summary for secondary (2°) docking of predicted bonding interactions in the hNQO1 active site (inter-atomic distances in Å)

1.3 Primary (1°) docking for mechanism two

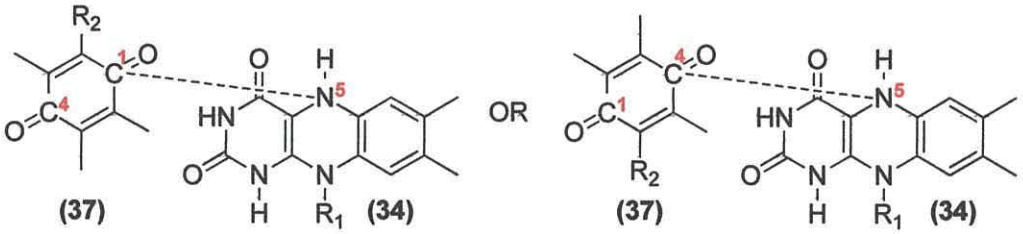

R_2 = trimethyl lock/aromatic substituent

	Interaction with $FADH_2$ (Å)								
Poses	**129**	**130**	**131**	**132***	**133**	**134***	**78**	**135**	**136**
[00]	3.4 (C^4)	5.0 (C^4)	4.0 (C^1)	4.4 (C^1)	4.2 (C^4)	6.8 (C^1)	11.1 (C^1)	11.0 (O^4)	3.9 (C^1)
[01]	4.3 (C^1)	4.2 (C^1)	4.7 (C^4)	4.7 (C^4)	6.6 (C^4)	6.3 (C^1)	10.9 (C^1)	10.9 (C^4)	10.7 (C^1)
[02]	3.3 (C^4)	4.0 (C^4)	10.3 (C^1)	8.3 (C^4)	3.3 (C^4)	4.9 (C^1)	11.1 (C^4)	10.7 (C^1)	10.3 (C^1)
[03]	3.7 (C^4)	3.3 (C^4)	3.2 (C^4)	6.0 (C^1)	4.1 (C^1)	5.5 (C^1)	3.8 (C^4)	8.5 (C^4)	11.2 (C^1)
[04]	3.5 (C^1)	5.5 (C^4)	5.6 (C^1)	5.0 (C^1)	3.9 (C^4)	10.0 (C^4)	11.1 (C^1)	3.9 (O^4)	10.1 (C^1)

Appendix 1.3.1 Primary (1°) docking distances (Å) between the N^5 of $FADH_2$ and either C^1 or C^4 of the quinone. Distances <4 Å are shown in yellow, whilst distance which is <4 Å with mechanism two but >4 Å with mechanism one is shown in green.

*Original structures submitted for primary (1°) docking contained errors converting from 2D to 3D. Corrected structures were submitted for secondary (2°) docking

Ligand	**Returned Pose of Ligand**	**Ligand-Protein interactions**
		Van der Waals (<5 Å)
133	[04]	Gln 104, Gly 149, Gly 150, Gly 152, Gly 193, His 161, His 194, Ile 160, Ile 192, Met 154, Phe 106, Ser 151, Ser 191, Thr 148, Thr 195, Trp 105, Tyr 155

Appendix 1.3.2 Additional Van der Waals interactions not specified for mechanism one

1.4 Primary (1°) docking for mechanism three

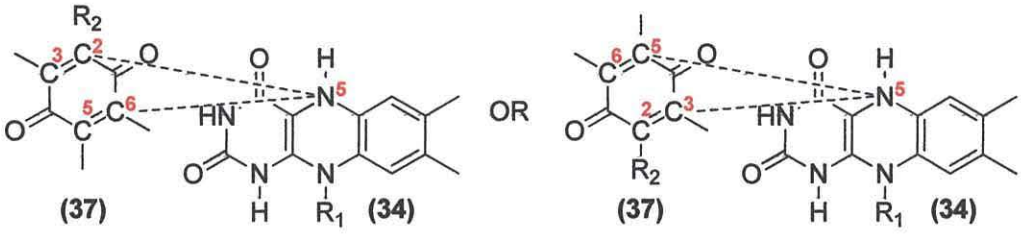

R_2 = trimethyl lock/aromatic substituent

	Interaction with $FADH_2$ (Å)								
Poses	**129**	**130**	**131**	**132***	**133**	**134***	**78**	**135**	**136**
[00]	3.8 (C^5)	4.7 (C^3)	3.4 (C^6)	3.9 (C^2)	3.5 (C^5)	5.9 (C^6)	10.5 (C^2)	10.6 (C^3)	4.4 (C^6)
[01]	3.5 (C^6)	3.8 (C^2)	4.0 (C^3)	4.1 (C^2)	5.7 (C^3)	6.4 (C^2)	10.7 (C^2)	10.7 (C^3)	9.8 (C^6)
[02]	3.7 (C^5)	4.6 (C^3)	10.4 (C^2)	7.3 (C^2)	3.7 (C^3)	5.1 (C^2)	10.7 (C^3)	10.5 (C^6)	9.7 (C^6)
[03]	4.0 (C^5)	3.6 (C^5)	3.6 (C^3)	4.8 (C^6)	3.4 (C^6)	5.6 (C^2)	3.4 (C^5)	8.8 (C^3)	11.0 (C^2)
[04]	4.0 (C^2)	5.7 (C^3)	6.2 (C^6)	5.2 (C^6)	3.4 (C^3)	9.9 (C^2)	11.0 (C^6)	4.0 (C^2)	9.6 (C^6)

Appendix 1.4.1 Primary (1°) docking distances (Å) between the N^5 of $FADH_2$ and either C^2, C^3, C^5 or C^6 of the quinone. Distances <4 Å are shown in yellow, whilst distances which are <4 Å with mechanism two but >4 Å with mechanism one and three are shown in green. Distances which are <4 Å with mechanism three but >4 Å with mechanism one and two are shown in blue.

*Original structures submitted for primary (1°) docking contained errors converting from 2D to 3D. Corrected structures would need to be submitted for secondary (2°) docking (i.e. **132** [00] could not be used)

Ligands	Returned Poses of Ligands	Ligand-Protein interactions
		Van der Waals (<5 Å)
129	[01]	Gly 149, Gly 150, Gly 193, His 161, His 194, Ile 192, Met 154, Phe 106, Ser 191, Thr 148, Trp 105, Tyr 155
130	[01]	Gln 104, Gly 149, Gly 150, His 161, Ile 160, Met 154, Phe 106, Thr 148, Trp 105
131	[00]	Gln 104, Gly 149, Gly 150, Gly 193, His 161, His 194, Ile 192, Met 154, Phe 106, Ser 191, Thr 148, Thr 195, Trp 105, Tyr 155, Tyr 190
132	[00]	Gly 149, Gly150, His 161, Ile 160, Met 154, Phe 106, Thr 148, Trp 105, Tyr 155
133	[00]	Gln 104, Gly 149, Gly 150, Gly 193, His 161, His 194, Ile 192, Met 154, Phe 106, Ser 191, Thr 147, Thr 148, Trp 105, Tyr 155
133	[03]	Gln 104, Gly 149, Gly 150, Gly 193, His 161, His 194, Ile 192, Met 154, Phe 106, Ser 191, Thr 148, Trp 105, Tyr 155

Appendix 1.4.2 Additional Van der Waals interactions not specified for mechanism one or two

2.0 Electrochemistry and crystallography

2.1 Electrochemical reaction set-up

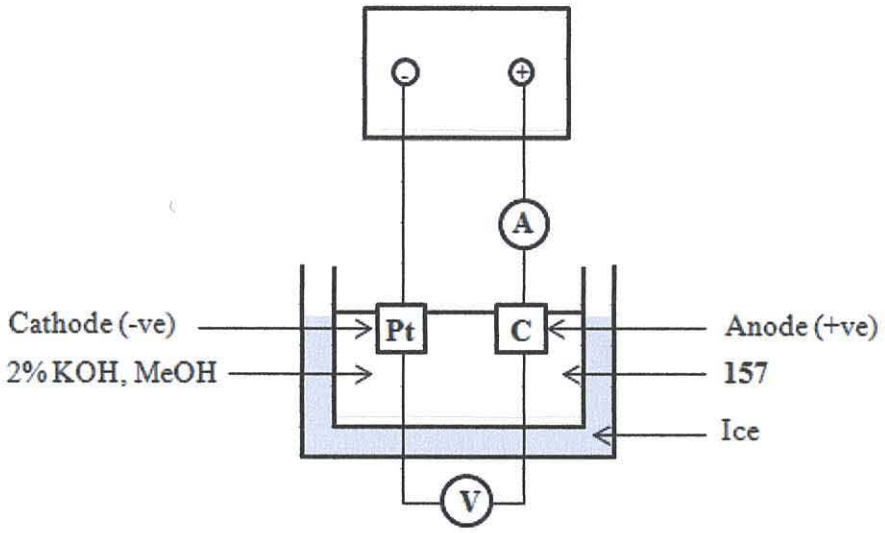

Appendix 2.1.1 Anodic oxidation of 1,4-dimethoxy-2,3,5-trimethylbenzene **157**

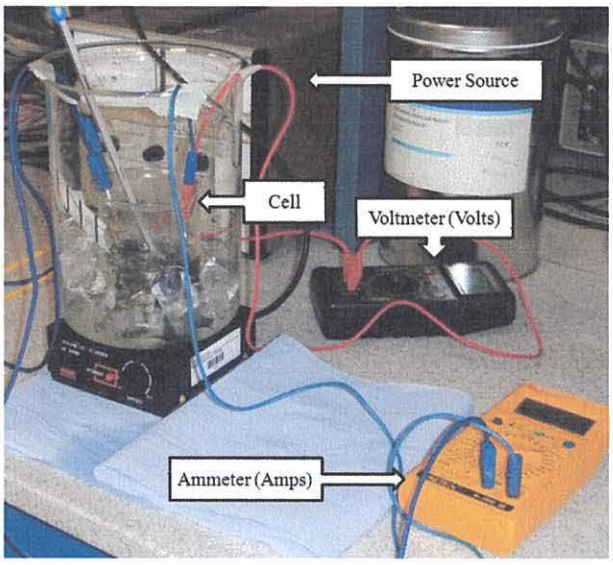

Appendix 2.1.2 Photograph of the apparatus

The anodic oxidation of **157** was performed using a platinum cathode and carbon felt anode. These were in turn connected to an ammeter (Amps), voltmeter (Volts) and a Farnell instruments LTD stabilised power supply, set to maintain a current of 1 Amp. Both the cathode and anode were submerged in a beaker containing the 1,4-dimethoxy-2,3,5-trimethylbenzene **157** dissolved in 2% methanolic potassium hydroxide. This was maintained at a temperature of <5 °C and the solution stirred vigorously throughout the oxidation process.

2.2 X-ray crystallography

2.2.1 (3aR,4R,10aR)-3a,4,6,7,7-Pentamethyl-3-phenyl-2-(phenylamino)-3a,4,7,8-tetrahydro-3*H*-chromeno[8,8a-d]imidazole-5,9-dione **143**

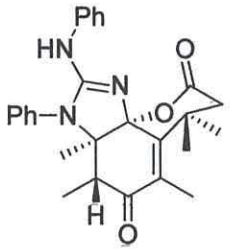

University of Southampton · School of Chemistry

EPSRC National Crystallography Service

Table 1. Crystal data and structure refinement.

Identification code	**2009src0297 CM/9/7**	
Empirical formula	$C_{27}H_{29}N_3O_3$	
Formula weight	443.53	
Temperature	120(2) K	
Wavelength	0.71073 Å	
Crystal system	Monoclinic	
Space group	$P2_1/c$	
Unit cell dimensions	a = 12.0632(15) Å	α = 90°
	b = 17.471(2) Å	β = 105.363(7)°
	c = 11.7628(11) Å	γ = 90°
Volume	2390.5(5) Å^3	
Z	4	
Density (calculated)	1.232 Mg / m^3	
Absorption coefficient	0.081 mm^{-1}	
F(000)	944	
Crystal	Fragment; Colourless	
Crystal size	0.20 × 0.10 × 0.03 mm^3	
θ range for data collection	2.92 – 26.63°	
Index ranges	$-15 \le h \le 15$, $-21 \le k \le 21$, $-14 \le l \le 14$	
Reflections collected	45452	
Independent reflections	4937 [R_{int} = 0.1872]	
Completeness to θ = 26.63°	98.1 %	
Absorption correction	Semi–empirical from equivalents	
Max. and min. transmission	0.9976 and 0.9840	
Refinement method	Full-matrix least-squares on F^2	
Data / restraints / parameters	4937 / 0 / 303	
Goodness-of-fit on F^2	1.113	
Final R indices [$F^2 > 2\sigma(F^2)$]	$R1$ = 0.1086, $wR2$ = 0.1678	
R indices (all data)	$R1$ = 0.1906, $wR2$ = 0.1953	
Largest diff. peak and hole	0.203 and –0.279 e Å^{-3}	

Diffractometer: *Nonius KappaCCD* area detector (ϕ scans and ω scans to fill *asymmetric unit* sphere). **Cell determination:** DirAx (Duisenberg, A.J.M.(1992). J. Appl. Cryst. 25, 92-96.) **Data collection:** Collect (Collect: Data collection software, R. Hooft, Nonius B.V., 1998). **Data reduction and cell refinement**: *Denzo* (Z. Otwinowski & W. Minor, *Methods in Enzymology* (1997) Vol. **276**: *Macromolecular Crystallography*, part A, pp. 307–326; C. W. Carter, Jr. & R. M. Sweet, Eds., Academic Press). **Absorption correction**: *SADABS Version 2.10.* (G. M. Sheldrick (2003)) Bruker AXS Inc., Madison, Wisconsin, USA. **Structure solution**: *SHELXS97* (G. M. Sheldrick, Acta Cryst. (1990) A**46** 467–473). **Structure refinement**: *SHELXL97* (G. M. Sheldrick (1997), University of Göttingen, Germany). **Graphics:** *ORTEP3 for Windows* (L. J. Farrugia, J. Appl. Crystallogr. 1997, 30, 565).

Table 2. Atomic coordinates [$\times 10^4$], equivalent isotropic displacement parameters [$Å^2 \times 10^3$] and site occupancy factors. U_{eq} is defined as one third of the trace of the orthogonalized U^{ij} tensor.

Atom	*x*	*y*	*z*	U_{eq}	*S.o.f.*
N1	1268(2)	3714(2)	−2865(2)	30(1)	1
N2	432(3)	2588(2)	−3825(2)	33(1)	1
N3	2303(3)	2591(2)	−2552(2)	33(1)	1
O1	5351(3)	4364(2)	−2508(3)	60(1)	1
O2	522(3)	3871(2)	77(2)	46(1)	1
O3	1914(2)	3679(1)	−778(2)	34(1)	1
C1	3119(3)	3206(2)	−1947(3)	33(1)	1
C2	3901(3)	2948(2)	−762(3)	42(1)	1
C3	3809(3)	3463(2)	−2812(3)	37(1)	1
C4	4686(3)	2880(3)	−2993(4)	49(1)	1
C5	4370(4)	4232(3)	−2446(3)	45(1)	1
C6	3712(3)	4833(2)	−2017(3)	39(1)	1
C7	4289(4)	5609(3)	−1898(4)	56(1)	1
C8	2700(3)	4660(2)	−1789(3)	35(1)	1
C9	1926(3)	5228(2)	−1364(3)	35(1)	1
C10	2517(4)	5520(2)	−112(3)	48(1)	1
C11	1552(4)	5904(2)	−2228(4)	50(1)	1
C12	804(3)	4827(2)	−1298(3)	35(1)	1
C13	1039(4)	4101(2)	−613(3)	36(1)	1
C14	2268(3)	3844(2)	−1884(3)	32(1)	1
C15	1298(3)	2988(2)	−3080(3)	30(1)	1
C16	−725(3)	2830(2)	−4196(3)	35(1)	1
C17	−1249(3)	3220(2)	−3457(4)	40(1)	1
C18	−2411(4)	3409(3)	−3833(4)	49(1)	1
C19	−3037(4)	3202(3)	−4949(4)	58(1)	1
C20	−2520(4)	2817(3)	−5688(4)	60(1)	1
C21	−1361(4)	2626(3)	−5310(3)	44(1)	1
C22	2223(3)	1859(2)	−1995(3)	35(1)	1
C23	1491(4)	1762(2)	−1274(3)	38(1)	1
C24	1420(4)	1068(3)	−742(3)	44(1)	1
C25	2091(4)	467(3)	−915(4)	58(1)	1
C26	2815(5)	551(3)	−1637(5)	78(2)	1
C27	2888(4)	1250(3)	−2185(5)	63(1)	1

Table 3. Bond lengths [Å] and angles [°].

N1–C15	1.295(5)	C9–C12	1.544(5)
N1–C14	1.449(5)	C9–C11	1.546(5)
N2–C15	1.364(5)	C10–H10A	0.9800
N2–C16	1.412(5)	C10–H10B	0.9800
N2–H2	0.8800	C10–H10C	0.9800
N3–C15	1.393(5)	C11–H11A	0.9800
N3–C22	1.451(5)	C11–H11B	0.9800
N3–C1	1.503(5)	C11–H11C	0.9800
O1–C5	1.226(5)	C12–C13	1.489(5)
O2–C13	1.215(4)	C12–H12A	0.9900
O3–C13	1.344(4)	C12–H12B	0.9900
O3–C14	1.500(4)	C16–C21	1.379(5)
C1–C14	1.530(5)	C16–C17	1.383(5)
C1–C2	1.530(5)	C17–C18	1.393(6)
C1–C3	1.542(5)	C17–H17	0.9500
C2–H2A	0.9800	C18–C19	1.379(6)
C2–H2B	0.9800	C18–H18	0.9500
C2–H2C	0.9800	C19–C20	1.372(7)
C3–C5	1.515(6)	C19–H19	0.9500
C3–C4	1.524(5)	C20–C21	1.391(6)
C3–H3	1.0000	C20–H20	0.9500
C4–H4A	0.9800	C21–H21	0.9500
C4–H4B	0.9800	C22–C27	1.385(6)
C4–H4C	0.9800	C22–C23	1.387(5)
C5–C6	1.484(6)	C23–C24	1.378(6)
C6–C8	1.351(5)	C23–H23	0.9500
C6–C7	1.513(6)	C24–C25	1.373(6)
C7–H7A	0.9800	C24–H24	0.9500
C7–H7B	0.9800	C25–C26	1.378(7)
C7–H7C	0.9800	C25–H25	0.9500
C8–C14	1.512(5)	C26–C27	1.395(7)
C8–C9	1.535(5)	C26–H26	0.9500
C9–C10	1.543(5)	C27–H27	0.9500

C15–N1–C14	104.4(3)	C4–C3–H3	106.8
C15–N2–C16	124.8(3)	C1–C3–H3	106.8
C15–N2–H2	117.6	C3–C4–H4A	109.5
C16–N2–H2	117.6	C3–C4–H4B	109.5
C15–N3–C22	119.1(3)	H4A–C4–H4B	109.5
C15–N3–C1	103.8(3)	C3–C4–H4C	109.5
C22–N3–C1	122.0(3)	H4A–C4–H4C	109.5
C13–O3–C14	115.8(3)	H4B–C4–H4C	109.5
N3–C1–C14	100.4(3)	O1–C5–C6	119.9(4)
N3–C1–C2	112.9(3)	O1–C5–C3	121.1(4)
C14–C1–C2	115.5(3)	C6–C5–C3	119.0(4)
N3–C1–C3	107.2(3)	C8–C6–C5	120.1(4)
C14–C1–C3	107.8(3)	C8–C6–C7	126.9(4)
C2–C1–C3	112.1(3)	C5–C6–C7	113.0(4)
C1–C2–H2A	109.5	C6–C7–H7A	109.5
C1–C2–H2B	109.5	C6–C7–H7B	109.5
H2A–C2–H2B	109.5	H7A–C7–H7B	109.5
C1–C2–H2C	109.5	C6–C7–H7C	109.5
H2A–C2–H2C	109.5	H7A–C7–H7C	109.5
H2B–C2–H2C	109.5	H7B–C7–H7C	109.5
C5–C3–C4	111.0(3)	C6–C8–C14	120.6(4)
C5–C3–C1	110.5(3)	C6–C8–C9	125.4(4)
C4–C3–C1	114.5(3)	C14–C8–C9	114.0(3)
C5–C3–H3	106.8	C8–C9–C10	110.9(3)

C8–C9–C12	109.9(3)	C25–C24–H24	120.1
C10–C9–C12	107.0(3)	C23–C24–H24	120.1
C8–C9–C11	112.1(3)	C24–C25–C26	120.3(5)
C10–C9–C11	110.8(3)	C24–C25–H25	119.8
C12–C9–C11	105.8(3)	C26–C25–H25	119.8
C9–C10–H10A	109.5	C25–C26–C27	120.4(5)
C9–C10–H10B	109.5	C25–C26–H26	119.8
H10A–C10–H10B	109.5	C27–C26–H26	119.8
C9–C10–H10C	109.5	C22–C27–C26	119.2(4)
H10A–C10–H10C	109.5	C22–C27–H27	120.4
H10B–C10–H10C	109.5	C26–C27–H27	120.4
C9–C11–H11A	109.5		
C9–C11–H11B	109.5		
H11A–C11–H11B	109.5		
C9–C11–H11C	109.5		
H11A–C11–H11C	109.5		
H11B–C11–H11C	109.5		
C13–C12–C9	111.7(3)		
C13–C12–H12A	109.3		
C9–C12–H12A	109.3		
C13–C12–H12B	109.3		
C9–C12–H12B	109.3		
H12A–C12–H12B	107.9		
O2–C13–O3	118.5(4)		
O2–C13–C12	125.7(4)		
O3–C13–C12	115.7(3)		
N1–C14–O3	107.0(3)		
N1–C14–C8	113.9(3)		
O3–C14–C8	106.8(3)		
N1–C14–C1	105.9(3)		
O3–C14–C1	104.5(3)		
C8–C14–C1	117.9(3)		
N1–C15–N2	124.8(3)		
N1–C15–N3	117.8(3)		
N2–C15–N3	117.3(3)		
C21–C16–C17	119.5(4)		
C21–C16–N2	118.2(4)		
C17–C16–N2	122.2(3)		
C16–C17–C18	120.4(4)		
C16–C17–H17	119.8		
C18–C17–H17	119.8		
C19–C18–C17	119.5(4)		
C19–C18–H18	120.3		
C17–C18–H18	120.3		
C20–C19–C18	120.3(4)		
C20–C19–H19	119.8		
C18–C19–H19	119.8		
C19–C20–C21	120.1(4)		
C19–C20–H20	119.9		
C21–C20–H20	119.9		
C16–C21–C20	120.1(4)		
C16–C21–H21	119.9		
C20–C21–H21	119.9		
C27–C22–C23	119.6(4)		
C27–C22–N3	119.5(4)		
C23–C22–N3	120.9(3)		
C24–C23–C22	120.8(4)		
C24–C23–H23	119.6		
C22–C23–H23	119.6		
C25–C24–C23	119.7(4)		

Symmetry transformations used to generate equivalent atoms:

Table 4. Anisotropic displacement parameters [$Å^2 \times 10^3$]. The anisotropic displacement factor exponent takes the form: $-2\pi^2[h^2a^{*2}U^{11} + \cdots + 2\,h\,k\,a^*\,b^*\,U^{12}]$.

Atom	U^{11}	U^{22}	U^{33}	U^{23}	U^{13}	U^{12}
N1	30(2)	31(2)	28(2)	−1(1)	7(1)	0(2)
N2	38(2)	33(2)	29(2)	−6(2)	10(2)	6(2)
N3	32(2)	37(2)	30(2)	−3(2)	8(1)	6(2)
O1	40(2)	82(3)	63(2)	−12(2)	21(2)	−14(2)
O2	63(2)	37(2)	50(2)	5(1)	37(2)	6(2)
O3	42(2)	33(2)	28(1)	1(1)	14(1)	7(1)
C1	31(2)	45(3)	23(2)	−4(2)	5(2)	2(2)
C2	41(2)	54(3)	27(2)	−5(2)	5(2)	11(2)
C3	29(2)	55(3)	28(2)	−5(2)	9(2)	1(2)
C4	34(2)	75(3)	40(2)	−10(2)	12(2)	12(2)
C5	34(3)	70(3)	31(2)	2(2)	7(2)	−7(2)
C6	33(2)	46(3)	37(2)	−1(2)	9(2)	−7(2)
C7	46(3)	61(3)	60(3)	3(3)	12(2)	−13(3)
C8	42(2)	39(3)	22(2)	1(2)	4(2)	2(2)
C9	39(2)	32(2)	34(2)	0(2)	10(2)	3(2)
C10	55(3)	41(3)	44(2)	−9(2)	10(2)	0(2)
C11	48(3)	42(3)	61(3)	10(2)	14(2)	−6(2)
C12	42(2)	32(2)	33(2)	−1(2)	14(2)	6(2)
C13	45(3)	33(2)	31(2)	−5(2)	14(2)	7(2)
C14	34(2)	40(2)	25(2)	−2(2)	11(2)	2(2)
C15	33(2)	37(3)	24(2)	1(2)	13(2)	4(2)
C16	37(2)	34(2)	34(2)	6(2)	11(2)	−5(2)
C17	38(2)	42(3)	41(2)	−1(2)	12(2)	−2(2)
C18	39(3)	41(3)	72(3)	4(2)	22(2)	1(2)
C19	28(2)	68(4)	75(3)	21(3)	5(3)	−8(2)
C20	41(3)	84(4)	47(3)	7(3)	−1(2)	−23(3)
C21	39(3)	56(3)	36(2)	−1(2)	11(2)	−12(2)
C22	38(2)	37(3)	30(2)	−3(2)	8(2)	6(2)
C23	47(3)	31(2)	34(2)	−3(2)	10(2)	9(2)
C24	49(3)	47(3)	35(2)	−3(2)	9(2)	1(2)
C25	67(3)	43(3)	62(3)	9(2)	15(3)	8(3)
C26	84(4)	45(3)	122(5)	20(3)	55(4)	31(3)
C27	69(3)	50(3)	83(4)	6(3)	43(3)	20(3)

Table 5. Hydrogen coordinates [$\times 10^4$] and isotropic displacement parameters [$Å^2 \times 10^3$].

Atom	*x*	*y*	*z*	U_{eq}	*S.o.f.*
H2	608	2147	–4094	40	1
H2A	3431	2803	–233	63	1
zH2B	4415	3369	–409	63	1
H2C	4359	2508	–884	63	1
H3	3242	3538	–3595	44	1
H4A	4968	3034	–3668	74	1
H4B	4323	2375	–3145	74	1
H4C	5331	2856	–2284	74	1
H7A	4296	5798	–2680	84	1
H7B	5080	5563	–1406	84	1
H7C	3864	5968	–1531	84	1
H10A	2723	5084	426	71	1
H10B	1990	5858	158	71	1
H10C	3213	5805	–127	71	1
H11A	2216	6232	–2203	76	1
H11B	956	6202	–2001	76	1
H11C	1245	5706	–3030	76	1
H12A	359	5175	–921	42	1
H12B	331	4715	–2106	42	1
H17	–814	3360	–2687	48	1
H18	–2769	3678	–3324	59	1
H19	–3831	3326	–5208	70	1
H20	–2955	2681	–6459	72	1
H21	–1008	2354	–5819	52	1
H23	1033	2179	–1146	45	1
H24	910	1006	–257	53	1
H25	2055	–8	–535	70	1
H26	3268	130	–1762	94	1
H27	3387	1308	–2683	76	1

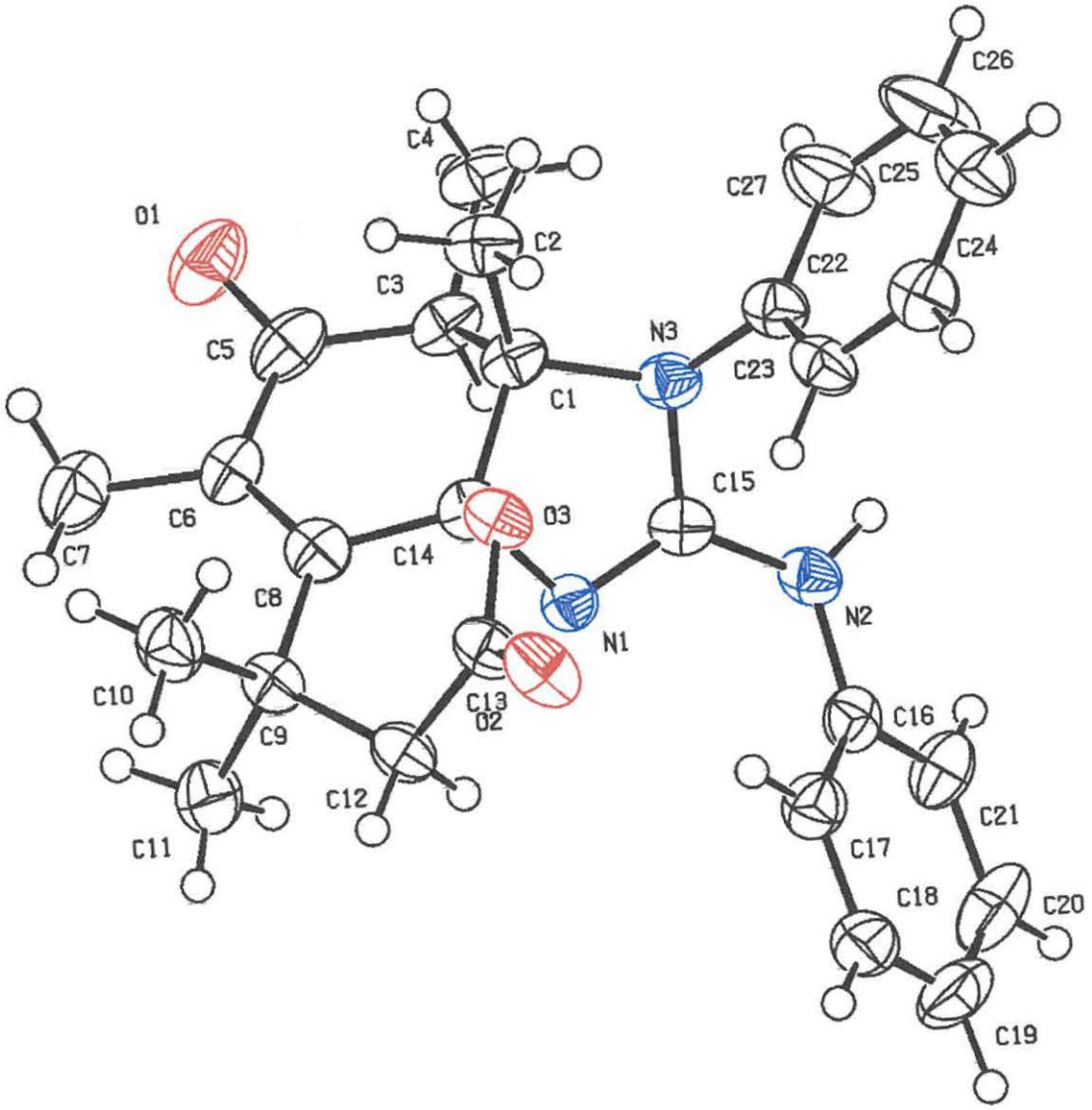
C26
C4
C27
C25
O1
C2
C24
C3
C22
C5
N3
C23
C1
C15
C6
O3
C7
C14
C8
N2
N1
C10
C13
O2
C16
C9
C12
C21
C11
C17
C18
C20
C19

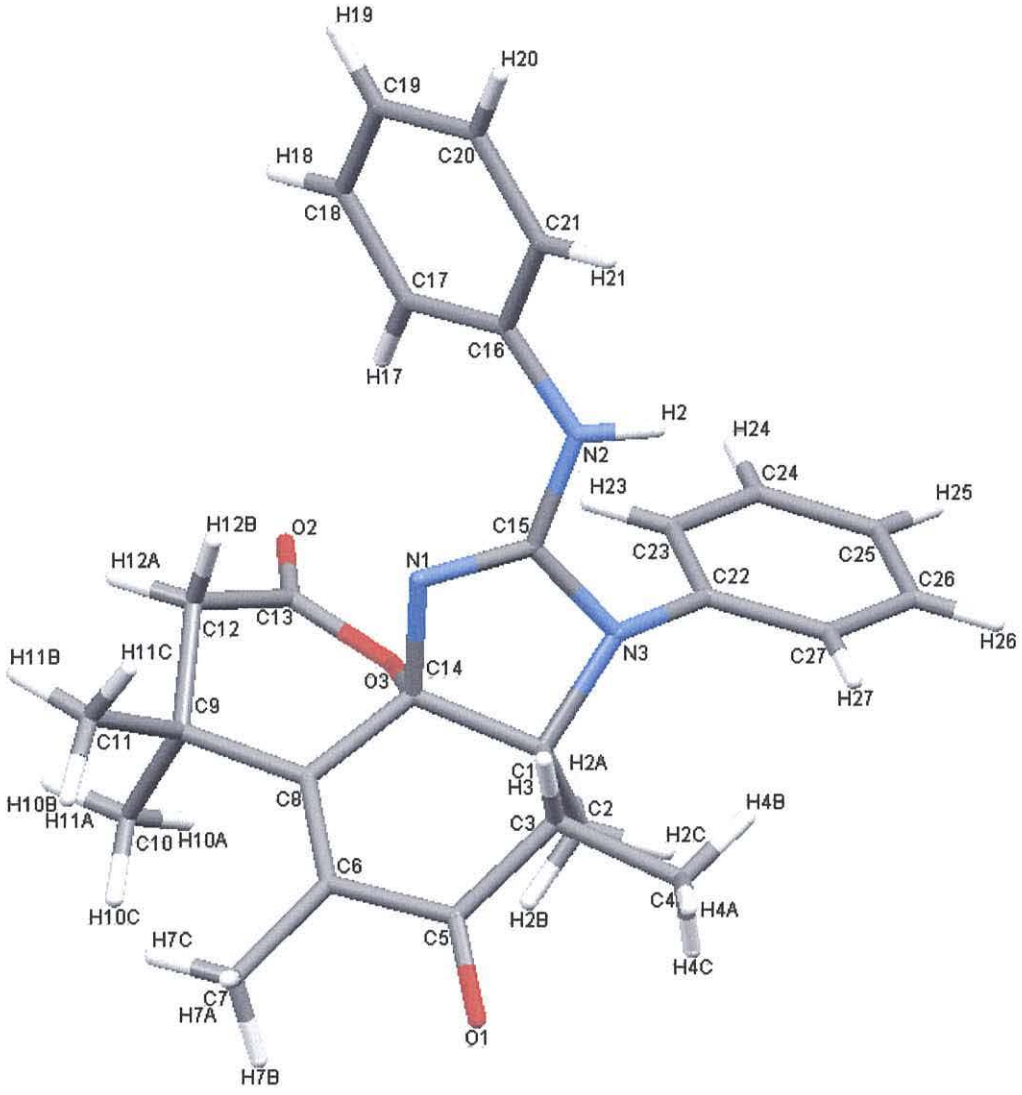
H19
H20
C19
H18
C20
C18
C21
H21
C17
C16
H17
H2
N2
H24
C24
H23
H25
C23
C25
C22
C26
H26
C27
H27
N3
C15
N1
H12B
O2
H12A
C12
C13
O3
C14
H11B
H11C
C9
C11
C1
H2A
H3
C8
C2
H4B
H10B
H11A
C10
H10A
C3
H2C
C6
C4
H4A
H10C
H2B
H7C
C5
H4C
C7
H7A
O1
H7B

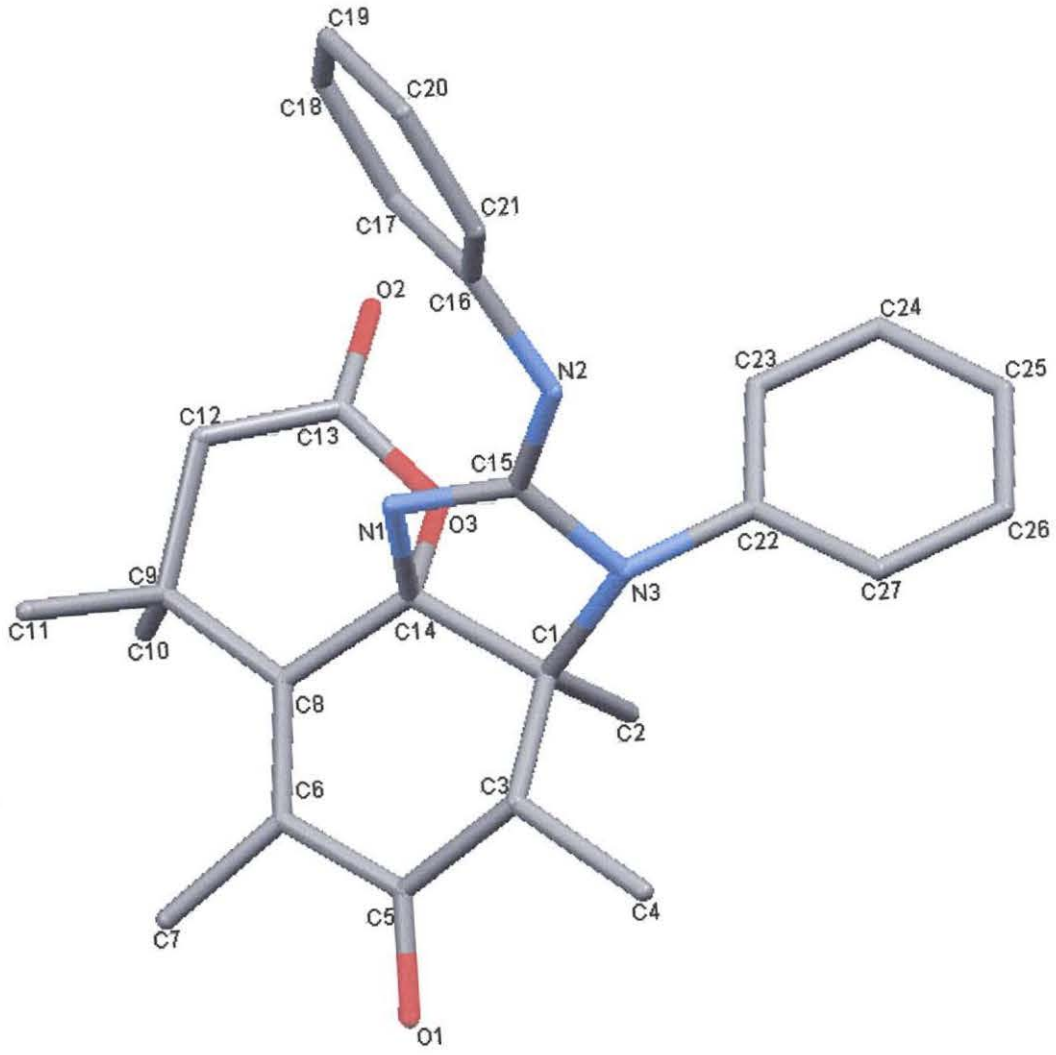
C19
C20
C18
C21
C17
C16
O2
N2
C24
C23
C25
C12
C13
C15
N1
O3
C22
C26
C9
N3
C27
C11
C10
C14
C1
C8
C2
C6
C3
C4
C5
C7
O1

2.2.2 2,3,5-Trimethyl-3'*H*-spiro[cyclohexa[2,5]diene-1,1'-isobenzofuran]-3',4-dione **160**

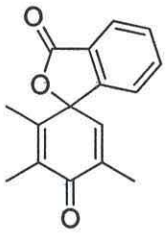

University of Southampton · School of Chemistry
EPSRC National Crystallography Service

Table 1. Crystal data and structure refinement details.

Identification code	**2010src0223**	
Empirical formula	$C_{16}H_{14}O_3$	
Formula weight	254.27	
Temperature	120(2) K	
Wavelength	0.71073 Å	
Crystal system	Monoclinic	
Space group	*P*21/*c*	
Unit cell dimensions	a = **7.5754(5) Å**	α = **90°**
	b = **19.7137(12) Å**	β = **101.678(4)°**
	c = **8.7909(4) Å**	γ = **90°**
Volume	1285.65(13) Å^3	
Z	4	
Density (calculated)	1.314 Mg / m^3	
Absorption coefficient	0.090 mm^{-1}	
F(000)	536	
Crystal	Shard; colourless	
Crystal size	0.40 × 0.10 × 0.04 mm^3	
θ range for data collection	2.93 – 27.48°	
Index ranges	$-9 \le h \le 9$, $-25 \le k \le 23$, $-10 \le l \le 11$	
Reflections collected	13309	
Independent reflections	2926 [R_{int} = 0.0578]	
Completeness to θ = 27.48°	99.1 %	
Absorption correction	Semi–empirical from equivalents	
Max. and min. transmission	0.9964 and 0.9648	
Refinement method	Full-matrix least-squares on F^2	
Data / restraints / parameters	2926 / 0 / 175	
Goodness-of-fit on F^2	1.085	
Final *R* indices [$F^2 > 2\sigma(F^2)$]	*R1* = 0.0756, *wR2* = 0.1576	
R indices (all data)	*R1* = 0.1069, *wR2* = 0.1781	
Largest diff. peak and hole	0.323 and –0.286 e Å^{-3}	

Diffractometer: *Nonius KappaCCD* area detector (ϕ scans and ω scans to fill *asymmetric unit* sphere). **Cell determination:** DirAx (Duisenberg, A.J.M.(1992). J. Appl. Cryst. 25, 92-96.) **Data collection:** Collect (Collect: Data collection software, R. Hooft, Nonius B.V., 1998). **Data reduction and cell refinement**: *Denzo* (Z. Otwinowski & W. Minor, *Methods in Enzymology* (1997) Vol. **276**: *Macromolecular Crystallography*, part A, pp. 307–326; C. W. Carter, Jr. & R. M. Sweet, Eds., Academic Press). **Absorption correction**: *SADABS* (Sheldrick, G. M. (2007). SADABS. Version 2007/2. Bruker AXS Inc., Madison, Wisconsin, USA.). **Structure solution**: *SHELXS97* (Sheldrick, G.M. (2008). Acta Cryst. A64, 112-122.). **Structure refinement**: *SHELXL97* (G Sheldrick, G.M. (2008). Acta Cryst. A64, 112-122.). **Graphics:** *CAMERON* (Watkin, D. M., Pearce, L. & Prout, C. K. (1993). Chemical Crystallography Lab, University of Oxford)

Special details:

Table 2. Atomic coordinates [$\times 10^4$], equivalent isotropic displacement parameters [$Å^2 \times 10^3$] and site occupancy factors. U_{eq} is defined as one third of the trace of the orthogonalized U^{ij} tensor.

Atom	*x*	*y*	*z*	U_{eq}	*S.o.f.*
C1	7224(3)	1032(1)	1540(3)	26(1)	1
C2	8891(3)	1419(1)	1294(3)	26(1)	1
C3	10652(3)	1383(1)	2126(3)	29(1)	1
C4	11896(3)	1820(1)	1681(3)	35(1)	1
C5	11410(4)	2268(2)	442(4)	44(1)	1
C6	9646(4)	2298(2)	−376(4)	44(1)	1
C7	8396(3)	1866(1)	85(3)	32(1)	1
C8	6449(3)	1798(1)	−534(3)	32(1)	1
C9	6755(3)	1252(1)	3029(3)	32(1)	1
C10	6933(4)	854(2)	4262(3)	38(1)	1
C11	7536(4)	148(2)	4147(3)	41(1)	1
C12	7712(3)	−126(1)	2601(4)	37(1)	1
C13	7455(3)	278(1)	1348(3)	28(1)	1
C14	6542(5)	1090(2)	5786(4)	58(1)	1
C15	8154(4)	−869(2)	2565(4)	52(1)	1
C16	7480(4)	49(2)	−268(3)	38(1)	1
O1	5808(2)	1293(1)	278(2)	29(1)	1
O2	5465(3)	2103(1)	−1555(2)	42(1)	1
O3	7830(3)	−212(1)	5312(3)	65(1)	1

Table 3. Bond lengths [Å] and angles [°].

C1–O1	1.471(3)	C6–C7–C8	129.6(2)
C1–C9	1.488(4)	O2–C8–O1	121.3(2)
C1–C13	1.511(3)	O2–C8–C7	130.7(3)
C1–C2	1.528(3)	O1–C8–C7	107.9(2)
C2–C7	1.373(4)	C10–C9–C1	123.1(3)
C2–C3	1.387(3)	C10–C9–H9	118.5
C3–C4	1.389(4)	C1–C9–H9	118.5
C3–H3	0.9500	C9–C10–C11	119.0(3)
C4–C5	1.394(4)	C9–C10–C14	122.7(3)
C4–H4	0.9500	C11–C10–C14	118.3(3)
C5–C6	1.385(4)	O3–C11–C10	119.6(3)
C5–H5	0.9500	O3–C11–C12	121.0(3)
C6–C7	1.393(4)	C10–C11–C12	119.4(2)
C6–H6	0.9500	C13–C12–C11	120.5(3)
C7–C8	1.472(4)	C13–C12–C15	123.8(3)
C8–O2	1.204(3)	C11–C12–C15	115.7(3)
C8–O1	1.370(3)	C12–C13–C16	125.1(3)
C9–C10	1.322(4)	C12–C13–C1	119.6(2)
C9–H9	0.9500	C16–C13–C1	115.3(2)
C10–C11	1.474(4)	C10–C14–H14A	109.5
C10–C14	1.504(4)	C10–C14–H14B	109.5
C11–O3	1.229(3)	H14A–C14–H14B	109.5
C11–C12	1.493(4)	C10–C14–H14C	109.5
C12–C13	1.341(4)	H14A–C14–H14C	109.5
C12–C15	1.504(4)	H14B–C14–H14C	109.5
C13–C16	1.494(4)	C12–C15–H15A	109.5
C14–H14A	0.9800	C12–C15–H15B	109.5
C14–H14B	0.9800	H15A–C15–H15B	109.5
C14–H14C	0.9800	C12–C15–H15C	109.5
C15–H15A	0.9800	H15A–C15–H15C	109.5
C15–H15B	0.9800	H15B–C15–H15C	109.5
C15–H15C	0.9800	C13–C16–H16A	109.5
C16–H16A	0.9800	C13–C16–H16B	109.5
C16–H16B	0.9800	H16A–C16–H16B	109.5
C16–H16C	0.9800	C13–C16–H16C	109.5
		H16A–C16–H16C	109.5
O1–C1–C9	107.15(19)	H16B–C16–H16C	109.5
O1–C1–C13	110.05(19)	C8–O1–C1	111.46(18)
C9–C1–C13	116.0(2)		
O1–C1–C2	102.49(19)		
C9–C1–C2	109.3(2)		
C13–C1–C2	111.0(2)		
C7–C2–C3	121.6(2)		
C7–C2–C1	109.0(2)		
C3–C2–C1	129.4(2)		
C2–C3–C4	117.1(2)		
C2–C3–H3	121.5		
C4–C3–H3	121.5		
C3–C4–C5	121.7(2)		
C3–C4–H4	119.1		
C5–C4–H4	119.1		
C6–C5–C4	120.5(3)		
C6–C5–H5	119.7		
C4–C5–H5	119.7		
C5–C6–C7	117.6(3)		
C5–C6–H6	121.2		
C7–C6–H6	121.2		
C2–C7–C6	121.5(2)		
C2–C7–C8	108.9(2)		

Symmetry transformations used to generate equivalent atoms:

Table 4. Anisotropic displacement parameters [$Å^2 \times 10^3$]. The anisotropic displacement factor exponent takes the form: $-2\pi^2[h^2a^{*2}U^{11} + \cdots + 2\,h\,k\,a^*\,b^*\,U^{12}]$.

Atom	U^{11}	U^{22}	U^{33}	U^{23}	U^{13}	U^{12}
C1	22(1)	24(1)	31(1)	1(1)	2(1)	0(1)
C2	25(1)	23(1)	30(1)	−3(1)	7(1)	0(1)
C3	26(1)	26(1)	33(1)	−3(1)	5(1)	1(1)
C4	23(1)	33(1)	50(2)	−3(1)	8(1)	1(1)
C5	29(1)	37(2)	68(2)	12(2)	16(1)	−1(1)
C6	32(2)	37(2)	63(2)	21(1)	12(1)	1(1)
C7	26(1)	27(1)	42(2)	3(1)	7(1)	3(1)
C8	30(1)	28(1)	39(2)	2(1)	7(1)	2(1)
C9	22(1)	36(2)	40(2)	−4(1)	8(1)	−3(1)
C10	27(1)	54(2)	34(2)	−1(1)	4(1)	−9(1)
C11	29(1)	48(2)	42(2)	16(1)	−2(1)	−12(1)
C12	24(1)	30(1)	54(2)	8(1)	0(1)	−5(1)
C13	21(1)	25(1)	38(1)	2(1)	2(1)	−2(1)
C14	46(2)	95(3)	36(2)	−7(2)	13(1)	−19(2)
C15	41(2)	31(2)	80(2)	13(2)	−1(2)	−2(1)
C16	33(1)	35(2)	47(2)	−8(1)	7(1)	−2(1)
O1	24(1)	28(1)	35(1)	5(1)	3(1)	1(1)
O2	32(1)	40(1)	51(1)	16(1)	0(1)	3(1)
O3	62(2)	72(2)	55(2)	35(1)	0(1)	−11(1)

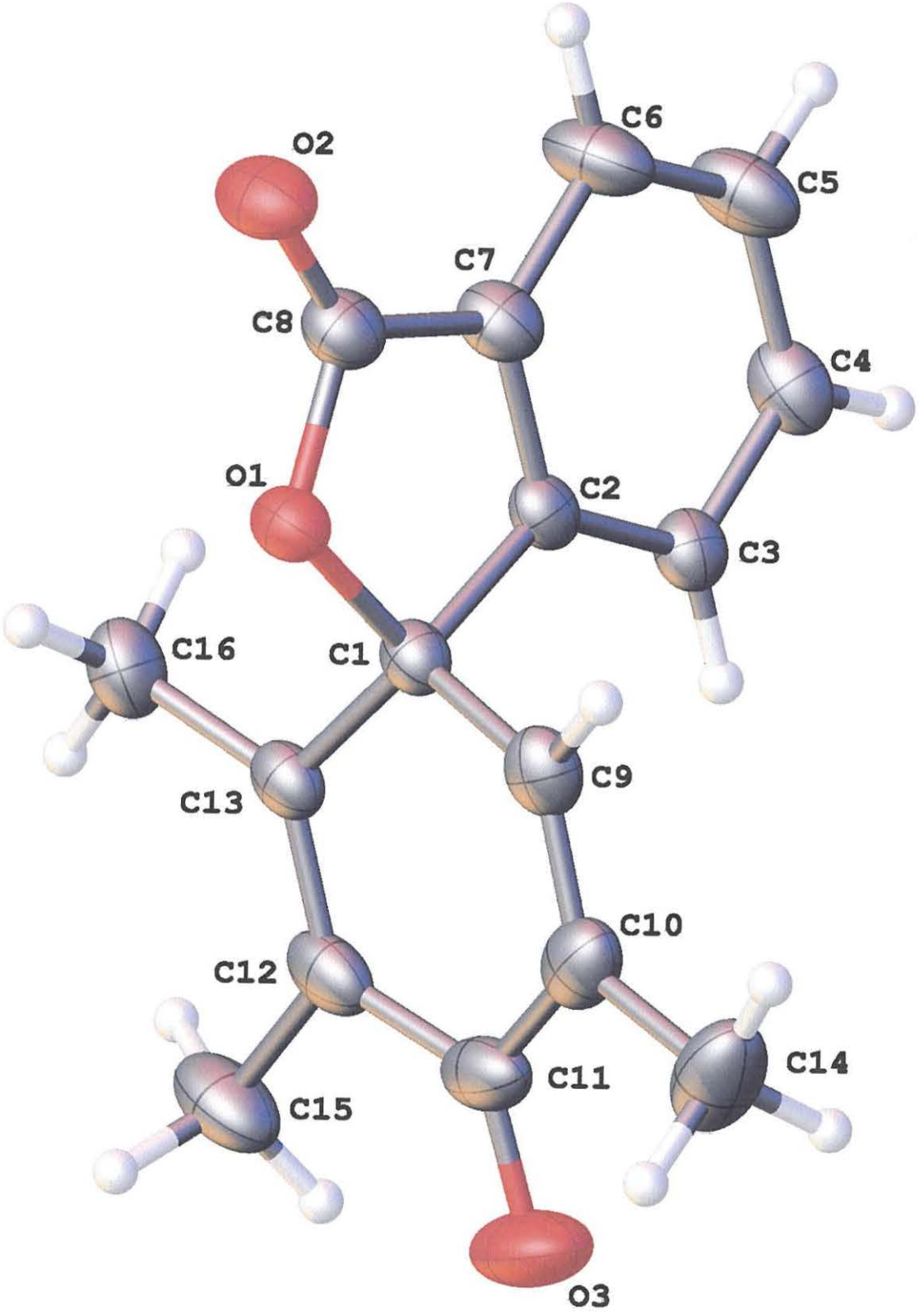
O2
C6
C5
C7
C8
C4
O1
C2
C3
C16
C1
C9
C13
C10
C12
C14
C11
C15
O3

2.2.3 2-Hydroxy-1,3,4-trimethyl-6*H*-benzo[c]chromen-6-one **120**

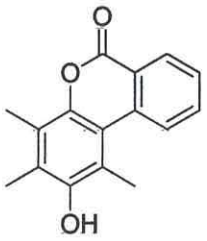

University of Southampton · School of Chemistry

EPSRC National Crystallography Service

Table 1. Crystal data and structure refinement details.

Identification code	**2010src0769**	
Empirical formula	$C_{16}H_{14}O_3$	
Formula weight	254.27	
Temperature	120(2) K	
Wavelength	0.71073 Å	
Crystal system	Monoclinic	
Space group	*P*21/*c*	
Unit cell dimensions	a = **7.2668(3) Å**	α = **90°**
	b = **9.4506(4) Å**	β = **92.275(3)°**
	c = **17.1427(8) Å**	γ = **90°**
Volume	1176.36(9) Å^3	
Z	4	
Density (calculated)	1.436 Mg / m^3	
Absorption coefficient	0.099 mm^{-1}	
F(000)	536	
Crystal	Fragment; colourless	
Crystal size	0.20 × 0.12 × 0.08 mm^3	
θ range for data collection	3.54 – 27.48°	
Index ranges	$-9 \le h \le 9$, $-12 \le k \le 12$, $-22 \le l \le 22$	
Reflections collected	15883	
Independent reflections	2705 [R_{int} = 0.0946]	
Completeness to θ = 27.48°	99.9 %	
Absorption correction	Semi–empirical from equivalents	
Max. and min. transmission	0.9921 and 0.9805	
Refinement method	Full-matrix least-squares on F^2	
Data / restraints / parameters	2705 / 0 / 176	
Goodness-of-fit on F^2	1.032	
Final *R* indices [$F^2 > 2\sigma(F^2)$]	*R1* = 0.0655, *wR2* = 0.1501	
R indices (all data)	*R1* = 0.1257, *wR2* = 0.1854	
Largest diff. peak and hole	0.295 and –0.353 e Å^{-3}	

Diffractometer: *Nonius KappaCCD* area detector (ϕ scans and ω scans to fill *asymmetric unit* sphere). **Cell determination:** DirAx (Duisenberg, A.J.M.(1992). J. Appl. Cryst. 25, 92-96.) **Data collection:** Collect (Collect: Data collection software, R. Hooft, Nonius B.V., 1998). **Data reduction and cell refinement**: *Denzo* (Z. Otwinowski & W. Minor, *Methods in Enzymology* (1997) Vol. **276**: *Macromolecular Crystallography*, part A, pp. 307–326; C. W. Carter, Jr. & R. M. Sweet, Eds., Academic Press). **Absorption correction**: *SADABS* (Sheldrick, G. M. (2007). SADABS. Version 2007/2. Bruker AXS Inc., Madison, Wisconsin, USA.). **Structure solution**: *SHELXS97* (Sheldrick, G.M. (2008). Acta Cryst. A64, 112-122.). **Structure refinement**: *SHELXL97* (G Sheldrick, G.M. (2008). Acta Cryst. A64, 112-122.). **Graphics:** *CAMERON* (Watkin, D. M., Pearce, L. & Prout, C. K. (1993). Chemical Crystallography Lab, University of Oxford)

Special details:

Table 2. Atomic coordinates [$\times 10^4$], equivalent isotropic displacement parameters [$Å^2 \times 10^3$] and site occupancy factors. U_{eq} is defined as one third of the trace of the orthogonalized U^{ij} tensor.

Atom	*x*	*y*	*z*	U_{eq}	*S.o.f.*
C1	1825(3)	7527(2)	381(2)	27(1)	1
C2	1546(3)	7282(2)	–455(1)	24(1)	1
C3	947(3)	8437(3)	–913(2)	29(1)	1
C4	791(3)	8315(3)	–1712(2)	31(1)	1
C5	1284(3)	7051(3)	–2061(2)	32(1)	1
C6	1839(3)	5899(3)	–1610(1)	28(1)	1
C7	1944(3)	5958(2)	–790(1)	23(1)	1
C8	2460(3)	4769(2)	–267(1)	20(1)	1
C9	2745(3)	3342(2)	–495(1)	24(1)	1
C10	3263(3)	2360(2)	77(1)	23(1)	1
C11	3507(3)	2693(2)	871(1)	22(1)	1
C12	3175(3)	4075(2)	1107(1)	21(1)	1
C13	2661(3)	5060(2)	534(1)	20(1)	1
C14	2453(4)	2786(3)	–1316(2)	40(1)	1
C15	4088(3)	1544(3)	1443(1)	29(1)	1
C16	3364(3)	4499(3)	1954(1)	27(1)	1
O1	1637(3)	8657(2)	715(1)	39(1)	1
O2	2358(2)	6412(2)	831(1)	26(1)	1
O3	3554(3)	994(2)	–173(1)	35(1)	1

Table 3. Bond lengths [Å] and angles [°].

C1–O1	1.222(3)	C9–C8–C7	126.3(2)
C1–O2	1.354(3)	C10–C9–C8	118.5(2)
C1–C2	1.458(3)	C10–C9–C14	116.7(2)
C2–C3	1.404(3)	C8–C9–C14	124.7(2)
C2–C7	1.411(3)	O3–C10–C9	116.5(2)
C3–C4	1.374(4)	O3–C10–C11	119.8(2)
C3–H3	0.9500	C9–C10–C11	123.7(2)
C4–C5	1.390(4)	C12–C11–C10	118.4(2)
C4–H4	0.9500	C12–C11–C15	122.2(2)
C5–C6	1.386(3)	C10–C11–C15	119.4(2)
C5–H5	0.9500	C11–C12–C13	117.9(2)
C6–C7	1.406(3)	C11–C12–C16	121.3(2)
C6–H6	0.9500	C13–C12–C16	120.9(2)
C7–C8	1.476(3)	C12–C13–O2	113.36(19)
C8–C13	1.402(3)	C12–C13–C8	125.0(2)
C8–C9	1.422(3)	O2–C13–C8	121.6(2)
C9–C10	1.391(3)	C9–C14–H14A	109.5
C9–C14	1.510(3)	C9–C14–H14B	109.5
C10–O3	1.380(3)	H14A–C14–H14B	109.5
C10–C11	1.402(3)	C9–C14–H14C	109.5
C11–C12	1.392(3)	H14A–C14–H14C	109.5
C11–C15	1.512(3)	H14B–C14–H14C	109.5
C12–C13	1.393(3)	C11–C15–H15A	109.5
C12–C16	1.506(3)	C11–C15–H15B	109.5
C13–O2	1.395(3)	H15A–C15–H15B	109.5
C14–H14A	0.9800	C11–C15–H15C	109.5
C14–H14B	0.9800	H15A–C15–H15C	109.5
C14–H14C	0.9800	H15B–C15–H15C	109.5
C15–H15A	0.9800	C12–C16–H16A	109.5
C15–H15B	0.9800	C12–C16–H16B	109.5
C15–H15C	0.9800	H16A–C16–H16B	109.5
C16–H16A	0.9800	C12–C16–H16C	109.5
C16–H16B	0.9800	H16A–C16–H16C	109.5
C16–H16C	0.9800	H16B–C16–H16C	109.5
O3–H3O	0.8400	C1–O2–C13	123.46(18)
		C10–O3–H3O	109.5
O1–C1–O2	116.7(2)		
O1–C1–C2	125.9(2)		
O2–C1–C2	117.5(2)		
C3–C2–C7	121.8(2)		
C3–C2–C1	117.0(2)		
C7–C2–C1	121.2(2)		
C4–C3–C2	120.2(2)		
C4–C3–H3	119.9		
C2–C3–H3	119.9		
C3–C4–C5	119.3(2)		
C3–C4–H4	120.4		
C5–C4–H4	120.4		
C6–C5–C4	120.6(2)		
C6–C5–H5	119.7		
C4–C5–H5	119.7		
C5–C6–C7	122.0(2)		
C5–C6–H6	119.0		
C7–C6–H6	119.0		
C6–C7–C2	115.9(2)		
C6–C7–C8	125.4(2)		
C2–C7–C8	118.6(2)		
C13–C8–C9	116.4(2)		
C13–C8–C7	117.3(2)		

Symmetry transformations used to generate equivalent atoms:

Table 4. Anisotropic displacement parameters [$Å^2 \times 10^3$]. The anisotropic displacement factor exponent takes the form: $-2\pi^2[h^2a^{*2}U^{11} + \cdots + 2\,h\,k\,a^*\,b^*\,U^{12}]$.

Atom	U^{11}	U^{22}	U^{33}	U^{23}	U^{13}	U^{12}
C1	31(1)	19(1)	33(2)	−1(1)	3(1)	3(1)
C2	21(1)	23(1)	29(1)	4(1)	1(1)	−1(1)
C3	25(1)	22(1)	42(2)	6(1)	2(1)	0(1)
C4	26(1)	33(2)	33(2)	15(1)	−1(1)	1(1)
C5	35(2)	37(2)	24(1)	7(1)	−1(1)	0(1)
C6	30(1)	27(1)	26(1)	2(1)	0(1)	0(1)
C7	20(1)	22(1)	26(1)	3(1)	1(1)	−2(1)
C8	18(1)	21(1)	22(1)	−1(1)	2(1)	−1(1)
C9	28(1)	22(1)	23(1)	−2(1)	2(1)	−2(1)
C10	23(1)	20(1)	26(1)	−3(1)	1(1)	2(1)
C11	22(1)	20(1)	24(1)	1(1)	0(1)	1(1)
C12	19(1)	24(1)	20(1)	−2(1)	1(1)	−1(1)
C13	20(1)	16(1)	24(1)	−2(1)	2(1)	−2(1)
C14	73(2)	21(1)	26(2)	−3(1)	2(1)	−1(1)
C15	31(1)	26(1)	29(1)	3(1)	−3(1)	3(1)
C16	28(1)	29(1)	24(1)	−3(1)	0(1)	2(1)
O1	53(1)	23(1)	40(1)	−5(1)	−1(1)	7(1)
O2	35(1)	19(1)	24(1)	−3(1)	1(1)	2(1)
O3	53(1)	19(1)	32(1)	−4(1)	2(1)	7(1)

Table 5. Hydrogen coordinates [$\times 10^4$] and isotropic displacement parameters [$Å^2 \times 10^3$].

Atom	*x*	*y*	*z*	U_{eq}	*S.o.f.*
H3	648	9306	−670	35	1
H4	352	9087	−2022	37	1
H5	1241	6975	−2614	39	1
H6	2157	5044	−1862	34	1
H14A	3476	3089	−1633	60	1
H14B	1294	3159	−1544	60	1
H14C	2401	1750	−1305	60	1
H15A	4420	1970	1951	43	1
H15B	5154	1038	1248	43	1
H15C	3068	879	1502	43	1
H16A	3288	5531	1996	41	1
H16B	4556	4175	2174	41	1
H16C	2371	4066	2241	41	1
H3O	3364	427	192	52	1

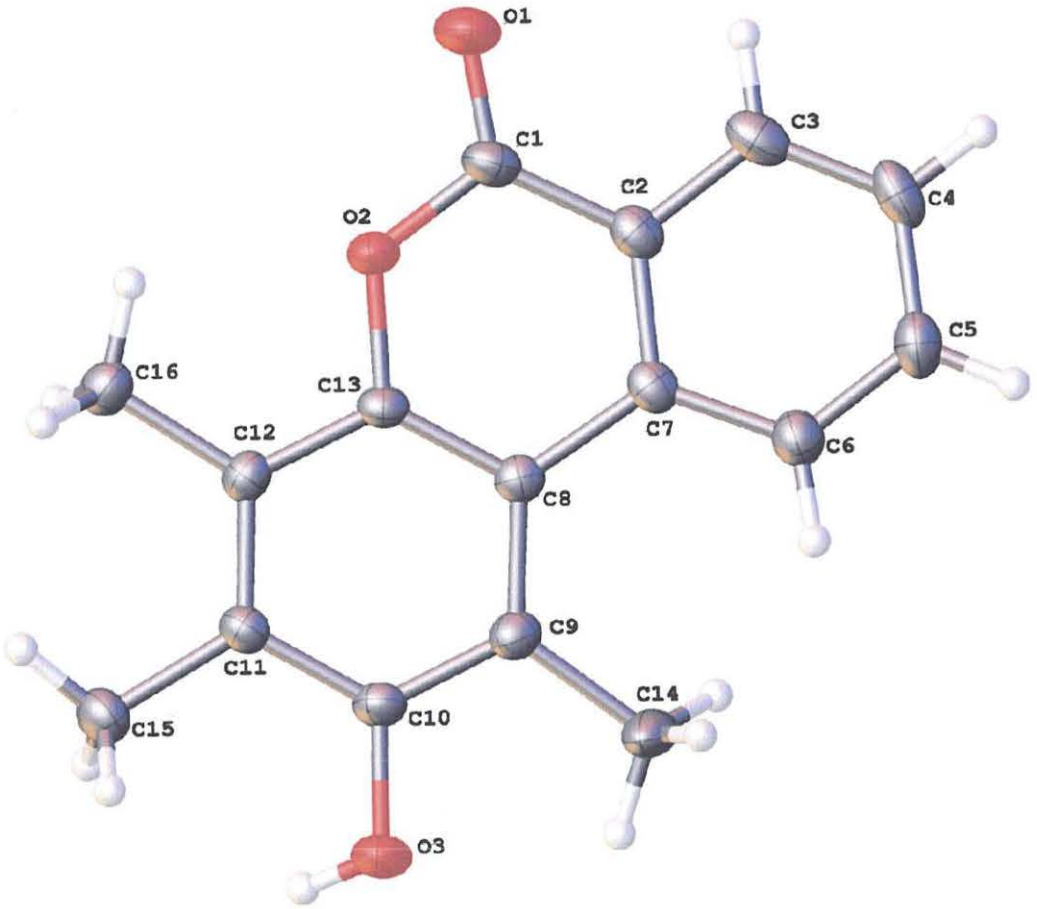
O1
C1
C3
C2
C4
O2
C5
C16
C13
C7
C12
C6
C8
C9
C11
C14
C15
C10
O3

2.2.4 (1R,6S)-6-Bromo-3,4,6-trimethyl-3'*H*-spiro[cyclohex[3]ene-1,1'-isobenzofuran]-2,3',5-trione **164**

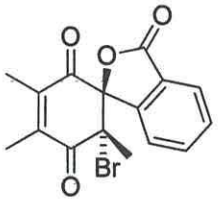

University of Southampton · School of Chemistry

EPSRC National Crystallography Service

Table 1. Crystal data and structure refinement details.

Identification code	**2010src0931a**	
Empirical formula	$C_{16}H_{13}BrO_4$	
Formula weight	349.17	
Temperature	120(2) K	
Wavelength	0.71073 Å	
Crystal system	Monoclinic	
Space group	*Pc*	
Unit cell dimensions	**a = 7.8811(7) Å**	**α = 90°**
	b = 11.9393(12) Å	**β = 111.263(5)°**
	c = 7.9987(7) Å	**γ = 90°**
Volume	701.40(11) Å^3	
Z	2	
Density (calculated)	1.653 Mg / m^3	
Absorption coefficient	2.943 mm^{-1}	
F(000)	352	
Crystal	Lath; colourless	
Crystal size	0.36 × 0.08 × 0.03 mm^3	
θ range for data collection	3.26 – 27.46°	
Index ranges	$-10 \le h \le 10$, $-14 \le k \le 15$, $-10 \le l \le 10$	
Reflections collected	9460	
Independent reflections	3035 [R_{int} = 0.0777]	
Completeness to θ = 27.46°	99.8 %	
Absorption correction	Semi–empirical from equivalents	
Max. and min. transmission	0.9169 and 0.4172	
Refinement method	Full-matrix least-squares on F^2	
Data / restraints / parameters	3035 / 2 / 193	
Goodness-of-fit on F^2	1.009	
Final R indices [$F^2 > 2\sigma(F^2)$]	$R1$ = 0.0479, $wR2$ = 0.0892	
R indices (all data)	$R1$ = 0.0683, $wR2$ = 0.0972	
Absolute structure parameter	0.021(12)	
Largest diff. peak and hole	0.357 and –0.606 e Å^{-3}	

Diffractometer: *Nonius KappaCCD* area detector (ϕ scans and ω scans to fill *asymmetric unit* sphere). **Cell determination:** DirAx (Duisenberg, A.J.M.(1992). J. Appl. Cryst. 25, 92-96.) **Data collection:** Collect (Collect: Data collection software, R. Hooft, Nonius B.V., 1998). **Data reduction and cell refinement**: *Denzo* (Z. Otwinowski & W. Minor, *Methods in Enzymology* (1997) Vol. **276**: *Macromolecular Crystallography*, part A, pp. 307–326; C. W. Carter, Jr. & R. M. Sweet, Eds., Academic Press). **Absorption correction**: *SADABS* (Sheldrick, G. M. (2007). SADABS. Version 2007/2. Bruker AXS Inc., Madison, Wisconsin, USA.). **Structure solution**: *SHELXS97* (Sheldrick, G.M. (2008). Acta Cryst. A64, 112-122.). **Structure refinement**: *SHELXL97* (G Sheldrick, G.M. (2008). Acta Cryst. A64, 112-122.). **Graphics:** *CAMERON* (Watkin, D. M., Pearce, L. & Prout, C. K. (1993). Chemical Crystallography Lab, University of Oxford)

Special details:

Table 2. Atomic coordinates [$\times 10^4$], equivalent isotropic displacement parameters [$Å^2 \times 10^3$] and site occupancy factors. U_{eq} is defined as one third of the trace of the orthogonalized U^{ij} tensor.

Atom	*x*	*y*	*z*	U_{eq}	*S.o.f.*
C1	1624(8)	4717(5)	8106(7)	26(1)	1
C2	3566(8)	4579(4)	8515(7)	20(1)	1
C3	4940(8)	5398(5)	9138(7)	26(1)	1
C4	6716(8)	5073(5)	9405(7)	25(1)	1
C5	7078(7)	3956(5)	9109(7)	26(1)	1
C6	5715(7)	3152(5)	8519(6)	23(1)	1
C7	3951(6)	3485(4)	8233(6)	18(1)	1
C8	2177(6)	2844(4)	7589(6)	16(1)	1
C9	1894(6)	1953(4)	8855(6)	19(1)	1
C10	–86(7)	1544(4)	8051(7)	19(1)	1
C11	–1032(7)	1495(4)	6073(6)	19(1)	1
C12	–230(7)	1868(4)	4957(6)	21(1)	1
C13	1652(6)	2324(4)	5695(6)	16(1)	1
C14	2466(7)	2333(4)	10807(6)	20(1)	1
C15	–2920(7)	987(5)	5416(7)	25(1)	1
C16	–1039(8)	1812(5)	2957(7)	28(1)	1
O1	721(6)	5509(3)	8206(6)	34(1)	1
O2	793(4)	3702(3)	7485(4)	20(1)	1
O3	–856(5)	1251(3)	9067(5)	27(1)	1
O4	2694(5)	2314(3)	4905(4)	22(1)	1
Br1	3341(1)	619(1)	8771(1)	26(1)	1

Table 3. Bond lengths [Å] and angles [°].

C1–O1	1.204(7)	O2–C8–C9	103.6(3)
C1–O2	1.381(6)	C7–C8–C9	117.5(4)
C1–C2	1.454(8)	O2–C8–C13	107.1(4)
C2–C7	1.378(7)	C7–C8–C13	115.0(4)
C2–C3	1.409(8)	C9–C8–C13	108.4(4)
C3–C4	1.393(8)	C14–C9–C10	113.6(4)
C3–H3	0.9500	C14–C9–C8	114.0(4)
C4–C5	1.402(8)	C10–C9–C8	108.2(4)
C4–H4	0.9500	C14–C9–Br1	108.3(3)
C5–C6	1.389(8)	C10–C9–Br1	103.9(3)
C5–H5	0.9500	C8–C9–Br1	108.1(3)
C6–C7	1.383(6)	O3–C10–C11	121.1(5)
C6–H6	0.9500	O3–C10–C9	119.0(4)
C7–C8	1.511(7)	C11–C10–C9	120.0(4)
C8–O2	1.476(5)	C12–C11–C10	121.3(5)
C8–C9	1.540(6)	C12–C11–C15	122.8(5)
C8–C13	1.548(6)	C10–C11–C15	115.9(4)
C9–C14	1.528(7)	C11–C12–C13	119.9(5)
C9–C10	1.536(7)	C11–C12–C16	125.2(5)
C9–Br1	1.975(5)	C13–C12–C16	114.8(4)
C10–O3	1.229(6)	O4–C13–C12	124.0(4)
C10–C11	1.485(7)	O4–C13–C8	121.8(4)
C11–C12	1.343(7)	C12–C13–C8	114.2(4)
C11–C15	1.513(7)	C9–C14–H14A	109.5
C12–C13	1.487(7)	C9–C14–H14B	109.5
C12–C16	1.493(7)	H14A–C14–H14B	109.5
C13–O4	1.204(5)	C9–C14–H14C	109.5
C14–H14A	0.9800	H14A–C14–H14C	109.5
C14–H14B	0.9800	H14B–C14–H14C	109.5
C14–H14C	0.9800	C11–C15–H15A	109.5
C15–H15A	0.9800	C11–C15–H15B	109.5
C15–H15B	0.9800	H15A–C15–H15B	109.5
C15–H15C	0.9800	C11–C15–H15C	109.5
C16–H16A	0.9800	H15A–C15–H15C	109.5
C16–H16B	0.9800	H15B–C15–H15C	109.5
C16–H16C	0.9800	C12–C16–H16A	109.5
		C12–C16–H16B	109.5
O1–C1–O2	119.9(5)	H16A–C16–H16B	109.5
O1–C1–C2	132.4(5)	C12–C16–H16C	109.5
O2–C1–C2	107.8(4)	H16A–C16–H16C	109.5
C7–C2–C3	122.0(5)	H16B–C16–H16C	109.5
C7–C2–C1	110.3(5)	C1–O2–C8	110.1(4)
C3–C2–C1	127.7(5)		
C4–C3–C2	117.4(5)		
C4–C3–H3	121.3		
C2–C3–H3	121.3		
C3–C4–C5	119.6(5)		
C3–C4–H4	120.2		
C5–C4–H4	120.2		
C6–C5–C4	122.4(5)		
C6–C5–H5	118.8		
C4–C5–H5	118.8		
C7–C6–C5	117.7(5)		
C7–C6–H6	121.2		
C5–C6–H6	121.2		
C2–C7–C6	120.9(5)		
C2–C7–C8	107.7(4)		
C6–C7–C8	131.4(5)		
O2–C8–C7	104.0(4)		

Symmetry transformations used to generate equivalent atoms:

Table 4. Anisotropic displacement parameters [$Å^2 \times 10^3$]. The anisotropic displacement factor exponent takes the form: $-2\pi^2[h^2a^{*2}U^{11} + \cdots + 2\,h\,k\,a^*\,b^*\,U^{12}]$.

Atom	U^{11}	U^{22}	U^{33}	U^{23}	U^{13}	U^{12}
C1	24(3)	18(3)	31(3)	−3(2)	4(3)	−5(2)
C2	18(3)	23(3)	17(3)	−1(2)	3(2)	−3(2)
C3	18(3)	29(4)	27(3)	−7(2)	4(3)	−4(3)
C4	17(3)	30(4)	27(3)	3(3)	7(3)	−7(2)
C5	15(3)	33(3)	30(3)	−6(2)	8(2)	0(2)
C6	19(3)	29(3)	19(3)	1(2)	7(2)	6(2)
C7	14(3)	23(3)	16(2)	−1(2)	5(2)	0(2)
C8	15(3)	15(3)	18(2)	3(2)	6(2)	8(2)
C9	16(3)	22(3)	20(3)	6(2)	9(2)	3(2)
C10	25(3)	12(2)	19(3)	2(2)	9(2)	0(2)
C11	16(3)	21(3)	21(3)	−2(2)	7(2)	1(2)
C12	22(3)	18(3)	22(3)	−1(2)	7(2)	1(2)
C13	18(3)	16(3)	14(2)	1(2)	4(2)	3(2)
C14	17(3)	28(3)	17(3)	2(2)	8(2)	−4(2)
C15	19(3)	35(3)	19(3)	−3(2)	5(2)	−7(2)
C16	29(3)	35(3)	17(3)	−3(2)	4(2)	−7(3)
O1	14(2)	22(2)	60(3)	−5(2)	7(2)	3(2)
O2	13(2)	19(2)	25(2)	0(2)	6(2)	3(1)
O3	26(2)	31(2)	27(2)	2(2)	14(2)	−4(2)
O4	23(2)	28(2)	18(2)	−1(2)	11(2)	−1(2)
Br1	26(1)	22(1)	31(1)	4(1)	12(1)	7(1)

Table 5. Hydrogen coordinates [$\times 10^4$] and isotropic displacement parameters [$Å^2 \times 10^3$].

Atom	*x*	*y*	*z*	U_{eq}	*S.o.f.*
H3	4664	6144	9367	31	1
H4	7677	5605	9786	30	1
H5	8299	3741	9320	31	1
H6	5986	2400	8319	27	1
H14A	3745	2566	11244	30	1
H14B	2315	1712	11542	30	1
H14C	1704	2964	10886	30	1
H15A	–3825	1574	4883	38	1
H15B	–3150	646	6428	38	1
H15C	–3006	413	4513	38	1
H16A	–424	1227	2529	42	1
H16B	–885	2535	2452	42	1
H16C	–2339	1636	2578	42	1

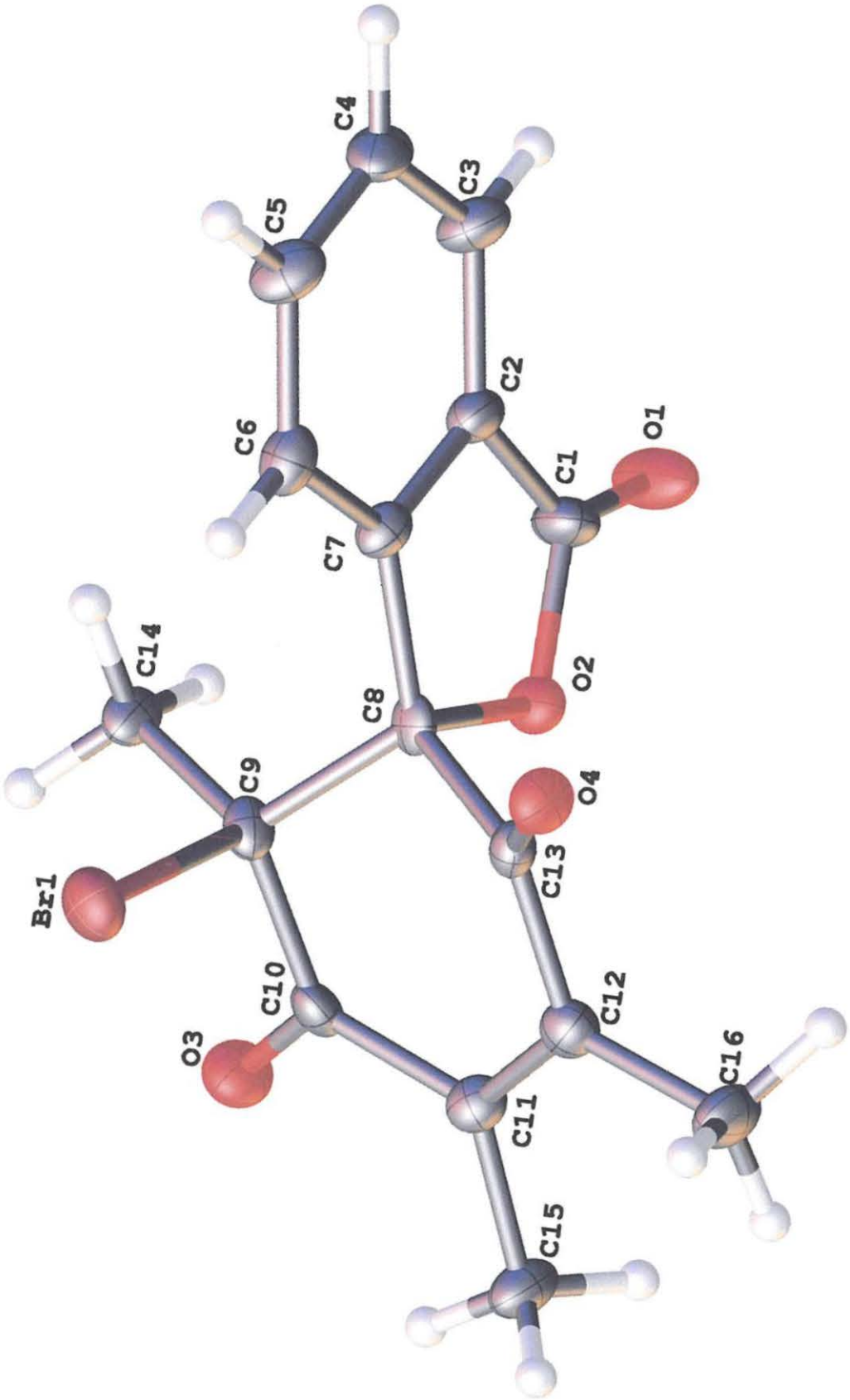
C4
C3
C5
C2
C6
O1
C1
C7
C14
O2
C8
C9
O4
Br1
C13
C10
C12
O3
C16
C11
C15

3.0 Enzymatic evaluation of compounds 129 and 130

3.1 Stability data for trimethyl-locked quinone delivery system

3.1.1 Compound 129

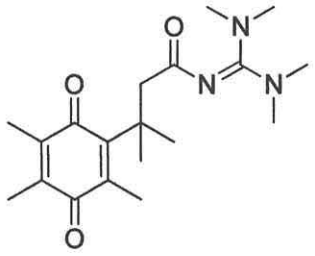

(129)

Time (min)	Retention Time (min)	Area %	Peak Area	Concentration (μM)*
0	3.622	48.79	1934726	86.10
7	3.563	47.82	2203163	98.05
14	3.575	48.82	1999575	88.99
21	3.572	48.46	2113616	94.06
28	3.585	54.25	2105335	93.69
35	3.572	50.61	2084255	92.76
42	3.568	45.22	2002439	89.11
49	3.575	47.27	2146306	95.52
56	3.570	46.10	2247050	100.00
63	3.582	49.29	2107511	93.79
70	3.593	48.24	2139406	95.21
77	3.602	50.94	2094809	93.22

Appendix 3.1.1.1 Stability data of 100 μM **129** in 10 mM phosphate buffer pH 7 at 37 °C

*Concentration (μM) = (area / 2247050) x 100 μM

3.1.2 Lactone 44

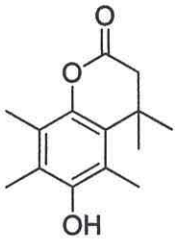

(44)

Time (min)	Retention Time (min)	Area %	Peak Area	Concentration (μM)*
0	2.237	5.50	218097	62.22
7	2.225	5.57	256497	73.17
14	2.227	7.46	305489	87.15
21	2.237	8.04	350528	100.00
28	2.233	7.17	278160	79.35
35	2.222	6.92	284854	81.26
42	2.218	6.87	304199	86.78
49	2.237	6.70	304411	86.84
56	2.223	6.34	309106	88.18
63	2.222	6.86	293481	83.73
70	2.245	6.26	277702	79.22
77	2.255	6.02	247416	70.58

Appendix 3.1.2.1 Stability data of 100 μM **44** in 10 mM phosphate buffer pH 7 at 37 °C

*Concentration (μM) = (area / 350528) x 100 μM

3.1.3 HPLC stability spectra for compound 129 and lactone 44

(a) t = 0 min

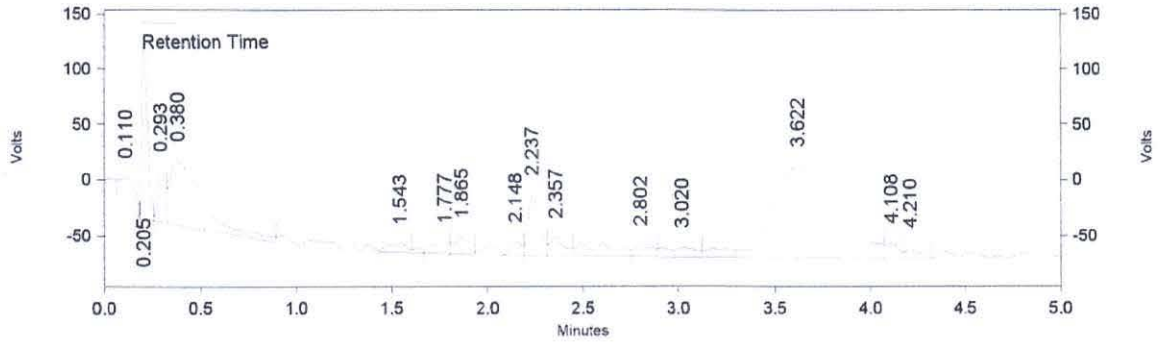

(b) t = 77 min

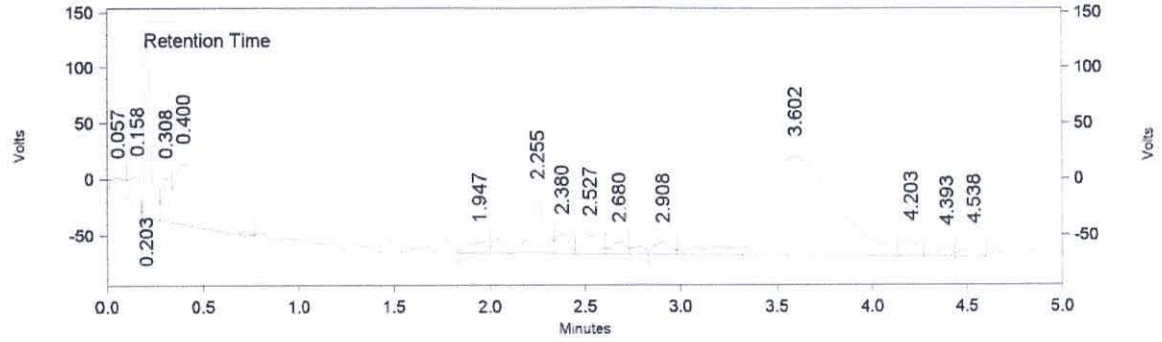

Appendix 3.1.3.1 Stability spectra of 100 µM **129** and 100 µM **44** in 10 mM phosphate buffer pH 7 at 37 °C

3.1.4 NADH 35

Time (min)	Retention Time (min)	Area %	Peak Area	Concentration (µM)*
0	0.162	25.35	1167647	470.03
7	0.153	27.67	1242105	500.00
14	0.152	26.28	1083633	436.21
21	0.152	23.87	1024799	412.53
28	0.152	26.73	1153550	464.35
35	0.152	24.22	1046723	421.35
42	0.153	29.37	1208470	486.46
49	0.152	29.30	1116520	449.45
56	0.150	28.78	1066149	429.17
63	0.153	26.16	1237234	498.04
70	0.153	25.05	1237125	498.00
77	0.152	25.47	1055493	424.88

Appendix 3.1.4.1 Stability data of 500 µM **35** in 10 mM phosphate buffer pH 7 at 37 °C

*Concentration (µM) = (area / 1242105) x 500 µM

3.2 Enzyme study data for trimethyl-locked quinone delivery system

3.2.1 Compound 129

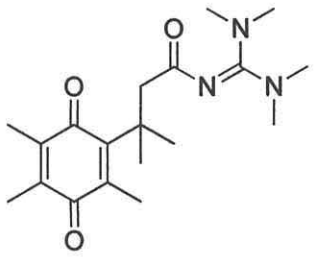

(129)

Time (min)	Retention Time (min)	Area %	Peak Area	Concentration (μM)*
0	5.175	10.65	1131715	100.00
10	5.220	6.48	911169	80.51
20	5.174	6.58	582499	51.47
30	5.209	3.76	400284	35.37
40	4.998	2.75	307842	27.20
50	5.065	0.89	121942	10.77
60	5.228	0.94	121928	10.77
70	0	0	0	0
80	0	0	0	0

Appendix 3.2.1.1 Effect of 0.5 μg hNQO1 on 100 μM **129** with 500 μM **35** at 37 °C (N=1)

*Concentration (μM) = (area/ 1131715) x 100 μM

Time (min)	Peak Area	Concentration (μM)*
0	526561	100.00
10	465837	88.47
20	266412	50.59
30	104779	19.90
40	63630	12.08
50	52940	10.05
60	87791	16.67
70	0	0
80	0	0

Appendix 3.2.1.2 Effect of 0.5 μg hNQO1 on 100 μM **129** with 500 μM **35** at 37 °C (N=2)

*Concentration (μM) = (area/ 526561) x 100 μM

Time (min)	Peak Area	Concentration (μM)*
0	904497	100.00
10	821631	90.84
20	528352	58.41
30	304227	33.63
40	226124	25.00
50	193000	21.34
60	93291	10.31
70	0	0
80	0	0

Appendix 3.2.1.3 Effect of 0.5 μg hNQO1 on 100 μM **129** with 500 μM **35** at 37 °C (N=3)

*Concentration (μM) = (area/ 904497) x 100 μM

3.2.2 Lactone 44

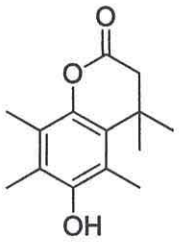

(44)

Time (min)	Retention Time (min)	Area %	Peak Area	Concentration (μM)*
0	0	0	0	0
0.1	2.780	1.32	140039	28.07
10	2.760	2.35	330343	66.22
20	2.782	2.53	223955	44.89
30	2.798	3.35	356438	71.45
40	2.803	3.16	353536	70.87
50	2.790	3.46	473342	94.89
60	2.767	3.84	498852	100.00
70	2.787	4.86	434363	87.07
80	2.805	4.72	352470	70.66

Appendix 3.2.2.1 Effect of 0.5 μg hNQO1 on 100 μM **44** with 500 μM **35** at 37 °C (N=1)

*Concentration (μM) = (area/ 498852) x 100 μM

Time (min)	Peak Area	Concentration (μM)*
0	0	0
0.1	-	-
10	358598	106.15
20	320143	94.76
30	309932	91.74
40	302623	89.58
50	344335	101.93
60	337829	100.00
70	291137	86.18
80	331220	98.04

Appendix 3.2.2.2 Effect of 0.5 μg hNQO1 on 100 μM **44** with 500 μM **35** at 37 °C (N=2)

*Concentration (μM) = (area/337829) x 100 μM

Time (min)	Peak Area	Concentration (μM)*
0	0	0
0.1	82245	18.91
10	293259	67.44
20	229490	52.78
30	310531	71.42
40	316699	72.84
50	280568	64.53
60	285866	65.74
70	306371	70.46
80	434814	100.00

Appendix 3.2.2.3 Effect of 0.5 μg hNQO1 on 100 μM **44** with 500 μM **35** at 37 °C (N=3)

*Concentration (μM) = (area/434814) x 100 μM

3.2.3 NADH 35

Time (min)	Retention Time (min)	Area %	Peak Area	Concentration (μM)*
0	0.210	21.64	2615945	500.00
10	0.212	15.50	2297400	439.11
20	0.215	21.05	2203381	421.14
30	0.218	18.55	2195608	419.66
40	0.218	16.33	2074234	396.46
50	0.212	12.92	1920287	367.04
60	0.215	15.96	2153779	411.66
70	0.213	19.08	1980293	378.50
80	0.213	24.96	2072600	396.15

Appendix 3.2.3.1 Effect of 0.5 μg hNQO1 on 500 μM **35** with 100 μM **129** at 37 °C (N=1)

*Concentration (μM) = (area/ 2615945) x 500 μM

Time (min)	Peak Area	Concentration (μM)*
0	2955063	500.00
10	2674009	452.45
20	2740160	463.64
30	2586772	437.68
40	2626500	444.41
50	2353199	398.16
60	2589195	438.09
70	2498430	422.74
80	2602819	440.40

Appendix 3.2.3.2 Effect of 0.5 μg hNQO1 on 500 μM **35** with 100 μM **129** at 37 °C (N=2)

*Concentration (μM) = (area/ 2955063) x 500 μM

Time (min)	Peak Area	Concentration (μM)*
0	2641215	500.00
10	2585139	489.38
20	2403000	454.90
30	2324902	440.12
40	2322702	439.70
50	2184498	413.54
60	2217158	419.72
70	2347797	444.45
80	2049667	388.02

Appendix 3.2.3.3 Effect of 0.5 μg hNQO1 on 500 μM **35** with 100 μM **129** at 37 °C (N=3)

*Concentration (μM) = (area/ 2641215) x 500 μM

3.2.4 Summary of enzyme study data concentrations (μM)

Time (min)	Average Concentration of 129 (μM)	Average Concentration of 44 (μM)	Average Concentration of 35 (μM)
0	100.00	0.00	500.00
0.1	-	23.49	-
10	86.61	79.94	460.31
20	53.49	64.14	446.56
30	29.63	78.20	432.49
40	21.43	77.76	426.86
50	14.05	87.12	392.91
60	12.58	88.58	423.16
70	0.00	81.24	415.23
80	0.00	89.57	408.19

Appendix 3.2.4.1 Average concentrations (μM) of **129**, **44** and **35** for N=1 to N=3 enzyme study

3.2.5 HPLC enzyme study spectra for compound 129

(a) t = 0.1 min

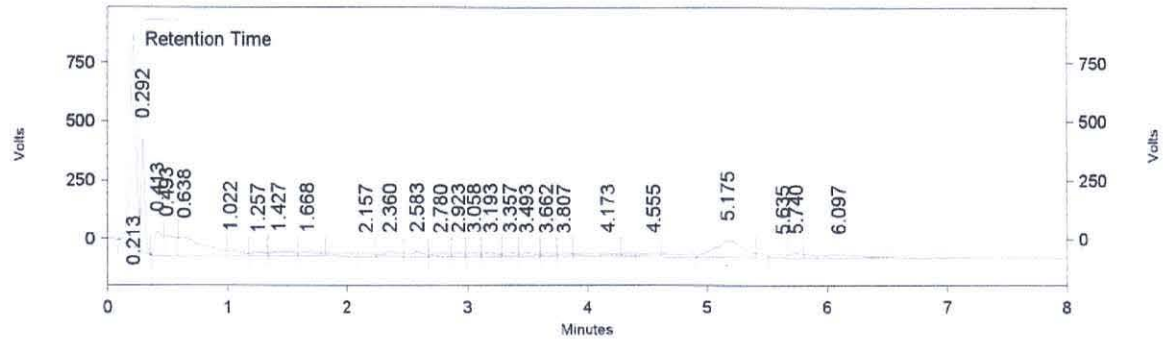

(b) t = 20 min

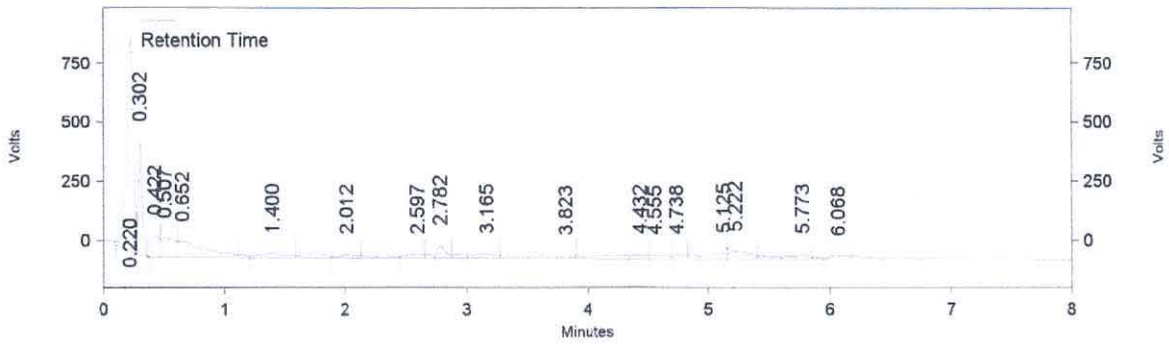

(c) t = 40 min

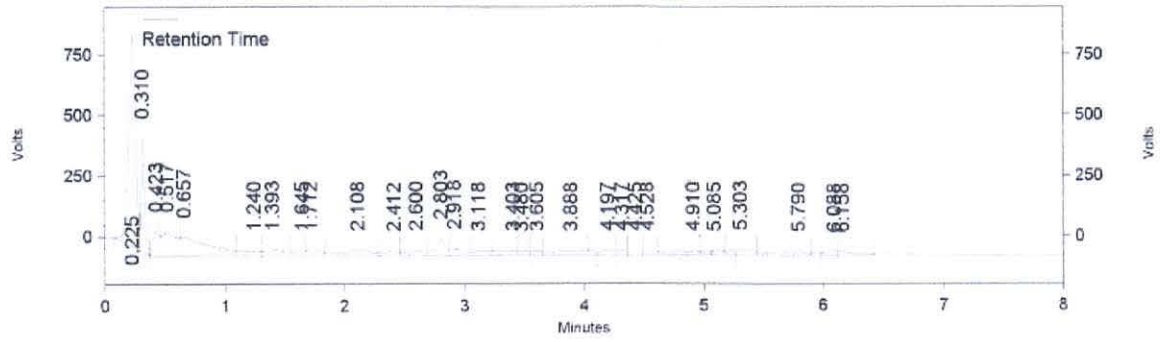

(d) t = 60 min

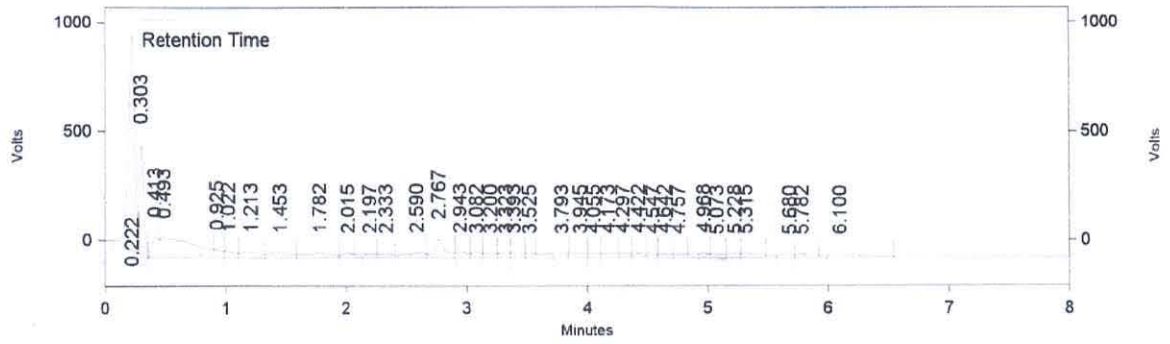

(e) t = 80 min

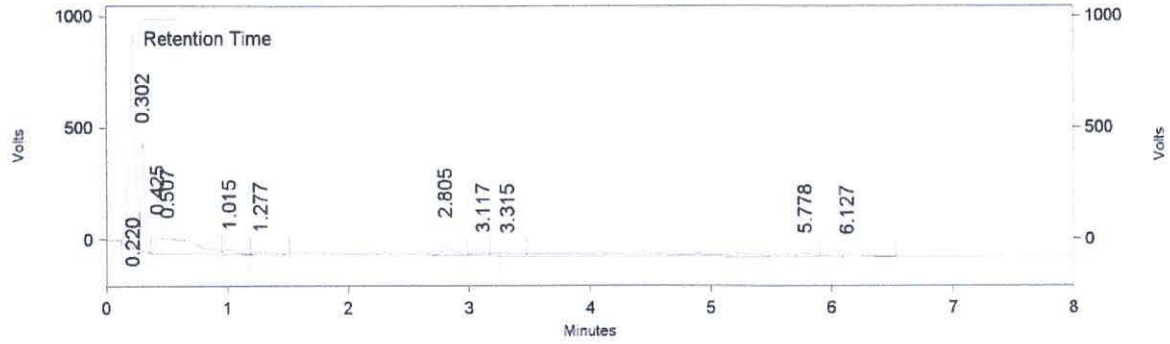

Appendix 3.2.5.1 Enzyme study spectra of N=1 showing the effect of 0.5 µg hNQO1 and 500 µM **35** on 100 µM **129** at 37 °C

3.3 Stability data for phenyl quinone delivery system

3.3.1 Compound 130

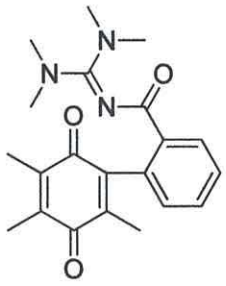

(130)

Time (min)	Retention Time (min)	Area %	Peak Area	Concentration (μM)*
0	9.093	15.743	2598114	97.49
20	9.103	20.085	2638151	98.99
40	9.115	20.327	2665117	100.00
60	9.110	19.955	2622273	98.39
80	9.115	19.809	2584294	96.97

Appendix 3.3.1.1 Stability data of 100 μM **130** in 10 mM phosphate buffer pH 7 at 37 °C

*Concentration (μM) = (area /2665117) x 100 μM

3.3.2 Lactone **120**

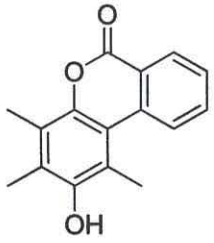

(120)

Time (min)	Retention Time (min)	Area %	Peak Area	Concentration (μM)*
0	9.963	5.599	924012	100.00
20	9.963	6.421	843373	91.27
40	9.967	6.307	826877	89.49
60	9.963	6.012	790073	85.50
80	9.970	5.505	718180	77.72

Appendix 3.3.2.1 Stability data of 100 μM **120** in 10 mM phosphate buffer pH 7 at 37 °C

*Concentration (μM) = (area / 924012) x 100 μM

3.3.3 HPLC stability spectra for compound 130 and lactone 120

(a) t = 0 min

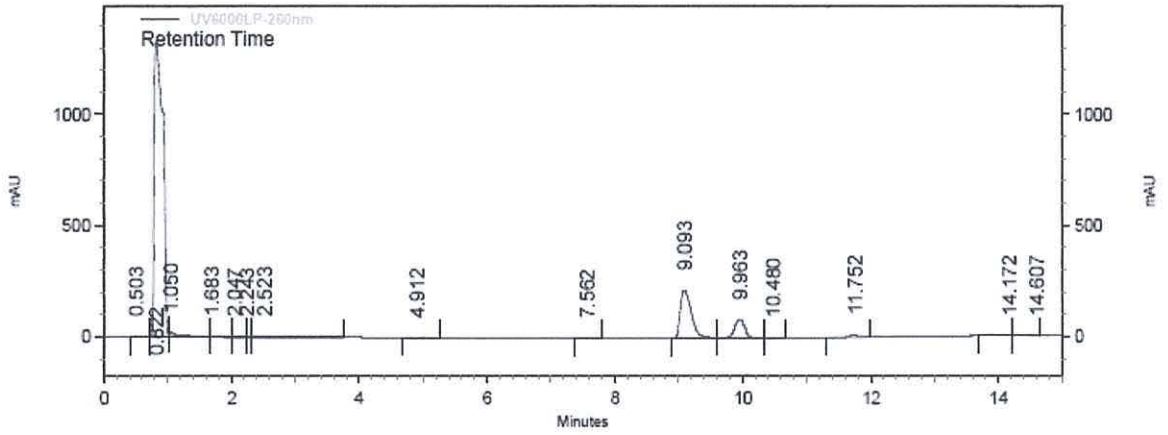

(b) t = 80 min

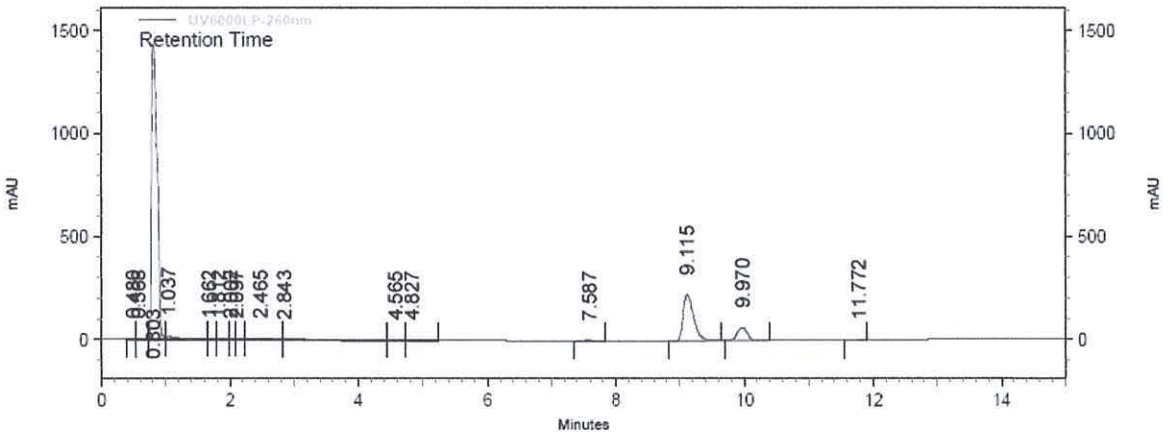

Appendix 3.3.3.1 Stability spectra of 100 μM **130** and 100 μM **120** in 10 mM phosphate buffer pH 7 at 37 °C

3.3.4 NADH 35

Time (min)	Retention Time (min)	Area %	Peak Area	Concentration (μM)*
0	0.827	84.453	5820751	500.00
20	0.807	86.189	5155542	442.86
40	0.808	86.206	5110561	438.99
60	0.807	75.793	5091765	437.38
80	0.805	75.648	5053718	434.11

Appendix 3.3.4.1 Stability data of 500 μM **35** in 10 mM phosphate buffer pH 7 at 37 °C

*Concentration (μM) = (area / 5820751) x 500 μM

3.4 Enzyme study data for phenyl quinone delivery system

3.4.1 Compound 130

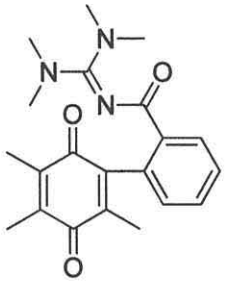

(130)

Time (min)	Retention Time (min)	Area %	Peak Area	Concentration (μM)*
0	8.865	19.936	3278240	100.00
20	8.912	9.884	1574778	48.04
40	8.980	7.043	1144080	34.90
60	8.848	5.999	911875	27.82
80	9.047	5.210	730799	22.29

Appendix 3.4.1.1 Effect of 0.5 μg hNQO1 on 100 μM **130** with 500 μM **35** at 37 °C (N=1)

*Concentration (μM) = (area / 3278240) x 100 μM

Time (min)	Retention Time (min)	Area %	Peak Area	Concentration (μM)*
0	8.917	19.635	3411045	100.00
20	9.003	10.717	1759267	51.58
40	8.987	8.611	1374866	40.31
60	8.938	6.808	1153858	33.83
80	8.912	6.691	1001690	29.37

Appendix 3.4.1.2 Effect of 0.5 μg hNQO1 on 100 μM **130** with 500 μM **35** at 37 °C (N=2)

*Concentration (μM) = (area / 3411045) x 100 μM

Time (min)	Retention Time (min)	Area %	Area	Concentration (μM)*
0	8.980	20.211	3274990	100.00
20	9.255	10.183	1476419	45.08
40	9.257	7.641	1059953	32.37
60	9.220	5.814	772324	23.58
80	9.178	4.335	568185	17.35

Appendix 3.4.1.3 Effect of 0.5 μg hNQO1 on 100 μM **130** with 500 μM **35** at 37 °C (N=3)

*Concentration (μM) = (area / 3274990) x 100 μM

3.4.2 Lactone 120

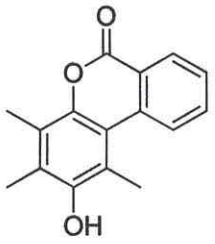

(120)

Time (min)	Retention Time (min)	Area %	Peak Area	Concentration (μM)*
0	0	0	0	0
0.1	9.578	1.300	213783	26.06
20	9.655	3.704	590107	71.92
40	9.723	4.008	651017	79.34
60	9.580	3.267	496612	60.53
80	9.785	2.351	329838	40.20

Appendix 3.4.2.1 Effect of 0.5 μg hNQO1 on 100 μM **120** with 500 μM **35** at 37 °C (N=1)

*Concentration (μM) = (area /820503) x 100 μM

Time (min)	Retention Time (min)	Area %	Area	Concentration (μM)*
0	0	0	0	0
0.1	9.693	1.063	184706	22.51
20	9.732	2.899	475856	58.00
40	9.767	3.503	559307	68.17
60	9.647	3.379	572786	69.81
80	9.672	2.469	369593	45.04

Appendix 3.4.2.2 Effect of 0.5 μg hNQO1 on 100 μM **120** with 500 μM **35** at 37 °C (N=2)

*Concentration (μM) = (area /820503) x 100 μM

Time (min)	Retention Time (min)	Area %	Area	Concentration (μM)*
0	0	0	0	0
0.1	9.643	1.346	218071	26.58
20	9.908	3.410	494411	60.26
40	9.910	4.967	688909	83.96
60	9.913	2.793	371017	45.22
80	9.932	2.271	297589	36.27

Appendix 3.4.2.3 Effect of 0.5 μg hNQO1 on 100 μM **120** with 500 μM **35** at 37 °C (N=3)

*Concentration (μM) = (area /820503) x 100 μM

Note: 820503 is the average concentration of lactone **120** at 100 μM (Appendix 3.3.2.1)

3.4.3 NADH 35

Time (min)	Retention Time (min)	Area %	Peak Area	Concentration (μM)*
0	0.925	93.682	5596750	500.00
20	0.863	85.214	5309702	474.36
40	0.860	86.568	5039368	450.20
60	0.840	88.272	4848404	433.14
80	0.847	89.962	4870124	435.09

Appendix 3.4.3.1 Effect of 0.5 μg hNQO1 on 500 μM **35** with 100 μM **130** at 37 °C (N=1)

*Concentration (μM) = (area / 5596750) x 500 μM

Time (min)	Retention Time (min)	Area %	Area	Concentration (μM)*
0	0.945	93.324	5767804	500.00
20	0.878	85.944	5482454	475.26
40	0.880	84.866	5127529	444.50
60	0.883	85.658	5361939	464.82
80	0.857	91.120	5056519	438.34

Appendix 3.4.3.2 Effect of 0.5 μg hNQO1 on 500 μM **35** with 100 μM **130** at 37 °C (N=2)

*Concentration (μM) = (area / 5767804) x 500 μM

Time (min)	Retention Time (min)	Area %	Area	Concentration (μM)*
0	0.973	90.825	5897723	500.00
20	0.863	92.909	5144572	436.15
40	0.845	88.540	4939013	418.72
60	0.835	89.912	4786742	405.81
80	0.830	94.811	4701612	398.60

Appendix 3.4.3.3 Effect of 0.5 μg hNQO1 on 500 μM **35** with 100 μM **130** at 37 °C (N=3)

*Concentration (μM) = (area / 5897723) x 500 μM

3.4.4 Summary of enzyme study data concentrations (μM)

Time (min)	Average Concentration of 130 (μM)	Average Concentration of 120 (μM)	Average Concentration of 35 (μM)
0	100.00	0.00	500.00
0.1	-	37.58	-
20	48.23	63.39	461.92
40	35.86	77.16	437.81
60	28.41	58.52	434.59
80	23.00	40.50	424.01

Appendix 3.4.4.1 Average concentrations (μM) of **130**, **120** and **35** for N=1 to N=3 enzyme study

3.4.5 HPLC enzyme study spectra for compound 130 and lactone 120

(a) t = 0.1 min

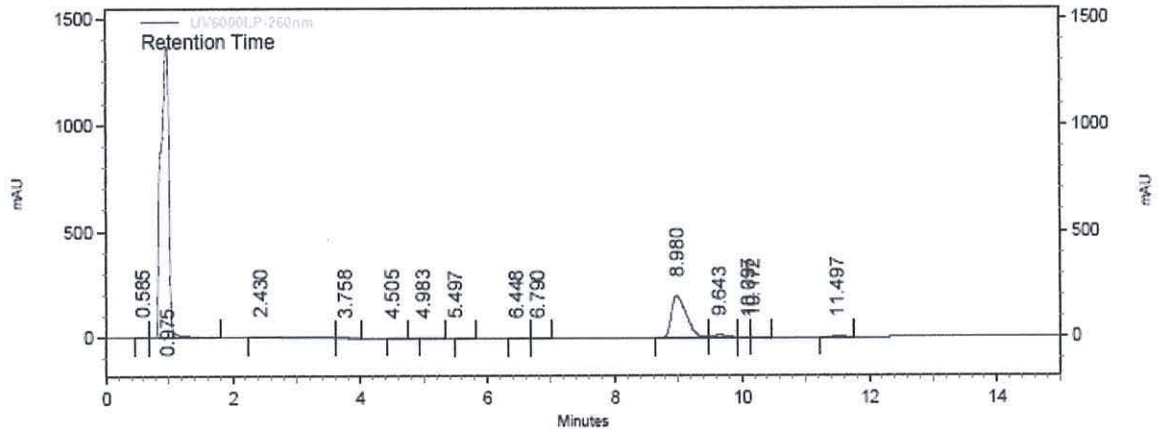

(b) t = 20 min

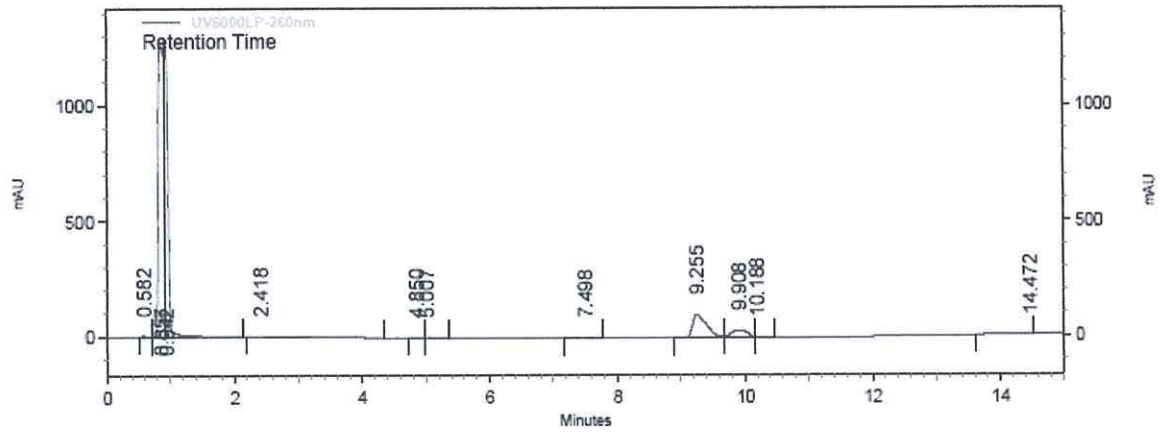

(c) t = 40 min

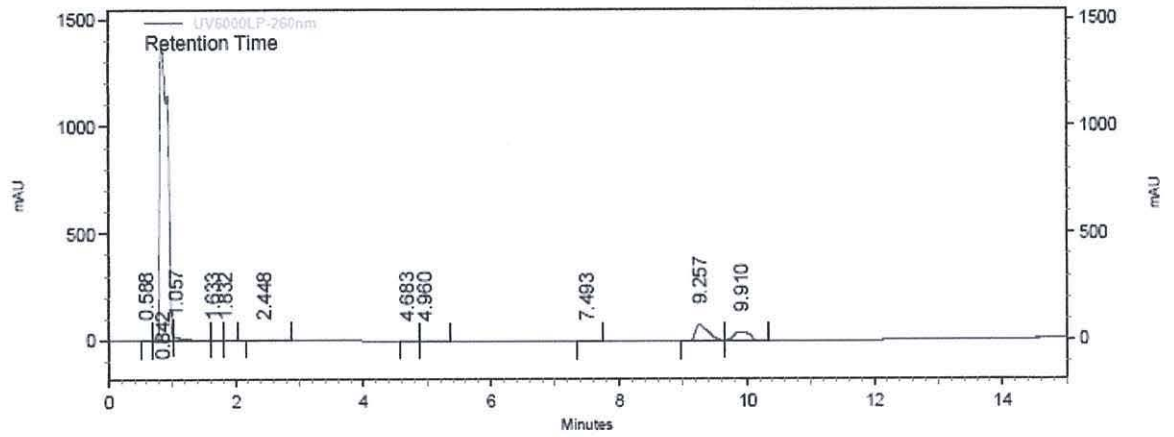

(d) t = 60 min

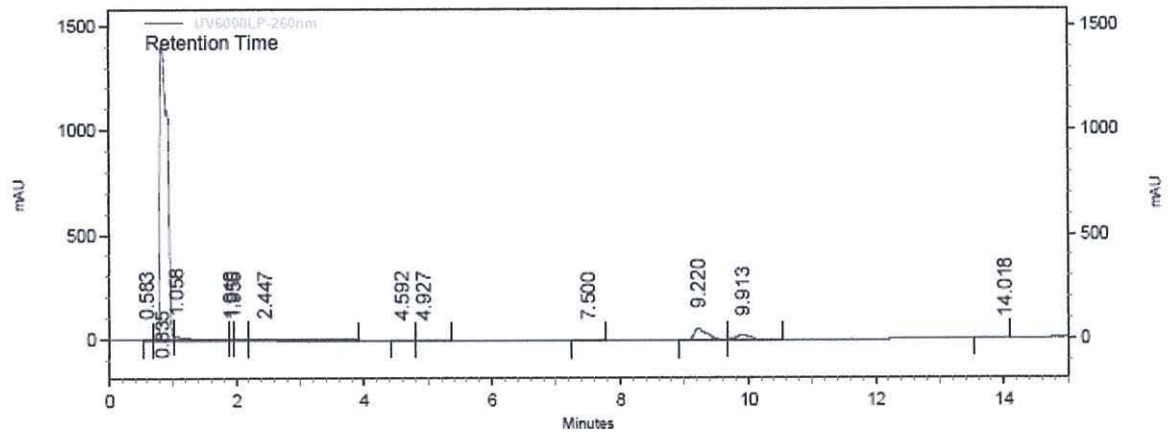

(e) t = 80 min

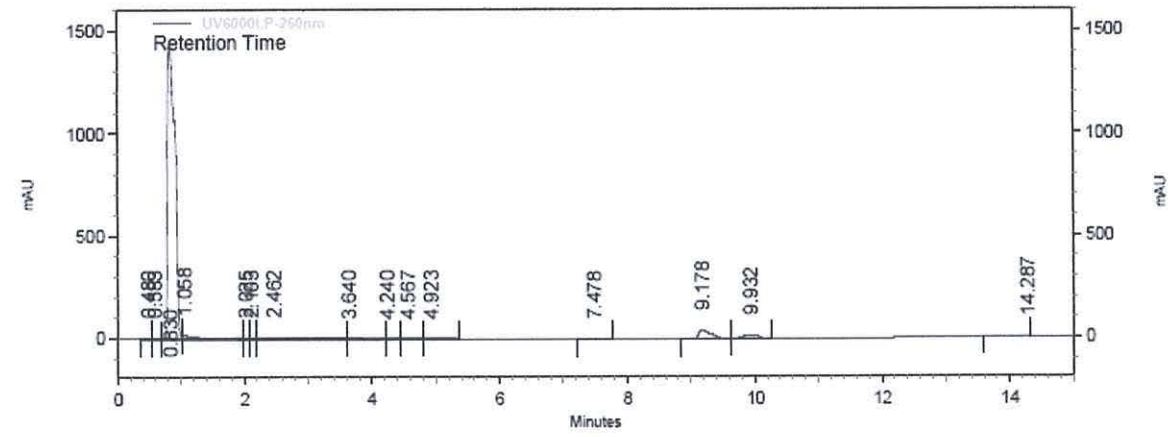

Appendix 3.4.5.1 Enzyme study spectra of N=3 showing the effect of 0.5 µg hNQO1 and 500 µM **35** on 100 µM **130** at 37 °C

The raw data (.pdf) for this HPLC section are provided in the supporting information. Awaiting additional raw data from Morvus Technology Ltd for N=2 and N=3 (Appendix 3.2).